INTESTINAL TARGETING OF SMALL MOLECULE MMP AND TGR5 LIGANDS FOR INFLAMMATORY BOWEL DISEASE

by

Maria Therese Pigott

Being a thesis submitted for the degree of Doctor of Philosophy in Pharmacy and Pharmaceutical Sciences

Under the supervision and direction of

Prof. John Gilmer and **Asst. Prof. Carlos Medina**

School of Pharmacy and Pharmaceutical Sciences

Trinity College Dublin

2018

Declaration

I declare that this thesis has not been submitted as an exercise for a degree at this or any other university and it is entirely my own work.

I agree to deposit this thesis in the University's open access institutional repository or allow the Library to do so on my behalf, subject to Irish Copyright Legislation and Trinity College Library conditions of use and acknowledgement.

Maria Therese Pigott

Summary

The aetiology of inflammatory bowel disease (IBD) is incompletely understood but it is generally accepted to involve a dysregulated intestinal immune response to commensal microbiota and an increase in intestinal permeability. Matrix metalloproteinases (MMPs), MMP-9 (gelatinase B) in particular, are implicated in this compromise of intestinal barrier structure and have further roles in the potentiation and augmentation of disease. Takeda G-protein coupled receptor 5 (TGR5), a bile acid receptor, is also involved in maintenance of intestinal barrier integrity and there is evidence to suggest that both these targets are accessible to modulators confined to the gut lumen. Expressed in many tissues and cell types and involved in many physiological processes, the potential of MMP and TGR5 modulators has been limited by unwanted off-target effects. We proposed that small molecule ligands designed to be confined to the gastrointestinal lumen through judicious modification of physicochemical properties could achieve non-systemic effects.

Suppression of oral absorption potential of an established gelatinase inhibitory scaffold was pursued by synthetic strategies to increase molecular weight and/or polarity including preparation of a dimer linked by a short PEG chain or introduction of a permanent charge. Bulky conjugates of an MMP inhibitor and lithocholic acid (LCA), the most potent endogenous bile acid agonist at TGR5, were also prepared. By virtue of their high molecular weight, such conjugates would be expected to have limited absorption potential and we hoped to retain activity at both targets.

Compound **53**, a permanently positively charged barbiturate-based gelatinase inhibitor, was a potent inhibitor of recombinant human MMP-9 as measured by fluorogenic assay and an uptake assay in Caco-2 cells indicated that it was a poor candidate for passive uptake. It was chosen for evaluation in a DSS mouse model of colitis to test the hypothesis that disease modifying effects can be achieved by inhibition of apically secreted gelatinases. The disease activity index (DAI) scores of the treated group were significantly lower than the DSS group indicating that treatment with compound **53** reduced the severity of DSS-induced colitis in mice. PCR analysis of the retained colon samples indicated that the pro-inflammatory cytokines TNF-α, IL-1β and IL-6 were downregulated at gene level in the treated group compared to the DSS control group and these downregulations were statistically significant.

The MMP-9 inhibitor – TGR5 agonist conjugates retained potent MMP-9 inhibition but activation of TGR5 showed tighter structural specificity than expected. Some compounds of the series caused accumulation of cAMP, the downstream second messenger of TGR5 activation, in human enterendocrine NCI-H716 cells but potency was much lower than LCA. It is yet unknown if this level of activity could exert a functional effect in the context of a gut confined agent in appropriate animal models. This work contributed to our knowledge of binding at the human TGR5 receptor, its SAR and capacity for chemical manipulation to achieve gut confinement. TGR5 agonists that are expected to be poor candidates for absorption by virtue of their polarity were also synthesised from LCA. These candidates retained activity at TGR5 and they are promising candidates for further study.

Acknowledgements

I wish to thank Prof. John Gilmer and Asst. Prof. Carlos Medina for their advice, guidance, ideas and inspirations in the past years. I have truly enjoyed being part of their team and thank them for the opportunity.

Thank you to Dr. Maria Jose Santos-Martinez for all her help and guidance in the lab. Thank you to Mr. Brian Talbot for the mass spec work and help with all kinds of technical difficulties. Thanks to Dr. John O' Brien for the NMR work and thanks to Dr. Brian Flood for help with the histology. A special thanks to Dr. Jun Wang and Dr. Gábor Radics for all their help in the chemistry lab and in the biology lab.

Thank you to all the Ph.D. students and postdocs, past and present, who make TCD a great place to be. I have met some wonderful people and made lifelong friends. Thanks also to my parents and sister Eimer who support me in everything I do and finally thanks to my husband Jason for his love and support.

Table of Contents

Table of Figures

Table of Tables

Table of Schemes

Abbreviations

ABC	ATP binding cassette
ACN	acetonitrile
Ac-PGP	N-acetylPro-Gly-Pro
ADAM	A disintegrin and metalloproteinase
ADME	absorption, distribution, metabolism, excretion
Ala	alanine
ANOVA	analysis of variance
Anti-TNF	anti-tumour necrosis factor
APCI	atmospheric pressure chemical ionization
APMA	*p*-aminophenylmercuric acetate
APS	ammonium persulfate
Arg	arginine
ARRIVE	Animal Research: Reporting of *In Vivo* Experiments
ASBT	apical sodium codependent bile acid transporter
ATP	adenosine triphosphate
ATR	attenuated total reflection
BOC	*tert*-butyloxycarbonyl
CA	cysteine array
cAMP	cyclic adenosine monophosphate
CBD	collagen binding domain
CCl_4	carbon tetrachloride
CD	Crohn's disease
CDCA	chenodeoxycholic acid
$CDCl_3$	deuterated chloroform
cDNA	complementary DNA
CHO	Chinese hamster ovarian
CI	confidence interval

COMU	(1-cyano-2-ethoxy-2-oxoethylidenamineooxy)–dimethylaminomorpholino carbenium hexafluorophosphate
CRP	c-reactive protein
d	doublet
D2	deiodinase 2
DABCO	1,4-diazabicyclo[2.2.2]octane
DAI	disease activity index
DCA	deoxycholic acid
DCC	N,N'-dicyclohexylcarbodiimide
DCM	dichloromethane
ddH_2O	double deionised water
DIPEA	N,N-Diisopropylethylamine
DMF	dimethylformamide
DMPU	1,3-dimethyl-3,4,5,6-tetrahydro-2(1H)-pyrimidinone
DMSO	dimethyl sulfoxide
DMSO-d6	deuterated DMSO
DNA	deoxyribonucleic acid
dNTPs	deoxyribose nucleoside triphosphates
DP IV	dipeptidyl peptidase IV
dsDNA	double-stranded DNA
DSS	dextran sodium sulfate
dUTP	deoxyuridine triphosphate
EC_{50}	effective concentration 50 percent
ECM	extracellular matrix
EGFR	epidermal growth factor receptor
EHS	Engelbreth-Holm-Swarm
eq.	equivalent
ESI	electrospray ionisation
Et_2O	diethyl ether
Et_3N	triethylamine

EtOAc	ethyl acetate
FN2	fibronectin type II
FXR	farnesoid X receptor
GIT	gastrointestinal tract
Gln	glutamine
GLP	glucagon-like peptide
Glu	glutamic acid
Gly	glycine
GPBAR1	G protein-coupled bile acid receptor 1
GPCRs	G protein-coupled receptors
GPI	glycosylphosphatidylinositol
H & E	hematoxylin and eosin
H_2	hydrogen gas
H_2O	water
HCl	hydrochloric acid
Hex	hexane
His	histidine
HN_3	hydrogen azide
HOBt	hydroxybenzotriazole
HPLC	high performance liquid chromatography
HRMS	high resolution mass spectrometry
IBD	inflammatory bowel disease
IBMX	3-isobutyl-1-methylxanthine
IC_{50}	inhibitory concentration 50 percent
IEC	intestinal epithelial cell
IFN	interferon
Ig	immunoglobulin
IL	interleukin
IL-2R	interleukin-2 receptor

ILC	innate lymphoid cell
Ile	isoleucine
IP	intraperitoneal
IR	infrared
IV	intravenous
IVCs	individually ventilated cages
JAK	Janus kinase
KO	knock-out
LAP	latency associated peptide
LC	liquid chromatography
LCA	lithocholic acid
Leu	leucine
$LiAlH_4$	lithium aluminium hydride
LOD	limit of detection
LTQ	linear trap quadrupole
LUMO	lowest unoccupied molecular orbital
m	multiplet
MAMPS	microbe associated molecular patterns
M-BAR	membrane-type bile acid receptor
MeOD	deuterated methanol
MeOH	methanol
Met	methionine
MMPs	matrix metalloproteinases
Mp	melting point
mRNA	messenger ribonucleic acid
MS	mass spectrometry
MW	microwave
N_2	nitrogen gas
Na_2SO_4	sodium sulfate

NaH	sodium hydride
$NaHCO_3$	sodium bicarbonate
NaN_3	sodium azide
NaOH	sodium hydroxide
NBS	N-bromosuccinimide
NFκB	nuclear factor-kappa B
NKT	natural killer T
NLRs	NOD-like receptors
NMR	nuclear magnetic resonance
NO	nitric oxide
NOD	nucleotide binding oligomerization domain
OCT	organic cation transporter
PBS	phosphate buffered saline
PCC	pyridinium chlorochromate
PCR	polymerase chain reaction
PEG	polyethylene glycol
P-gp	P-glycoprotein
PKA	protein kinase A
PLGA	poly [DL-lactide-co-glycolide]
PMA	phorbol 12-myristate
PPh_3	triphenylphospine
Pro	proline
RNA	ribonucleic acid
ROS	reactive oxygen species
rRNA	ribosomal ribonucleic acid
RT	room temperature
s	singlet
SAR	structure activity relationship
SC	solute carrier

scid	severely combined immunodeficiency
SD	standard deviation
SDS	sodium dodecyl sulfate
SDS-PAGE	sodium dodecyl sulfate polyacrylamide gel electrophoresis
SEM	standard error of the mean
siRNAs	small interfering RNAs
ssDNA	single-stranded DNA
t	triplet
T3	iodothyronine
T4	thyroxine
TACE	TNF-converting enzyme
TCA	taurocholic acid
TDCA	taurodeoxycholic acid
TEMED	tetramethylethylenediamine
TFA	trifluoroacetic acid
TGF-β	transforming growth factor-beta
TGR5	Takeda G protein-coupled receptor 5
T_H1	T helper 1
THF	tetrahydrofuran
TIMP	tissue inhibitor of matrix metalloproteinases
TLC	thin layer chromatography
TLR	toll-like receptor
TM	transmembrane
TNBS	trinitrobenzene sulfonic acid
TNF	tumour necrosis factor
tPSA	total polar surface area
TRAF2	TNF receptor-associated factor 2
T_{Reg}	regulatory T
Tyr	tyrosine

UC	ulcerative colitis
UDCA	ursodeoxycholic acid
UNG	uracil-N glycosylase
UPLC	ultra performance liquid chromatography
USP	United States Pharmacopoeia
Val	valine

Chapter 1. Introduction

1.1 Inflammatory bowel disease

Inflammatory bowel disease (IBD) comprises a number of idiopathic chronic inflammatory intestinal conditions including Crohn's disease (CD) and ulcerative colitis (UC). The pathogenesis is incompletely understood but it is generally accepted to involve an increase in intestinal permeability combined with or leading to dysregulation of the intestinal immune response to commensal microbiota in genetically susceptible individuals leading to gastrointestinal injury.[1] IBD has no cure and the aim of interventions (medical, surgical or other) is to treat active disease to control symptoms, improve quality of life, induce remission and thereafter maintain remission. Colonoscopic surveillance measures are recommended for prevention and early detection of associated colorectal cancers in patients with extensive UC.[1]

1.1.1 Impact of IBD

IBD affects an estimated 1.5 million Americans and 2.2 million Europeans[2] posing a significant challenge and economic burden to healthcare systems.[3] With increasing incidence in the developing world,[2] this is rising globally. Most commonly presenting during the second or third decade of life, IBD will require management throughout the patient's lifetime. Uncontrolled it can have debilitating effects on quality of life, ability to work, have relationships and plan a family. While associated with significant morbidity, mortality rates in IBD patients do not differ substantially from the general population.[4]

1.1.2 Ulcerative colitis

UC usually affects the rectum and may extend proximally to the colon to a variable extent. The inflammation is continuous and diffuse affecting only the mucosal layer and has a relapsing-remitting pattern.[5] A representative image[6] of the endoscopic appearance can be seen in panel B of Figure 1. Histologically, there is distorted crypt architecture and cryptitis and there may be crypt abscesses.[5]

A **B**

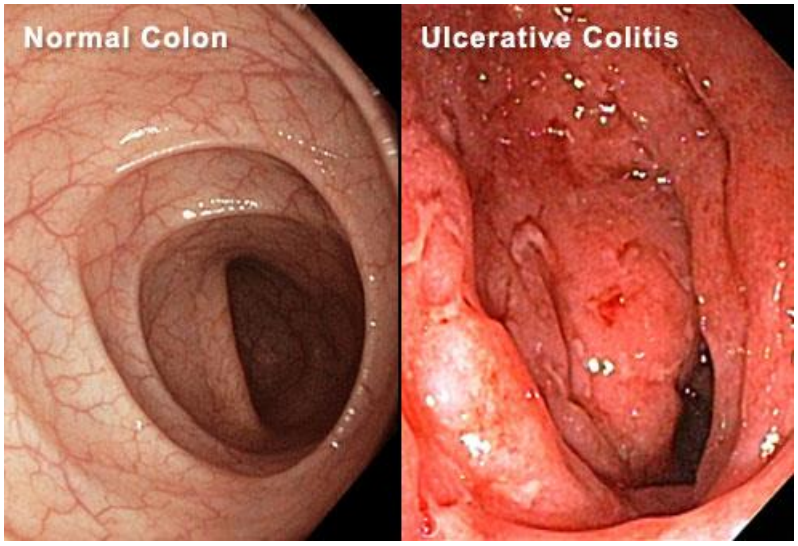

Figure 1. Representative endoscopy images of A: normal colon and B: ulcerative colitis of the colon. Image taken from www.webmd.com6

Pharmacological intervention is based on clinical severity and regions of the gastrointestinal tract (GIT) affected with consideration for the patient's age, preferences and co-morbidities.[7] Symptoms are typically bloody diarrhoea with passage of mucus and abdominal cramping. Disease activity is typically described as mild (up to four bloody stools daily and no systemic involvement, moderate (four to six bloody stools daily and minimal systemic involvement) or severe (more than six stools daily and signs of systemic involvement such as fever, tachycardia, anaemia or raised erythrocyte sedimentation rate).[5] Treatment is generally a step-up approach.[7] To induce remission in disease affecting the rectum (proctitis) or the rectum and sigmoid (proctosigmoiditis) a topical aminosalicylate as a suppository or enema is indicated which may be combined with an oral aminosalicylate. Where an aminosalicylate is not tolerated or contraindicated a topical or oral corticosteroid can be used. Oral prednisolone is indicated in moderate or severely active cases not requiring hospitalisation or surgery. Where the presentation involves the colon distal to the splenic flexure (left-sided colitis) or is extensive involving the entire colon (pancolitis) a high induction dose of an oral aminosalicylate is indicated and may be combined with a topical aminosalicylate or beclomethasone dipropionate. More severe cases will require oral prednisolone.[7] Anti-tumour necrosis factor (anti-TNF) agents such as adalimumab or infliximab are licensed for moderately to severely active ulcerative colitis which has not responded to conventional therapies or in patients who are intolerant or have medical contraindications for such therapies.[8, 9]

1.1.3 Crohn's disease

In the case of CD, the inflammation is discontinuous and segmented extending transmurally and complications include strictures, fistulae, fissures and abscesses. Representative images of the endoscopic appearance in Crohn's disease can be seen in Figure 2. While most commonly affecting the terminal ileum, it may affect any region of the GIT from the mouth to the anus.[5]

A **B**

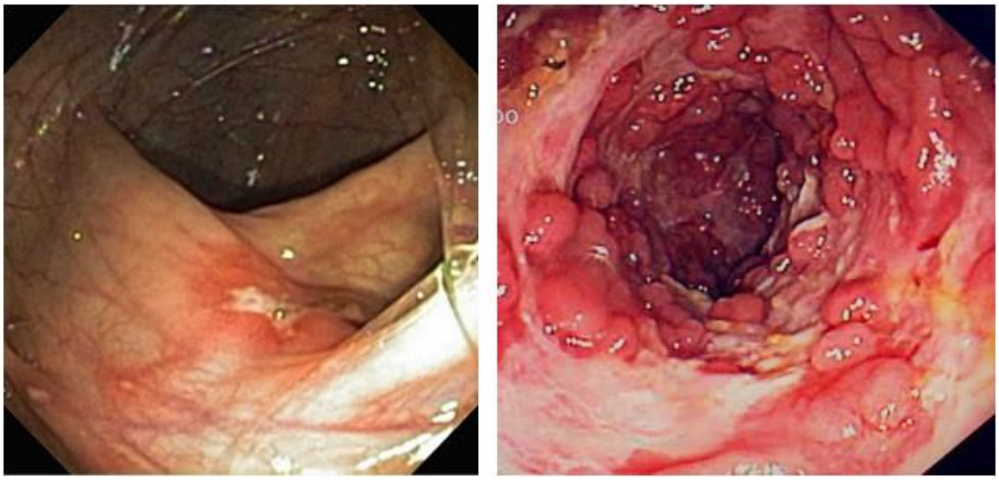

*Figure 2. Endoscopic appearance of Crohn's disease **A**: Localized ulcerations in mild colonic disease **B**: Severe colonic disease with pseudopolyps. Image taken from www.mcgillibd.ca*

Symptoms of Crohn's disease include diarrhoea, abdominal pain, weight loss and sometimes malaise, anorexia, nausea, vomiting and fever.[5] For most patients, the disease will follow a chronic remitting and relapsing course with only 10 – 13% of patients maintaining remission for several years. Disease behaviour can vary and progression from non-stricturing and non-penetrating presentation to stricturing and penetrating is often seen[10] so that after 20 years most CD patients will have required surgery.[5] Management options include drug therapy, attention to nutrition, smoking cessation and frequently surgery.[11] Like UC, the aim of drug treatment is to reduce symptoms, promote mucosal healing, induce and maintain remission. Monotherapy with a conventional glucocorticosteroid such as prednisolone is first line therapy for first presentation or a single exacerbation in 12 months and where this is not appropriate 5-aminosalicylic acid or budesonide can be considered as appropriate. When there are two or more exacerbations in 12 months or the steroid cannot be tapered, azathioprine, mercaptopurine or methotrexate can be added.[11] Anti-TNF agents are recommended as treatment options for moderately or

severely active CD which has not responded to conventional treatment or in patients who are intolerant or have medical contraindications for such therapies.[8, 9] Patients requiring hospitalisation for severely active disease require intravenous (IV) corticosteroids. Those that remain unresponsive can be treated with ciclosporin, tacrolimus or an anti-TNF agent. The main agents for maintenance of remission are azathioprine and mercaptopurine or alternatively methotrexate with optional addition of an anti-TNF agent to maintain a steroid-free or steroid-spared remission.[11]

1.1.4 Contributory factors in IBD - the host, the environment and the microbiota

IBD is most prevalent in northern Europe and North America and has been thought of as a disease of westernized society.[3] This is most certainly in part due to race and ethnicity. However, the increasing incidence in developing countries of Asia[12] and Africa[13] suggests a role for environmental factors in disease initiation. Better access to healthcare and improved diagnoses may contribute to an increase in recorded prevalence[14] but correlations to industrialisation and increased incidence in migrants from low-prevalence areas to high-prevalence areas supports a role for lifestyle effects.[15]

The role of genetics as a contributory factor in disease pathogenesis is supported by twin studies and familial studies particularly in CD[16] and in 2001, linkage analyses identified variants in the nucleotide binding oligomerization domain containing 2 (NOD2 or CARD15) gene.[17] Since then more than 160 IBD risk loci have been identified that indicate involvement of innate immunity, adaptive immunity, autophagy and intestinal epithelial barrier function.[18] Many of these risk loci are also associated with other immune-mediated disorders such as diabetes mellitus and rheumatoid arthritis.[18] It is not understood why many individuals who carry these gene variants do not develop the disease while others do.

Aspects of modern lifestyle have been linked with IBD but findings between studies exploring environmental risk factors are often inconsistent.[19] Generally, there is increased risk associated with urban living,[20] repeated exposure to antibiotics[21] and a westernized diet.[22] Reduced risk has been associated with being breastfed,[23] having a large family and living on a farm.[24] These trends concur with the hygiene hypothesis that improvements in water, food and housing sanitary conditions correlate with increased incidence of autoimmune and chronic inflammatory conditions. This hypothesis was initially proposed by Strachan who correlated hay fever incidence to family size and position in the

household in childhood.[25] It is thought that exposure from birth dictates gut microbial colonization, a diverse and well-balanced exposure promoting immune tolerance. Experimental studies show that smoking is beneficial in UC but in CD smoking cessation is an effective therapeutic intervention.[26] The beneficial effect in UC is thought to be due to increased mucus production and decreased production of proinflammatory cytokines and nitric oxide[27] but nicotine patches have failed to show efficacy as maintenance therapy.[28] IBD has been correlated to aspects of a westernized diet including high carbohydrate consumption, high polyunsaturated fat consumption and low fibre consumption.[29] The diet effect in disease is not clear but effects of diet on the microbiota have been established. Environmental, dietary, microbial and host factors are interrelated and can be confounding in experimental studies.

Bacteria are an absolute requirement for IBD pathogenesis. Researchers failed to induce colitis in germ-free mice despite a genetic predisposition.[30] In addition, antibiotics such as metronidazole can be beneficial in colitis.[31] In normal physiology, bacterial colonization of the gut is essential for normal nutrient uptake, intestinal barrier function and appropriate immune response to pathogens. Beneficial commensals have anti-inflammatory actions inducing regulatory immune responses including regulatory T (T_{Reg}) -cells and interleukin-10 (IL-10).[32] Thousands of species from many genera have been found in the microbiota, make-up differing between individuals and GIT location within an individual modulated by diet and health status.[33] The composition of the microbiota is altered in IBD, both quantitatively and qualitatively.[34] In humans, the microbiota is dominated by members of the Firmicutes and Bacteroidetes phyla. In IBD, a depletion of some species including Bacteroidetes and overall diversity has been identified as well an increase in other phyla such as Proteobacteria.[34] Associations have been made with some pathogens such as *Escherichia coli*[35] and a model of IBD can be induced in rodents by infection with *Salmonella typhimurium*.[36] However, there does not seem to be a single causative organism in the disease and the association is multifactorial involving the homeostasis of the microbiota itself and its interactions with both the innate and adaptive immune systems.[33] A combination of genetic and environmental factors leads to loss of protective bacteria and dysbiosis. Colitogenic bacteria activate T helper 1 (T_H1) and T_H17 cells which leads to chronic inflammation[32] and a colitogenic microbiota allowed to develop in an immunodeficient mouse strain can induce colitis in healthy immunocompetent mice.[37] The roles of the microbiota in homeostasis and pathology are illustrated in Figure 3.

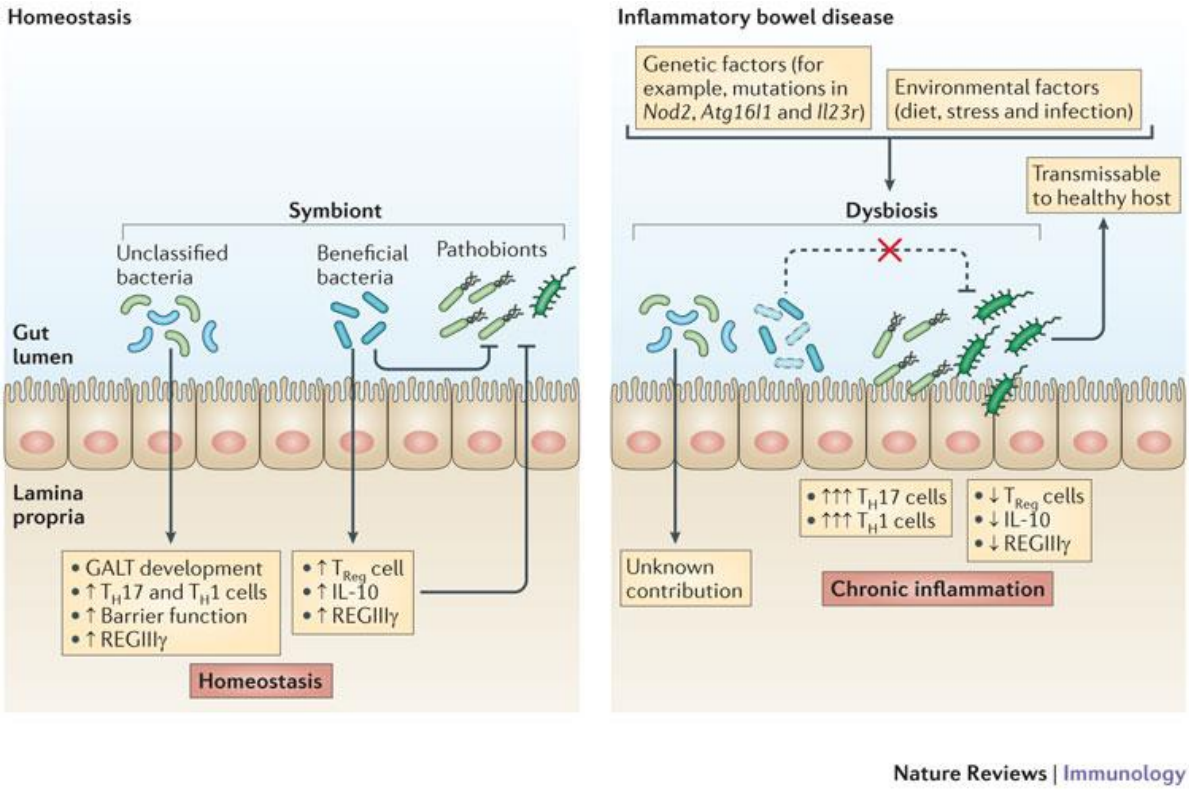

Figure 3. Protective roles of the gut microbiota in normal homeostasis (left-hand side) and pathogenic roles in IBD (right-hand side). Image taken from Kamada et al.[32]

1.1.5 Immunopathology of IBD

The epithelium of the intestine is the barrier between the immune cells of the lamina propria and food and microbe derived antigens in the gut lumen. It is made up of absorptive enterocytes, mucus-producing goblet cells, hormone-producing enteroendocrine cells and growth factor and antimicrobial peptide producing paneth cells.[38] Tight junctions between the cells prevent the paracellular transport of most substances. In addition, the epithelium is coated with a protective layer of mucus which contains mucins and antimicrobials and a lower bacterial density than the gut lumen. In IBD patients, the epithelial barrier is leaky in both inflamed and non-inflamed areas.[39, 40] There is evidence that this compromise of barrier integrity precedes disease onset and healthy first degree relatives of IBD patients exhibit enhanced permeability.[16] IBD patients can have loss of goblet cells and the pattern of mucin expression is altered.[41, 42]

In addition to its barrier function, the epithelium has a role in communicating the status of the luminal contents to the immune cells of the lamina propria. It senses commensals, pathogens and other antigens through pattern recognition receptors, the toll-like receptor family (TLRs) on the cell membrane and cytosolic NOD-like receptors (NLRs).[43]

Necessary for normal homeostasis of gut barrier integrity, the TLR family are together capable of recognising most microbe associated molecular patterns (MAMPS) and recognition triggers intracellular signalling pathways culminating in activation of the nuclear factor-kappa B (NF-κB) pathway.[43]

NOD1 and NOD2 proteins perform a recognition function intracellularly and a NOD2 mutation was one of the first susceptibility genes recognised.[44] Models of NOD2 overexpression stimulated with peptidoglycan-derived muramyl dipeptide results in NF-κB activation and a feedback loop increases NOD2 expression in the inflammatory condition[45] but *in vitro* models have shown both negative and positive regulation of this pathway by NOD2 mutations.[1] Functioning NOD2 is also necessary for effective autophagy[46] and it regulates paneth cell functions influencing the production of antimicrobial α-defensins.[47]

In IBD, the quantitative and qualitative expression of TLRs is altered. Healthy intestinal cells constitutively express TLR3 and TLR5 basolaterally and TLR2 and TLR4 are barely detectable. TLR4 is strongly upregulated in both CD and UC while TLR3 is downregulated in CD.[48] Such alterations in the innate immune mechanisms of the epithelial layer lead to dysregulated microbial recognition and clearance and inappropriate immune response.

Aberrations in the innate immune system trigger aberrations in the adaptive immune system. Dendritic cells express the entire spectrum of TLRs and NODs and can activate or silence T cell responses[49] as well as control the opening of tight junctions and expression of tight junction proteins.[50] In healthy individuals, these cells induce T-cell unresponsiveness stimulating naïve T-cell differentiation into regulatory CD4+ T-cells such as T_H3 cells. On identifying a pathogen, they acquire a mature activated phenotype and induce immunity by switching to effector T-cell responses such as T_H1, T_H2 or T_H17.[49] In IBD, the dendritic cell population has an increased frequency of mature cells with prolonged survival and aberrant expression of pattern recognition receptors inappropriately activates the immune response.[1] The pathogenesis of CD has been thought of as predominantly driven by T_H1 cells with increased expression of interferon-γ (IFN-γ), TNF-α and IL-12. UC is predominantly driven by T_H2 cells with increased expression of IL-4, IL-5 and IL-13.[51] IBD emerges as a result of dysregulation of T_H1, T_H2, and T_H17 and perhaps other T_H subsets.[51] This is combined with insufficient T_{Reg} suppressor function, accumulation of activated T-cells due to apoptosis resistance, disrupted balances in natural killer T (NKT) cells and innate lymphoid cells (ILCs) and inhibition of immunoregulatory and tolerance inducing transforming growth factor – β (TGF- β) signalling. Chemokines

which promote or direct inflammatory cell infiltrate are found at higher levels in IBD tissue than in normal mucosa.[1] This dysregulation of the innate and adaptive immune systems leads to inflammation initiation and persistence leading to a chronic inflammatory state.

1.1.6 Emerging therapies for IBD

The complexity of diverse pathways at play in IBD offers many potential therapeutic targets and the success of anti-TNF therapies has ignited interest in developing biologics for other molecular targets.[52] Other pro-inflammatory cytokines that have been investigated include IL-12/IL-23, the IL-2 receptor (IL-2R), and IFN-γ. While there have been some indications of clinical benefit in early trials in some cases, durable clinical responses have not been observed. Ustekinumab, a monoclonal antibody targeting IL-12 and IL-23 did not demonstrate significant benefit in phase II trials in patients with moderate to severe CD but did induce response in a subset of patients who had previously failed to respond to anti-TNF therapies.[53] Similarly, anti-IFN-γ therapy with the humanized antibody fontolizumab produced small delayed clinical benefit in patients with moderate to severe CD but did reduce C-reactive protein (CRP) levels.[54] Targeting of IL-2R signalling in UC with the monoclonal antibody basiliximab did not improve disease activity in a corticosteroid-refractory population.[55]

Blockade of signalling pathways downstream of cytokines has also been investigated. Tofacitinib is a small molecule inhibitor of the Janus kinase (JAK) family of proteins. In phase II trials it was effective for induction of remission in UC and the benefit was thought to be via JAK 1 inhibition with downregulation of IL-6 and IFN-γ.[56] Administration of anti-inflammatory cytokines such as IL-10, IL-11 and IFN-β which might influence the T_{reg}/T_H balance was also disappointing clinically.[52] Biologics aimed at inducing T-cell apoptosis do show evidence of clinical response but have also been associated with serious adverse events. Visilizumab, a monoclonal antibody targeting the T-cell receptor CD3, was not efficacious in severe IV corticosteroid-refractory UC and caused cytokine release syndrome in the majority of patients including cardiac events.[57]

Inhibition of leucocyte infiltration by targeting integrins has proved a successful approach. The monoclonal antibody Vedolizumab specifically recognizes the $\alpha_4\beta_7$ integrin selectively blocking gut lymphocyte trafficking without interfering with trafficking to the central nervous system, a problematic off-target effect of other integrin targeting agents such as natalizumab. In phase III trials, vedolizumab was effective for inducing and maintaining a

response and remission in CD and UC patients with adequate safety.[58, 59] Vedolizumab has progressed to the clinic and is licensed for the treatment of adult patients with moderate to severely active UC or CD who have had an inadequate response with, lost response to, or were intolerant to either conventional therapy or a TNF antagonist.

1.1.7 Limitations of current and emerging therapies

The success of anti-TNF agents has transformed the clinical management of IBD but such agents and new novel biologics have limitations in terms of efficacy, safety and cost. Approximately 10 - 30% of patients do not respond to initial anti-TNF treatment and a significant proportion of patients lose response in part due to the formation of antibodies.[60] Anti-TNF agents are associated with adverse effects such as infections and malignancies[61] and it is reasonable to expect that emerging selective biologics will also have antigenic potential and target-mediated toxicities. Biologics require parenteral administration and the production costs are high. In the age of biologics, there is still a need for novel small molecule drug treatments either as monotherapies or adjunct therapies.[62] Small molecule drugs are generally amenable to oral administration and the costs of chemical synthesis are generally lower than biotechnologies which should translate to more reasonable treatment related costs.

With the availability of biologics, the goal of therapy has evolved from attaining symptomatic relief and remission to achieving mucosal healing or deep remission.[63] However, no clear indications are yet available regarding the optimum time for drug withdrawal.[64] Continuing therapy to maintain remission must be balanced with the significant adverse side effects of long term biologic therapy and there is a need for the development of small molecule biologic-sparing therapies.

1.1.8 Matrix metalloproteinases (MMPs) and Takeda G protein-coupled receptor 5 (TGR5)

In this work, we have examined two potential targets for small molecule therapeutics in IBD, the MMPs and TGR5. MMPs are implicated in the compromise of intestinal barrier structure seen in IBD through degradation of the extracellular matrix (ECM) and inhibition has disease ameliorating effects in models of colitis.[65] MMP-9 can be considered a downstream effector of TNF-α and the clinical effects of anti-TNF agents have been attributed in part to MMP-9 downregulation.[66-68] TGR5 activation has a role to play in maintaining intestinal barrier integrity[69] and agonists display disease modifying effects in

colitis also.[70] There is evidence to suggest that these targets may also be luminally accessible to gut-confined agents. We propose that luminal inhibition of MMPs and/or luminal activation of TGR5 could achieve disease-modifying effects in IBD and limited systemic exposure could eliminate unacceptable off-target adverse effects. With full mucosal healing within reach in the clinic, ECM modelling manipulation by small molecule therapeutics could be a promising approach as a monotherapy, an adjunct to immunomodulators or as a biologic-sparing agent.

1.2 Gut-restricted drugs

Gut-restricted drugs are a subgroup of oral agents which act within the intestinal lumen to achieve a therapeutic effect which can be local or systemic but neither the drug nor active metabolites should be appreciably absorbed.[71] Such minimisation of systemic exposure and off-target systemic effects could facilitate the reduction or complete avoidance of side-effects that might otherwise limit the 'druggability' of the target. Proteomic analysis of preparations of brush border membranes isolated from murine jejunum identified 570 proteins including 45 transporters, 20 digestive enzymes and 105 signalling proteins.[72] Further work is needed to establish the physiological or pathophysiological roles of these proteins and to determine if they are apically expressed or secreted and potential for modulation by a gut-confined agent. Gut-restricted therapeutics are not a new concept but emerging potential drug targets will ignite interest in physicochemical space which may have been disregarded.

Good absorption from the GIT is generally required for good bioavailability of systemic orally administered drugs. For this, a drug candidate should have reasonable aqueous solubility, ability to permeate the lipid membrane, chemical stability in the environments encountered during GI transit and resistance to hydrolysis by enzymes found in the intestinal lumen such as those normally required for the digestion of food. Some solubility, stability and resistance to enzyme action are still required by an agent designed to be gut-confined but design should restrict permeability as much as possible while retaining the desired biological action in the gut. Permeability, the velocity of passage through a membrane barrier, is fundamental to absorption. Membrane permeation of systemic drugs is predominantly by passive diffusion but can also be by active transport and/or paracellular transport through tight junctions. A minor pathway involves M cell sampling of luminal contents by endocytosis where a substance is engulfed by the membrane and transported through the cytoplasm in a vesicle for release on the other side.[73]

The Lipinski rules (rules derived by Lipinski *et al.*)[74, 75] allow the profiling of absorption potential from chemical structure. While they have long been applied in selection of candidates for oral delivery into the systemic circulation, they could equally be used to design or select candidates with low permeability for intestinal targeting.

Poor absorption is more likely when:

- the molecular weight is greater than 500
- there are more than 5 hydrogen bond donor groups
- there are more than 10 hydrogen bond acceptor groups
- the Log P value is greater than 5

Increasing molecular weight reduces aqueous solubility reducing the concentration gradient for passive diffusion. Increased size is also a barrier to passage through the tightly packed side chains of the lipid membrane. Hydrogen bonds increase water solubility and must be broken for a compound to permeate the lipid bilayer. The lipophilicity of a compound can be numerically represented by Log P, the Log of the partition coefficient of the compound between an organic phase e.g. octanol and an aqueous phase e.g. buffer at a pH where the compound is in the neutral form. GI absorption by passive diffusion after oral dosing is generally best for compounds at a moderate Log P of 0 – 3, a balance of lipophilicity and hydrophilicity facilitating sufficient aqueous solubility but also sufficient lipid bilayer permeability.

The work by Veber *et al.*[76] established an alternative set of rules to Lipinski's. A molecule is likely to have poor absorption if it has greater than 10 rotatable bonds and a polar surface area greater than 140 $Å^2$, a function of molecular weight and the total number of hydrogen bond donors and acceptors.

Applying Lipinski's rules to the design of a gut confined drug candidate will produce a relatively large, polar molecule incapable of absorption by the passive, transcellular route. By passive diffusion, a compound follows a concentration gradient from the intestinal lumen through the lipid bilayer, the cytoplasm and through the basolateral membrane to the capillary blood vessels. However, this does not preclude passage through the tight junctions or transporter mediated active transport. Generally, paracellular transport is available to small polar molecules. A second pathway has been reported involving time dependent openings between the tight junction proteins permeable to molecules with

molecular weights up to several Kg/mol.[71] Molecular rigidity and cross-sectional diameter may limit tight junction permeability. Molecules may undergo active transport by binding to a transmembrane protein transporter which facilitates passage of the molecule through the membrane. Transport can occur against a concentration gradient but there must be an affinity of the drug for the transporter.

Gut-restricted drugs are in clinical use, in the drug discovery pipeline and used as probes to further our understanding of physiological and pathophysiological processes. Some have been serendipitously discovered while others are the result of deliberate structural modifications. They target luminal small molecules and enzymes or membrane proteins expressed on the surface of the gut epithelium. In other approaches local absorption is facilitated for activity in the gut wall without considerable systemic exposure. The pharmacodynamic effect may be local or systemic.

Targeting drug delivery is a logical consideration in the selection of an appropriate administration route and pharmaceutical formulation. The benefits of local delivery to achieve high concentration of active agent at the target site to maximise pharmacological on-target therapeutic effects whilst minimising off-target systemic effects have long been recognised. The most common utilization of this approach is topical administration to the skin but topical administration also encompasses application to any mucous membrane and so includes administration to the eye, ear, lungs and rectum. Topical administration to the GIT can be achieved by the oral or rectal routes but the oral route remains more acceptable to patients than the rectal route.

Various strategies are used to selectively target pharmacological agents to their site of action including prodrugs, antedrugs, pharmaceutical formulation and judicious modification of physicochemical properties.

1.2.1 Prodrugs

In this strategy, a non-absorbable prodrug undergoes local metabolism in the target area of the GIT releasing the active pharmacological agent. Sulfasalazine (1), a treatment for inflammatory bowel disease, is an example of this approach. When Salazopyrin® 500 mg tablets are orally administered, around 90% of the dose reaches the colon. There, it is cleaved by colonic bacterial azoreductases to release 5-aminosalicylic acid (2) which exerts a local anti-inflammatory effect and sulfapyridine (3) which is largely absorbed (Figure 4).[77]

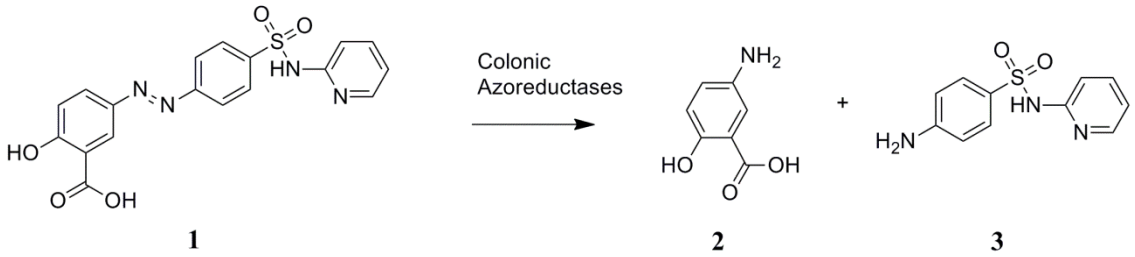

*Figure 4. Structure of sulfasalazine (**1**) and the products of it metabolism by colonic azoreductases, 5-aminosalicylic acid (**2**) and sulfapyridine (**3**)*

Side effects are mostly attributed to circulating sulfapyridine and so other analogues have been designed e.g. olsalazine (**4**), which is composed of two molecules of 5-aminosalicylic acid (**2**, Figure 5). In humans, olsalazine is negligibly absorbed and local 5-aminosalicylic concentrations in the colon 1000 times the plasma level can be achieved.[78]

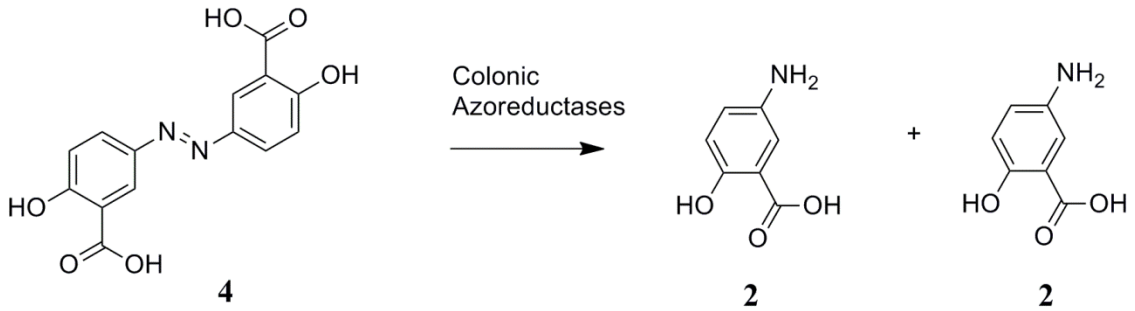

*Figure 5. Structure of olsalazine (**4**) and the product of its metabolism by colonic azoreductases, two equivalents of 5-aminosalicylic acid (**2**)*

Colonic bacteria possess other enzymes which can be utilized for prodrug metabolism including nitroreductases, phosphatases and glycosidases. The unique glycosidase activity of the colon has been utilized in the design of steroid glycoside prodrug systems. The drug glycosides were larger in molecular weight and usually more hydrophilic than the drugs themselves and so membrane permeability of the intact prodrug was limited. Percentage distribution to the lower intestine was dependent on the lability of the prodrug to hydrolysis which in turn had dependency on the aglycone, the attached sugar and the glycosidic linkage employed.[79] For example, when the 21-β-D-glucoside of dexamethasone (**5**, Figure 6) was administered to the stomachs of rats, nearly 60% of the administered dose reached the cecum whereas when free dexamethasone (**6**) was administered, it was almost entirely absorbed in the small intestine with less than 1% reaching the cecum.[80]

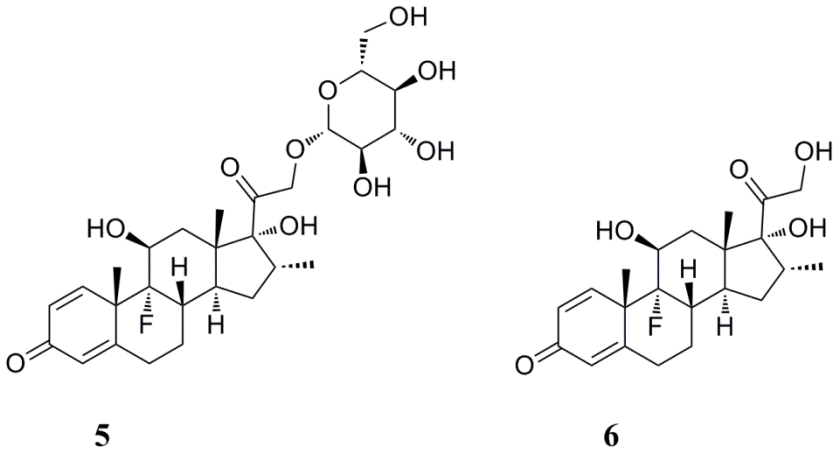

*Figure 6. Chemical structures of the 21-β-D-glucoside of dexamethasone (**5**) and free dexamethasone (**6**)*

1.2.2 Antedrugs

Antedrugs or 'soft drugs' are designed to act locally but also to be rapidly metabolised before or on entry to the systemic circulation. This approach was applied to the development of phosphonamide-based MMP inhibitors as antipsoriatic drugs.[81] Potent inhibitors of some MMPs, these compounds were shown to inhibit the shedding of epidermal growth factors, amphiregulin and heparin-binding EGF-like growth factor, which contribute to the epidermal hyperproliferation in psoriasis. MMPs are thought to be responsible for processing of these growth factors. Topical application of compound **7** (Figure 7) significantly reduced TPA-induced epidermal hyperplasia in a mouse model of

psoriasis and rapidly decomposed in human plasma to compound **8** which was further hydrolysed to inactive metabolites **9** and **10**. This work indicated that the antedrug approach could be viable in the treatment of psoriasis.[81]

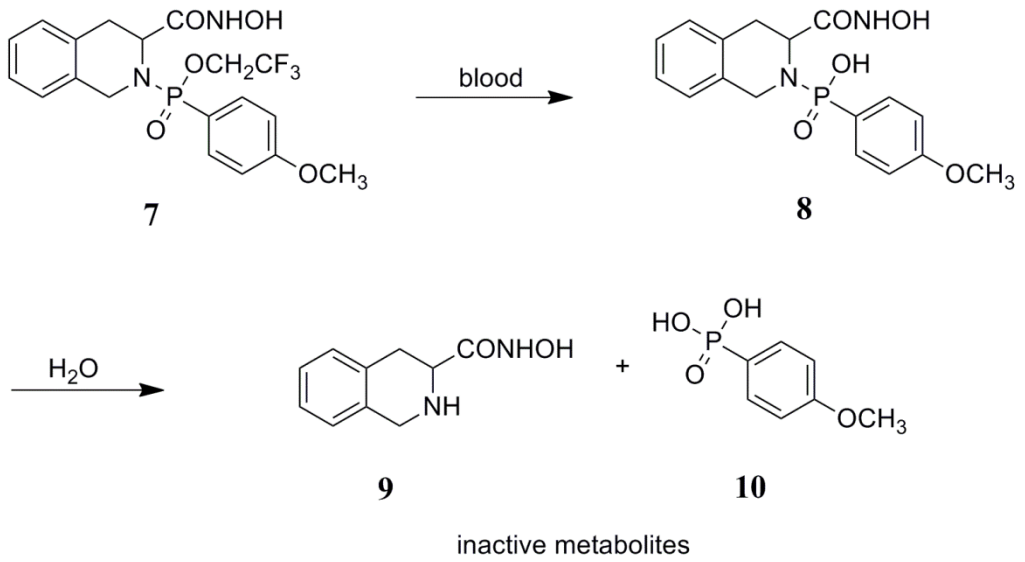

7 **8** **9** **10**

*Figure 7. Chemical structure of compound **7**, a phosphonamide-based MMP inhibitor, which rapidly decomposes in human plasma to compound **8** with subsequent hydrolysis to inactive metabolites **9** and **10**. Compound **7** is an example of an antedrug.*

Clinical utilization of the antedrug budesonide (**11**, Figure 8) in treating CD illustrates the value of this approach in treating bowel conditions. Formulated as a gastro-resistant oral dosage form, e.g. Entocort® CR, it is considered a locally acting glucocorticosteroid. Following absorption, it undergoes extensive first pass metabolism to metabolites of low glucocorticoid activity including 16α-hydroxyprednisolone (**12**). At doses clinically equivalent to prednisolone it gives significantly less hypothalamic pituitary adrenal axis suppression and less bone loss.[82]

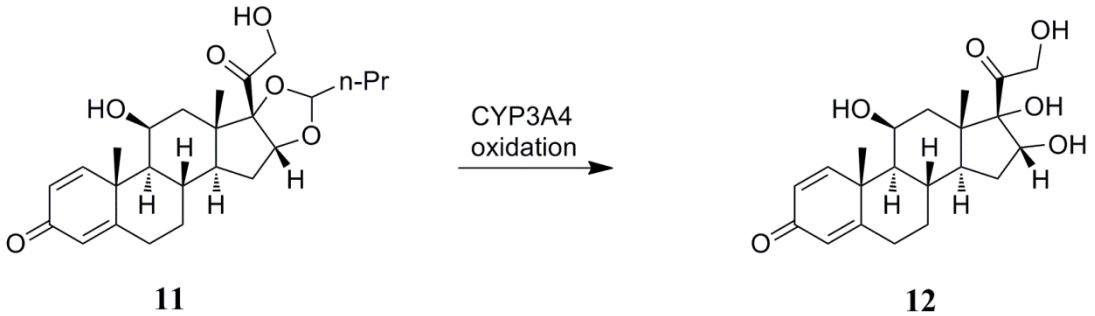

11 **12**

*Figure 8. The antedrug budesonide (**11**) undergoes CYP3A4-mediated oxidation to 16α-hydroxyprednisolone (**12**)*

1.2.3 Pharmaceutical formulations

Pharmaceutical approaches can be utilized for drug delivery to the colon. A pH dependent system has probably translated most effectively to marketed products. Asacolon® gastro-resistant tablets contain mesalazine and are coated with a pH responsive polymer, Eudragit® (methacrylic acid-methylmethacrylate copolymer (1:2)). Insoluble in acid pH, the coating protects the drug core from disintegration in the stomach and in the small intestine until it reaches the more basic pH of the lower intestine. Mesalazine is only released in the terminal ileum and colon when the pH $\geq$ 7 and the coating dissolves. Absorption is minimised and approximately 75% of the administered dose remains in the gut lumen and the mucosal tissue.[83]

Time dependent formulations can be designed to resist release until the estimated transit time to the colon has passed. In the Pulsincap™ system,[84] the drug is contained in a non-disintegrating capsule with an enteric coated cap. On gastric-emptying to the small intestine, the cap dissolves and a hydrogel plug then swells to block drug release. After a lag phase, which can be controlled by the properties of the plug employed, the plug is swelled to the point of ejection and the drug is released. *In vivo*, there can still be considerable variance in distribution due to the variation in intestinal transit times. Control over time to release can also be achieved by an osmotic system where swelling of a polymer can be controlled to push a drug gel out of the formulation.[85] Pressure-controlled drug delivery systems release drug load when a pressure limit is exceeded by the strong peristaltic waves of the colon.[85] The bacterial microflora of the colon derive energy by enzymatic digestion of polysaccharides that travel through the GIT undigested. Such polysaccharides, natural or chemically modified, and other synthetic polymers amenable to bacterial enzyme digestion can be used to coat and protect a drug material or as a carrier matrix or hydrogel.[86]

Nanoparticle technologies offer drug targeting solutions to many organs and tissues including the colon[87] and claim advantages over more conventional formulation approaches. Similarly able to protect and transit drug load to the site of action, appropriately sized nano systems can selectively target inflamed tissue in the bowel over healthy tissue. Nanoparticles exhibit mucoadhesivity and can be taken up by immune cells and so can accumulate in inflamed tissue where inflammatory cell infiltrate and mucus are greater.[88] Lamprecht *et al.* used a biodegradable poly [DL-lactide-co-glycolide] (PLGA) nanoparticle system for delivery of rolipram in a 2,4,6-trinitrobenzenesulfonic acid

(TNBS) model of colitis in rats. In comparison to the group administered rolipram solution, the nanoparticle group had a reduced adverse effect index indicative of reduced systemic exposure and the anti-inflammatory effect was sustained longer after drug withdrawal.[89]

1.2.4 Modification or utilisation of physicochemical properties

Poor absorption potential can be conferred on promising leads at intestinal targets by manipulation of physicochemical properties. Introduction of a permanent charge has been successfully used by Tremont *et al.* to increase polarity and thereby reduce permeability in a series of apical sodium codependent bile acid transporter (ASBT) inhibitors.[90, 91] Primarily apically expressed on the distal ileum, ASBT is a promising target for a gut-confined small molecule ligand and inhibition should be an effective approach to lower serum LDL cholesterol. This is because reduction of bile acid retrieval is predicted to increase cholesterol metabolism. A palatable, potent, non-absorbed ASBT inhibitor could offer advantages over current therapies. A potent pharmacophore based on a core benzothiepine ring structure was identified. Structure activity relationship (SAR) studies established that the phenyl group at position five of the ring could tolerate the introduction of a polar/charged substituent whilst maintaining good potency. A series of non-systemic candidates were synthesized by attachment of a positively charged quaternary ammonium group via a short linker. *In vitro* potency and *in vivo* efficacy were maintained with minimal systemic exposure. Compounds **13** and **14** in Figure 9 are examples of compounds in the series. Anionic inhibitors were also shown to be efficacious and poorly absorbed. While monocarboxylic acid analogues did not have satisfactorily limited systemic exposure, diacid analogues such as compound **15** in Figure 9 did.[90, 91]

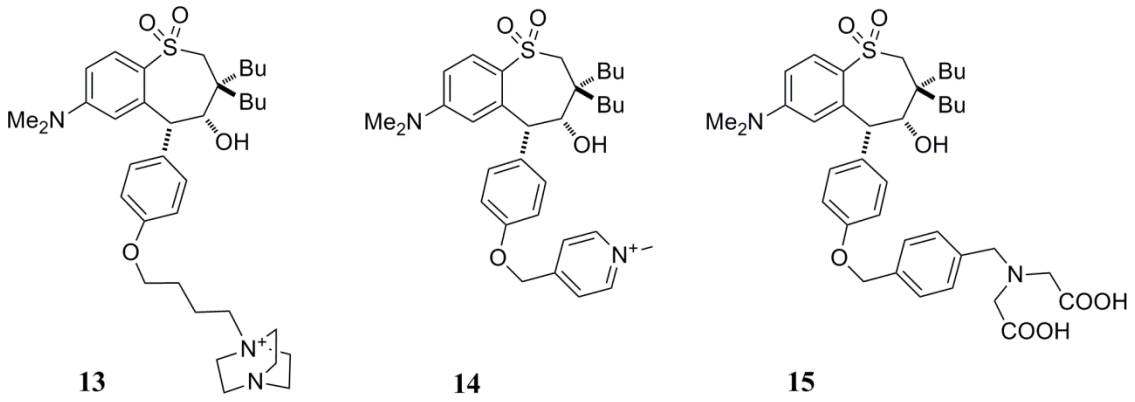

Figure 9. Chemical structures of non-absorbable ASBT inhibitors designed and synthesized by Tremont et al.

Highly lipophilic compounds are likely to have poor permeability. Increasing lipophilicity decreases aqueous solubility and may also increase clearance, reducing systemic exposure further. Orlistat (**16**, Figure 10) is an example of an orally administered, poorly absorbed, lipophilic drug in clinical use for obesity which exerts its therapeutic effect by inhibition of enzymes in the gut lumen. It covalently binds gastric and pancreatic lipases in the stomach and small intestine through reaction with its β-lactone group. Dietary fats cannot be digested to absorbable units and are excreted in the faeces reducing caloric intake.[92]

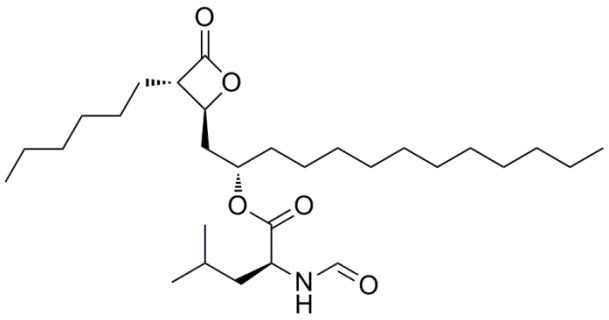

16

*Figure 10. Chemical structure of orlistat (**16**)*

Fexaramine (**17,** Figure 11) was synthesized by Fang *et al*. as a highly lipophilic agonist of the intestinal farnesoid X receptor (FXR).[93] Bile acid secretion after a meal has been shown to selectively activate intestinal FXR in contrast to systemic therapies and the group hoped to mimic this effect. Serum levels indicated some systemic exposure on oral administration to mice but the level was below the EC_{50}. Intraperitoneal (IP) administration upregulated target genes in the liver, kidney and gut but upregulated expression on oral administration was restricted to the intestinal genes. This work illustrates that selective pharmacodynamic effects may be achieved by biased distribution, though puzzlingly, FXR is a nuclear receptor in the gut enterocytes, requiring cellular uptake for activation. Oral fexaramine also showed substantial benefits in a mouse model of obesity. It protected against diet-induced weight gain, enhanced glucose tolerance and decreased inflammation, effects not normally associated with FXR agonism. It is thought that the effects of fexaramine were in part due to activation of TGR5-mediated pathways. The metabolic effects seen are known downstream effects of TGR5 signalling and the results were tempered in *TGR5*$^{-/-}$ mice.[93]

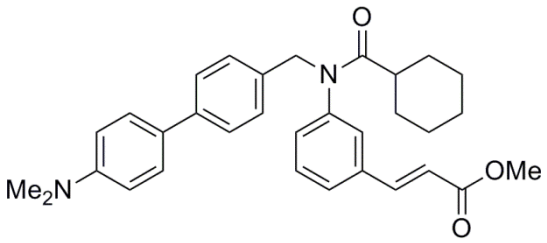

17

*Figure 11. Chemical structure of fexaramine (**17**)*

The efflux capabilities of the enterocytes can also be exploited to achieve gut-biased delivery. During *in vitro* profiling of a series of diacylglycerol acyltransferase 1 inhibitors, Serrano-Wu *et al.* found compound **18** (Figure 12) to be a nanomolar inhibitor with strong efflux potential in Caco-2 cells and this was confirmed in a MDR1-MDCK assay.[94] Following oral dosing to rats, the concentration of **18** in duodenal enterocytes was over 20-fold higher than the level detected in the portal vein or plasma and this concentration was maintained and increased over 17 h indicating recycling of **18** in the intestine through the efflux system. Biosynthesis of triglycerides in enterocytes into chylomicrons for passage to the systemic circulation is in part mediated by diacylglycerol acyltransferase-1 in the small intestine and 2 h after an Intralipid® challenge, intracellular triglyceride levels were reduced by 67% in rats treated with **18** compared with vehicle treated rats.[94]

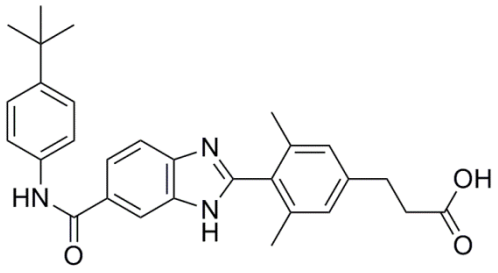

18

*Figure 12. Chemical structure of compound **18**, a diacylglycerol acyltransferase 1 inhibitor*

Vancomycin (**19**, Figure 13) is an example of a natural product which by virtue of its high molecule weight and ionisable groups, has negligible absorption from the gastrointestinal tract. It is used to treat *Clostridium difficile* infection of the GI tract by oral administration but must be administered IV for the treatment of systemic infection. It is excreted unchanged in the faeces.[95]

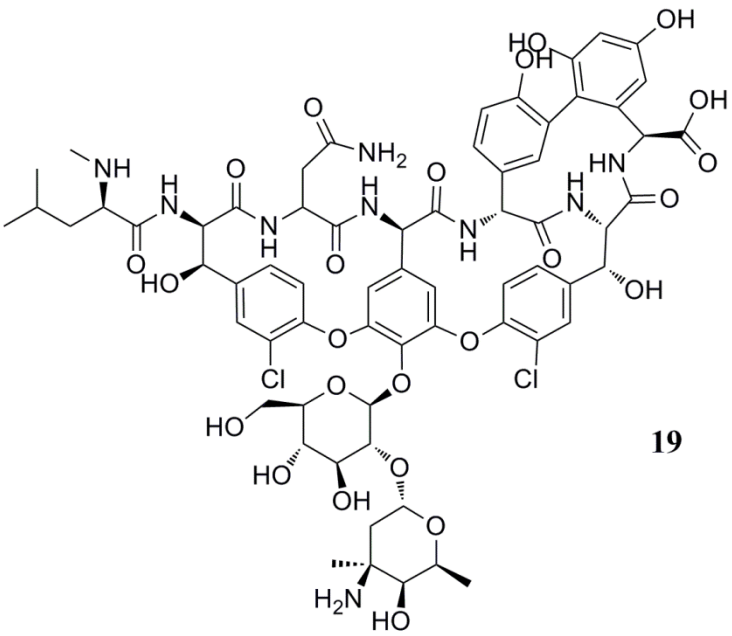

*Figure 13. Chemical structure of vancomycin (**19**)*

Absorption potential can be reduced by increasing molecular weight. Duan *et al*. used a dimerising approach to synthesize a gut-confined TGR5 agonist for treatment of type 2 diabetes. Linking two molecules of the pharmacophore, compound **20**, by a hydrophilic eight unit polyethylene glycol (PEG) chain, the dimer, compound **21**, had a molecular weight of 1401 g/mol and a calculated polar surface area of 223 $Å^2$ (Figure 14). The dimer produced blood glucose lowering effects comparable to the parent compound in mice but the associated side effect of gallbladder filling was much reduced despite evidence of some systemic exposure.[96]

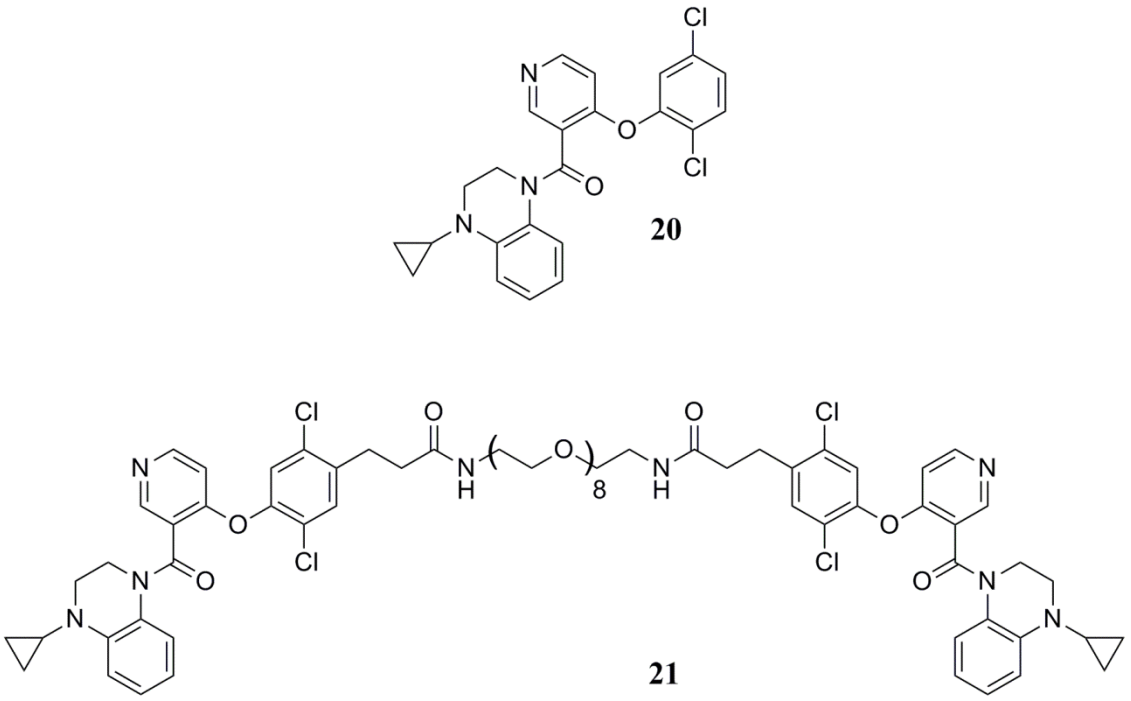

*Figure 14. Chemical structure of compound **20**, a TGR5 agonist and compound **21**, a PEG chain-linked dimer of **20***

Chapter 2. Design, synthesis and evaluation of a gut-confined MMP inhibitor

2.1 Introduction to MMPs

MMPs are zinc and calcium-dependent endopeptidases belonging to the metzincin superfamily of metalloproteinases.[65] Comprising a family of about 24 enzymes in humans, collectively they have the ability to degrade all structural components of the ECM.[67] Conventionally, MMPs were classified based on preferred substrate and/or cellular location as collagenases (MMP-1, -8, -13 and -18), gelatinases (MMP-2 and -9), stromelysins (MMP-3, -7, -10 and -11), elastase (MMP-12), membrane type MMPs (MMP-14, -15, -16, -17, -24 and -25) and others (MMP-19, -20, -23, -26, -27 and -28).[97] An alternative approach utilises domain organisation classifying them as archetypal MMPs, matrilysins, gelatinases or convertase-activatable MMPs.[98, 99] They have crucial roles in any physiological process requiring matrix remodelling including wound healing, reproduction, embryogenesis and angiogenesis. They also play central roles in immunity modulation by facilitating the release and/or direct activation of signalling molecules. The involvement of MMPs in disease pathologies such as cancer has been well established and has made them attractive targets for drug discovery.

2.1.1 MMP Structure

MMPs are multidomain proteins that are approximately 130 – 260 residues in length.[65] A schematic representation of the structure of human MMPs can be seen in Figure 15. All MMPs have similar domain organizations and most consist of an amino-terminal signal peptide (pre-domain), a propeptide (prodomain), a catalytic domain, a linker (hinge) region and a hemopexin-like domain at the carboxy terminal end with some exceptions. Matrilysins contain the minimal domain organization required for secretion, latency and activity and do not contain a linker or hemopexin-like domain The pre-domain targets the enzyme to the endoplasmic reticulum for transport out of the cell. Synthesized with intact pro-domains, pro-MMPs are inactive zymogens and most MMPs are secreted in this form. In the pro-forms interaction between a cysteine in the prodomain and the zinc ion of the catalytic site maintains the inactive state. Disruption of this interaction, activation of the cysteine switch, leads to activation. The length and flexibility of the linker region contributes to function by facilitating protein substrate interaction and independent movement of the catalytic and hemopexin-like domains. MMP-9 has the longest linker region of the MMPs at 72 amino acid residues. The hemopexin-like domain can contain binding sites outside of the catalytic centre (exosites) important as secondary substrate binding sites for substrate localisation and for interaction with TIMPs and cell-surface

molecules.[100] Gelatinases contain fibronectin type II (FN2) modules that improve collagen binding efficiency. Convertase-activatable MMPs contain an insert in the propeptide that is targeted by furin-like proteases. The membrane-associated MMPs in this class are membrane-anchored via glycosylphosphatidylinositol (GPI) or type I or type II transmembrane (TM) segments. MMP-23A and MMP-23B contain unique cysteine array (CA) and immunoglobulin (Ig)-like domains in their C-terminal region.[99]

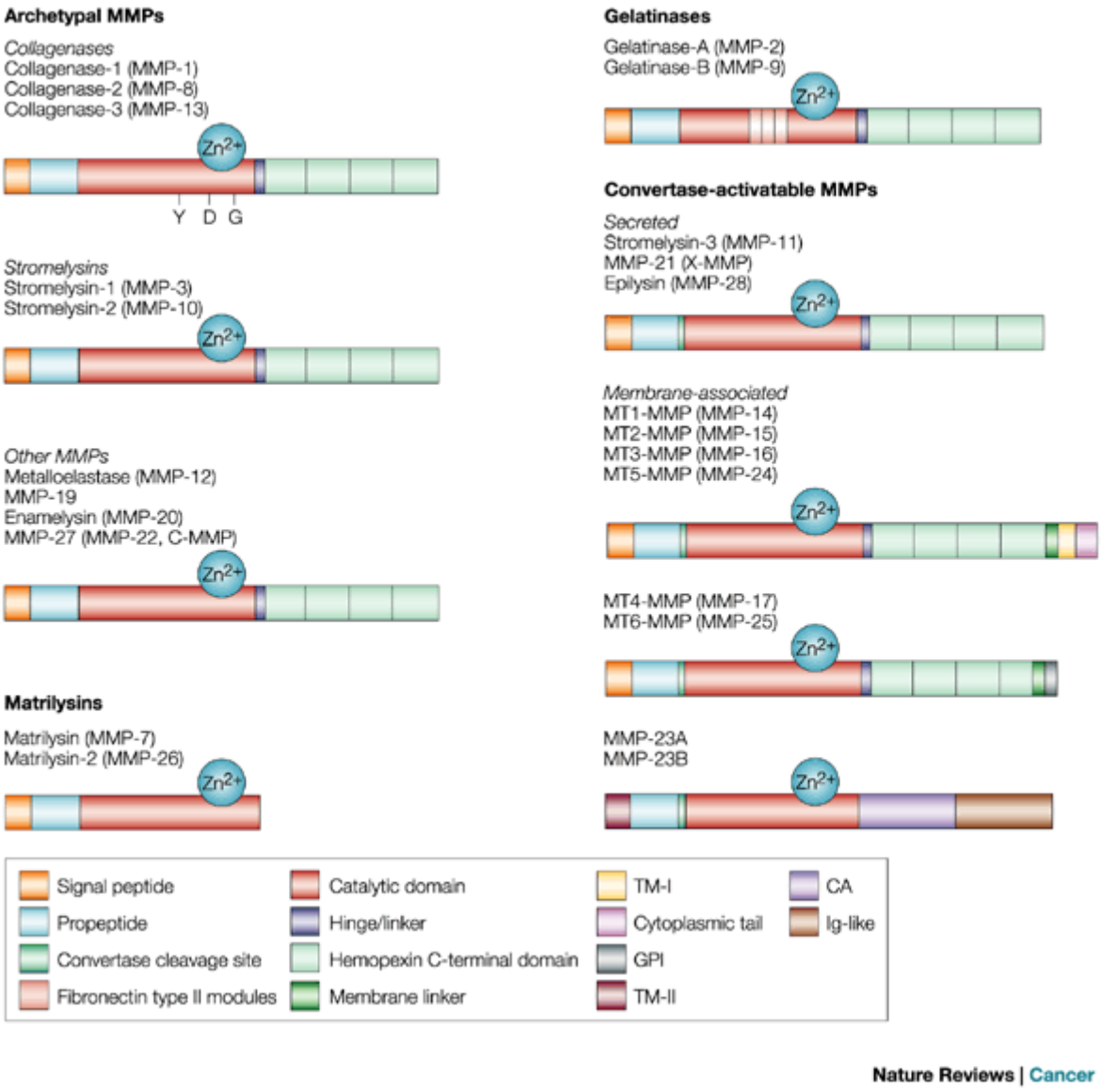

Figure 15. Schematic representation of the structure of the human MMPs classified according to domain organisation as archetypal MMPs, matrilysins, gelatinases and convertase-activatable MMPs. Image taken from Overall et al.[96]

2.1.2 MMPs in disease pathologies

The MMP-mediated activities of cell migration, differentiation, proliferation, angiogenesis, apoptosis, inflammation and platelet aggregation in normal physiological processes can contribute to disease pathologies when dysregulated. The involvement of MMPs in cancer and angiogenesis has received most attention[101] and MMP levels have prognostic biomarker value in cancers of the breast,[102] prostate,[103] lung[104] pancreas,[105] and ovaries.[106] In cardiovascular disease, MMPs have roles in atherosclerosis contributing to plaque formation, instability and rupture.[107] Post-infarction, transcriptional upregulation of MMP-9 is associated with a higher degree of adverse ventricular remodelling which is associated with greater functional impairment and development of heart failure.[108] Inflammation is characteristic of autoimmune diseases and MMP activities are implicated in diseases such as arthritis,[109] diabetes[110] and multiple sclerosis[111] as well as in IBD.

2.1.3 Regulation of MMPs

Having significant destructive capabilities, MMPs are tightly regulated at the level of gene expression, compartmentalization in the cell, pro-enzyme activation and enzyme inhibition. They are transcriptionally responsive to growth factors and pro-inflammatory cytokines such as TNF and IL-1.[67] The tissue inhibitors of matrix metalloproteinases (TIMPs) are endogenous reversible inhibitors of MMPs. They target the active site, binding in a substrate like manner in a 1:1 complex, the catalytic Zn coordinated by an N-terminal cysteine residue.[112] There are four known 20 – 29 kDa secreted TIMPs (TIMP-1, -2, -3, and -4).[113] The four TIMPs can inhibit all MMPs however they show varying specificities. For instance, TIMP-1 inhibits MMP-9 with a high affinity, whereas TIMP-2 inhibits MMP-2.[113] In addition to inhibition by TIMPs, MMPs are also inhibited by non-specific circulating α-2 macroglobulin.

2.1.4 Mechanism of substrate proteolysis

A mechanism for substrate proteolysis at the active site was proposed by Lovejoy *et al.*[114] Consisting of a 5-stranded β sheet, two α helices and several surface loops, the catalytic domain has a notch on its surface containing the active site cleft. In this cleft, formed in part by a highly conserved Met 1, 4, β-turn, the catalytic zinc ion is coordinated by the imidazolyl sidechains of three histidine residues His401, His405 and His411 as part of the consensus sequence HExxHxxGxxH. In the free enzyme, a water molecule is H-bonded to a conserved Glu residue and coordinated to the zinc atom. On docking of a ligand, the

carbonyl group of the scissile amide also coordinates to the zinc ion. This carbonyl undergoes nucleophilic attack by a hydroxide ion generated by donation of a proton to Glu by H_2O. The resulting tetrahedral intermediate is stabilized by the zinc ion. Transfer of the proton to the amide nitrogen causes a rearrangement and bond hydrolysis.

2.1.5 Synthetic MMP Inhibitors

2.1.5.1 Active site targeted MMP inhibitors

In the active site there are six pockets in the enzyme structure three of which are located on one side of the active site zinc atom designated S1, S2 and S3 and three of which are located on the other side of the zinc atom designated S1', S2' and S3' after Schechter and Berger.[115] The substrate binding groove is relatively open from S3 to S1 but narrows at S1' and S2' before opening out at S3'.[100] Significant interactions take place between the S1' and S2' pockets and ligand moieties of the enzyme substrate or inhibitor designated P1' and P2'. The S1'pocket is a deep pocket penetrating the enzyme surface whereas S2' is a shallower solvent exposed cleft. In MMP-9 the S1' pocket has been described as a continuous pore exiting to solvent at the lower surface of the protein. The wall of the cavity is mainly formed by the sidechains of Tyr423, Leu188, Leu397, Val398, His401 and Leu418. A specificity loop arches around the pocket and can separate the lower part of the S1' cavity from bulk solvent. Some of the earliest synthetic MMP inhibitors were structural analogues designed to mimic endogenous substrates. Generally, such peptidomimietic inhibitors bind reversibly, chelating the catalytic zinc. The S1' pocket is usually occupied sometimes accompanied by occupancy of subsites along the extended binding site. The scissile bond of the modelled substrate is modified in the inhibitor to prevent hydrolysis and while the inhibitor remains bound the enzyme remains inhibited.

Pre-clinical studies of broad spectrum active site MMP inhibitors were promising and more than 50 such MMP inhibitors have been investigated in clinical trials.[65] One of the first inhibitors to reach clinical trials was batimastat (**22**), a hydroxamate-containing peptidomimetic based on a principal cleavage site in type I collagen (Figure 16). It is a broad spectrum, competitive MMP inhibitor but due to lack of solubility could only be administered by direct injection into body cavities. In phase I trials it was administered intraperitoneally or intrapleurally to patients with malignant ascites or malignant pleural effusion. It did show efficacy but development was halted as it was considered to have limited potential due to unfavourable physicochemical properties and pharmacokinetics.[116] Marimastat (**23**, Figure 16), its orally available analogue, showed some promise in early

trials but efficacy could not be established in randomized Phase III trials and patients developed musculoskeletal toxicities.[117] On reflection, it is likely that the failure of marimastat and other MMP inhibitors to subsequently enter trials was at least in part due to poor trial design. As MMP inhibitors are cytostatic rather than cytotoxic, the conventional measures of efficacy applied were not appropriate end-points for treatment assessment.[118] Also, pre-clinical animal studies were conducted in the early stages of disease progression whereas human trials were in advanced stages of disease. Broad spectrum inhibition caused unacceptable side-effects of musculoskeletal pain and inflammation and as a result subsequent trials were conducted with inadequate doses. [65]

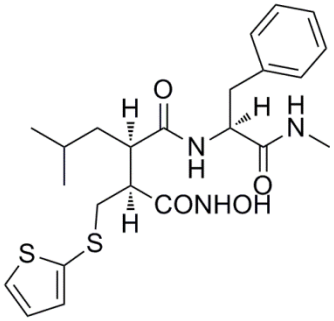

22

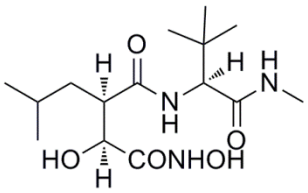

23

*Figure 16. Structure of batimastat (**22**) and marimastat (**23**)*

Promising *in vitro* and *in vivo* results of hydroxamate peptidomimetics did not translate to the clinic. The availability of MMP crystal structures has allowed structure and fragment based drug design and other zinc chelating groups have been identified such as sulphydryls, carboxylates, phosphonates and heterocycles some with favourable pharmacokinetics to the hydroxamates.[115] However, the development of a small molecule selective inhibitor has remained elusive due to the highly conserved nature of the active site in this enzyme family.

2.1.5.2 Allosteric inhibition

The exosites of MMPs provide opportunities for allosteric inhibition.[112] MMP-2 and MMP-9 are the only MMPs to possess three FN2 repeats otherwise known as a collagen binding domain (CBD) which contributes to binding by positioning substrate molecules relative to the active site for cleavage. A CBD binding site specific peptide has been shown to inhibit gelatinolytic activity and while this approach was not selective for MMP-2 over MMP-9, it was selective for the gelatinases over other MMPs.[119]

2.1.5.3 Inhibition by tetracyclines

Tetracycline antibiotics can inhibit MMPs. While the mechanism is not completely understood it seems to involve some direct inhibition and a concurrent downregulation of expression.[120] Direct inhibition does not involve interaction with the catalytic zinc but rather with the structural zinc and/or calcium ions, destabilizing the tertiary structure. Doxycycline (**24**, Figure 17), is the only MMP inhibitor in clinical use. Periostat® 20 mg film-coated tablets contain doxycycline and at dose levels well below effective anti-microbial levels, it reduces elevated collagenase activity in chronic adult periodontitis.[121]

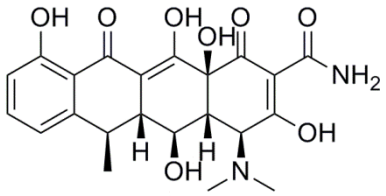

24

*Figure 17. Structure of doxycycline (**24**)*

2.1.5.4 Mechanism based inhibition

SB-3ct (**25**, Figure 18) is a mechanism-based inhibitor of the gelatinases, a form of irreversible inhibition where the inhibitor is covalently bound. Coordination of the thiirane of SB-3ct with the active site zinc ion positions it for nucleophilic attack by a resident active site nucleophile.[122] The diaryl ether occupies the S1' pocket and the inhibitor is covalently bound in the active site rendering the enzyme catalytically inactive.

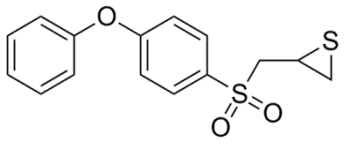

25

*Figure 18. Structure of the mechanism based gelatinase inhibitor, SB-3ct (**25**)*

2.1.5.5 Inhibition by small interfering RNAs (siRNAs)

Capable of sequence-specific post-transcriptional gene silencing, siRNAs can be used to downregulate MMP protein synthesis. Reductions in cancer cell invasiveness have been demonstrated in chondrosarcoma[123] and glioblastoma[124] cells *in vitro* through siRNA-mediated reduction of MMP-2. Utilisation of this strategy poses significant drug delivery challenges as siRNAs do not readily cross cell membranes and are effectively cleared by the body. The potential in local delivery has been demonstrated and siRNA impregnated wound dressing materials have improved diabetic wound healing in a mouse model.[125]

2.1.5.6 Biologic inhibitors of the MMPs

MMP sub-type selectivity has been achieved with monoclonal antibodies.[126] REGA-3G12 is a murine monoclonal antibody prepared by hybridoma technologies against human MMP-9. Selective for MMP-9 over the closely related MMP-2 and other MMPs, it recognises the amino terminal section of the catalytic domain but does not interact with the catalytic zinc.[126] The ability of REGA-3G12 to inhibit MMP-9 mediated gelatin degradation has been demonstrated *in vitro* and the prevention of IL-8 induced stem cell mobilisation in rhesus monkeys illustrates it has *in vivo* effects.[127] In some cases, an antibody may be designed to target a single function of an enzyme. Shiryaev *et al*. designed 9E8, a mouse antibody against MT1-MMP (MMP-14) which could selectively block its function of MMP-2 activation while other proteolytic functions remained intact.[128]

2.1.6 MMPs in IBD

The dysregulated immune response in IBD promotes aberrant expression and activation of MMPs and there is a body of evidence supporting roles for MMPs in the destructive remodelling and reduced gut barrier function seen in IBD. Total MMP proteolytic activity is upregulated in tissue homogenates from UC and CD patients[129] and the ratio of MMPs to TIMPs is also increased.[130, 131] Broad spectrum inhibition of MMPs has been consistently shown in several studies by a variety of agents to ameliorate the effects of TNBS-induced colitis or dextran sodium sulfate (DSS)-induced colitis in rodents.[132-134] Several members of the MMP family including collagenases, stromelysins and gelatinases have been implicated in IBD.[135]

Due to their potentially destructive effects on native collagen, the distribution of collagenases is strictly controlled in normal physiology. In IBD pathogenesis, MMP-1

(collagenase-1) is expressed by myofibroblasts and macrophages and is associated with ulceration. Expressed by smooth muscle cells also, it is considered to be involved in cell migration and remodelling.[135] MMP-8 (collagenase-2) is upregulated predominantly in epithelial cells in IBD and is thought to contribute to ECM destruction[136] as is MMP-13 (collagenase-3).[68] MMP-3 (Stromelysin-1) is induced consistently in human IBD and in animal models of the disease. It is associated with fistula formation[137] and facilitates T-cell mediated injury.[138] MMP-10 (Stromelysin-2) is associated with wound healing, *MMP-10*$^{-/-}$ mice having delayed healing of DSS-induced ulcers.[139] MMP-7 (matrilysin) also appears to be involved in repair and healing. In the mouse it activates antimicrobial α-defensins but this does not seem to be conserved in humans.[135]

Of the MMPs, the gelatinases have received most attention in IBD research. MMP-9 expression in adult tissues is confined to neutrophils, macrophages and osteoclasts.[135] MMP-9 is consistently upregulated in IBD[129] and tissue and plasma levels in IBD patients correlate with disease activity.[140, 141] MMP-9 is upregulated in rodent models of colitis and the severity of DSS-induced colitis in mice has been attenuated by gelatinase-selective antibody treatment.[142] In *MMP-9*$^{-/-}$ mice the results reported are contradictory. Santana *et al*. reported *MMP-9*$^{-/-}$ mice to be less susceptible to DSS colitis compared to wild-type mice as indicated by improved survival and indices of epithelial injury.[143] In contrast, de Bruyn *et al*. found no differences in clinical or histopathological parameters after genetic inhibition of MMP-9 in DSS mouse models causing them to question the validity of MMP-9 as a drug target in IBD.[144] They proposed that MMP-9 upregulation is a consequence rather than a cause of intestinal inflammation. The reasons for these contradictory results are not clear but it should be considered that compensatory activity of other pathways and enzymes may obscure the role of MMP-9 in a knockout model. De Bruyn *et al*. also found that two peptide inhibitors with established efficacy towards MMP-9 did not ameliorate the colitis induced by their DSS protocols. In contrast, pharmacological inhibition of MMP-9 has been shown to attenuate DSS colitis in the mouse by other research groups using a variety of inhibitor types and a destructive role for MMP-9 in the pathology of IBD is generally accepted.

MMP-2 is believed to oppose MMP-9 in IBD progression. MMP-2 is constitutively expressed by epithelial cells and the lamina propria and it is upregulated in IBD. Epithelial barrier integrity is compromised in *MMP-2*$^{-/-}$ mice and they are more susceptible to chemical or bacterial-induced colitis than wild-type mice, suggesting MMP-2 has a role in epithelial barrier regulation.[145] The gelatinases are structurally similar and have similar

substrate specificities. Their opposing functions may be due to differences in their non-matrix substrates, MMP-2 lacking a 56-residue type V collagen-like domain of MMP-9. Work in a double knockout model suggests that the destructive action of MMP-9 is dominant over any protective action of MMP-2 and that global gelatinase inhibiton may be desirable in IBD.[146]

2.1.7 MMP-9, is it luminally accessible?

During inflammation in IBD, MMP-9 is expressed by intestinal epithelial cells (IECs) as well as immune cells. It is detectable in the faeces of IBD patients and its presence moreover is correlated with endoscopically assessed disease activity. Indeed its faecal concentration has similar diagnostic accuracy to calprotectin.[147] Work in the Medina group has shown that treatment of the IEC line, Caco-2, with TNF-α and IL-1β stimulates secretion of gelatinases into the media.[67] This models the *in viv*o condition, primary epithelial cells isolated from patients with active IBD having upregulated MMP-9 mRNA and supernatants from such primary cultures having functional MMP activity.[148] *In vitro* work has also shown that MMP-9 impairs cell adhesion and wound healing activity in Caco-2 cells.[149] Studies in IBD tissue have usually identified neutrophils to be the major source of pathologic MMP-9.[129] However, Castaneda *et al.*, through neutrophil transmigration studies and bone marrow chimeras in mouse models of colitis, concluded that epithelial-derived MMP-9 is responsible for colitic damage.[149] This is in line with observations that epithelial damage precedes inflammatory infiltration in colitis models.[143] A transgenic mouse model (*Tg-villin-MMP-9*) specifically overexpressing MMP-9 in the intestinal epithelium exhibited spontaneous goblet cell depletion and increased epithelial proliferation and apoptosis as well as increased expression of the proinflammatory cytokine Kc, the mouse homologue of human IL-8. This mouse model exhibited more severe inflammation in response to DSS or bacterial induced colitis compared to wild type mice. In IBD tissues, inflammatory cells infiltrating the mucosa closely approach the epithelial cell layer. More than an intestinal barrier, the epithelium communicates luminal status to the immune system but there is evidence that this communication is two-way. Al-Ghadban *et al*. demonstrated communication between intestinal epithelial cell lines and the monocytic cell line THP-1 in co-culture through gap junctions and proposed that this communication plays a role in dysregulation of intestinal barrier function seen in IBD.[150] In line with this, the epithelial cell lines secreted increased levels of MMP-9 when treated with conditioned media from activated THP-1 cells. Colitis models suggest that epithelial-derived MMP-9 has a role in early stages of disease compromising the gut barrier allowing

luminal contents to further activate the immune system. In human IBD, there is also evidence to support that increased permeability precedes disease initiation. MMP-9 is a terminal effector of the inflammatory cascade. It is upregulated and activated by a variety of cytokines and growth factors and activated by other MMPs including MMP-1, -2, -3 and -7. MMP-9 contributes to the tissue damage associated with IBD but it also regulates it. In addition to facilitating increases in epithelial and endothelial permeability by ECM degradation, MMP-9 potentiates a feed forward mechanism of inflammation by activation of chemokines and cytokines and augmentation of chemotaxis.

Evidence for the pathological involvement of MMPs in IBD is compelling but in cancer trials, the viability of MMP inhibition as a therapeutic approach was extinguished by the poor safety profile associated with broad spectrum inhibition. Despite decades of research efforts selective inhibition by a small molecule inhibitor has remained elusive. Selectivity has been achieved with monoclonal antibodies but while this selectivity is attractive, there may be an even more intractable problem in separating regional and temporal roles of patho/physiological MMP-9 targets. Many MMPs have been validated as anti-targets including MMP-9. For instance, MMP-9 is implicated in the resolution of inflammation in asthma.[151] It is necessary for the effective clearance of immune cells by establishing a transepithelial chemokine gradient. Allergen challenged *MMP-9*$^{-/-}$ mice exhibit increased inflammatory cell death compared to wild-type mice due to decreased MMP-9 mediated cell egression into the airways. Pertinent inhibition can be successful as demonstrated by the widespread clinical use of the tetracyclines. We propose that an inhibitor designed to be confined to the gastrointestinal lumen to achieve a non-systemic effect could achieve disease modifying effects in IBD. This would in addition allow us to test the hypothesis that disease modifying effects in IBD could be achieved by inhibition of apically secreted gelatinases in the intestinal lumen and at disease sites where high induction is expected.

2.2 Chapter objective

The objective of this chapter was to test the hypothesis that disease-modifying effects could be achieved in a model of IBD by inhibition of apically secreted gelatinases in the intestinal lumen.

2.2.1 Specific objectives

- To design and synthesize a candidate for testing the chapter hypothesis. This candidate should be a potent small molecule inhibitor of the gelatinases and resistant to degradation and metabolism in the environments of the GIT.

- To assess the potential of the candidate for absorption.

- To test the candidate in a DSS mouse model of colitis. The treatment effect would be assessed at clinical level, histological level and by examination of pro-inflammatory cytokines at gene level.

2.3 Establishing the MMP inhibitory scaffold

The barbiturate class was chosen as a suitable scaffold for modification to a gut-confined inhibitor. The MMP inhibitory potency of barbiturates has been widely reported in the literature including work by the Gilmer and Medina groups.[152, 153] The potential for barbiturates as MMP inhibitors was first identified in 2001 when workers at Hoffman La-Roche identified RO200-1770 (**26**, Figure 19) as an inhibitor of MMP-8 in a high-throughput screen.[154]

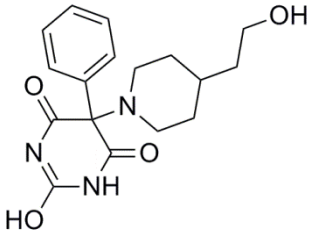

26

*Figure 19. Structure of RO200-1770 (**26**)*

Barbiturates are a class of CNS depressants derived from barbituric acid or 2,4,6,-trioxohexahydropyrimidine (**27**, Figure 20). Barbituric acid itself lacks central depressant activity but substitution of alkyl or aryl groups at position 5 confer sedative-hypnotic activity. As sedatives, they have almost completely been superseded by the benzodiazepines which possess a more favourable therapeutic index. They continue to be employed in some instances in the treatment of convulsions and ultrashort-acting agents continue to be used in anaesthesia.[155] MMP inhibitory activity is primarily due to coordination of the ionised barbiturate ring to the zinc ion of the active site of the enzyme. In addition, appropriate C-5 substituents, P1' and P2', can bind in the S1' and S2' pockets of the enzyme.

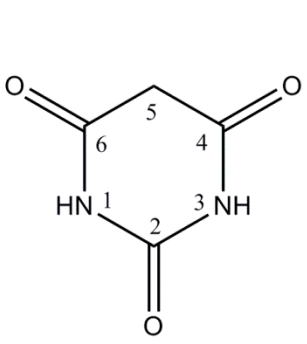

27

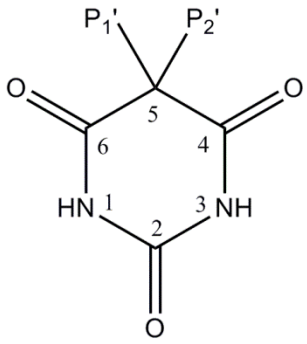

28

*Figure 20. Structure of barbituric acid (**27**) and 5-disubstituted barbituric acid (**28**)*

Tochowicz *et al*. prepared a mutant of the truncated catalytic domain of human MMP-9 and co-crystallized it with several small molecule inhibitors including RO-206-0222 (**29**), a barbituric acid derivative doubly substituted at C-5 with a phenoxyphenyl and pyrimidine-piperazine moiety as represented in Figure 21.[156] This work provides us with much information about barbiturate interaction with the MMP-9 active site.

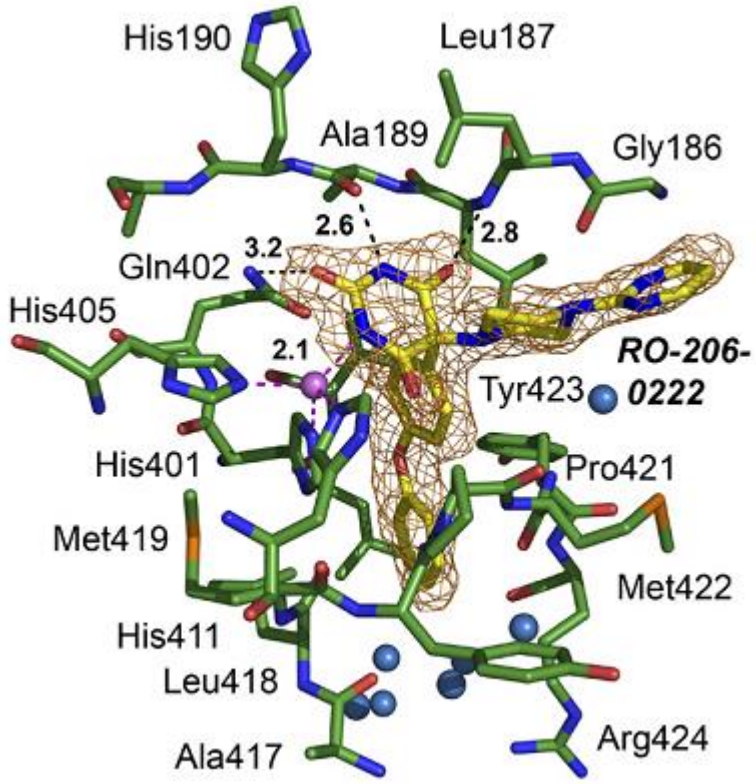

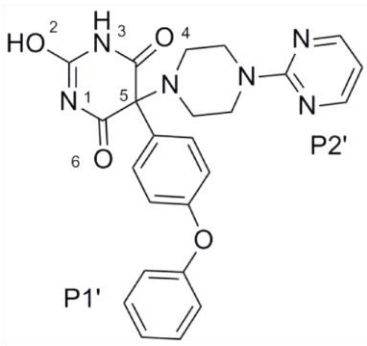

29

*Figure 21. Chemical structure of RO-206-0222 (**29**) and stereo representation of the active site region of the mini-MMP-9 RO-206-0222 complex. The compound and mini-MMP-9 are shown as stick models with nitrogen atoms in blue, oxygen atoms in red, compound carbon atoms in yellow and mini-MMP-9 carbon atoms in green. Coordinate bonds to the catalytic zinc ion in purple and intermolecular hydrogen bonds are shown as broken lines with distances in Å (reproduced from Tochowicz et al.[57])*

Active site interactions favour the enol form of the barbiturate ring and the catalytic zinc is coordinated in a distorted tetrahedral manner by the nitrogen atom at position 3 of the barbiturate and the nitrogen atoms of the three His residues. The hydroxyl oxygen of the enol form is positioned where the catalytic H_2O molecule is expected and forms a hydrogen bond with the carboxamide nitrogen of Gln402. The $H_1 – N_1$ and $C_6 = O_6$ groups hydrogen bond to the Ala189 carbonyl group and the Ile188 NH group. The two C-5 substituents orientate into the S1' and S2' pockets. The proximal phenyl ring stacks on the imidazole ring of His401 and the ether oxygen interacts with the slightly positively

charged aromatic edge of Tyr423. The distal phenyl ring interacts with Leu418, Tyr420 and Arg424 towards the bottom of the S1' pocket. The S2' pocket is bordered on one side by Gly186-Leu187 and Pro421-Met422 on the other. The piperazine P2' moiety is in the chair conformation between these groups and the distal pyrimidine ring is allowed to solvent with only minor contacts with Gly186.

In agreement with available literature, previous work in the Gilmer group found that substitution by a phenoxyphenyl group at C-5 conferred greater inhibitory potency than benzyloxyphenyl or phenyl groups for the gelatinases. In MMP-9, the S1' pocket is deep similar to that of MMPs -2, -3, -11, -12, -13 and -14 in contrast to the shallower pocket of MMPs -1, -7, -8 and -16. We decided to maintain the phenoxyphenyl substituent on the core barbiturate scaffold as it contributes to potency and a degree of selectivity over the shallower MMPs. The S2' pocket is shallow and P2' substituents are allowed out to solvent as demonstrated by the mini-MMP-9 barbiturate complex crystal structure providing an opportunity for further derivation without detrimental effects on inhibitory potency.

2.4 Synthesis of the phenoxyphenyl substituted barbiturate scaffold

Synthesis of the barbiturate scaffold was achieved in four steps as outlined in Scheme 1 similar to that described by Breyholz *et al.*[157] The phenoxyphenyl substituent is generated in the first step before preparation of the substituted malonate ester in step two. Reaction with urea in the third step forms the barbiturate ring. In step four, the C-5 hydrogen is functionalized to bromine, a good leaving group for further elaboration.

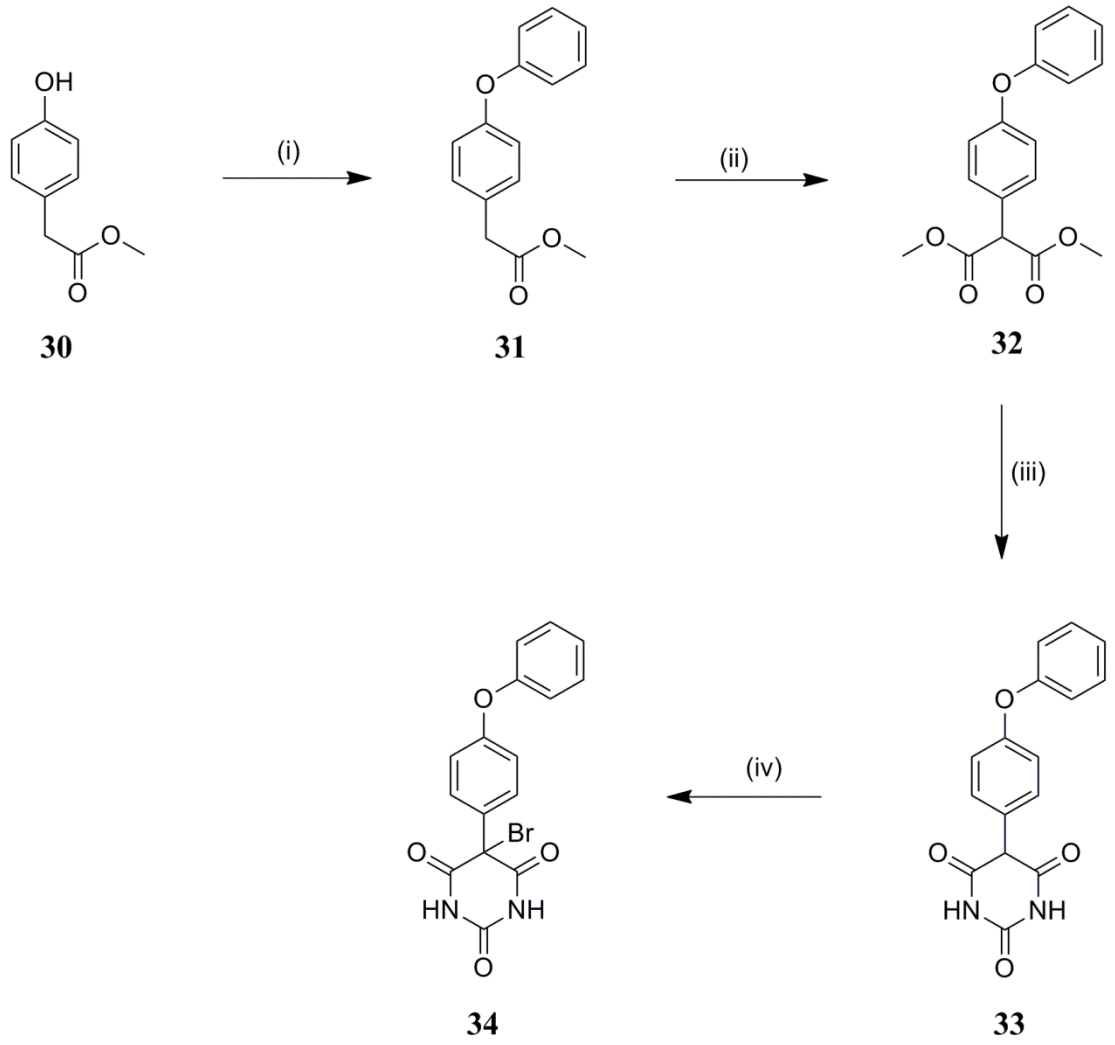

(i) $C_6H_5B(OH)_2$, copper (II) acetate, pyridine, DCM, RT, 48 h (ii) $(CH_3O)_2CO$, NaH, anhydrous THF, 90^oC, 5 h (iii) Na, urea, EtOH, 100^oC, 7 h (iv) Br_2, HBr, H_2O, 0^oC, 5 h

Scheme 1. Four step synthesis of the phenoxyphenyl substituted barbiturate scaffold

In the first step of our synthesis, diaryl ether synthesis was achieved by coupling phenylboronic acid to methyl-4-hydroxy phenyl acetate (**30**) via Chan-Lam coupling, also known as Chan-Evans-Lam coupling. This coupling is catalyzed in the presence of copper and proceeds in air at room temperature. The catalytic cycle involves ligand exchange, transmetallation, reductive elimination and oxidation (Figure 22) but it is unclear which or how many copper oxidation states are involved. In our case, copper acetate was used as a source of copper (II) at one equivalency and pyridine was used as the ligand. The reaction was carried out at room temperature in ambient air in DCM. Yields achieved were never >30%. Work by Evans *et al.*[158] on optimisation of Chan-Lam coupling reaction conditions identified phenol and diphenyl ether as unwanted side-products. From this it was assumed that there was competitive arylation of water and competition of the resulting phenol with phenolic substrate. These side products were identified even under anhydrous conditions and the source of water is thought to be degradation of phenylboronic acid. Evans *et al.* counteracted this side reaction by the inclusion of powdered molecular sieves in the reaction mixture. It was also our experience that the inclusion of sieves counteracted the diminished yields. The grade of DCM used, anhydrous or technical, or the atmospheric conditions used, N_2 or ambient, were not found to impact the yield obtained. The reactions were carried out with technical grade DCM in ambient air. A ready supply of oxygen should promote the oxidation step.

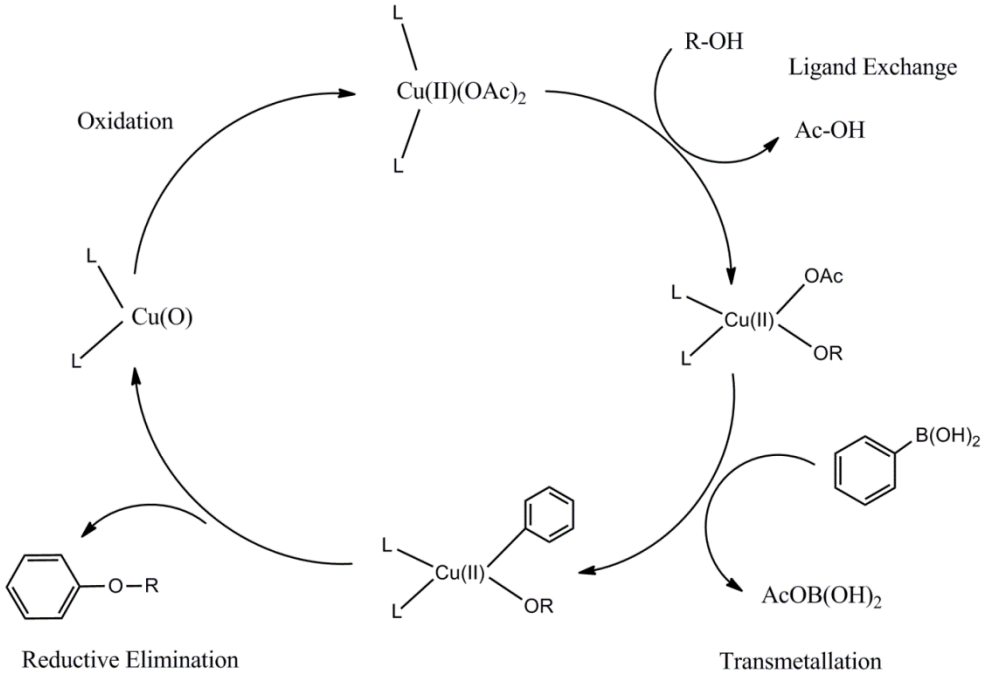

Figure 22. Proposed mechanism of Chan-Lam coupling

Step two involved a Claisen ester condensation between the enolizable methyl 2-(4-phenoxyphenyl)acetate (**31**) and the unenolizable but electrophilic dimethyl carbonate. The proposed mechanism is outlined in Figure 23. In the first step of the mechanism, sodium hydride (NaH) extracts an acidic α-proton resulting in the formation of an enolate anion which is stabilized by electron delocalization. The enolate ion nucleophilically attacks a carbonyl carbon of the dimethyl carbonate. Carbonates are suitable starting materials for this reaction type as they are not enolizable themselves lacking α hydrogens and are more electrophilic than the enolizable ester. The carbonate should react with the enolate anion faster than the ester itself limiting any self-condensation side reactions. The greater electrophilicity of the carbonate is explained by the fact that both oxygen atoms adjacent to the carbonyl group can exert their full inductive effect to increase reactivity. A methoxy group is eliminated to yield the product. The reaction was carried out in anhydrous THF as NaH is deactivated by water and on reaction produces NaOH as well as H_2 gas which could cause ester hydrolysis. The reaction mixture was refluxed at 90°C and was seen to turn an orange colour within the first hour. When the reaction was complete after approximately 5 h the mixture was poured onto iced-water and the product was extracted with DCM. This product (**32**) could be used in the next step without further purification.

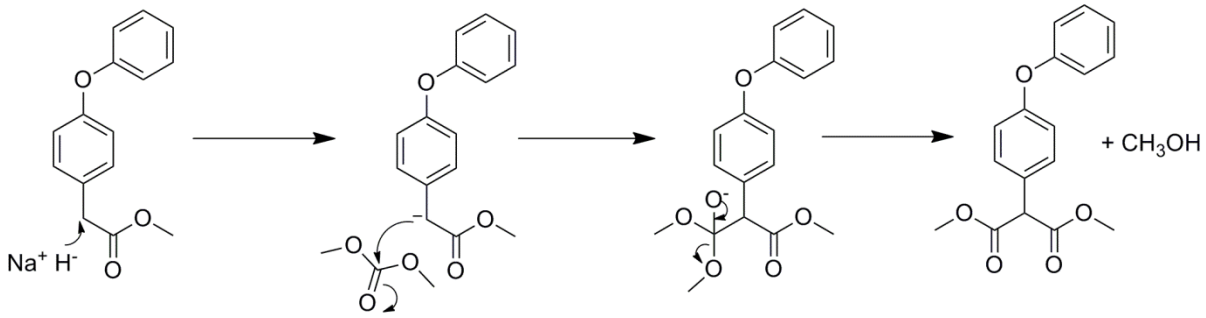

Figure 23. Proposed mechanism of step two in synthesis of the phenoxyphenyl substituted barbiturate scaffold, a Claisen ester condensation

The barbiturate ring was formed by reaction of **32** with urea in the presence of sodium ethoxide at elevated temperatures. Sodium ethoxide was generated *in situ* by dissolving sodium in HPLC grade ethanol. Urea was then added, dissolved and the mixture brought to reflux at 90ºC. Once refluxing had commenced, **32** was added dropwise in ethanol over the first 30 min and off-white precipitates began to form within 1 h. The generally accepted mechanism for this classical reaction is deprotonation of urea by the strong base and nucleophilic attack on the ester carbonyl with loss of methoxide. A second nucleophilic attack completes the cyclocondensation with removal of a further methoxide molecule

(Figure 24). When the reaction was complete, the mixture was poured onto ice, the precipitates dispersing to a cloudy orange mixture. Acidification to pH 2 with 1 M HCl precipitated the barbiturate product (**33**). This collected product contained some impurities which were removed by refluxing the material in ethyl acetate: methanol 3:1. The impurities dissolved readily while the barbiturate remained insoluble in the hot solvent.

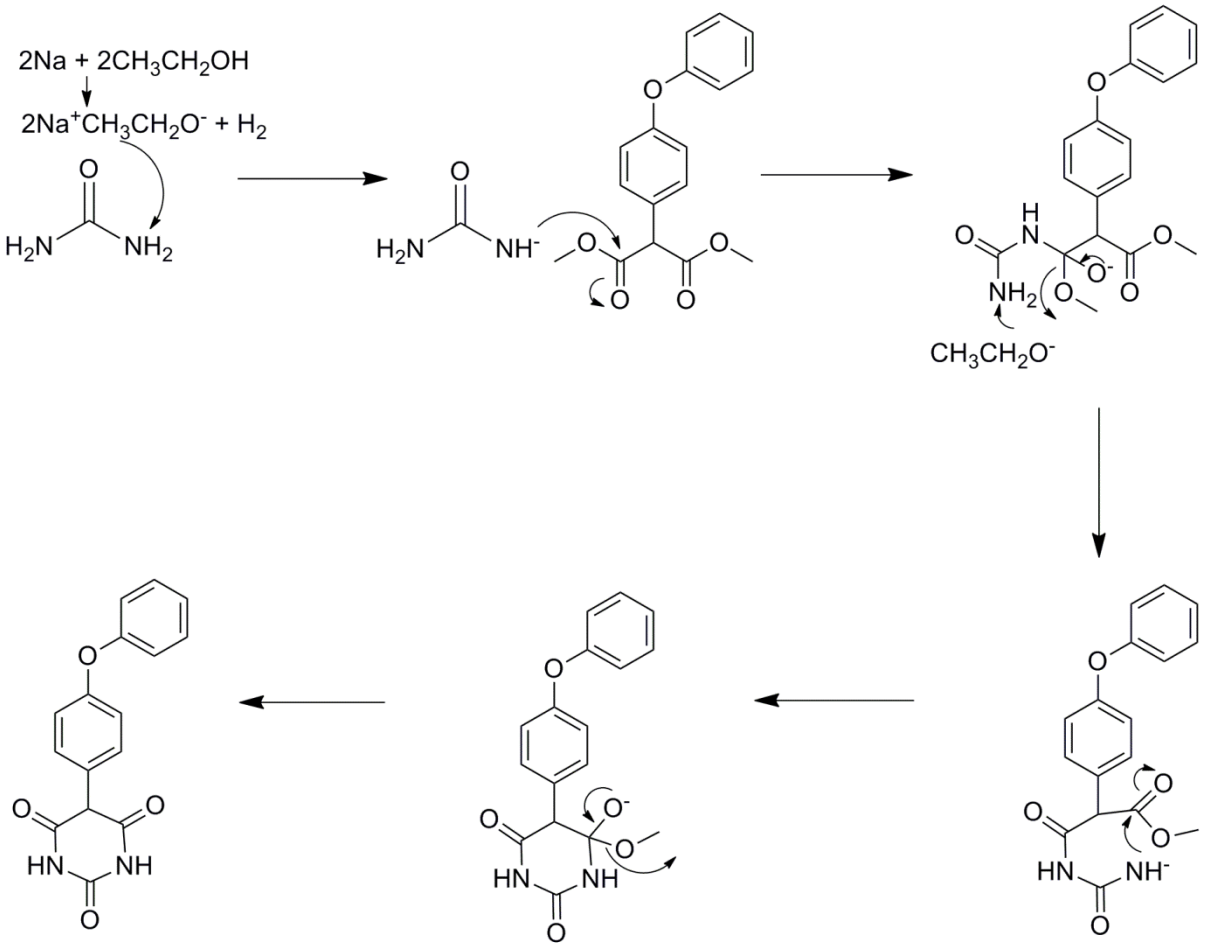

Figure 24. Proposed mechanism of step three in synthesis of the phenoxyphenyl substituted barbiturate scaffold, barbiturate ring synthesis

Position 5 of the barbiturate ring was functionalised by bromination. Radical bromination was pursued by treatment with bromine in the presence of hydrobromic acid in water a 0 - 5°C. Under the influence of light, a molecule of Br_2 is homolytically cleaved to produce two bromine radicals. This radical can abstract a proton from position 5 of the barbiturate ring producing a molecule of HBr and a barbiturate radical. Reaction of this barbiturate radical with a further molecule of Br_2 produces the desired brominated product (**34**) and a bromine radical propagating the reaction further (Figure 25).

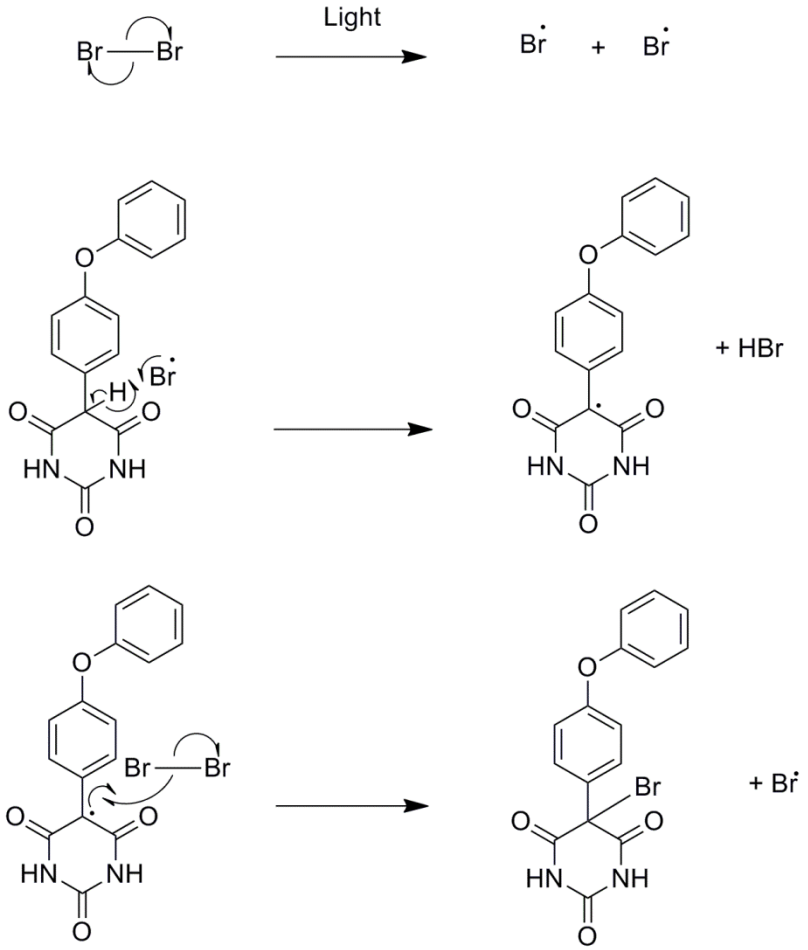

Figure 25. Proposed mechanism of step four in synthesis of the phenoxyphenyl substituted barbiturate scaffold, free radical bromination

Compound **34** was used as a starting material for derivatisation of P2'. Previous work in the Gilmer group established that a P2' substitution by homopiperazine or piperazine gave good gelatinase inhibition and that potency was tolerant of further derivation by substitution at the distal N. The C-5 bromine is amenable to nucleophilic substitution by a primary or secondary amine in methanol at room temperature. One derivative was produced by substitution of an amino monofuntionalised 3-unit PEG chain at position 5 to yield compound **35**, the structure of which can be seen in Figure 26.

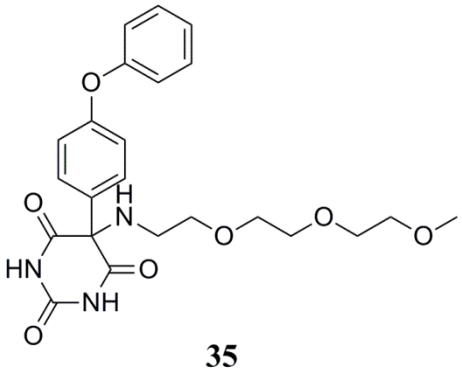

35

*Figure 26. Structure of compound **35***

However, in ^{1}H NMR characterisation of **35**, some of the signals in the aromatic region integrated lower than expected as can be seen in Figure 27.

A

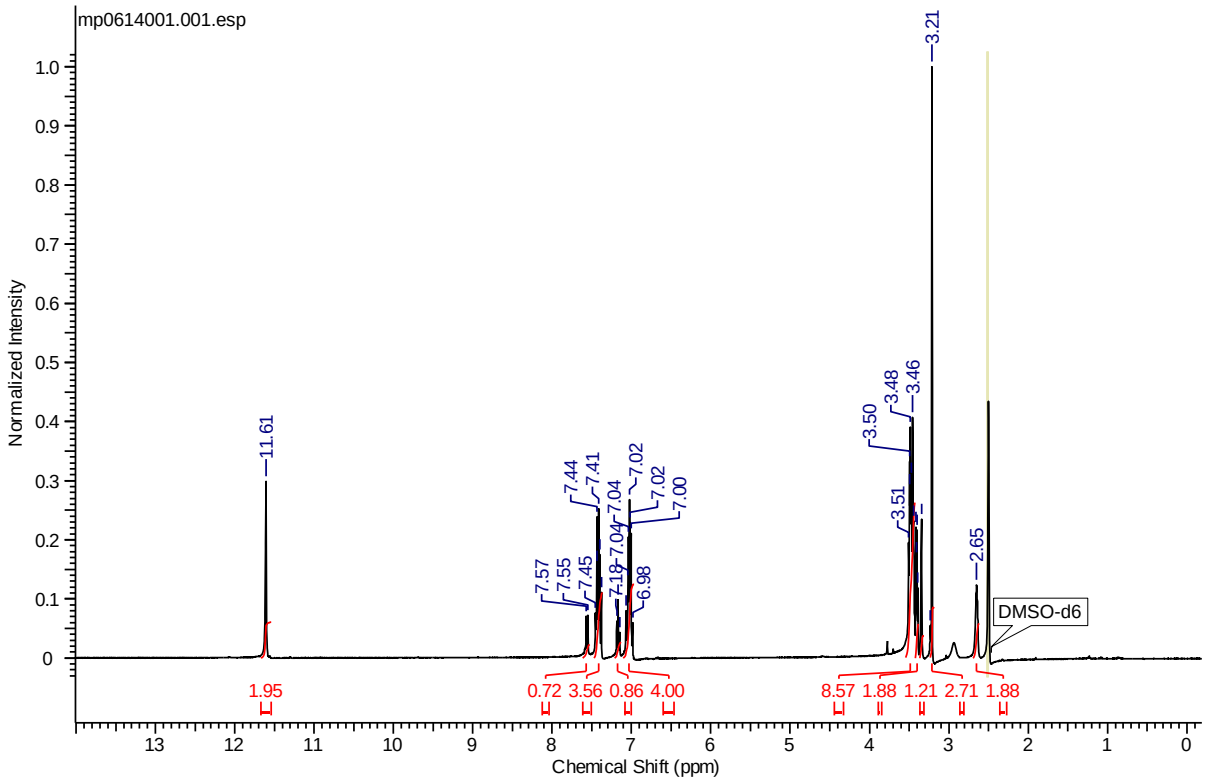

B

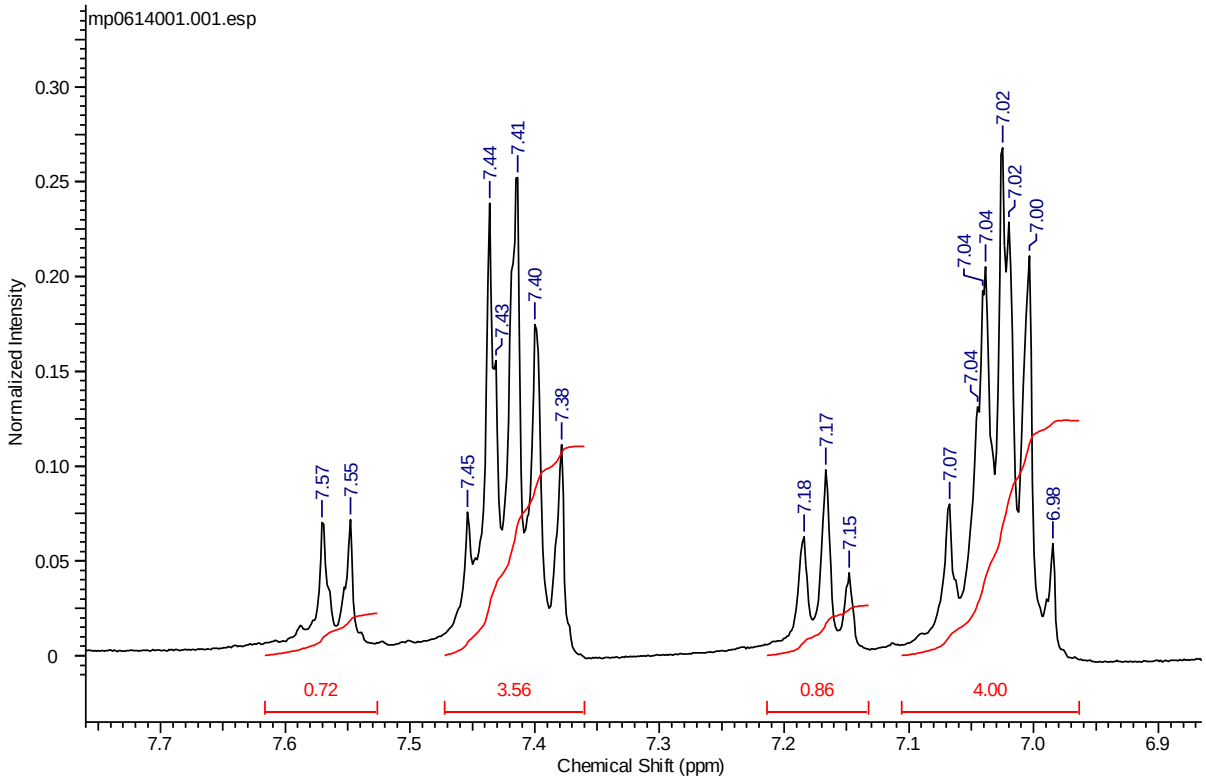

*Figure 27. ^{1}H NMR spectrum of compound **35** **A**: Full spectrum; **B**: Zoom of aromatic region*

The significance of this was underlined by the appearance of two peaks in the HPLC chromatogram of **35** (Figure 28).

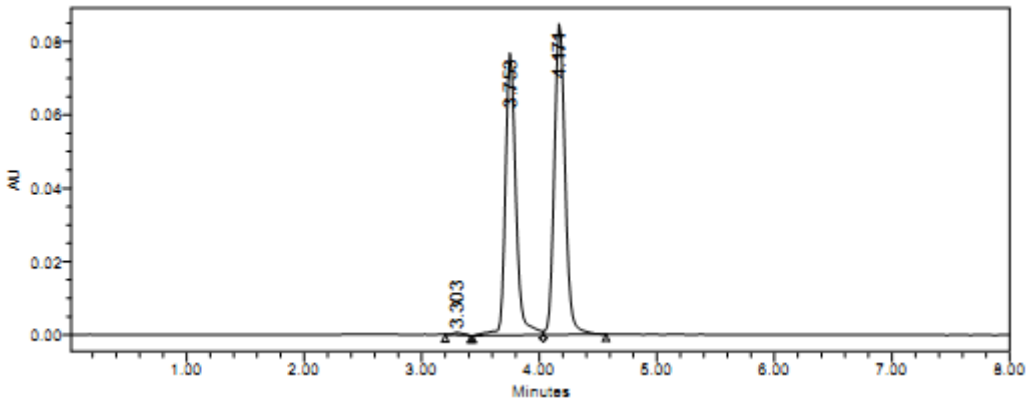

*Figure 28. HPLC chromatogram of compound **35***

It was initially proposed that this could be a tautomeric behaviour. Shifting tautomeric equilibriums had been observed in NMR analysis of the barbiturate compounds. Tautomeric interconversion can be slow and has been reported to be slow enough to allow separation of tautomers by HPLC. If tautomers were responsible, it should be possible to cause a shift in the equilibrium proportionality by a change in pH or by heating but no change in the chromatogram was observed. The chromatographic peaks were isolated by collection of the appropriate fractions from a HPLC analytical column and left overnight to allow equilibration. On re-analysis no changes in the chromatograms of the fractions were observed. NMR analysis of each peak revealed that the spectra differed in the aromatic regions. The peak at the longer retention time of 4.2 min did not have a signal corresponding to the *para* proton and the aromatic region of the spectrum indicates the presence of two *para* disubstituted phenyl rings (Figure 29). The doublet at 7.56 ppm integrating for 2 protons is coupled to the doublet at 7.05 ppm where J = 9.16 Hz and the doublet at 7.44 ppm is coupled to the doublet at 6.99 ppm where J = 8.54 Hz, these coupling constants characteristic of *ortho* coupling. It was deduced that the bromination step was yielding a mixed product of monobrominated material and dibrominated material. The oxygen of the diaryl ether was sufficiently electron donating to allow electrophilic aromatic substitution of the *para* proton of the distal phenyl ring. The ^{1}H NMR of the peak at retention time 3.7 min contained a signal for the *para* proton which integrated for one proton as expected (Figure 30).

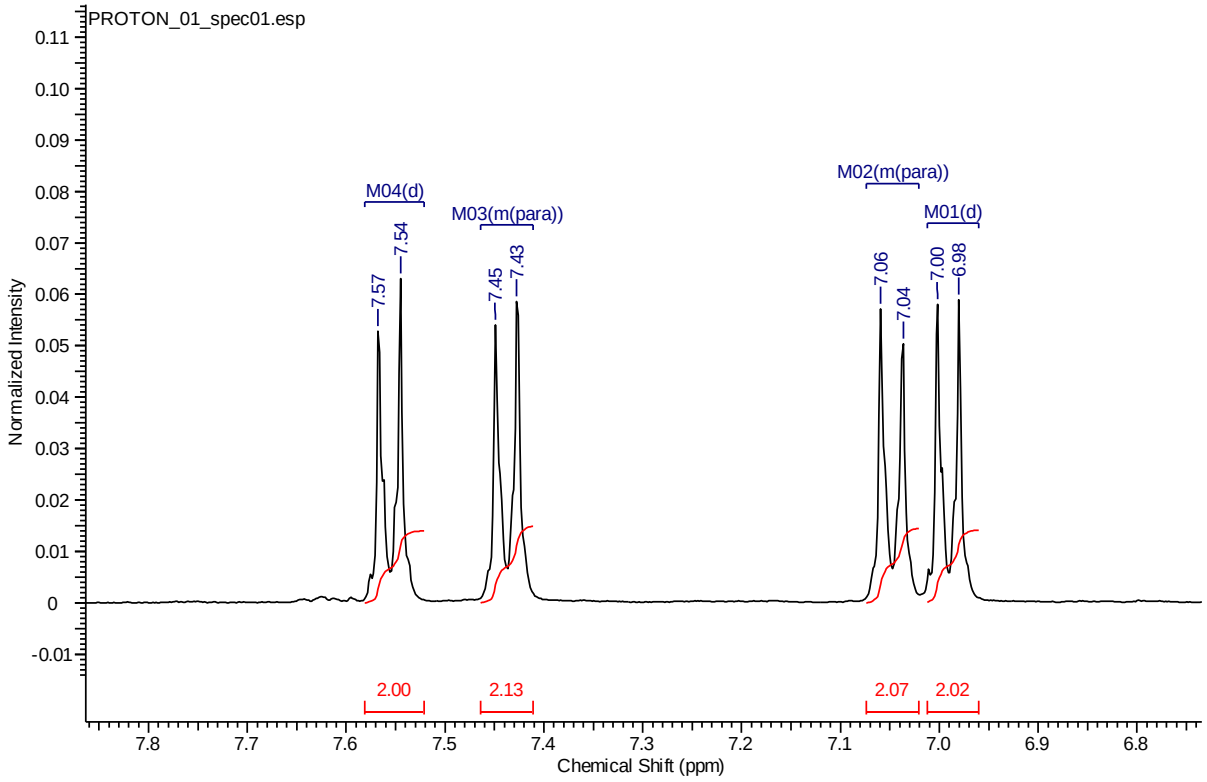

*Figure 29. Aromatic region of ^{1}H NMR of HPLC peak at retention time of 4.2 min of compound **35***

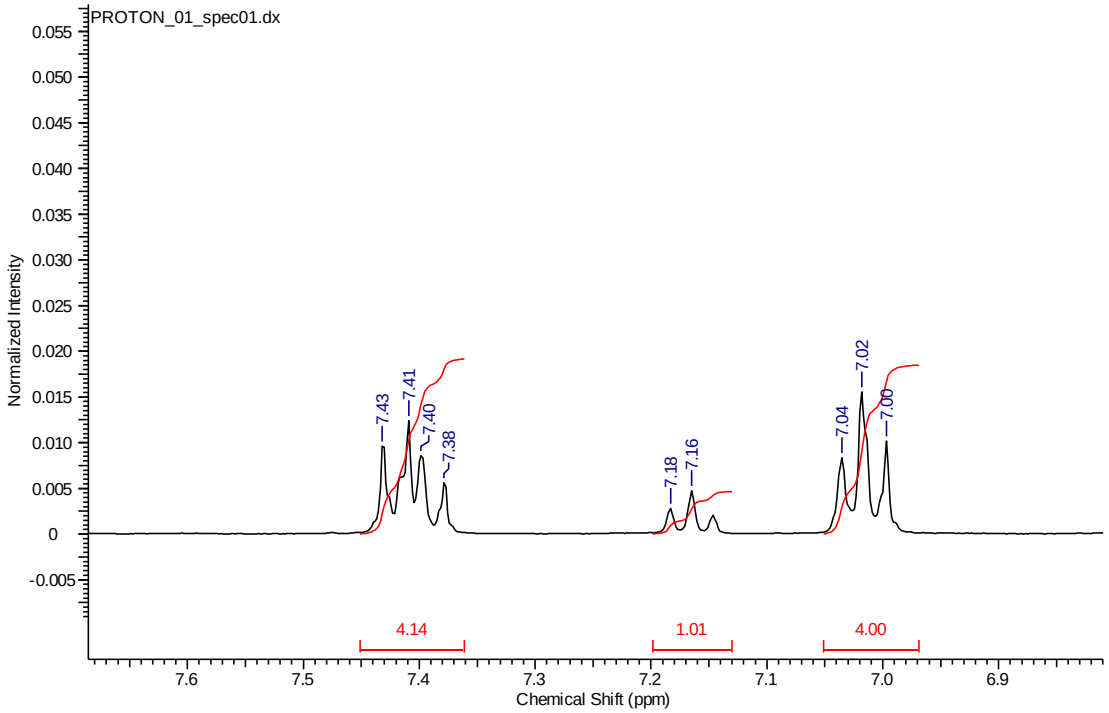

*Figure 30. Aromatic region of ^{1}H NMR of HPLC peak at retention time of 3.7 min of compound **35***

Separation of these products was not feasible by manual flash column chromatography. They were not separable on TLC and there was degradation in solution. Selective bromination was pursued. Lowering the equivalencies of Br_2 and HBr and reducing the temperature to – 20°C by the addition of salt to the reaction mixture over an acetone-ice bath did improve the product ratio but did not achieve full selectivity. The monobrominated product was obtained by N-bromosuccinimide (NBS) bromination. The use of NBS keeps the concentration of bromine in the reaction system low. NBS reagent will contain a small amount of bromine and a catalytic amount of dibenzoyl peroxide initiates the reaction. In the first propagation step, one molecule of HBr is produced. Reaction of one molecule of HBr with NBS yields one molecule of Br_2 and succinimide and so Br_2 is slowly released as the reaction proceeds.

Pursuit of the dibrominated product was expected to be straightforward. However it proved difficult to encourage the reaction beyond 90% completion. Radical bromination reactions slow or stop as chain terminating steps consume one or both of the reactive intermediates. This and the scale dependency of bromination reactions prompted us to pursue the dibrominated material by using a *p*-brominated phenylboronic starting material in step 1. The four step synthesis was carried out as before and the barbiturate was brominated using HBr and Br_2 to afford compound **39** seen below in Figure 31.

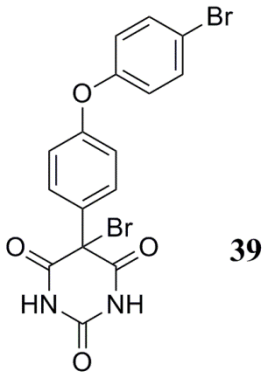

39

*Figure 31. Structure of compound **39***

2.5 Barbiturate tautomerism

Barbiturates can undergo prototropic tautomerism or addition of a proton at one molecular site and its removal from another[159] (Figure 32).

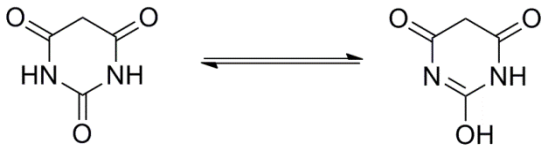

Figure 32. Tautomerism of barbituric acid

The equilibrium between tautomers is dynamic, dependent on factors such as pH and solvent. This behaviour has made the barbiturates challenging to work with. The change in structure on tautomer interconversion changes the compound's physical and chemical properties and changing solubilities have been observed on many occasions in this work. These changes may also affect biological activities and as tautomeric forms may be substituent dependent, similar compounds may not exhibit biological potencies as expected.[159]

The tautomeric behaviour of compound **39** could be seen in NMR analysis in deuterated DMSO. The spectrum in Figure 33 taken immediately after sample preparation contains two signals at 11.66 ppm and 11.55 ppm of the barbiturate ring nitrogens integrating for 0.8 and 1.2 protons indicating the presence of two tautomeric forms of the molecule. The aromatic zoomed region also shows a mixture of tautomers. In the spectrum of the same sample obtained 24 h after sample preparation in Figure 34, it can be seen that the compound has resolved to one tautomeric form. There is one N-H signal at 11.54 ppm integrating for two protons and the aromatic region now integrates as expected with a coupling pattern typical of a *para*-substituted benzene ring system. A similar behaviour was observed in the ^{13}C spectrum (Figure 35). In the first spectrum every expected signal was duplicated indicating two similar species and the two signals at 75.7 ppm and 55.5 ppm were assigned to C-5. After 24 h, the carbon spectrum also resolved to one species.

A

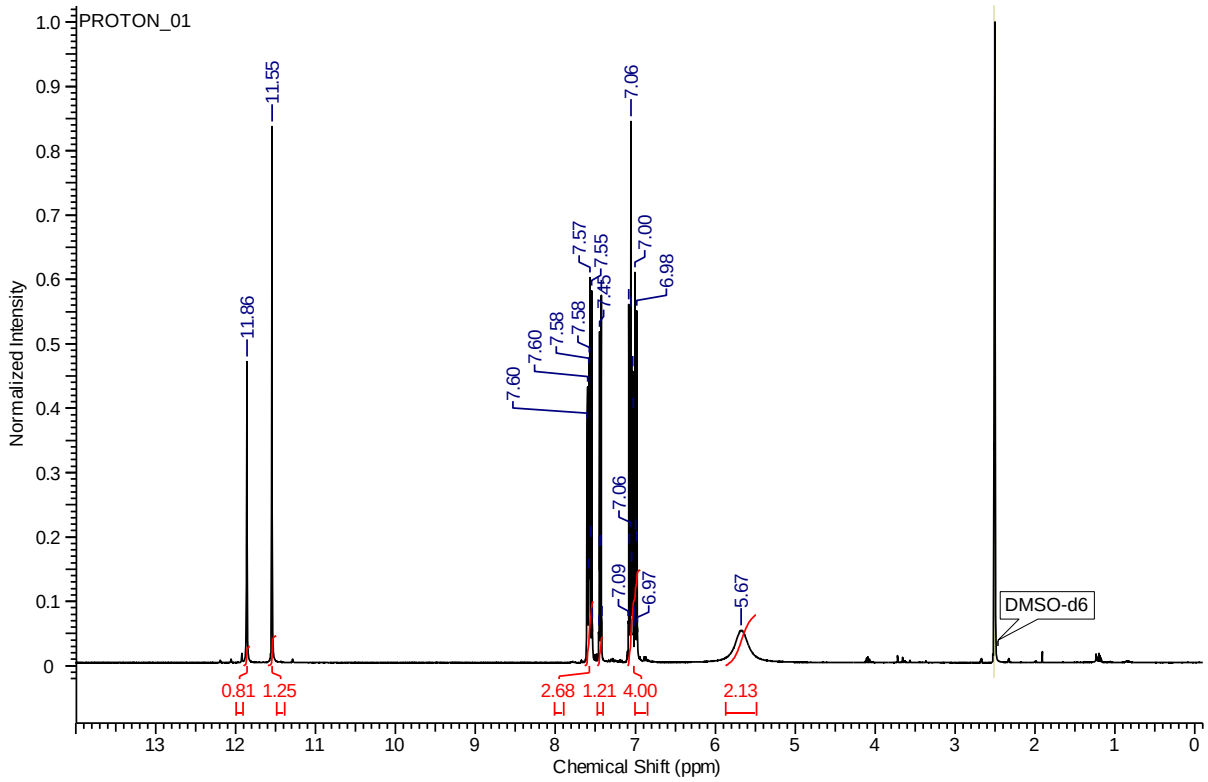

B

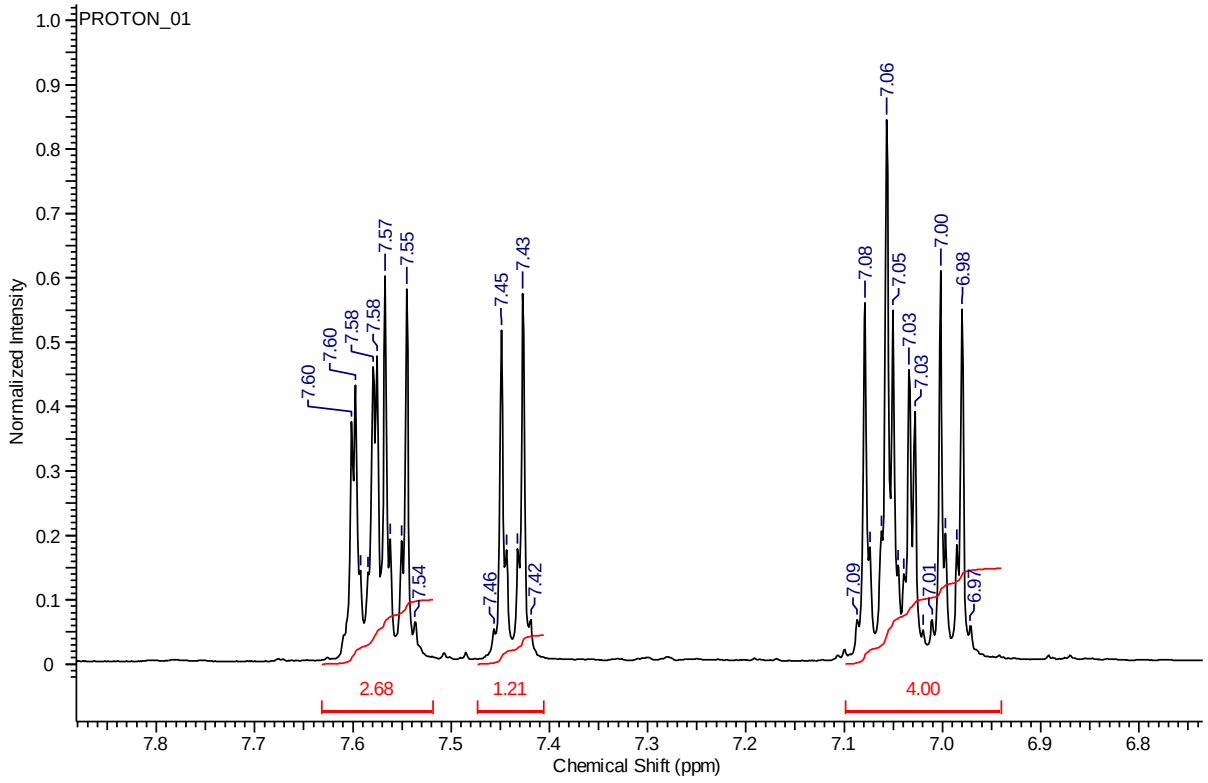

Figure 33. ^{1}*H NMR of compound* ***39*** *taken immediately on sample preparation* ***A****: Full spectrum* ***B****: Zoom of aromatic region*

A

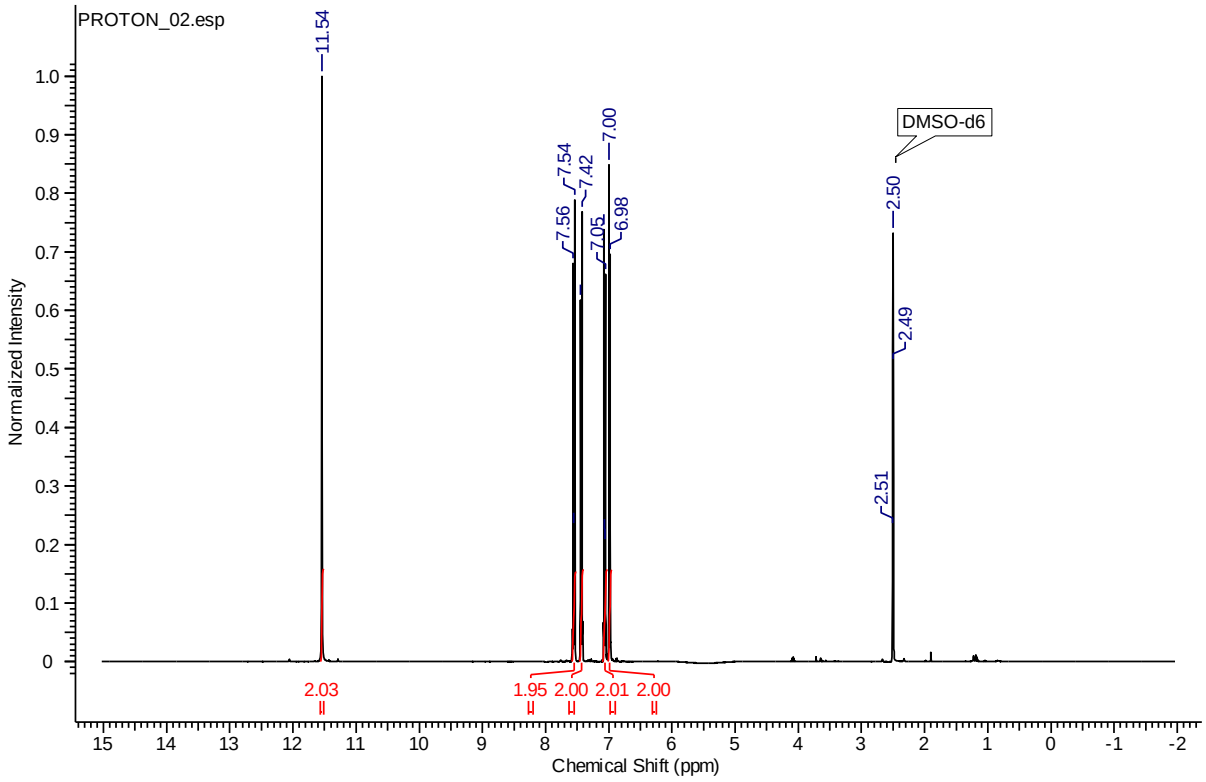

B

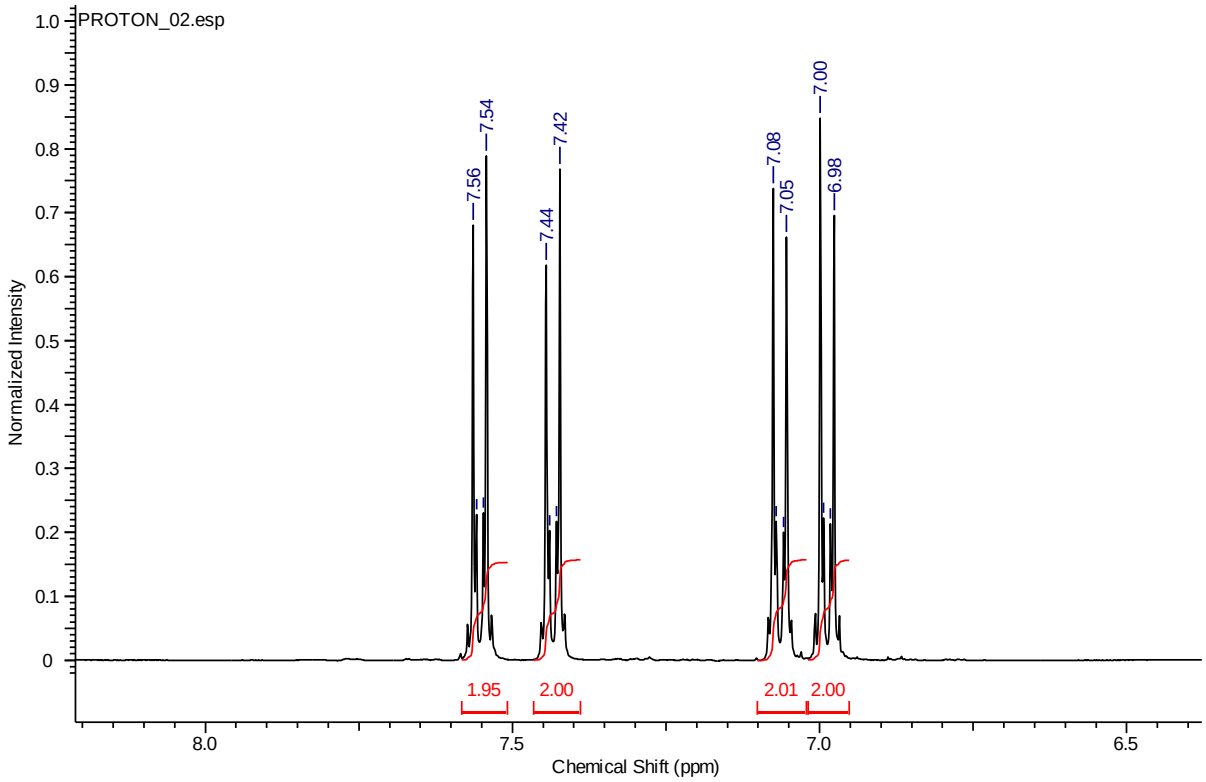

Figure 34. ^{1} *H NMR of compound* ***39*** *taken 24 h after sample preparation* ***A****: Full spectrum* ***B****: Zoom of aromatic region*

A

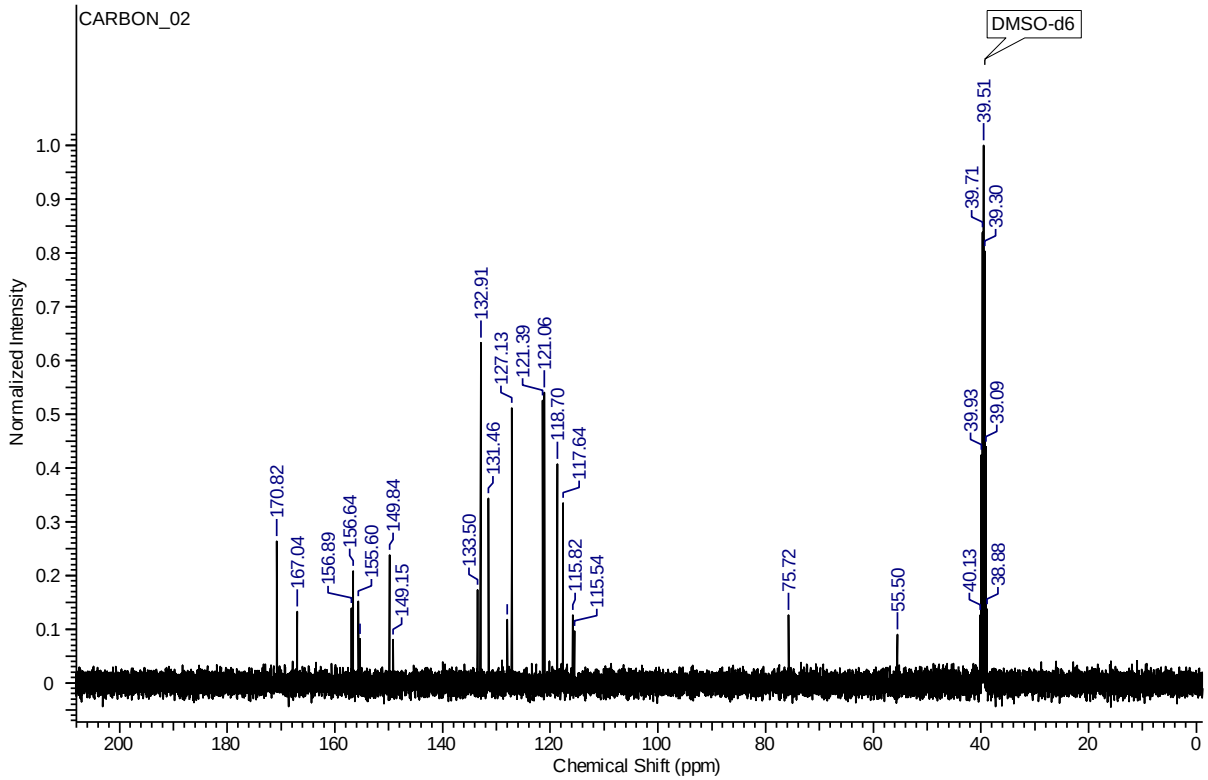

B

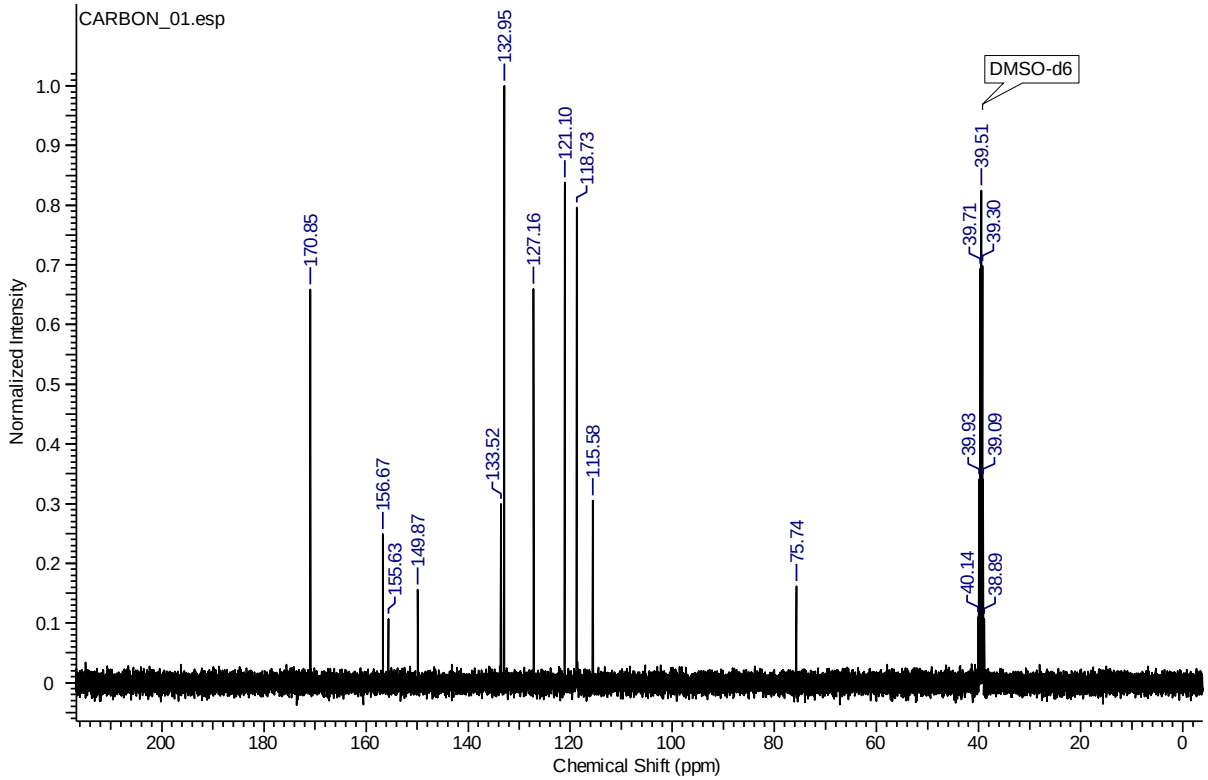

Figure 35. ^{13}*C NMR of compound* ***39*** *taken* ***A****: immediately after sample preparation* ***B****: 24 h after sample preparation*

Compound **39** (Figure 31) was chosen as the MMP inhibitory scaffold in the design of candidate gut-confined MMP inhibitors. The bromine *para* substitution on the distal phenyl ring was maintained because it was difficult to avoid producing. Bromo-substitution was in addition expected to contribute to selectivity for MMPs with deep S1' pockets such as the gelatinases over MMPs with shallow S1' pockets such as MMP-7.

2.6 Design and synthesis of a non-absorbable gelatinase inhibitor

With an MMP inhibitory scaffold established, strategies for suppressing oral absorption were considered. Synthesis efforts would focus on the P2' substituent where inhibitory potency was tolerant of further substitution. The following strategies were considered:

- Attachment of a hydrophilic chain or polymer to increase molecular weight and polarity
- Introduction of a permanent charge

2.6.1 Synthesis of a non-absorbable inhibitor by pegylation

The first strategy considered in the pursuit of a non-absorbable inhibitor candidate was attachment of a hydrophilic polymer at P2'. Polyethylene glycol (PEG) was selected for incorporation. PEG groups are known to be non-toxic and non-antigenic and they can increase water solubility.[160, 161] Reduced lipophilicity and increased molecular weight should reduce absorption potential.

Pegylation is now a commonly pursued strategy for modifying a therapeutic agent's pharmacokinetic profile facilitating manipulation of its pharmacodynamics. To date, the most important clinical application of drug pegylation has been the extension of half-life of parenteral biologics. PEG incorporation reduces renal clearance and may slow metabolism.[162] The increased bioavailability compensates for any reduced potency and the conferred increased water solubility may also be desirable. PEGs range from LMW to HMW and can be employed as permanently bonded PEG drugs, drug conjugate linkers or as prodrugs designed to be cleaved.

2.6.1.1 Synthesis of a 3-unit pegylated barbiturate

A 3-unit monofunctional PEG group with one hydroxyl end group (**40**) was functionalized to an amine (**43**) in a three step synthesis (Scheme 2) for substitution of the C-5 bromine of **39**.

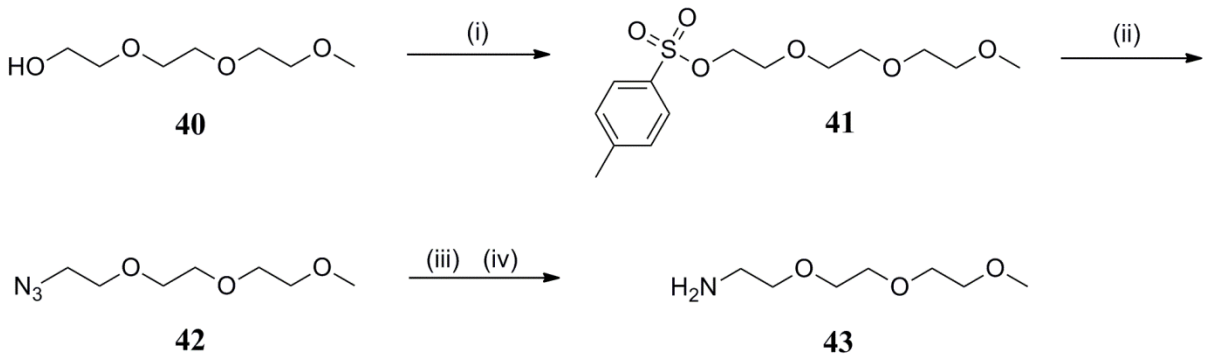

(i) tosyl chloride, Et_3N, anhydrous DCM, N_2, 0°C – RT, 1 h, (ii) NaN_3, DMF, 60°C, 24 h
(iii) PPh_3, anhydrous THF, N_2, 12 h (iv) H_2O, 12 h

Scheme 2. Three step synthesis of compound 43

The alcohol was first converted to a tosylate (**41**), a better substrate for nucleophilic attack by reaction with tosyl chloride in anhydrous DCM with triethylamine as base. A lone pair of electrons from the hydroxyl group attacks the electrophilic sulfur of tosyl chloride expelling the chloride anion in an S_N2 mechanism. A proton is extracted from the positively charged intermediate by the chloride anion forming HCl which is trapped by triethylamine in triethylamine hydrochloride salt and yielding the tosylate product. Treatment of **41** with sodium azide in 1,3-dimethyl-3,4,5,6-tetrahydro-2(1H)-pyrimidinone (DMPU) solvent yielded the azide (**42**). The electron rich azide ion is a good nucleophile and attacks the electrophilic carbon α to the tosylate displacing it. The azide (**42**) was then reduced to the amine (**43**) via the Staudinger reaction. Triphenylphosphine reacts with the azide by nucleophilic addition of the phosphine to the terminal nitrogen to generate a phosphazide, which loses N_2 to form an iminophosphorane. Hydrolysis in water yields the amine (**43**) and the triphenylphosphine oxide by-product (Figure 36).

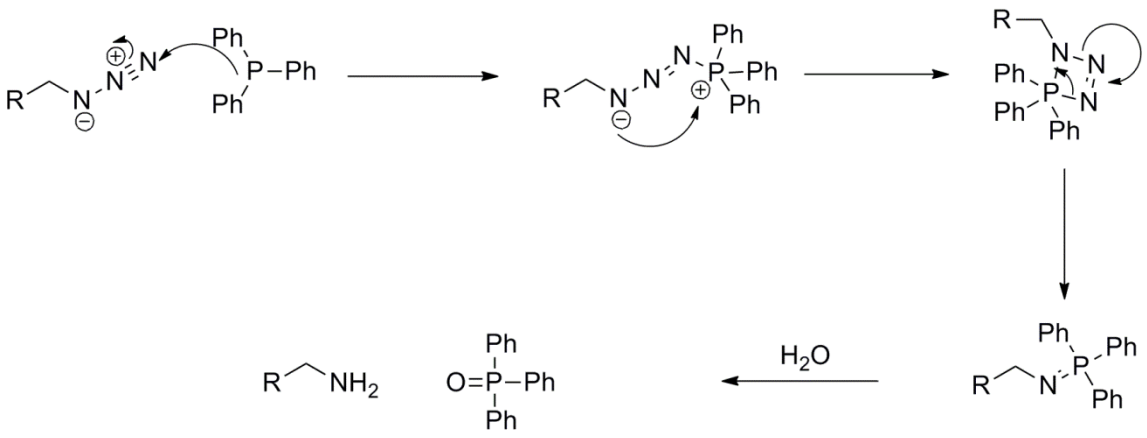

Figure 36. Proposed mechanism of the Staudinger reaction

The C-5 bromine of compound **39** is amenable to nucleophilic substitution by a primary or secondary amine in methanol at room temperature. The reaction is thought to follow an S_N2 mechanism. As a tertiary structure, approach of the amine nucleophile should be heavily sterically hindered and it could be presumed that an S_N1 mechanism would take precedence. In this case however, the bromide leaving group is adjacent to a carbonyl group. The neighbouring carbon atoms are electrophilic and their lowest unoccupied molecular orbitals (LUMOs) can combine to form a new LUMO of lower energy. This increased reactivity facilitates nucleophilic attack and increases the rate of S_N2 reaction so that it is likely to be the dominant mechanism. Polar, protic methanol is generally a solvent choice suited to promoting an S_N1 mechanism but was found to be suitable here. The starting material is soluble in methanol but the disubstituted products are not soluble in some cases and precipitate out of solution facilitating product isolation by simple filtration. The amine functionalised PEG (**43**) was stirred with **39** in methanol for 24 h and the pegylated product (**44**) was isolated by flash column chromatography (Scheme 3). The product was somewhat hygroscopic.

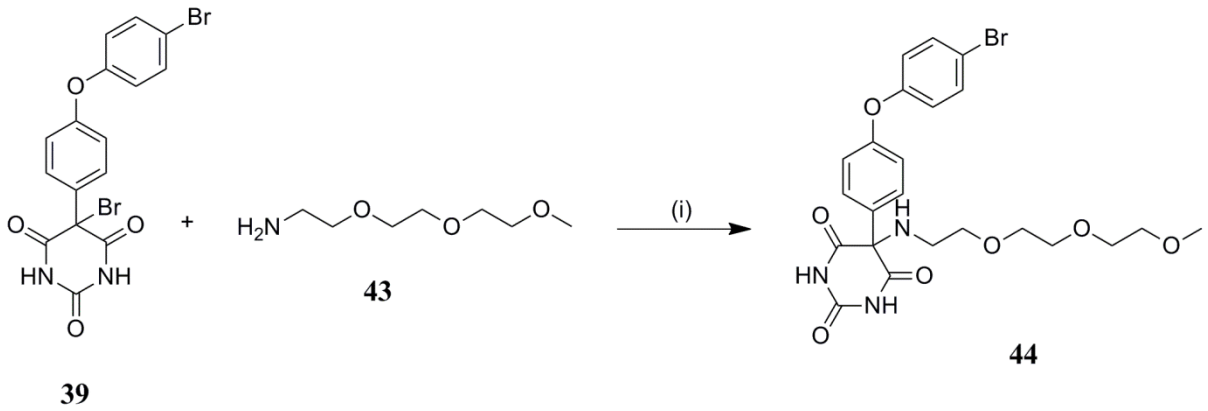

(i) MeOH, RT, 24 h

Scheme 3. Synthesis of compound 44

2.6.1.2 Synthesis of a PEG chain-linked barbiturate inhibitor dimer

We sought to increase molecular weight and reduce absorption potential by dimerization of the MMP inhibitor. MMP-9 is secreted in monomeric, heterodimeric and homodimeric forms and is the only MMP known to form homodimers.[163] A suitably spaced inhibitor dimer could offer increased affinity over the monomeric form or other MMP species. Wang *et al*. studied homodimeric compounds of 5-homopiperazine barbiturates linked by alkyl chains from 2 – 20 carbons in length[164] and MMP-9 inhibition was maintained. A 3-unit PEG chain-linked barbiturate dimer, compound **49**, was synthesized using the synthesis route for **44** but in this case the starting PEG material was a bifunctional alcohol, each terminus acting as a reaction centre in the synthesis (Scheme 4).

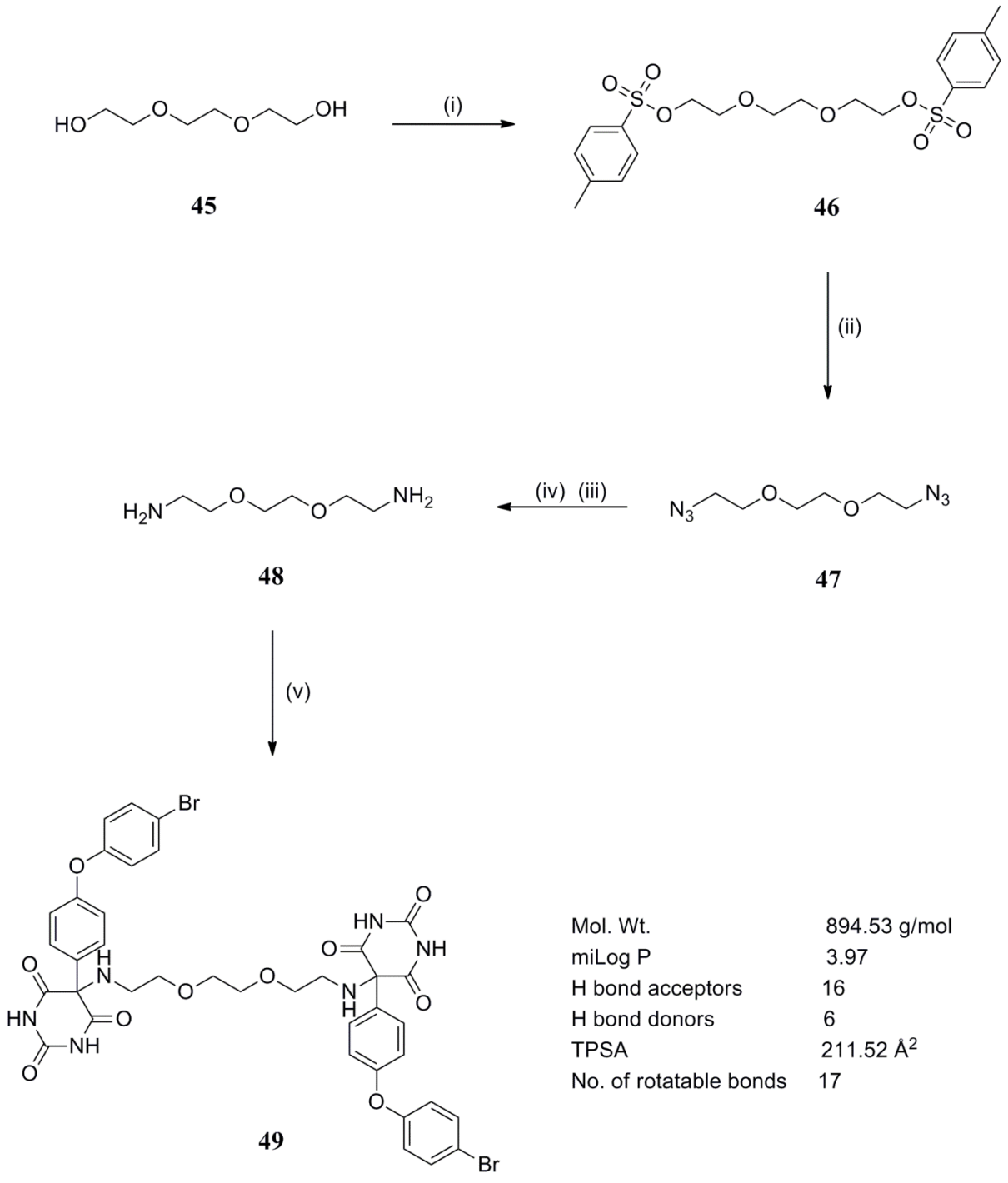

(i) Tosyl chloride, Et_3N, anhydrous DCM, N_2, 0°C – RT, 1 h, (ii) NaN_3, DMPU, RT, 24 h (iii) PPh_3, anhydrous THF, N_2, 12 h (iv) H_2O, 12 h (v) compound **39,** MeOH, RT, 24 h

Scheme 4. Synthesis of compound 49; Molecular properties of 49 calculated and/or predicted by the molinspiration molecular property calculation web tool [165]

The molecular properties of compound **49** in Scheme 4 were calculated and/or predicted by the *molinspiration* molecular property calculation web tool.[165] With a molecular weight of greater than 500, > 10 H-bond acceptors and > 5 H-bond donors, **49** breaches several of Lipinski's so-called rules for good oral absorption.[74, 75] With a calculated total polar surface area of 211.52 $Å^2$ and 17 rotatable bonds, it also contravenes Veber's rules for good absorption.[76] Compound **49**, however, did not have good solubility in MeOH, H_2O or DMSO.

2.6.2 Synthesis of a non-absorbable inhibitor by incorporation of a permanent positive charge

It is generally accepted that a permanently charged compound will have a poor absorption profile. The arrow poison curare contains the quaternary ammonium alkaloid tubocurarine (**50**, Figure 37). Naturally occurring in the bark and stem of *Chondodendron tomentosum*, a stemmed, woody vine, it is a competitive antagonist of nicotinic receptors inhibiting the action of acetylcholine leading to muscle relaxation and paralysis. It was used by South American natives to hunt animals and they were able to eat the meat without experiencing the toxic effects of the poison as it was unable to pass into the systemic circulation from the oral route.[155]

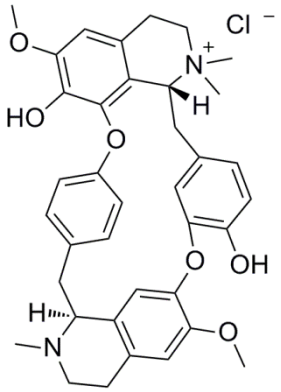

50

*Figure 37. Structure of tubocurarine chloride (**50**)*

Quaternary ammonium muscle relaxants are in clinical use as neuromuscular blocking agents in anaesthesia. They are parenterally administered and have minimal absorption by the oral route as established in pharmacokinetic profiling. The incorporation of a positive charge has been used by others in the design of non-systemic drugs. Huang & Tremont *et al*. designed non-systemic ASBT inhibitors as described in Chapter one. They attached an

alkyl chain linked 1,4-diazabicyclo[2.2.2]octane (DABCO) moiety to the core inhibitor molecule to confer low systemic absorption while retaining potency. Its crystallinity and non-hygroscopicity were advantages over PEG-linked candidates in the series.[91]

2.6.2.1 Synthesis of compound 53

A permanent positive charge was incorporated into the P2' substituent in synthesis of compound **53** as outlined in Scheme 5. Compound **39** was substituted at C-5 with 4-piperidine ethanol to produce compound **51**. The primary alcohol was then converted to the mesylate (**52**) by reaction with methanesulfonyl chloride in the presence of triethylamine in anhydrous DCM. Compound **52** was treated with two equivalents of DABCO in acetonitrile at room temperature for one week. Nucleophilic attack by DABCO and expulsion of the leaving group yields the quaternary ammonium compound with methanesulfonate anion as its counterion. The positive charge reduces the nucleophilicity of the distal N reducing dimerisation potential. In an attempt to improve reaction time, a greater equivalency of DABCO was trialled but the resulting NMR indicated that the product contained a mixture of DABCO salts. Isolation of the polar product was achieved by solid phase extraction on reverse phase silica.

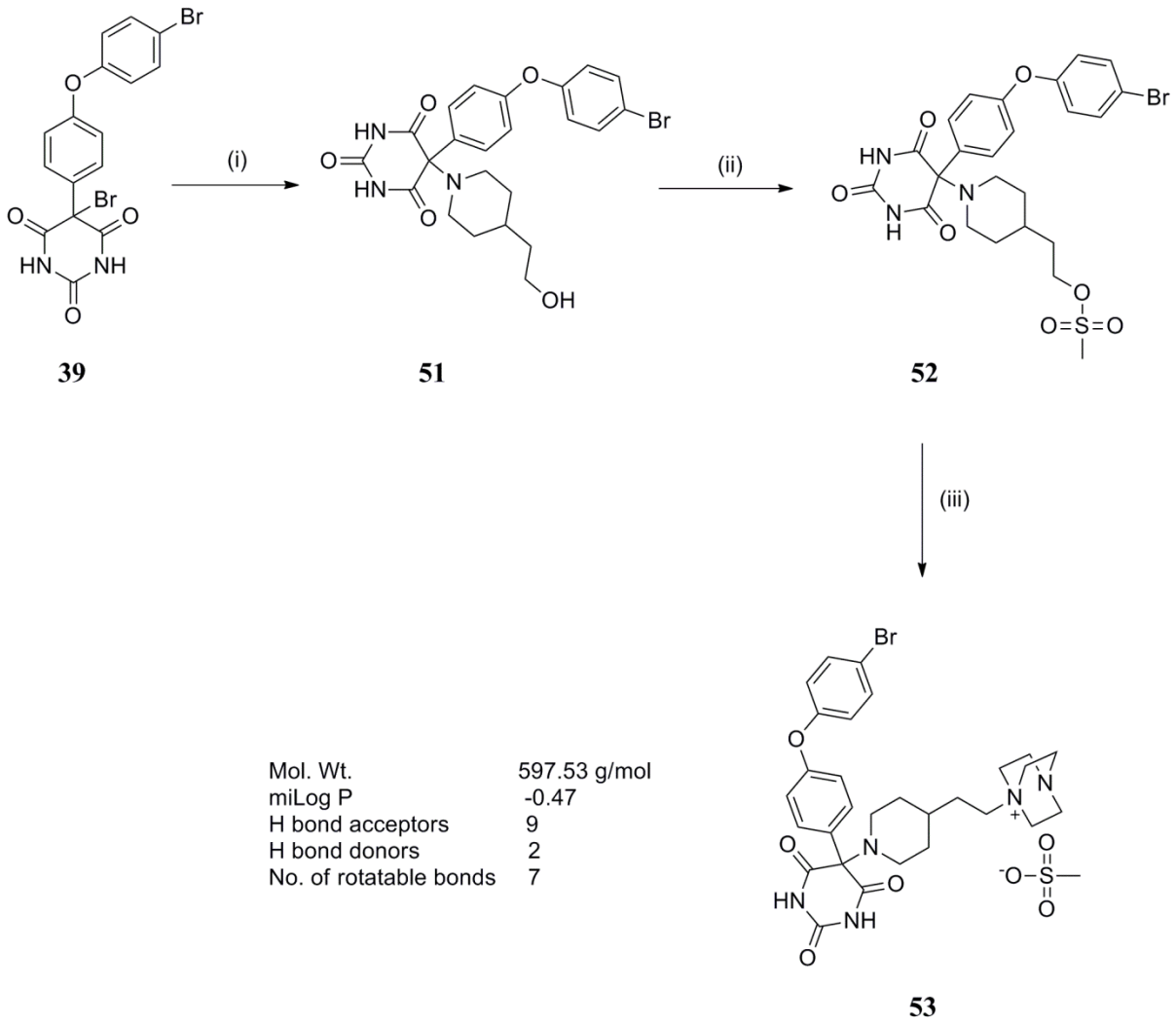

39 **51** **52** **53**

(i) 4-piperidine ethanol, MeOH, RT, 24 h, (ii) mesyl chloride, NEt_3, anhydrous DCM, N_2, 0°C – RT, 24 h, (iii) DABCO, ACN, RT, 7 d

Scheme 5. Synthesis of compound 53; Molecular properties calculated and/or predicted by the molinspiration molecular property calculation web tool [165]

Permanently positively charged, compound **53** would not be readily passively absorbed and with a molecular weight of greater than 500, evidence would suggest that it would not be a candidate for apical organic cation transporters in the GIT.

2.7 Characterisation of compound 53

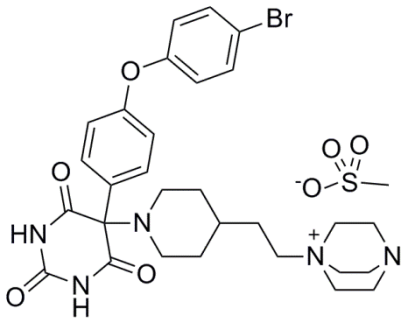

*Figure 38. Structure of compound **53***

Compound **53** (Figure 38**)** was characterised by ^{1}H NMR, ^{13}C NMR, infrared (IR) spectroscopy and high resolution mass spectrometry (HRMS). The ^{1}H NMR spectrum of compound **53** was referenced to the deuterated DMSO solvent peak at 2.5 ppm. The spectrum also contained an accompanying solvent peak for water at 3.33 ppm. Broad signals were observed in the spectrum of **53** (Figure 39) which was likely due to the timeframe of tautomer interconversion of the compound.

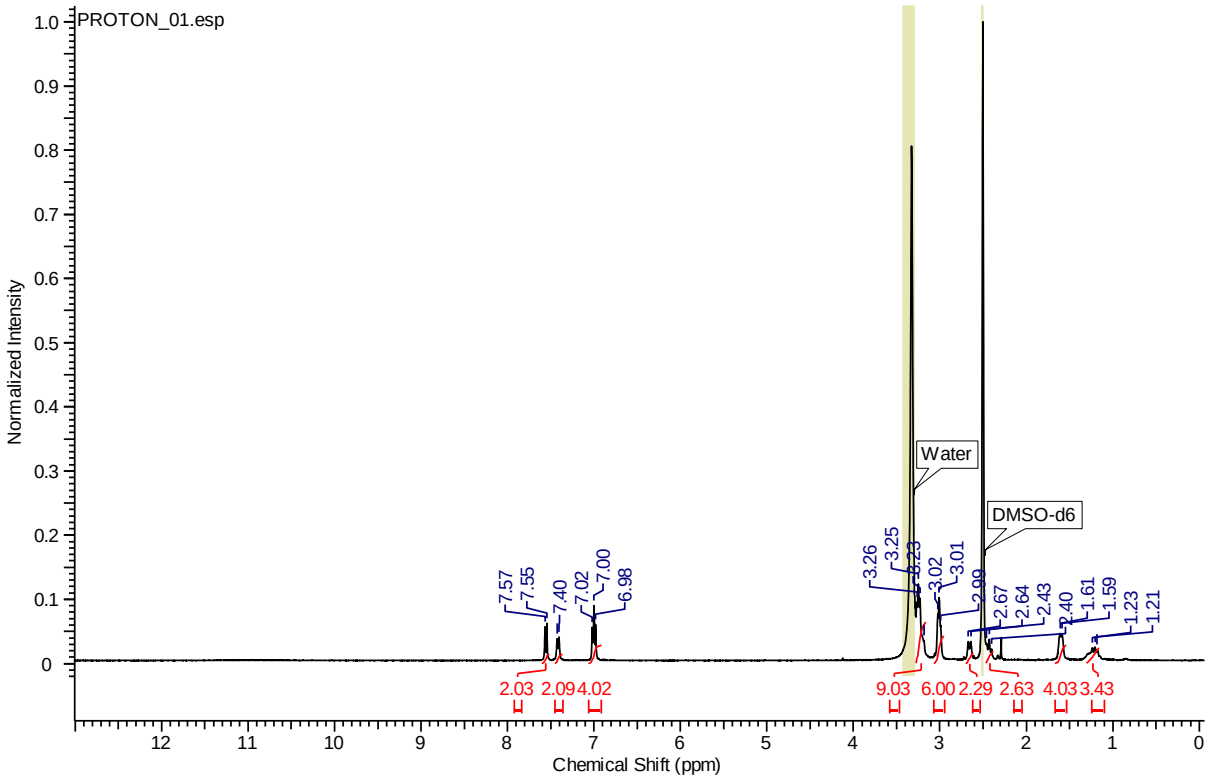

*Figure 39 . ^{1}H NMR spectrum of compound **53***

In the upfield region of the spectrum in Figure 40, the broad multiplet integrating for three protons from 1.15 - 1.30 ppm is attributed to overlapping signals of the CH of the piperidine moiety and the adjacent CH_2 of the two carbon chain linker. Integrating for four protons, the multiplet from 1.54 - 1.66 ppm is attributed to the piperidine CH_2 protons beta to the piperidine nitrogen. Deshielded alpha to the nitrogen, the remaining four CH_2 protons of the piperidine moiety resonate farther downfield as two multiplets at 2.38 - 2.47 ppm and 2.62 - 2.70 ppm. Further deshielded again by proximity to electronegative nitrogens the 12 protons of the DABCO moiety resonate as two multiplets. The multiplet at 2.94 – 3.07 ppm integrates for six protons. The other multiplet is shouldered on the water peak and overlaps with the multiplet of the CH_2 protons of the chain linker alpha to the positively charged DABCO nitrogen.

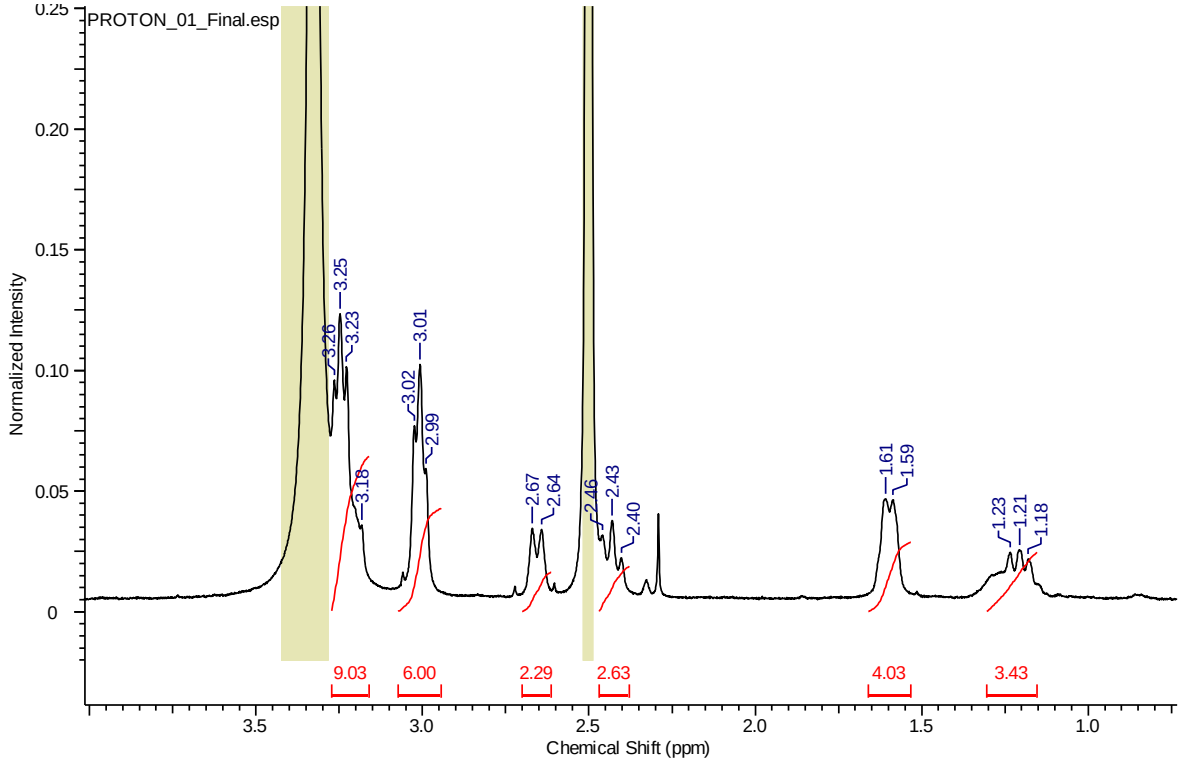

*Figure 40. Zoom of upfield region of the ^1H NMR spectrum of compound **53***

The downfield region of the spectrum can be seen in Figure 41. The protons of the *para*-substituted phenoxyphenyl substituent resonate downfield in the aromatic region as two coupled doublets each integrating for two protons and a multiplet integrating for four protons.

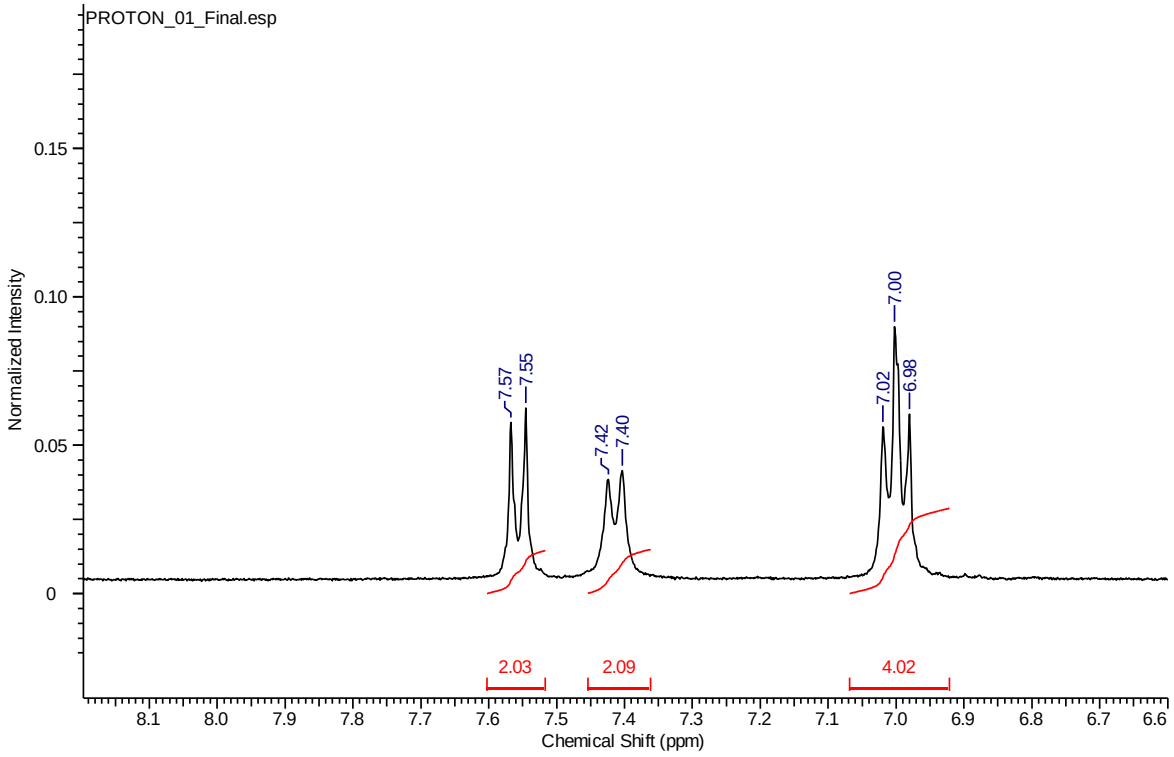

*Figure 41. Zoom of downfield region of the ^{1}H NMR spectrum of compound **53***

The protons of the barbiturate ring did not appear in the spectrum. This was not unexpected and the presence of the barbiturate ring was confirmed in the ^{13}C NMR spectrum.

In the ^{13}C NMR spectrum of compound **53** (Figure 42) the barbiturate ring produced three signals. C-4 and C-6 of the ring are equivalent and produce the signal at 172.4 ppm. The signal for the disubstituted C-5 appears at 73.8 ppm. The remaining barbiturate ring carbon, C-2, resonates at approximately 150 ppm. In the spectrum of compound **53**, the signal at 152.8 is most likely due to C-2. The phenoxyphenyl substituent contains 12 aromatic carbons for which eight signals are expected. These signals can be seen in the spectrum of compound **53** between 115 ppm and 157 ppm. The spectrum of compound **53** contains four signals in the region between 40 ppm and 70 ppm, at 44.7 ppm, 47.8 ppm, 51.5 ppm and 61.6 ppm. One of these signals can be attributed to the two equivalent -CH_2 carbons alpha to the piperidine nitrogen. The DABCO moiety contains two sets of three chemically equivalent –CH_2 carbons which produce two signals in this region. The fourth signal is due to the -CH_2 of the chain linker alpha to the positively charged nitrogen atom. In the upfield region of the spectrum between 25 ppm and 35 ppm, the three signals at 27.4 ppm, 32.4 ppm and 33.6 ppm can be assigned to the two remaining equivalent -CH_2 carbons and the –CH carbon of the piperidine moiety and the -CH_2 of the chain linker. The

spectrum was referenced to the deuterated DMSO solvent peak at 39.5 ppm which is thought to overlap the signal of the methanesulfonate counterion.

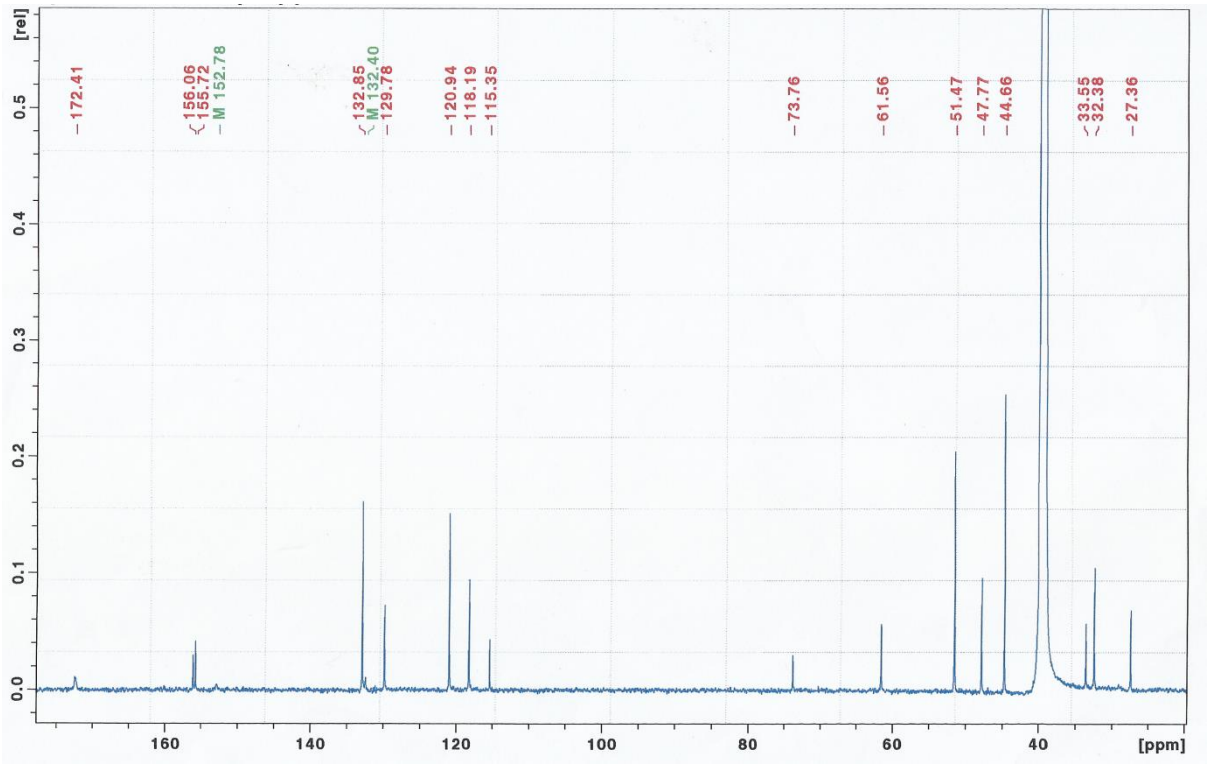

*Figure 42. ^{13}C NMR spectrum of compound **53***

The high resolution mass spectrum of compound **53** can be seen in Figure 43. As a quaternary ammonium salt, compound **53** bears a permanent positive charge and was expected on electrospray ionisation to produce a molecular ion with m/z equal to the exact mass of the cation. Containing one bromine atom, the spectrum of **53** should contain two peaks in the molecular ion region of approximately equal height separated by two m/z units corresponding to the two approximately equally abundant isotopes of bromine, ^{79}Br and ^{81}Br. The calculated exact mass for $C_{29}H_{35}BrN_5O_4^+$ is 596.1867 and the mass found was 596.1875. The mass error between the theoretical m/z and that experimentally observed was 1.34 ppm. The second peak at (m+2)/z of 598.1846 confirms the presence of one bromine atom in the molecule.

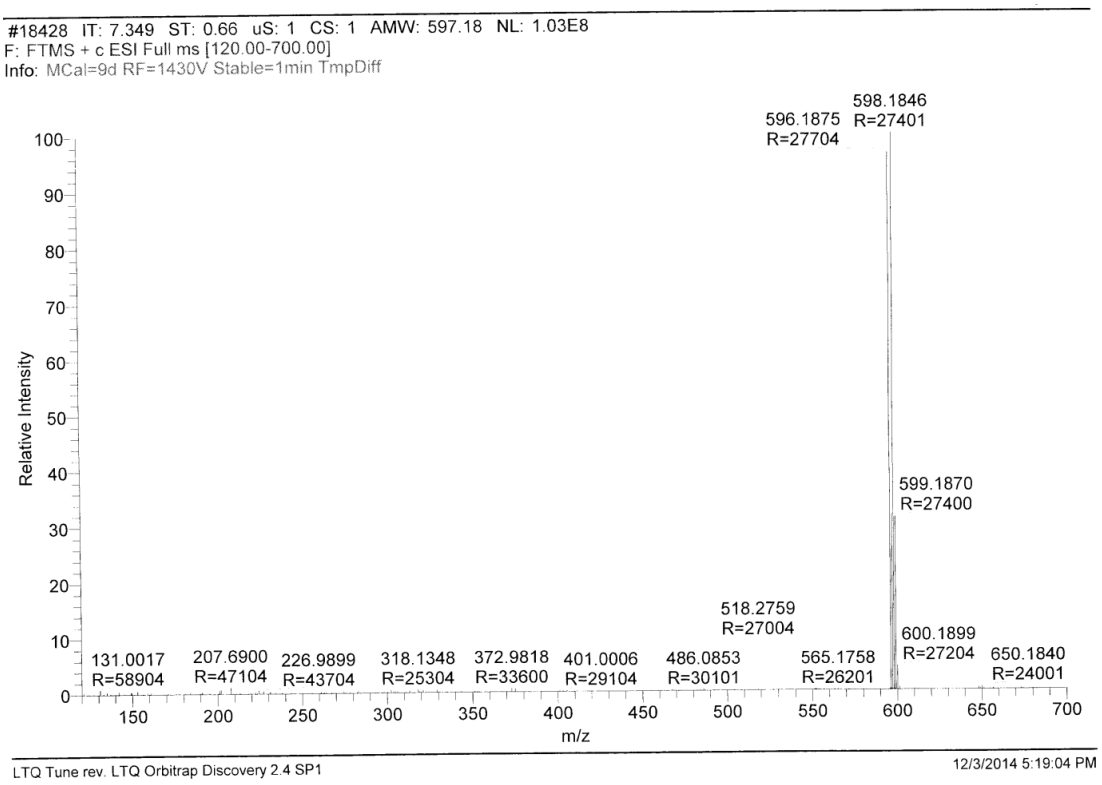

*Figure 43. HRMS of compound **53***

The IR spectrum of compound **53** can be seen in Figure 44. The strong band at 1234 cm^{-1} is consistent with the C-O stretch of an aryl ether. The bands around 1700 cm^{-1} can be attributed to C=O stretches of the barbiturate ring.

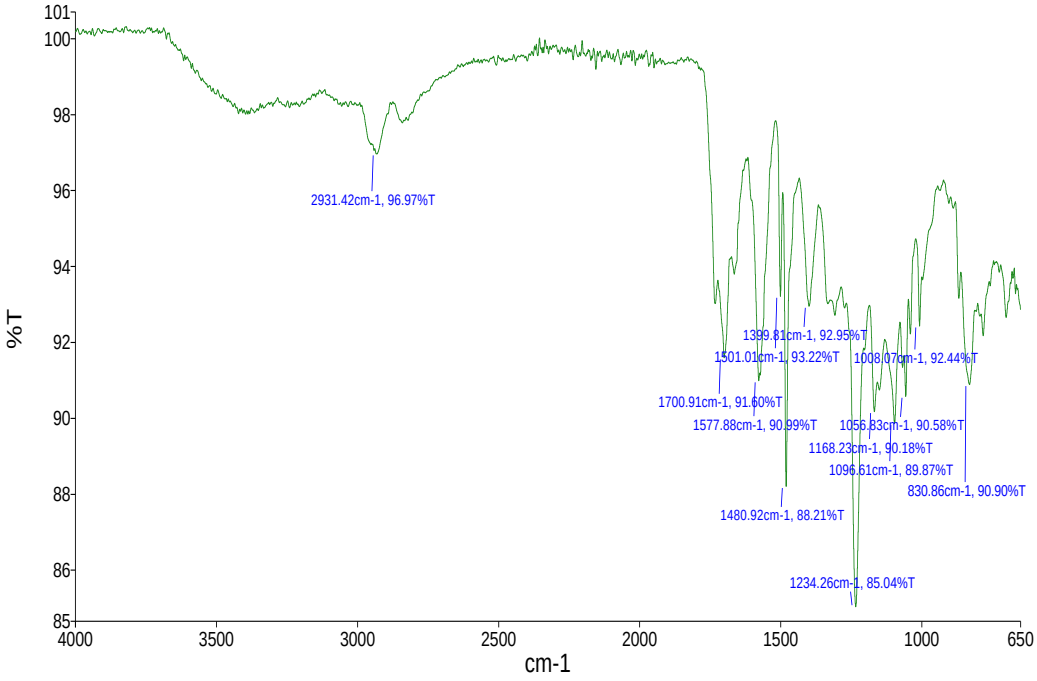

*Figure 44. IR spectrum of compound **53***

2.8 *In vitro* evaluation of MMP-9 inhibitory potency

The inhibitory potency of candidate compounds against recombinant human MMP-9, (R&D systems, UK) was measured in a fluorogenic assay. Briefly, proteinase activity was measured after incubation of *p*-aminophenylmercuric acetate (APMA)-activated MMP-9 and the test concentration of inhibitor at 37°C for 45 min. After incubation, a fluorescent substrate was added and the remaining proteinase activity in the test well cleaved an amide bond between a fluorescent group and a quencher group in the substrate causing an increase in fluorescence. The substrate used was MCA-Pro-Leu-Gly-Leu-DPA-Ala-Arg-NH_2 (R&D systems, UK) which is cleaved at the Gly-Leu bond by MMP-9.[166] The fluorescence was monitored at 10 time points over the initial 10 min of reaction in a plate reader with excitation and emission wavelengths set to 320 nm and 405 nm, respectively. The fluorescence is plotted as a function of time and the slope of this linear plot is calculated. The decrease in slope in comparison to the positive control (buffer + MMP-9 + substrate) provided a measure of inhibition. The % inhibition was calculated using the formula below

$$\%\ Inhibition = \left(1 - \frac{Slope(inhibitor)}{Slope(positive\ control)}\right) \times 100\%$$

Inhibitor test concentrations were selected to cover from 0% to 100% inhibition and nonlinear regression analysis of the sigmoidal dose-response curve established the IC_{50} and 95% confidence interval (CI).

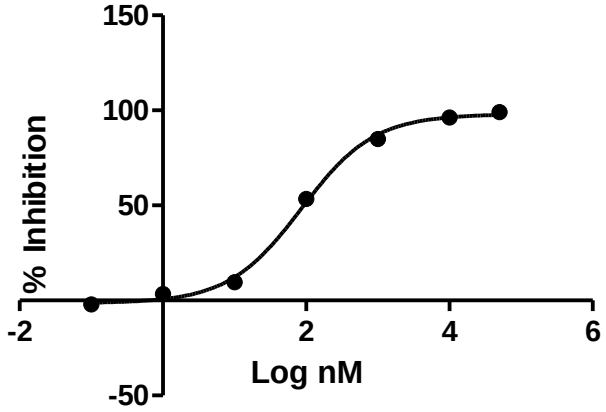

*Figure 45. Recombinant human MMP-9 inhibition curve of compound **49** established over seven concentrations in duplicate; IC_{50} 85.8 nM, 95% CI (66.7, 110.5)*

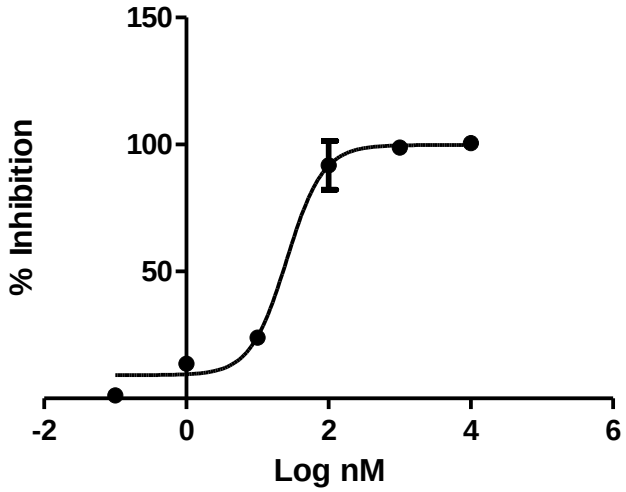

*Figure 46. Recombinant human MMP-9 inhibition curve of compound **51** established over six concentrations in duplicate; IC_{50} 25.8 nM, 95% CI (14.5, 45.9)*

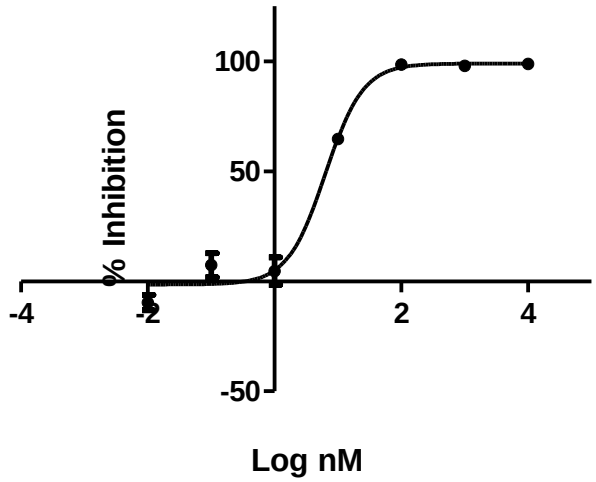

*Figure 47. Recombinant human MMP-9 inhibition curve of compound **53** established over seven concentrations in duplicate; IC_{50} 6.3 nM, 95% CI (4.1, 9.7)*

Compound **49** was a potent inhibitor of MMP-9 with an IC_{50} of 85.8 nM (Figure 45). Compound **53** was more potent again with an IC_{50} of 6.3 nM (Figure 47). Interestingly, it was more potent than its synthetic precursor, compound **51**, which was found to have an IC_{50} of 25.8 nM (Figure 46). Based on its potency and excellent H_2O solubility, compound **53** was chosen for further evaluation.

2.9 Stability of compound 53 in the environments of the GIT

Stability in the environments of the GIT is required for delivery of the inhibitor to its target area in the colon by the oral route. The stability of **53** was examined in simulated gastric fluid over 4 h. Simulated gastric fluid was prepared according to the United States Pharmacopoeia (USP) 2010.[167] Containing salt, pepsin and hydrochloric acid, it has a pH of approximately 1.2 to represent normal gastric pH which is in the range 1 – 3. The compound was prepared at 100 µM in simulated gastric fluid, incubated at 37°C and samples were taken at time 0, 10 min, 20 min, 30 min, 1 h, 2 h and 4 h and analysed immediately by HPLC. Similarly, the stability of **53** was examined in simulated intestinal fluid prepared according to the USP 2010.[167] Containing monobasic potassium phosphate, sodium hydroxide and pancreatin, it is pH adjusted to pH 6.8 to represent the higher pH of the small intestine. The stability was examined over 6 h to simulate the longer residence time in the small intestine.

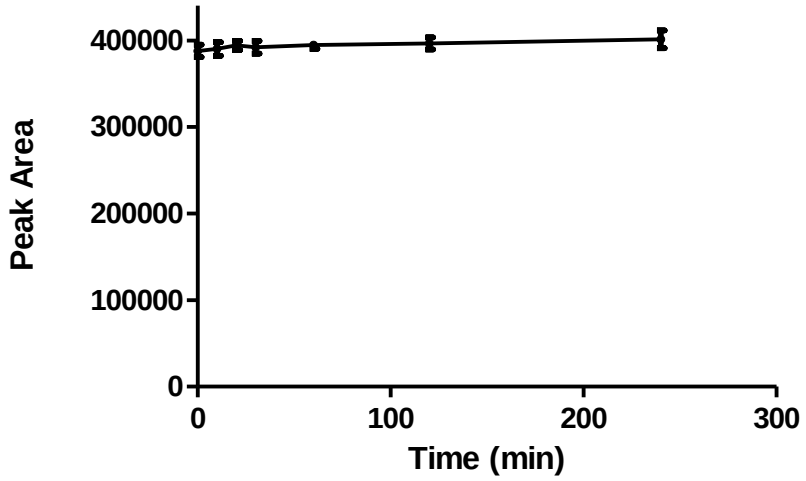

*Figure 48. Graph of HPLC peak area of compound **53** 100 µM in simulated gastric fluid incubated at 37°C over 4 h. The points and error bars represent mean peak area ± SD at that sampling time point carried out in triplicate in three separate experiments on three different days.*

There was no loss of peak area while incubated at 37°C in simulated gastric fluid for 4 h indicating that **53** is stable in the presence of pepsin at the acidic pH of the stomach (Figure 48).

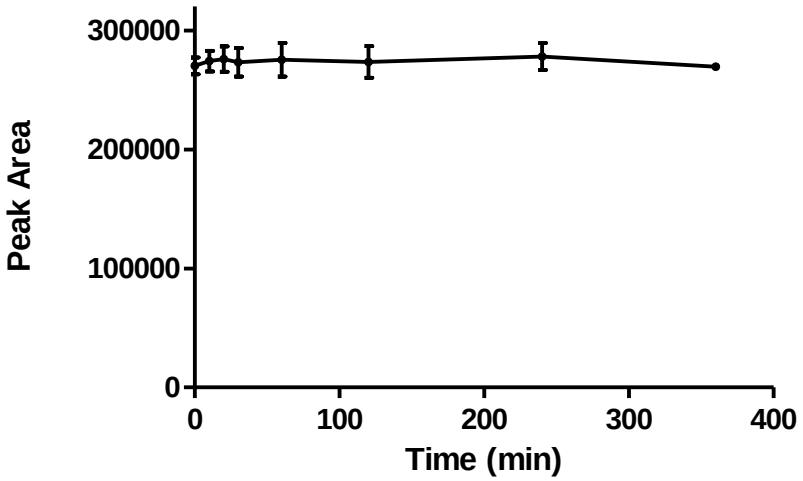

*Figure 49. Graph of HPLC peak area of compound **53** 100 µM in simulated intestinal fluid incubated at 37°C over 6 h. The points and error bars represent mean peak area ± SD at that sampling time point carried out in triplicate in three separate experiments on three different days*

There was no loss of peak area while incubated at 37°C in simulated intestinal fluid for 6 h (Figure 49) indicating that **53** is stable in the presence of pancreatin at the basic pH of the small intestine.

2.10 Caco-2 cell uptake assay

A Caco-2 cell uptake assay was undertaken to probe the absorption potential of **53**. The Caco-2 cell line is a human epithelial cell line from a colorectal adenocarcinoma of the colon which upon reaching confluence expresses characteristics of enterocytic differentiation.[168] The uptake assay performed here measured the concentration of drug inside cells that are cultured in the usual cell culture plates or flasks. The cells were incubated at 37°C with the compound in media and at a particular time point the medium was completely removed and the cells were gently washed and lysed. The lysate was analysed by HPLC for the presence of compound. The model did not consider paracellular diffusion or aspects of facilitated transport that might be present in a functional monolayer but it was a pragmatic approach to estimating the capacity for test article to penetrate a cell membrane.

The best known cell layer model of the intestinal epithelial cells is the Caco-2 monolayer model. The cells are cultured on a porous filter support insert providing an apical and basolateral compartment in the cell culture plate. The cells are cultured for approximately

21 days and in this time they grow to confluence, develop microvilli on the apical surface and increasingly express transporter proteins. Before an assay is carried out, a measure of transepithelial electrical resistance indicates if the monolayer is continuous and the tight junctions intact. The simplest experiment using this monolayer involves treatment of the monolayer with the test compound in buffered solution on the apical side. Buffer is placed on the basolateral side. The compound diffuses and/or is transported through the monolayer and by taking aliquots from the apical and basolateral compartments at appropriate time points for analysis, the rate of permeation can be calculated. Modifications to the experiment include use of pH gradients or sink conditions where the test compound is sequestered on the basolateral side.

Passive diffusion is the predominant mechanism of transport of small molecule drugs and this is what we sought to investigate here using an adherent monolayer rather than a functional barrier as in the usual Caco-2 set up. Initially, RIPA buffer was used to lyse the cells but a component of this buffer was found to complicate the analysis of the samples by HPLC. There was retention of a component of the matrix on the HPLC column leading to a regular cycling baseline. Instead, the washed cells were gently scraped into PBS. Before analysis the cells were pelleted, the PBS removed and the cells lysed in acetonitrile with sonication. This solution was suitable for direct analysis by HPLC after centrifugation to remove insoluble cellular debris. This approach had dual benefits of simplifying the analysis and concentrating the lysate, thereby enhancing the ability to detect absorbed compound. To ensure there was no loss of water-soluble test compound to the pelleted material, the pellet was dispersed in 200 µL of ddH_2O and sonicated before preparation for HPLC analysis as for the acetonitrile samples.

Compound **53** and its synthetic precursor, compound **51**, were examined in this assay at a test concentration of 10 µM to examine the effect of the DABCO moiety on passive absorption potential. The assay was carried out in triplicate in three different passage numbers on three different days. Compound **51** was detected in the conditioned media and in all the cell lysates indicating its uptake into the cells during the incubation. Compound **53** was detected only in the collected media samples. No peak corresponding to it was found in the cell lysate chromatograms (Figure 50).

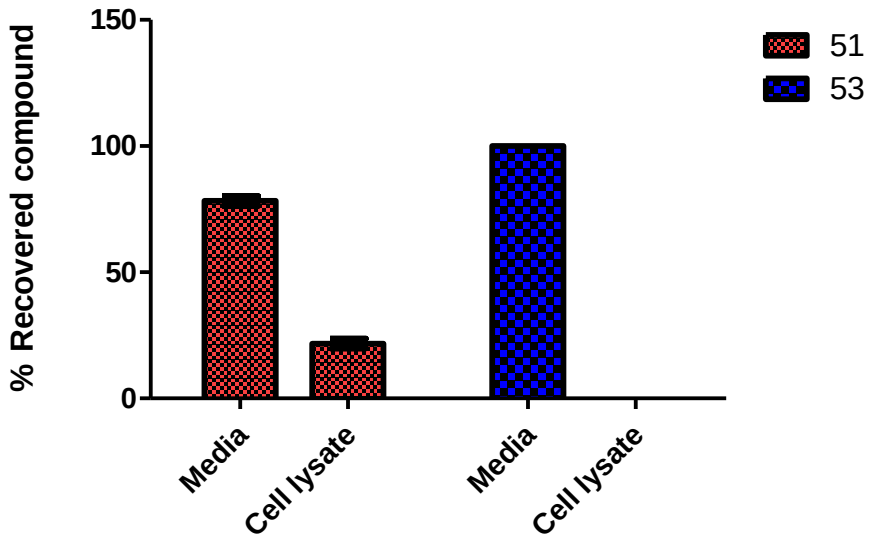

*Figure 50. Results of Caco-2 cell uptake assay for **51** and **53**. Bar chart represents the proportion of total recovered compound detected in the cell culture conditioned media and in the cell lysate for **51** and **53** in the Caco-2 cell uptake assay. The bar chart was generated from the data of experiments in triplicate in three different passage numbers and the error bars represent ± SEM*

As compound **53** was a potent MMP-9 inhibitor, exhibited stability in the environmental conditions of the GIT and demonstrated limited absorption potential, it was assessed *in vivo* in a DSS mouse model of colitis.

2.11 *In vivo* assessment of compound 53

Animal models of disease allow us to investigate disease pathologies and the potential benefit of interventions, pharmacological or other. Animal models of intestinal inflammation include genetically engineered, adoptive transfer, spontaneous and induced models.[169] Genetically engineered models include knock-out (KO) models in which a target gene can be inactivated in the body or conditionally in a particular tissue type or organ. Alternatively, transgenics can be designed to overexpress a particular gene. In the adoptive transfer model, intestinal inflammation is induced by transfer of certain cell types to immunocompromised animals. This model has been used to probe the role of T-cells in colitis.[170] Strains of animal that spontaneously develop intestinal inflammation or an inappropriate immune response are particularly useful as they do not require exogenous manipulation to model colitis. Colitis can be chemically induced in mice with normal immune function by administration of DSS or carrageenan in drinking water or by rectal administration of the hapten TNBS, the hapten oxazolone or acetic acid. Colitis can also be bacterially induced and *Salmonella typhimurium* is commonly used.[170]

DSS is a synthetic sulfated polysaccharide composed of dextran and sulfated anhydro-glucose units. Oral administration of DSS 2 - 10% w/v in drinking water for five to seven days produces an acute colitis in rodents and chronic colitis can be induced by cycling periods of DSS treatment with usual drinking water.[170] The DSS model is useful in that it is easy to perform, produces reproducible results and is relatively cheap. However, the severity of the induced pathology and reproducibility is dependent on a variety of factors including the DSS molecular weight, the DSS source, dose, duration, animal strain and sex[170] and so optimisation of the model may be required. The effects of DSS can be severe and can potentially cause mortality of experimental animals during the course of the experiment or other unacceptable side effects such as excessive weight loss. The model has clinical and histological similarities to UC but it must be considered that the colitis is due to acute chemical injury rather than a chronic inflammation and so will differ from IBD in aspects of immunopathology. DSS can induce colitis in T-cell and B-cell deficient severely combined immunodeficiency (scid) mice indicating that acute damage is initiated by the innate immune system.[171] There is increased production of macrophage-derived IL-1β, IL-6 and TNF-α.[172] The adaptive immune system is subsequently activated and chronic colitis is mediated by a combination of T_H1 and T_H2 responses.[173] It was thought that DSS was directly toxic to the epithelial cells[174] but the work of Laroui *et al*. established that DSS can associate with medium-chain length fatty acids to form nano-sized vesicles which can

penetrate the epithelial cells allowing the dextran moiety to activate inflammatory signalling pathways.[175] The DSS model is widely reported facilitating the rapid screening of drug candidates for potential effects in IBD and was chosen as a model for evaluation of compound **53** *in vivo*.

2.11.1 Experimental animals

The *in vivo* experiment was carried out with approval of the Animal Research Ethics Committee, Trinity College and licensed by the Department of Health under Section 8 of the Cruelty to Animals Act, 1876 and adhered to ARRIVE guidelines. A total of 24 male BALB/c mice (Comparative Medicines Unit, Trinity College Dublin) were used. Animals were maintained in a restricted access room in the facility at 23°C with 12 hour: 12 hour light-dark cycles and access to drinking water and standard food pellets *ad libitum*. Animals were housed in individually ventilated cages (IVCs) with a maximum of five animals per cage with standard bedding and enrichment and allowed to settle to conditions for 10 days before the experiment was commenced.

2.11.2 Experimental design

Animals were randomly assigned to experimental groups and one animal constituted an experimental unit. Ten animals were assigned to each of the treatment group and DSS group and four animals were assigned to the sham group. Animals caged together were in the same experimental group.

2.11.3 *In vivo* experimental procedures

Colitis was induced by oral DSS (mol. wt. 40,000; TdB consultancy, Sweden) at 5% w/v in the usual drinking water. On day 0 of the experiment, the usual drinking water of the positive control DSS group and the treatment group was replaced with the DSS solution and consumption was monitored for the duration of the experiment. The sham group continued to drink the usual drinking water. The treatment group were administered compound **53** at a dose of 10 mg/Kg by oral gavage once daily in the morning from day 0 to day 6 and the DSS group received the water vehicle by oral gavage. The animals were weighed and examined for signs of softened stool or diarrhoea or evidence of blood in the stool or rectal bleeding. Diarrhoea was defined as the presence of faecal matter adherent to the fur or tail and rectal bleeding as the visible presence of blood around the rectal area. Each animal was assigned a disease activity index (DAI) score for weight loss, stool

consistency and presence of blood as in Table 1 and these scores were combined and averaged to generate the daily score.

Table 1. DAI scoring system for daily clinical assessment of the DSS induced colitis mouse model

DAI Score	Weight Loss (%)	Stool Consistency	Presence of Blood
0	<1	Normal	None
1	1 - 5	-	-
2	5 - 10	Soft stool	Blood in stool
3	11 - 15	-	-
4	>15	Diarrhoea	Gross rectal bleeding

At the endpoint of the experiment on day 6, the animals were euthanized by cervical dislocation by Dr. Carlos Medina, School of Pharmacy, Trinity College, Dublin. A mid-laparotomy was performed and the distal colon was removed for future histological analysis, protein analysis and RNA analysis.

The development and progression of the disease in each group as quantified by the group mean DAI score ± SEM from the beginning of the experiment on day 0 to the termination of the experiment on day 6 can be seen in Figure 51.

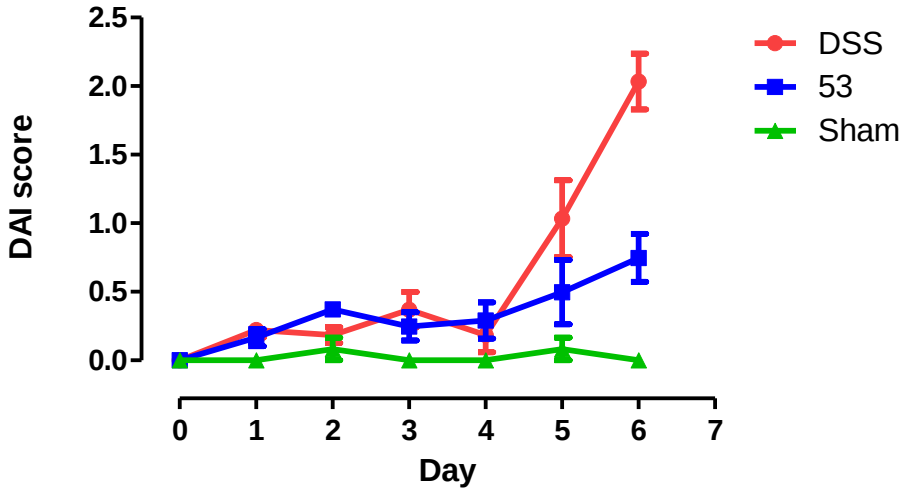

Figure 51. Graph of disease progression from day 0 to day 6 in each experimental group quantified by the daily group mean DAI ± SEM

As expected, the animals in the sham group did not develop colitis. The progression of the disease in the positive control group and the treatment group was similar from day 0 to day 4 but on day 5, the symptoms of colitis in the positive control group were trending to greater than that of the treatment group. By day 6, the treatment had significantly ameliorated the severity of the DSS induced colitis, the treated group scoring significantly clinically better than the DSS group by one-way ANOVA as can be seen in Figure 52.

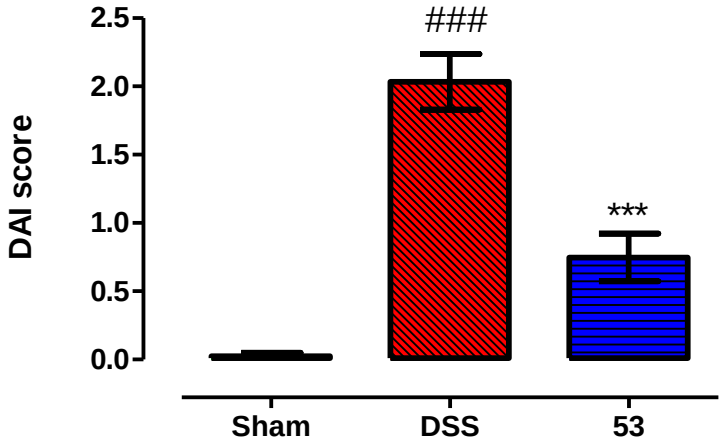

*Figure 52. Histogram of the mean DAI scores ± SEM of the experimental groups on day 6. ### p < 0.001 vs sham; *** p < 0.001 vs DSS group*

The contributions of the clinical symptoms to the final DAI scores on day 6 are represented in Figure 46 for the experimental groups and in Figure 47 for the experimental units.

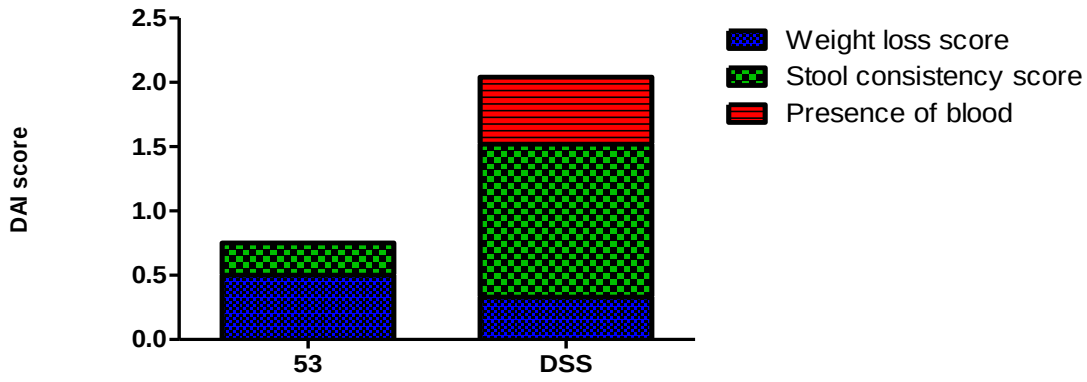

Figure 53. Stacked bar chart illustrating the clinical symptom contribution to the mean DAI score for the DSS group and treatment group on day 6

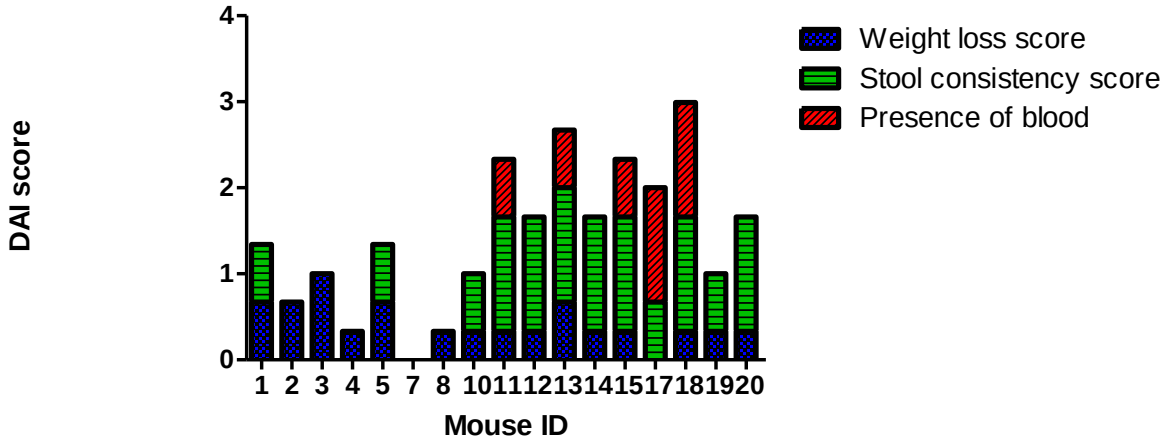

Figure 54. Stacked bar chart illustrating the clinical symptom contribution to the mean DAI score for each experimental unit in the DSS group and treatment group on day 6 mouse IDs 1 – 10: treated group; mouse IDs 11 – 20: DSS group

No animal in the treated group exhibited symptoms of blood in stool or rectal bleeding whereas five of the mice in the DSS group scored for presence of blood on the last day. All individuals in the DSS group had a stool consistency indicative of colitis but more than half the treated group registered a normal stool consistency on the final day. We were concerned that there was a trend to greater weight loss in the treated group but in Figure 55 it can be seen that the weight change in the DSS group and in the treatment group followed a similar course. The stress induced by oral gavage appears to have caused some weight loss in the first two days as has been documented in other studies.[176, 177] This was followed by partial to full recovery over days 3 to 4 until the colitis came into effect from day 4. No weight loss was observed in the sham group.

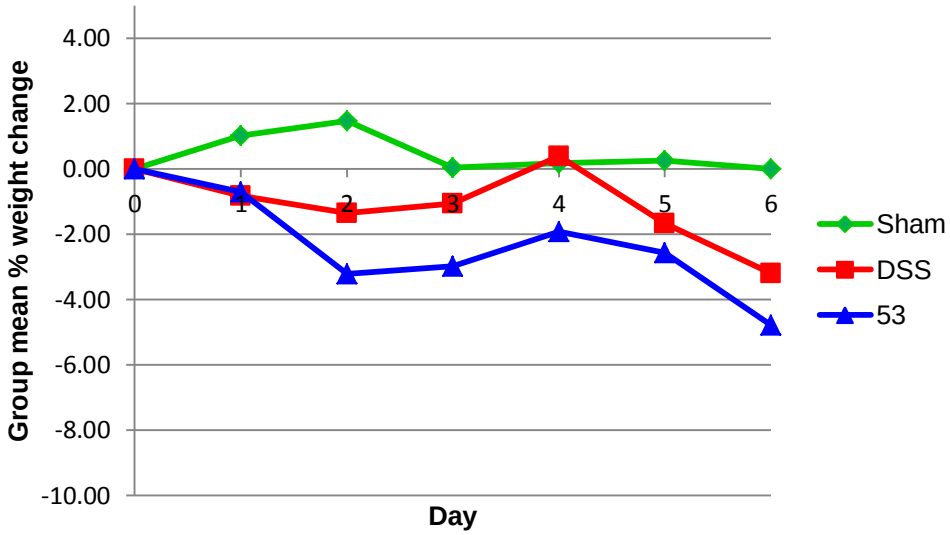

Figure 55. Graph of mean weight change progression in the experimental groups from day 0 to day 6

2.12 Histological analysis of colon tissue samples

Retained tissue samples were histologically analysed for signs of inflammation. To prepare sections for staining the tissue samples were first subjected to an automated tissue processing protocol which resulted in dehydrated, clarified and paraffin infiltrated colon samples. Following processing, the colon tissue samples were paraffin embedded, sectioned and mounted on glass slides for staining with hematoxylin and eosin (H & E). The standard H & E histological stain uses two separate dyes to stain the nucleus and cytoplasm of connective tissue. Hematoxylin is a dark purple basic dye that will stain chromatin within the nucleus leaving it a dark purple/blue colour. Eosin is a dark orange-red acidic dye that stains cytoplasmic material and ECM material various shades of red,

pink and orange. The staining protocol deparaffinises the tissue in xylene and passes it through a step gradient of decreasing ethanol concentrations to rehydrate the tissue before staining. After staining, the tissue is then dehydrated in a series of increasing ethanol concentrations before clearing in xylene. The slides are then mounted and coverslipped.

2.12.1 H&E histological analysis

Colitis severity was assessed by scoring inflammatory cell infiltration and tissue damage according to the scoring system outlined in Table 2. Histological scoring was performed blind by Dr. Brian Flood, School of Biochemistry and Immunology, TBSI, Trinity College Dublin.

Table 2. Colitis severity histological scoring system

Infiltration	Score
Occasional infiltration in lamina propria	0
Increased infiltrate in lamina propria (predominantly at base of crypts)	1
Extension of infiltrate into mucosa	2
Transmural extension of infiltrate	3
Tissue damage	Score
No mucosal damage	0
Partial (<50%) loss of crypts in large areas	1
Partial to total (50-100%) loss of crypts in large areas	2
Total loss of crypts in large areas and epithelial loss	3

A combined score for each experimental unit was calculated by summing the scores obtained for infiltration and tissue damage and dividing by 2.

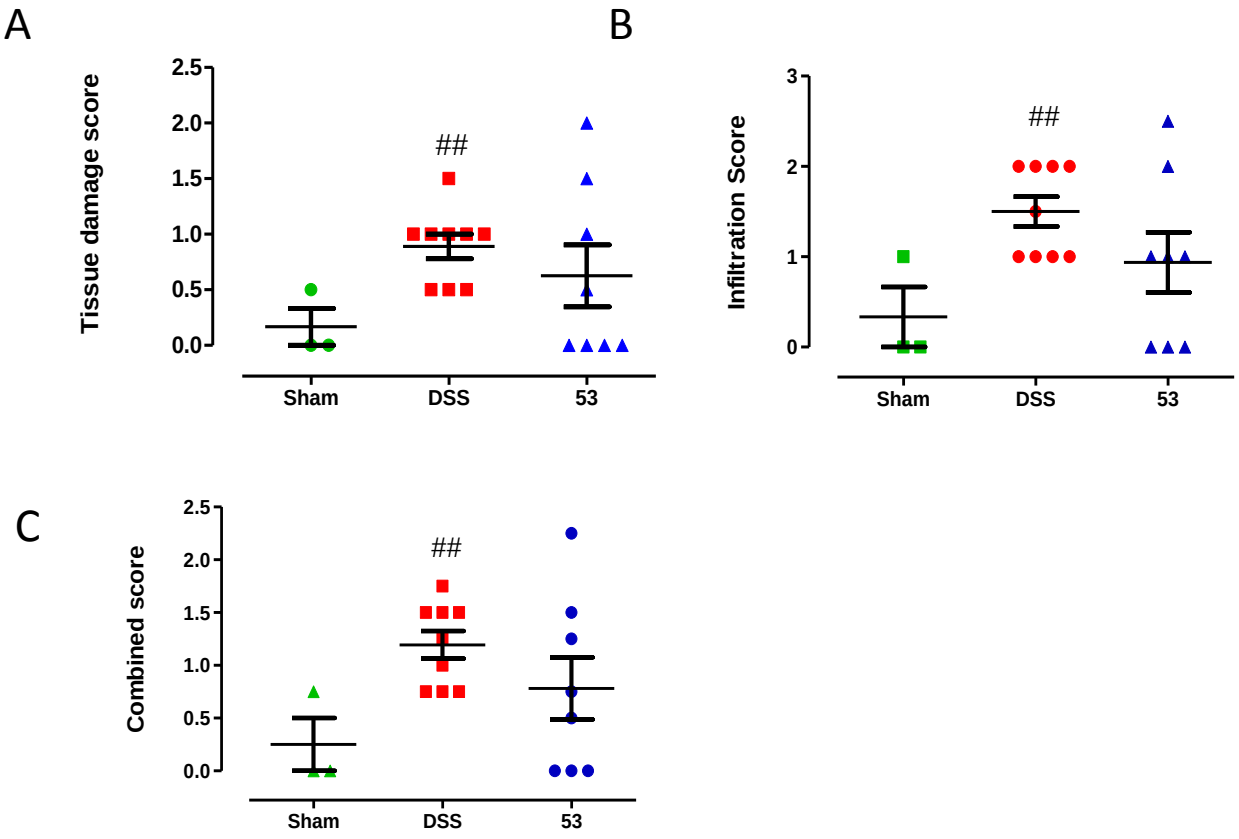

Figure 56. Histological scores of the grouped experimental units; A: tissue damage; B: inflammatory cell infiltration; C: combined score of tissue damage and infiltration; ## p < 0.01 vs sham

In the treatment group, four mice were scored zero for tissue damage indicating no mucosal damage was observed and three of the group were scored zero for infiltration indicating only occasional infiltration of inflammatory cells in the lamina propria. In contrast, every experimental unit in the DSS group had at least partial loss of crypts and increased evidence of infiltrate. However, there was high variability in the treatment group with some individuals exhibiting epithelial damage and inflammation comparable to the DSS group. The mean tissue damage score of the treatment group was not significantly different from that of the positive control group by a two-tailed unpaired t-test (*p* value = 0.4968). Statistical analysis of the infiltration scores assigned was similar. The mean of the treatment group could not be statistically distinguished from the mean of the positive control group by a two-tailed unpaired t-test (*p* value = 0.3278). In healthy tissue with normal crypt architecture, the base of the crypt sits on the muscularis mucosa. In DSS

induced colitis, shortening of the crypts and loss of the basal third of the crypt is one of the earliest histological changes. As the disease condition progresses there is further crypt loss and thinning of the epithelium until crypt loss can be described as total. The surface epithelium may show erosion. The first sign of accompanying inflammation is enlargement of the lamina propria. The inflammatory cell infiltrate in the lamina propria is increased in comparison to normal tissue. This mixed infiltrate of both acute and chronic inflammatory cells extends into the mucosa and submucosa and into the epithelial cells themselves inducing cryptitis or crypt abscesses.[178]

Representative images from each group can be seen in Figure 57. In panels A and B, the intact crypt architecture extends to the muscularis mucosa which is characteristic of normal healthy tissue from an animal in the sham group. In panels C and D, images from an animal in the DSS group show the effect of DSS on the tissue. There is loss of basal portions of crypts in all areas with complete loss in some areas accompanied by enlargement of the lamina propria and inflammatory cell infiltrate. In panels E and F, the attenuating effect of the treatment on the DSS colitis can be seen. While there is some crypt loss and increased infiltrate due to DSS, the crypt architecture has largely remained intact.

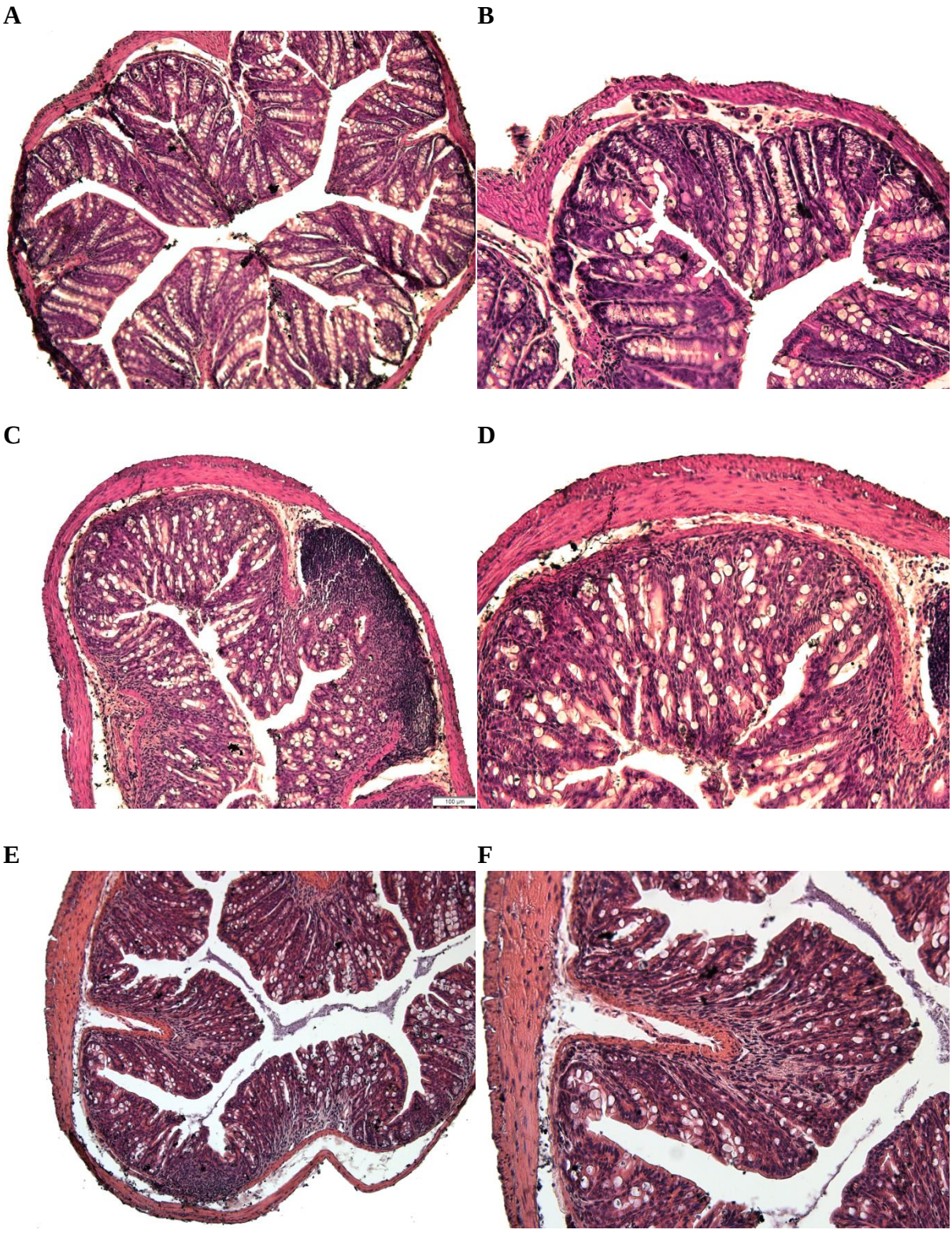

*Figure 57. Representative histology images from the experimental groups **A**: sham 10× magnification **B**: sham 20× **C**: DSS 10× **D**: DSS 20× **E**: Treatment 10× **F**: Treatment 20×*

2.13 The effect of compound 53 treatment on pro-inflammatory cytokines at gene level

Having observed that compound **53** could attenuate the severity of DSS colitis in mice, we wanted to examine if there was an anti-inflammatory effect at gene level. The treatment effect of **53** on the mRNA of TNF-α, IL-1β and IL-6 in colon tissue samples retained from the DSS mouse model was examined.

2.13.1 RNA Isolation

Total RNA was isolated using the RNAqueous® Kit (Applied Biosystems), a column-based system, according to the manufacturer's instructions. The procedure involves disruption of the sample with a proprietary lysis buffer, a high concentration guanidinium salt solution that lyses the cells and denatures endogenous RNAses. The sample is diluted with an ethanol solution to make the RNA competent for binding to the glass fibre filter in the RNAqueous filter cartridge. As the lysate ethanol mixture is pulled through the filter, the RNA is bound while most cellular contents pass through. A sequence of washes removes contaminants before the RNA is eluted by warmed elution buffer, a very low ionic strength solution. The RNA was quantified and normalized for reverse transcription.

2.13.2 Reverse Transcription

Total RNA was quantitatively converted to single-stranded cDNA for PCR applications using a High Capacity cDNA Reverse Transcription Kit (Applied Biosystems) according to the manufacturer's protocol. Briefly, a 2× reverse transcription mastermix is prepared to which an equal quantity of RNA template is added. Reverse transcription is then performed in a thermal cycler. The kit uses a random primer scheme for initiating cDNA synthesis. The synthesis occurs efficiently with all species of RNA molecules present, including mRNA and rRNA. The reverse transcription reaction must generate products directly dependent on the amount of input RNA template and in all test cases, this kit has yielded quantitative conversion of mRNA and 18S ribosomal RNA.

2.13.3 Polymerase chain reaction (PCR)

In this step, DNA polymerase amplified the cDNA synthesized from the RNA samples. PCR involves an initial denaturation step at 95° to separate double-stranded DNA (dsDNA) into single-stranded DNA (ssDNA). The temperature is then lowered to 60° to promote annealing of the primer to the template. Extension by a DNA polymerase

generates a new strand. We used Taqman® gene expression assays (Applied Biosystems) in our analysis which contain sequence specific forward and reverse primers and a probe detection system. The probe is an oligonucleotide labelled with a reporter dye at the 5' end and a quencher moiety at the 3' end. As the DNA polymerase extends from the primer, it encounters the probe situated on the same strand and hydrolyses the reporter dye into solution causing an increase in fluorescence. As cycles of denaturation, annealing and extension proceed, there is exponential amplification of the amplicon and the fluorescent signal produced is directly proportional to amplicon yield. In conjunction with the Taqman® gene expression assays and the cDNA templates, we used Taqman® Universal PCR MasterMix II, with UNG (Applied Biosystems) to prepare the samples for PCR. Supplied at 2× concentration, it contains Amplitaq Gold® DNA Polymerase, dNTPs (with dUTP), ROX™ passive reference, uracil-N glycosylase (UNG) and optimized buffer components. Eukaryotic 18S was used as the endogenous control and the results were analysed by the comparative C_T method.[179] For a sample, the difference between the C_T of the gene of interest and the C_T of the endogenous reference gene (18S) is the ΔC_T value. Fold change in comparison to a reference sample is given by $2^{-\Delta\Delta CT}$ where $\Delta\Delta C_T$ is the difference between the ΔC_T of the sample and the ΔC_T of the reference sample. Fold change was calculated with reference to a median animal from the sham group. Fold change results were Log transformed to allow the application of parametric statistical tests. One-way ANOVA was applied and where the result was significant, Bonferroni's multiple comparison test was applied as post-test.

2.13.4 The effect of compound 53 treatment on IL-1β at gene level

The expression of IL-1β mRNA was upregulated in the DSS group in comparison to the sham group as expected ($p < 0.01$). The expression of IL-1β was reduced by 6.4 fold in the treated group in comparison to the DSS group and this reduction was statistically significant as shown in Figure 58A. The expression of IL-1β at gene level also correlated well with the DAI score as shown in Figure 58B.

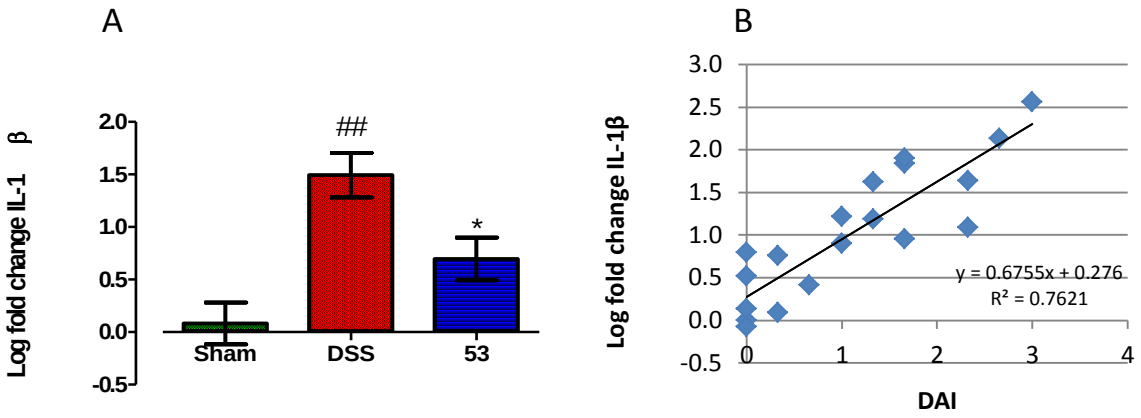

*Figure 58. Effect of compound **53** treatment on IL-1β expression at gene level in a murine DSS model of colitis. **A**: Histogram of the mean Log fold change in IL-1β ± SEM in the experimental group, ## $p < 0.01$ vs sham; * $p < 0.05$ vs DSS group **B**: Graph of linear regression of Log fold change in IL-1β mRNA on day 6 DAI score, $r^2 = 0.76$*

2.13.5 The effect of compound 53 treatment on TNF-α at gene level

The expression of TNF-α mRNA was upregulated in the DSS group in comparison to the sham group as expected ($p < 0.01$). The expression of *TNF-α* was reduced by 7.4 fold in the treated group in comparison to the DSS group and this reduction was statistically significant as shown in Figure 59A. The expression of TNF-α at gene level correlated well with the DAI score as shown in Figure 59B.

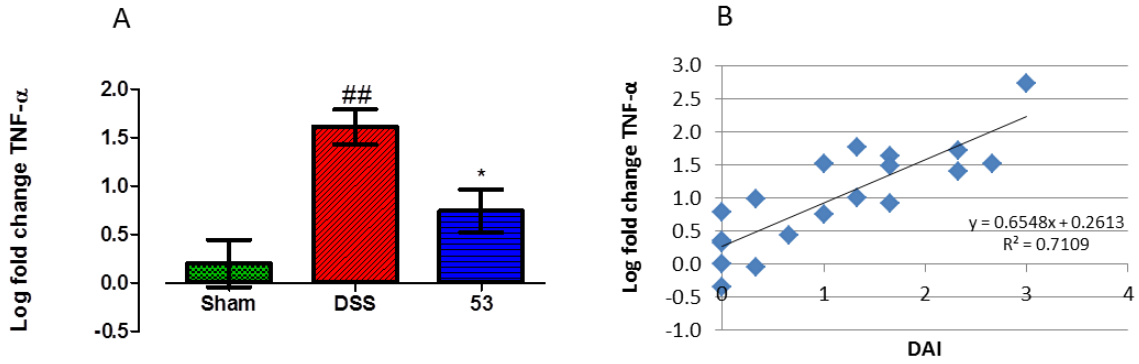

*Figure 59. Effect of compound **53** treatment on TNF-α expression at gene level in a murine DSS model of colitis. **A**: Histogram of the mean Log fold change in TNF-α ± SEM in the experimental groups, ## p < 0.01 vs sham; * p < 0.05 vs DSS group **B**:Graph of linear regression of Log fold change in TNF-α mRNA on day 6 DAI score, r^2= 0.71*

2.13.6 The effect of compound 53 treatment on IL-6 at gene level

The expression of IL-6 mRNA was upregulated in the DSS group in comparison to the sham group as expected (p < 0.01). The expression of *IL-6* was reduced by 9.3 fold in the treated group in comparison to the DSS group and this reduction was statistically significant as shown in Figure 53A. There was also good correlation between the expression of IL-6 at gene level and the DAI score as shown in Figure 53B.

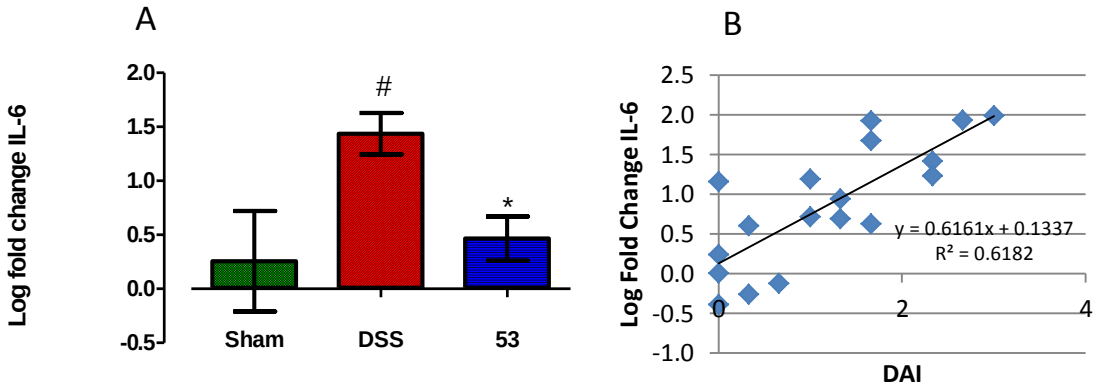

*Figure 60. Effect of compound **53** treatment on IL-6 expression at gene level in a murine DSS model of colitis. **A**:Histogram of the mean Log fold change in IL-6 ± SEM in the experimental groups, # p < 0.05 vs sham; * p < 0.05 vs DSS group **B**:Graph of linear regression of Log fold change in IL-6 mRNA on day 6 DAI score, r^2= 0.61*

2.13.7 The effect of compound 53 treatment on MMP-9 and MMP-2 proteolytic activity

MMP-9 activity in the colon samples was assessed by zymography. Gross and Lapière developed an assay to detect collagen degradation in tadpole tissue describing an MMP for the first time in 1962.[180] Zymography involves the study and visualization of enzyme activity by substrate conversion. The proteins are separated according to molecular weight by sodium dodecyl sulfate polyacrylamide gel electrophoresis (SDS-PAGE) under nonreducing conditions.[181, 182] The polyacrylamide separating gel is co-polymerized with a suitable substrate, gelatin in the case of the gelatinases MMP-2 and MMP-9. During electrophoresis the MMPs are reversibly denatured but in the subsequent washing step exchange of the SDS with Triton X-100 allows the enzyme to partially renature. Incubation of the gel allows the reactivated enzymes to digest the gelatin. After incubation, staining with Coomassie Blue reveals the MMPs as clear bands on a blue background. These bands can be quantified by densitometry. Proenzyme forms can be detected as a different band corresponding to their higher molecular weight.

The protein samples were prepared by cell disruption in homogenization buffer with added aprotinin 60 µg/mL and leupeptin 10 µg/mL as protease inhibitors. The samples were quantified for total protein using the Bio-Rad protein assay and normalized before zymography. The Bio-Rad protein assay is a colorimetric assay based on the Bradford dye-binding method.[183] The absorbance maximum for an acidic solution of Coomassie brilliant Blue G – 250 dye shifts from 465 nm to 595 nm when binding to protein occurs, visible as a colour shift from green-red to blue. At appropriate ratios of dye volume to sample concentration, Beer's law can be applied to quantitate total protein concentration by measuring the absorbance at 595 nm. A standard curve was prepared using serial dilutions of bovine serum albumin standard in the concentration range 400 – 0 µg/mL. Conditioned media from HT1080 cells stimulated with phorbol 12-myristate (PMA) at a concentration of 10 µM for 24 h was provided by Dr. Jun Wang, School of Pharmacy, TCD and used as a control in zymography to identify the bands. HT1080 cells have been shown by Lohi *et al*. to secrete 92 kDa proMMP-9 and 72 kDa proMMP-2 with partial proteolysis of proMMP-2 to active forms on stimulation with PMA[184] and this method has been used by the Gilmer and Medina groups also.[185]

In the representative gel in Figure 61 panel C, the gelatinase bands in the HT1080 control in the left hand lane are indicated. In the samples, the bands positioned slightly above the HT1080 92 kDa MMP-9 are attributed to murine MMP-9. Highly glycosylated, it appears at 105 - 110 kDa.[186]

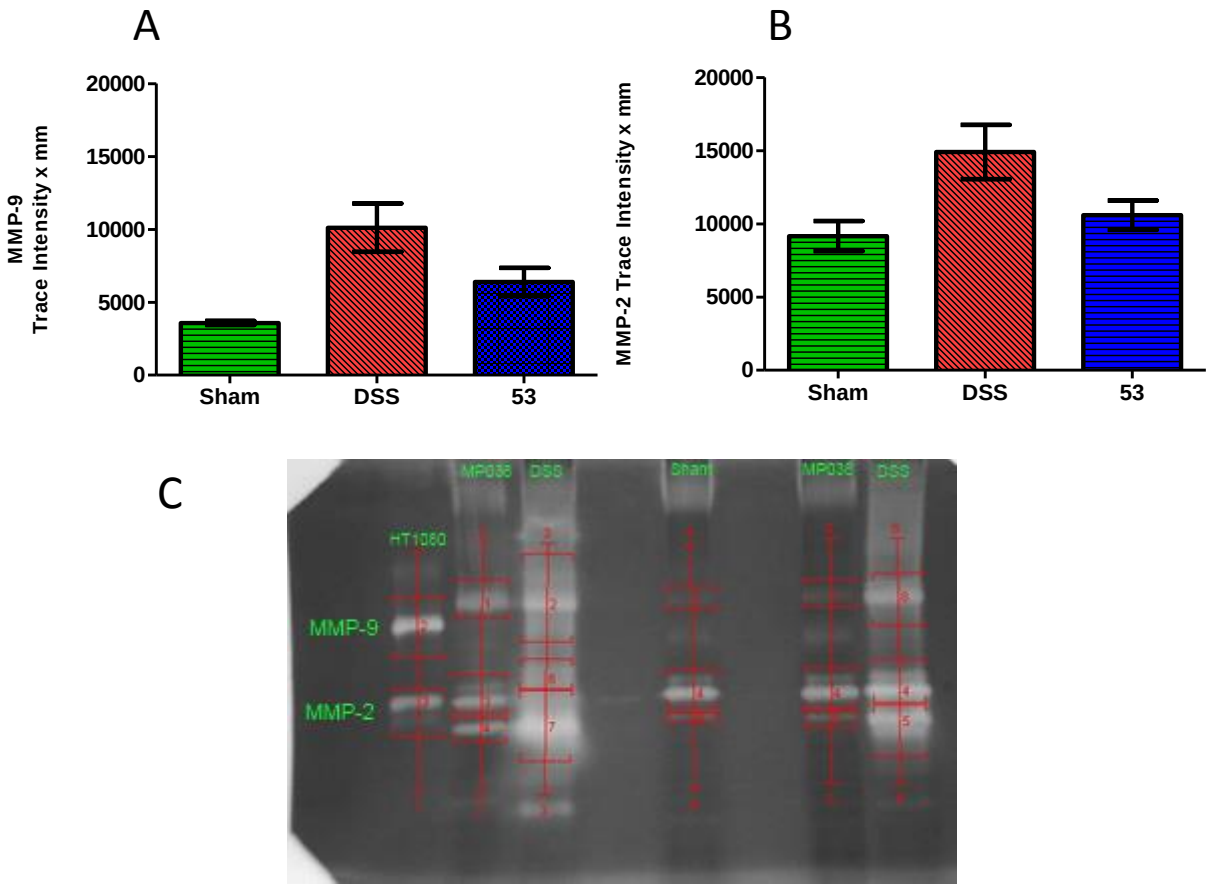

*Figure 61. Effect of compound **53** treatment on MMP-9 and MMP-2 proteolytic activity in a murine DSS model of colitis **A**: Histogram of the group mean MMP-9 band intensity ± SEM determined by zymography **B**: Histogram of the group mean total MMP-2 band intensity ± SEM determined by zymography **C**: Representative zymography gel. Representative samples in lanes from left to right HT1080 control; treated group; DSS group; sham group; treated group; DSS group*

MMP-9 activity is negligible in the sham group. Exposure to DSS upregulated MMP-9 at protein level and there is a trend to reduced MMP-9 activity in the treated group in comparison to the DSS group but by an unpaired two-tailed t-test this reduction is not statistically significant (p value = 0.09; panel A Figure 61). MMP-2 is constitutively expressed and a strong band corresponding to MMP-2 was seen in sham samples. Several

bands were seen in close proximity to the HT1080 MMP-2 control attributed to proMMP-2 and activated forms thereof. The densitometry measurements of these bands were summed to yield a value for total MMP-2 potential proteolytic activity. Exposure to DSS upregulated MMP-2 at protein level. There was a trend to reduced MMP-2 activity in the treated group in comparison to the DSS group but by an unpaired two-tailed t-test this reduction is not statistically significant (p value = 0.07; panel B Figure 61).

2.14 Discussion

Compound **53** was designed to be an active site directed gelatinase inhibitor but with limited intestinal absorption potential. Based on an established barbiturate scaffold, the C-5 substituents occupy the S1' and S2' pockets of the enzyme and the barbiturate ring co-ordinates the catalytic Zn of the active site. Compound **53** is a potent inhibitor of human MMP-9 with an IC_{50} of 6.34 nM as measured by fluorogenic assay. Designed devoid of functional groups generally labile to the endogenous enzymes of the GIT such as esters or amides, **53** was found to be stable in simulated conditions of the stomach and small intestine for time durations exceeding expected residence times. When initially considering the introduction of a permanent positive charge as an absorption limiting strategy, we were concerned that repulsion between the Zn and quaternary ammonium group might be detrimental to potency. On the contrary, potency was improved over synthetic precursors. Perhaps any repulsive forces encourage correct orientation and approach of the inhibitor to the enzyme. As a quaternary ammonium salt, **53** has excellent water solubility and ease of solvation may contribute to potency.

The membrane permeability of compound **53** was reduced relative to compound **51**, its synthetic precursor. Carrying a permanent positive charge, it would not be expected to have good passive uptake potential. This was demonstrated in a model of passive uptake in Caco-2 cells. Compound **53** was not detected in the cell lysate. The positively charged DABCO derived moiety, however, may not preclude carrier mediated uptake or paracellular transport through the tight junctions. Enterocytes are equipped with an array of transport proteins some specialists in cation transport.[187] Members of the solute carrier (SLC) transporters, OCTN1 and OCTN2 mediate uptake of cations from the gut lumen by cation exchange. The primary physiological function of OCTN2 in the gut is uptake of L-carnitine and while OCTN1 also facilitates carnitine absorption its primary endogenous substrate is ergothioneine. On the basolateral membrane, OCT1 mediates uptake of small, hydrophilic cations into enterocytes.[188, 189] The ATP binding cassette (ABC) efflux transporters are abundantly expressed on the apical membrane and efflux is ATP-driven allowing efflux against a concentration gradient. One of the most widely studied, P-glycoprotein (P-gp) is responsible for efflux of xenobiotics and toxins in the gut and is implicated in reducing the bioavailability of many drugs. The substrates of P-gp are diverse, ranging in size from 200 Da to over 1000 Da and can be charged or neutral, hydrophobic or amphipathic or more hydrophilic. Type II cations, often polyvalent and bulky with a size > 500 Da have been found to be substrates.[190] Most OCT research has

focused on transport in the kidney and liver where they are more abundantly expressed and the SAR available in the literature is limited but with a molecular weight of 598 g/mol, compound **53** is larger than the currently known substrates of OCTs. Paracellular transport through the tight junctions in the intestinal epithelium is generally only available to small polar molecules with molecular radii < 4.5 Å.[191] A second 'leak' pathway is available to larger molecules and permeability to molecules with molecular weights up to several Kg/mol has been reported. This transport can be considered as transient openings in the epithelium and is a minor absorption pathway.[192]

A gut confined drug candidate cannot be unequivocally determined as strictly gut-confined. It is inevitable that some fraction of the drug or metabolites thereof will reach the systemic circulation. In this context we equate gut-confined to gut-limited, an approach which maximises drug concentration at the target disease site whilst minimising systemic exposure sufficiently to offer an acceptable safety profile. The physicochemical properties of **53**, in particular its charge and molecular weight of > 500 Da, make it a poor candidate for absorption. While a 'leaky' damaged epithelium in IBD could theoretically facilitate systemic exposure, such a drug should still be gut-limited, the compromised surface area comprising only a fraction of the total surface area for absorption in the GIT.

Treatment with compound **53** reduced the severity of DSS-induced colitis in mice and ANOVA analysis of the group DAI scores on the final day of the experiment indicated that the effect was statistically significant ($p < 0.001$). Histological analysis of retained colon samples from the DSS model confirmed the development of colitis in the DSS treated animals. In the DSS control group, all animals exhibited tissue damage and crypt loss combined with increased levels of inflammatory cell infiltrate. More than half the animals in the group had registered scores for rectal bleeding on the last day and the entire group exhibited altered stool consistency. There was high variability in the treated group, some animals having histology scores comparable to the DSS control group and some animals scoring comparable to normal healthy tissue samples of the sham group. We do not know if this could be due to variable response to the treatment between different experimental units and/or the small sample size may mean the experiment is underpowered. With this high variability in the samples, the treatment group cannot be statistically distinguished from the other groups. However, the results do indicate a clinically significant effect occurred. In the treatment group, half the animals were blindly scored 0 for tissue damage indicating no mucosal damage and three of the group were scored 0 for infiltration indicating only occasional infiltration of inflammatory cells in the lamina propria

characteristic of healthy non-inflamed tissue. Combined with the clinical observation that no treated animal developed blood in stool or rectal bleeding over the course of the experiment and more than half the group registered normal stool consistency scores on the last day, it is possible to conclude there was a treatment effect.

PCR analysis of the colon samples retained from the colitis model indicated that the clinical effect of the treatment was reflected at gene level by a reduction in mRNA markers of inflammation. The pro-inflammatory cytokines TNF-α, IL-1β and IL-6 were downregulated 7.4 fold, 6.4 fold and 9.3 fold respectively at gene level in the treated group compared to the DSS control group and these downregulations were statistically significant. Loss of immune tolerance in IBD triggers excessive cytokine responses. In response to TLR signalling, antigen presenting cells (APCs) such as dendritic cells and macrophages produce pro-inflammatory cytokines.[193] There is increased activation of the IL-1 system and IL-1β levels in the colon correlate with disease activity in UC patients.[194] IL-1β further activates APCs and promotes T-cell activation and survival.[195] IL-6 is also upregulated in IBD tissues[196] and it activates multiple cell types further augmenting cytokine production and prolongs effector T-cell survival. Blockade of IL-6 signalling is associated with reduced levels of IFNγ, TNF and IL-1β and a pilot study of human anti-IL-6 receptor monoclonal antibody in active Crohn's disease patients over 12 weeks found a clinical effect.[197] The roles of TNF in IBD pathology are many.[193] It is produced membrane–bound but undergoes cleavage by TNF-converting enzyme (TACE or ADAM17) to release soluble TNF. However it is the membrane bound form that is most implicated in IBD, selective antagonists of soluble TNF failing to show clinical effect. It is produced by many cell types including macrophages, dendritic cells, T-cells, adipocytes and fibroblasts and also targets many cell types. In endothelial cells it promotes angiogenesis and hypervascularization. It activates macrophages and T-cells to pro-inflammatory cytokine production including IL-6, IL-1β and further TNF and prolongs effector T-cell survival via induction of TNF receptor-associated factor 2 (TRAF2) and activation of NF-κB. TNF impairs intestinal barrier function directly by activating cell death pathways such as receptor-interacting protein kinase induced necroptosis and indirectly by driving MMP production altering MMP/TIMP balances.[193] The clinical success of anti-TNF agents can be attributed to the pleiotropy of its effects in IBD. Blockade of TNF obstructs many damaging pathways at play in IBD simultaneously. Targeting other cytokines has yielded disappointing results in some cases despite strong

evidence of involvement in pathology perhaps due to the availability of compensatory mechanisms in this complex network.

Roles for MMPs beyond simple matrix remodelling continue to unfold including cell signalling and chemokine and cytokine processing. Likewise, the ECM must be thought of as more than an architectural scaffold for the body's processes. The ECM itself has signalling functions acting as a source of signalling ligands. Growth factors embedded in the ECM may be released by general matrix degradation or in some cases a pro- or bound form is cleaved to release the mature form. The example of transforming growth factor-beta (TGF-β) illustrates the crucial roles MMPs can play. TGF-β is secreted to the ECM in a latent complex and activation by disruption of its association to a latency associated peptide (LAP) can be mediated by MMP-2 or -9 leading to release of mature ligand.[198] ECM components can themselves act as signals exerting physiological effects upon liberation by MMPs e.g. the anti-angiogenic peptide tumstatin is generated by MMP-9 cleavage of the α3 chain of collagen IV.[199] Cells receive mechanosensory signals from the ECM and exhibit durotaxis or migration based on the stiffness gradient of the ECM.[200, 201] Changes in the matrix may initiate or potentiate disease.

In the present work, analysis of MMP-9 at protein level by zymography indicated there was a trend to reduced MMP-9 activity in the tissue homogenate of the treated group compared to the DSS group. Care must be taken in the interpretation of zymography results as it cannot distinguish between an active species and a species inhibited by a non-covalently bound inhibitor. During zymography, endogenous TIMPs and introduced MMP inhibitors will be dissociated from the enzyme during electrophoresis. For this reason, bands must be considered to represent potential activity as they may not represent true activity *in vivo*. Any reduction in band intensity we see in the treated group is a secondary effect to disruption of the self-potentiating cycle of inflammation. Inhibition of MMP-9 released on exposure to DSS reduces matrix degradation dampening the inflammatory response, reducing cytokine induction and further downstream production and secretion of MMP-9. Xu *et al*. demonstrated that chronic neutrophilic inflammation is self-propagating and MMP-9 dependent.[202] In inflammation, chemokines act on CXCR1 and CXCR2 receptors on neutrophils to induce chemotaxis. Il-8 is one such chemokine and also triggers release of MMP-9 from neutrophil storage granules. An MMP hydrolysis product of collagen, N-acetylPro-Gly-Pro (Ac-PGP), can also act on CXC receptors causing neutrophil influx and release of MMP-9. This finding that matrix-derived chemokines can augment their own production in a positive feed-forward loop illustrates the role of MMP-

9 in chronic inflammation. Koelink *et al*. investigated PGP in IBD. They demonstrated that this pathway is active in DSS colitis and that PGP neutralisation could ameliorate disease severity.[203]

2.15 Conclusion

ECM degradation is not an end result of the IBD inflammatory process but rather a dynamic contributor to disease activity with the ability to maintain and augment a vicious cycle of disease activity. In the DSS mouse model, inhibition of local luminally secreted MMPs by compound **53** disrupted this cycle to significantly reduce disease activity as indicated by the clinical scores and reduction in mRNA markers of inflammation. This is the first example of a non-systemic approach to MMP inhibition to target pathophysiological roles in the intestinal tract. The work suggests that disease modifying MMP inhibitors for inflammatory bowel diseases may be efficacious topically and that pathophysiological enzyme is luminally accessible.

Chapter 3. Design, synthesis and *in vitro* evaluation of gut-confined TGR5 agonists and MMP inhibitor-TGR5 agonist conjugates

3.1 Introduction to TGR5

TGR5 also known as membrane-type bile acid receptor (M-BAR), or G protein-coupled bile acid receptor 1 (GPBAR1) is a member of the rhodopsin-like subfamily of G protein-coupled receptors (GPCRs).[204] It is conserved in mammals, expressed in various organs and cell types with diverse physiological roles dependent on tissue type.[204] It was first discovered in 2002 as a cell surface receptor for bile acids[205] but also responds to semisynthetic, synthetic and natural agonists.[206, 207] Cell surface ligand binding at the receptor releases the $G\alpha_s$ subunit of the associated G protein on the inner surface of the membrane which directly stimulates adenylate cyclase to produce cyclic adenosine monophosphate (cAMP) from ATP. The increase in the intracellular second messenger cAMP activates downstream effects depending on cell and tissue type often involving activation of protein kinase A (PKA).[208] TGR5 can also bind to other G proteins.[209]

3.1.1 Physiological roles of TGR5

Functional in diverse cell types, the physiological roles of TGR5 include bile acid homeostasis,[210] glucose homeostasis,[211] metabolism,[212] neural roles[213] and immune system regulation. It is involved in bile acid homeostasis regulating bile composition and bile flow through activity in gall bladder epithelial cells, gall bladder smooth muscle and cholangiocytes.[210] TGR5 also influences glucose homeostasis. Activation induces glucagon-like peptide-1 (GLP-1) secretion improving insulin sensitivity and glycemic control.[211] TGR5 activation increases energy expenditure. In mouse brown adipose tissue and human skeletal muscle, it induces deiodinase 2 (D2). This enzyme converts inactive thyroxine (T4) to active iodothyronine (T3) increasing mitochondrial oxidative phosphorylation via the thyroid hormone receptor.[212] Its action in the enteric nervous system in response to bile acid has been shown to slow intestinal motility but its roles in the central nervous system are largely unknown. TGR5 signalling can modulate the immune system and it is expressed in several immune cell types including monocytes, macrophages, endothelial cells, enteroendocrine cells and dendritic cells. In several models, treatment of TGR5 expressing macrophages with a TGR5 agonist decreased cytokine production.[69, 214, 215] This anti-inflammatory effect seems to be mediated by downstream NF-κB pathway inhibition.[214]

3.1.2 TGR5 as a drug target

Most research into TGR5 as a drug target has focused on its role in glucose homeostasis and its role in limiting body weight gain.[216] Administration of TGR5 agonists improves glucose homeostasis in high-fat diet fed mice and may prove an alternative blood glucose lowering therapy to GLP-1 receptor agonists or dipeptidyl-peptidase (DPP) IV inhibitors. From its initial discovery in 2002, TGR5 was associated with modulation of the immune system, Kawamata *et al*. reporting high expression in human monocytes and rabbit alveolar macrophages.[205] TGR5 stimulation dampens the inflammatory response and so has a potential role in conditions such as liver disease, coronary artery disease and IBD. TGR5 activity exerts a protective effect against atheroma development in a mouse model of atherosclerosis by dampening inflammation and lipid accumulation through its modulation of monocyte to macrophage differentiation.[217] Interestingly, decreased plasma levels of the most potent endogenous agonist of TGR5, lithocholic acid (LCA), have been found to be a predictor of atherosclerosis in a small pilot observational study.[218] In the liver, the roles of TGR5 are complex with potential pharmacological implications for agonists and antagonists. TGR5 activation has been linked with vascular hepatic disorders and hepatic encephalopathy through its stimulation of nitric oxide (NO) and reactive oxygen species (ROS).[219] Further research is necessary to establish if these are potential applications for TGR5 antagonists. Also, cholestatic pruritus might be amenable to TGR5 antagonist treatment. Historically linked to increased circulating bile acid levels, it has been shown to be TGR5 mediated in mice.[220] TGR5 agonism, through its anti-inflammatory effects, has potential application in non-alcoholic fatty liver disease.[221] TGR5 in IBD is discussed later in the section entitled 'TGR5 in IBD'.

3.1.3 TGR5 as an anti-target

Expressed at a higher level in the gallbladder than other tissues, systemic TGR5 stimulation has been consistently shown to induce gallbladder filling by relaxation of gallbladder smooth muscle.[222] This occurs with non-bile acid as well as bile acid structures in a dose-dependent manner at dose levels below that necessary to induce a measurable increase in GLP-1 secretion.[223] Infusion of TGR5 agonists has also been shown to reduce vascular tone in dogs causing a drop in blood pressure combined with reflex tachycardia and a positive inotropic response.[224] Gallbladder and cardiac side effects have been the main obstacles in the development of TGR5 agonist drugs. Bile acids have been implicated in gastrointestinal cell carcinogenesis and some *in vitro* research has shown the

involvement of TGR5 signalling via the EGFR-extracellular signal-regulated kinase 1/2 pathway.[225]

3.1.4 TGR5 in IBD

TGR5 is purported as a drug target for IBD.[219] In the gut, the receptor is expressed in the enteric ganglia, the muscularis externa, the muscularis mucosa, in some types of enterocytes and in lamina propria mononuclear cells. While widely reported as expressed in enterocytes, intestinal epithelial TGR5 seems mostly expressed in the enteroendocrine cells such as L-cells. Expression is higher in colonic L-cells than ileal L-cells and they also express FXR. Enteroendocrine cells, comprising 1% of the total cells of the intestinal mucosa, act as sensors in the gut, sensing nutrients, metabolites and bacterial products by virtue of an array of GPCRs and relay status information to the brain and periphery via neurons and hormones. L-cells express/process the proglucagon peptide which is cleaved to produce GLP-1, GLP-2 and oxyntomodulin.[226]

TGR5 has a role in the regulation of intestinal barrier structure. *TGR5*$^{-/-}$ mice have been shown to have altered gut architecture and increased gut permeability compared to wild-type mice and were more susceptible to DSS induced colitis.[69] This gut barrier maintenance function of TGR5 has been attributed to GLP-2 release. When Sakanaka *et al*. found that the selective TGR5 agonist betulinic acid dose dependently suppressed the disease activity index in a DSS mouse model and reduced mRNA expression of IL-1β, IL-6 and TNF-α, they concluded that this disease modifying effect was at least in part due to GLP-2 release as co-administration of a GLP-2 receptor antagonist reversed the effects in part.[70] The enhancement of mucosal epithelial cell proliferation by GLP-2 and its analogues is well described[227] and Drucker *et al*. found that treatment of an acute colitis model with a GLP-2 analogue enhanced colon length, crypt depth, mucosal area and integrity.[228] There was significant reversal of weight loss not due to increased food intake and reduced expression of IL-1α. An exploratory study on the effects of teduglutide, a sub-cutaneously administered GLP-2 analogue in clinical use for short bowel syndrome, as a single therapy in patients with moderate to severe CD found that it was safe and effective.[229] After eight weeks, over half of the highest dose level treatment group were in remission compared to a third of the placebo group. Adverse effects were mild including abdominal pain and injection site reactions.

GLP-2 stimulation through TGR5 agonism could be a strategy to regenerate the intestinal epithelium. There is evidence of altered GLP-2 levels in the inflammatory condition. An

increase in circulating plasma levels of active GLP-2 in association with reduced levels of dipeptidyl peptidase IV (DP IV) has been found in IBD patients.[230] Increased synthesis or secretion and/or reduced degradation may contribute to endogenous repair as pair of a compensatory mechanism to tissue destruction.

In addition to GLP-2 stimulation, the anti-inflammatory effects of TGR5 can have beneficial effects in IBD. Dendritic cells function as antigen-presenting cells and have a role in immunological homeostasis. Dysregulated cytokine production by dendritic cells has been implicated in the pathogenesis of chronic inflammatory conditions such as IBD, e.g. IL-12 produced promotes a T_H1 cell immune response. While mature dendritic cells do not express a detectable level of TGR5 receptors, treatment of monocytes with bile acid or a TGR5 agonist has been shown to affect DC differentiation and the resultant biological phenotype. Ichikawa *et al.* showed that bile acids induce a IL-12 hypo-producing dendritic cell via a TGR5 dependent pathway suggesting a role for TGR5 agonism in immune modulation.[231] Yoneno *et al*. have demonstrated that CD14+ macrophages isolated from the lamina propria of CD patient specimens express TGR5 and that agonist treatment suppressed bacterially stimulated TNF-α production.[215]

3.1.5 TGR5, is it luminally accessible?

The wide distribution of TGR5 and the unavoidable side effects of systemic exposure such as gallbladder filling are limitations to its clinical applications as a drug target and have prompted research into selective tissue activation. The expression of TGR5 on L-cells and reports of apparent luminal activation have led to the hypothesis that the receptor may be luminally accessible to a gut-confined agent. Local activation could achieve disease modifying effects in IBD while avoiding some of the off-target effects associated with systemic exposure. Administration of taurocholic acid (TCA) as an enema promptly stimulated increased circulating levels of GLP-1 in a dose-dependent manner in healthy humans leading Wu *et al*. to speculate that topical application of bile acid could be a viable therapeutic approach for type II diabetes.[232] The observation that anionic exchange resins clinically used as cholesterol lowering agents also have glycemia lowering effects, substantiated the case for luminal accessibility. Harach *et al*. demonstrated that this effect is through enhanced GLP-1 secretion in a TGR5 dependent pathway.[233] This was due to increased bile acid delivery to the colon and induced proglucagon mRNA, by activation of cAMP responsive elements in the gene promoter. While certain that concentration of bile acids in the colon is responsible for GLP-1 increased secretion, it cannot be stated

unequivocally that this is due to luminal activation on enteroendocrine L-cells. It is possible that intestinal flora metabolism of bile acids in the colon facilitates passive absorption and basolateral accumulation of TGR5 agonists. However, there were no significant differences in body weight changes between TGR5 expressing mice and knockouts which would be an indicator of systemic exposure.

In demonstrating that GLP-1 release by taurodeoxycholic acid (TDCA)-stimulated primary mouse intestinal cells was TGR5-dependent, Brighton *et al.* also showed that GLP-1 release in intact tissue in response to bile acids is primarily by basolateral activation.[234] Using perfused intact mouse small intestinal tissue and Ussing chambers, treatment with TDCA on the basolateral side was more effective than on the apical side and cotreatment with an ASBT inhibitor blocked the apical treatment effect only. This implies that TGR5 may not be sufficiently luminally accessible to elicit an adequate *in vivo* response. Ullmer *et al*. also concluded that L cells are stimulated through a mechanism other than direct stimulation in the gut lumen.[235] They identified a potent and efficacious agonist with excellent bioavailability that produced peptide induction levels by the oral or IV administration routes that correlated with systemic agonist levels. Also, when derivatised by tauro conjugation to a still potent but now poorly absorbed candidate, efficacy was only maintained for IV administration.

However, such models may not reflect the inflammatory condition. Inflammation has been shown to modulate colonic TGR5 expression, with increased expression observed in rodent models of colitis and the inflamed colonic tissues of CD patients.[69] Also, expression in the small intestine may not be an accurate reflection of colonic expression or the mouse may not reflect the human.

Ma *et al*. designed and synthesized a poorly absorbed dual acting TGR5 agonist and DPP-IV inhibitor by linking a TGR5 agonist via a six unit PEG chain linker to the DPP-IV inhibitor, linagliptin.[236] The resulting high molecular weight, polar molecule had poor permeability and was shown to have GLP-1 induced glucose lowering effects without gall bladder filling effects in mice. Similarly, Duan *et al*. synthesized a PEG-linked dimer of a TGR5 agonist achieving desired effects on glucose homeostasis[96] as described in the introduction to this thesis.

Even though the luminal accessibility of TGR5 has been disputed, treatment effects have been achieved by various groups with non-systemic approaches. Even if full gut

confinement is not achieved, it appears that a gut biased approach can achieve desired pharmacological effects with minimised adverse effects.

3.2 TGR5 ligands

Endogenous ligands for TGR5, the bile acids, have been used to probe the functions of the receptor but a desire for a specific ligand has prompted research into semi-synthetic bile acid derivatives as well as other agonists from natural and synthetic sources.

3.2.1 Bile acids

The anti-inflammatory effects of secondary bile acids in the down regulation of cytokines such as IL-1β, IL-6 and TNF-α have been attributed to TGR5. The endogenous bile acids have similar efficacy at the receptor with lithocholic acid (LCA, **54**) being the most potent (EC_{50} = 0.58 μM) followed by deoxycholic acid (DCA, **55**) (EC_{50} = 1.25 μM), chenodeoxycholic acid (CDCA, **56**) (EC_{50} = 6.71 μM) and cholic acid (CA, **57**) (EC_{50} = 13.6 μM). The conjugated forms of each, to both taurine and glycine, have EC_{50}s in the low micromolar range also. The tauro form of LCA (**58**) is the most potent with an EC_{50} of 0.29 μM, approximately half that of the parent acid while the glycol form (**59**) has a similar EC_{50} to the acid of 0.54 μM. These values were established by Sato *et al.* by CRE-driven luciferase reporter assays in TGR5-transfected Chinese hamster ovarian (CHO) cells and reported in 2008.[237]

LCA is a secondary bile acid formed in the lumen of the intestine by bacterial metabolism of the primary bile acid chenodeoxycholic acid.[238] With the other primary bile acid in humans, cholic acid, CDCA is synthesized in the liver from cholesterol and conjugated to glycine or taurine before secretion. In the intestine, one transformation of CDCA salt is deconjugation and dehydroxylation to LCA. Along with the primary bile acids and DCA, the secondary bile acid of cholic acid, LCA can be reabsorbed by active transport into the enterohepatic circulation as well passively absorbed in the colon. However LCA does not tend to accumulate in the bile as it is sulfated at C-3 (**60**) and conjugated in the liver. Ursodeoxycholic acid (UDCA, **61**) is another tertiary bile acid derived from CDCA by epimerisation.[238]

Bile acids are saturated steroid structures with a 5 carbon sidechain at C-24. In the higher vertebrates the A and B rings are cis-fused and the C-5 hydrogen is in the β orientation giving a curved structure. The structures of the major bile acids in humans can be seen in Figure 55.

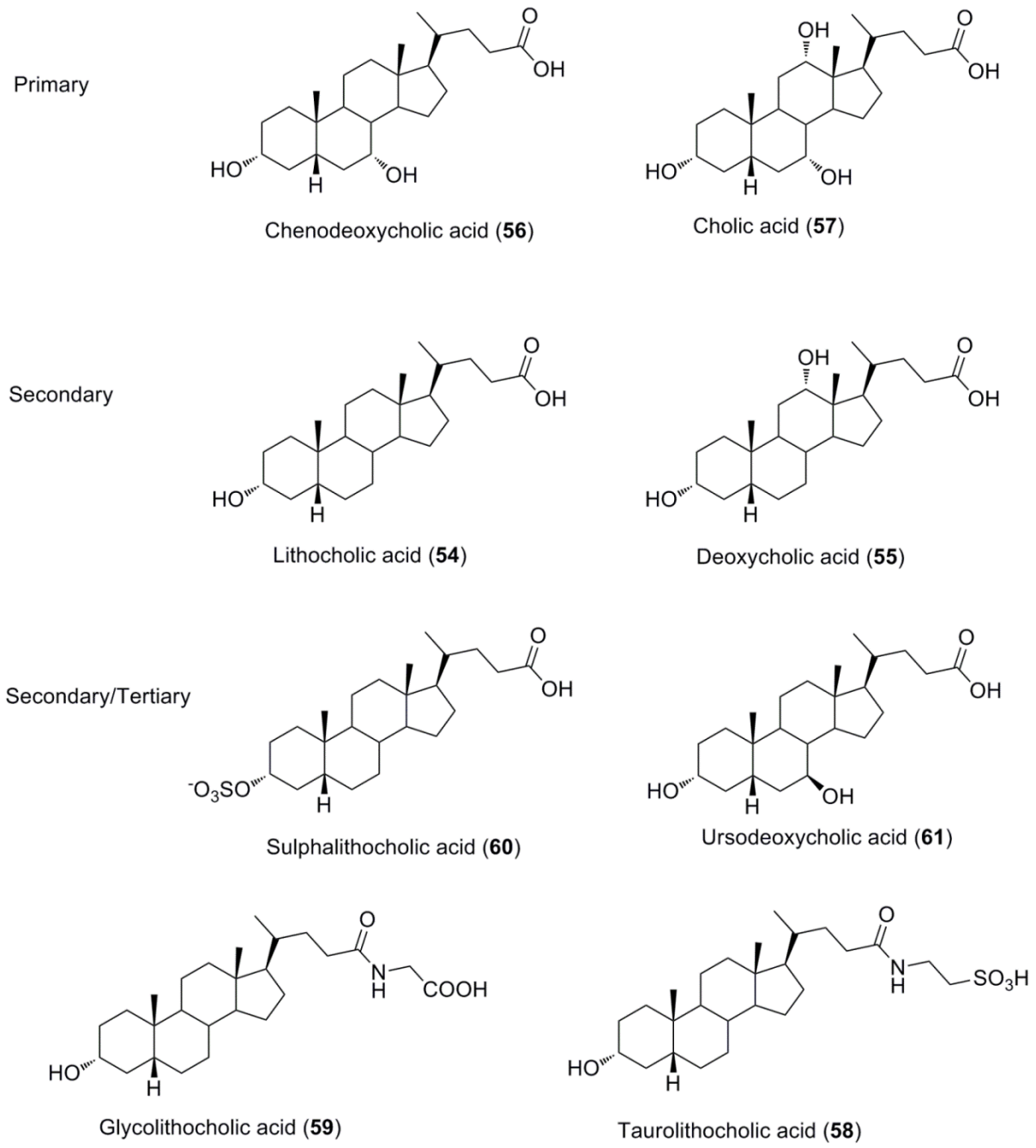

Figure 62. Structures of the major primary, secondary and tertiary human bile acids and the conjugate derivatives of lithocholic acid

3.2.2 Semi-synthetic bile acids

SAR studies on semi-synthetic bile acid derivatives found that introduction of a methyl group at C-23(S) conferred some selectivity for TGR5 over the nuclear bile acid receptor FXR.[239]

Structural modifications of the bile acid scaffold produced INT-777 (**62,** Figure 63), where a 6-α ethyl group and 23(S) - methyl have been inserted into cholic acid.[240] INT-777 is a selective TGR5 agonist and has proved a useful probe in delineating non-genomic effects of TGR5 in the absence of FXR activation.

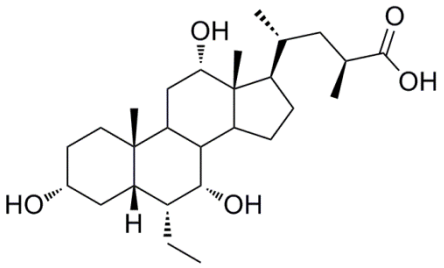

62

*Figure 63. Structure of INT-777 (**62**)*

3.2.3 Natural products

Olive (*Olea europeaea*) leaves are a traditional herbal remedy with anti-diabetic and anti-hypertensive properties. The pentacyclic triterpenoid constituent oleanoic acid (**63,** Figure 64**)** was isolated and shown to be a TGR5 agonist with an EC_{50} comparable to LCA. Sato *et al*. demonstrated that oleanolic acid could improve metabolic homeostasis in mice fed a high-fat diet through TGR5 agonist activity.[241] Screening of naturally derived triterpenoids identified other agonists including betulinic acid (**64**) and ursolic acid (**65**) (Figure 64). Betulinic acid can be extracted from white birch (*Betula platyphylla suk.*) bark[242] and ursolic acid is widely occurring in herbs and fruits including apple peel.[243] In contrast to endogenous bile acids, these agonists showed high selectivity for TGR5 over FXR which prompted investigation of the SAR of semi-synthetic triterpenoid derivatives. Despite potent *in vitro* results, these derivatives were disappointing *in vivo* due to metabolic instability.[244]

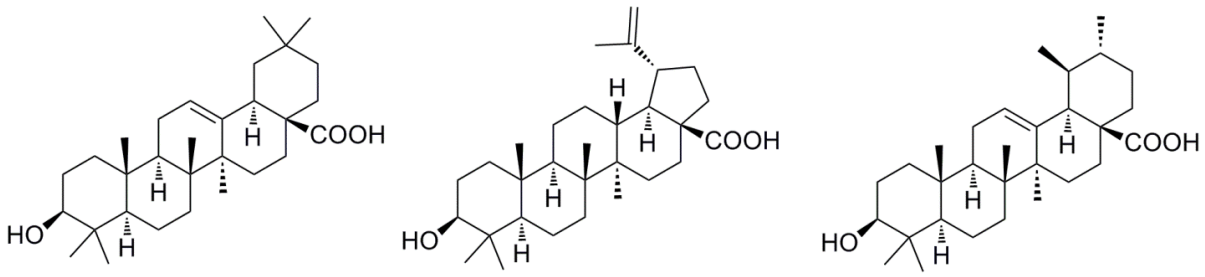

63 **64** **65**

*Figure 64. Structures of oleanoic acid (**63**), betulinic acid (**64**) and ursolic acid (**65**)*

3.3 Synthetic agonists at TGR5

Library screenings have identified many chemical classes with TGR5 agonist activity including tetrahydropyrimidines, carboaxamides, quinolines, triazoles imidazoles, isoquinolines, oxazepines and sulfonamides.[206, 245] While diverse, many representative compounds of these classes contain aromatic moieties separated by a central scaffold and are quite lipophilic.[206] It is not clear if such non steroid ligands bind at the same site as bile acids at the same region within the binding site or at a different site altogether.

3.4 Chapter objective

In this chapter we sought to design and synthesize conjugates of a TGR5 agonist and an MMP inhibitor retaining activity at both targets. As far as we are aware, there are no such dual-acting agents reported. We also sought to design gut-confined TGR5 agonists based on bile acid. Successful candidates would have potential to achieve disease modifying effects in IBD by target modulation in the gut lumen with limited potential for off-target effects.

3.4.1 Specific objectives

- To probe the structural requirements for bile acid binding at TGR5 and amenability to further derivation
- To synthesize conjugates of a bile acid TGR5 agonist and an MMP inhibitor
- To evaluate the TGR5 agonist activity of the synthesized conjugates *in vitro*
- To evaluate the MMP inhibitory activity of the synthesized conjugates *in vitro*
- To design and synthesize LCA-based TGR5 agonists with limited absorption potential and evaluate TGR5 agonist activity *in vitro*

3.5 Synthesis discussions

From the available literature, it appears that both MMP-9 and TGR5 are potential targets for modulation in IBD. Our previous work in chapter 2 had shown that MMP-9 is luminally accessible but TGR5 is still contentious. We sought to design and synthesize conjugates of an MMP inhibitor and a TGR5 agonist which could retain the pharmacological action of each component. Covalent linking of an MMP inhibitor to a TGR5 agonist will yield a compound of high molecular weight which will contravene some of Lipinski's rules and thus likely be a poor candidate for absorption.

We decided to focus on LCA as the TGR5 agonist component. SAR indicates that there is some tolerance to structural modification at C-24 as indicated by the activity of the parent acid and its conjugated forms. Also, the natural triterpenoids are likely to be binding at the same site as the bile acids further indicating tolerance. We focused on the barbiturate scaffold as the MMP-inhibitory component, a potent inhibitor scaffold that we know is tolerant to an array of P2' substitutions.

3.5.1 Synthesis of TGR5 agonist – MMP inhibitor conjugates, Group 1

3.5.1.1 Synthesis of piperazine and homopiperazine-linked conjugates

The first compounds proposed were amide couplings of the C-24 of LCA to a P2' substituent of the barbiturate MMP inhibitor. It is likely from the available literature that the acid group of LCA is a requirement for activity and conversion to an amide may be detrimental to TGR5 activity. We proposed that perhaps the barbiturate ring could provide the affinities provided by a carboxylic acid in this case. The pK_a of LCA has been reported as approximately 5 and conjugation lowers the pK_a due to the induction effect of the carbonyl of the amide group. The pK_a of barbituric acid is 4.12 and 5, 5'- disubstituted barbituric acids would be expected to have higher pK_a values in the range of 6 – 8. Previous work in the Gilmer group on the barbiturate scaffold had shown that potent MMP inhibition was intact on C-5 substitution with piperazine or homopiperazine and there was tolerance for further derivatisation at the distal N.[152]

The piperazine or homopiperazine-linked conjugates, **72** and **73**, were synthesized in two steps as in Scheme 6. In the first step, compound **39** was treated with two equivalents of piperazine or homopiperazine respectively in MeOH at RT for 24 h. The products, **70** and **71**, precipitated during the course of the reaction and could be isolated by filtration and used in the subsequent amide coupling step to LCA without further purification. Formation

of an amide bond using conventional coupling methods involves activation of a carboxylic acid by an activating group followed by nucleophilic displacement by the amine to form the amide bond in the presence of the coupling reagent, base and solvent. Coupling reagents including carbodiimides such as N, N–dicylohexylcarbodiimide facilitate such couplings and often require benzotriazole-type activators such as hydroxybenzotriazole (HOBt) to increase reaction rate and suppress racemization.[246] The propensity of benzotriazoles to degradation is potentially explosive. In our case, amide coupling of LCA to a barbiturate derivative was achieved using COMU coupling reagent. COMU or (1-cyano-2-ethoxy-2-oxoethylidenamineooxy)–dimethylaminomorpholino carbenium hexafluorophosphate (**66**) is a uronium salt derived from ethyl 2-cyano-2-(hydroxyimino)acetate (Oxyma, **67**) and a morpholonium-based immonium moiety and the structure can be seen in Figure 65.

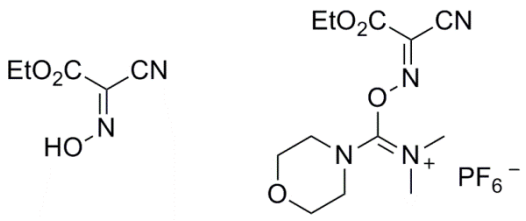

*Figure 65. Chemical structure of Oxyma (**67**) and COMU (**66**)*

Oxyma functions as a good leaving group and the morpholino group functions as a proton acceptor contributing to reactivity while also conferring stability on the reagent.[247] COMU is amenable to solution or solid phase peptide synthesis. In our case, COMU couplings were carried out in solution in DMF with one equivalent of base. One equivalent of COMU was added at 0°C and after 1 h the reaction was allowed to RT and monitored by TLC. The urea and oxime by-products of COMU are soluble in H_2O and can be removed by typical acid/base/H_2O extractions. This was found to be a major advantage of COMU coupling over DCC coupling. However, equivalency of the reagent is still required in the reaction.

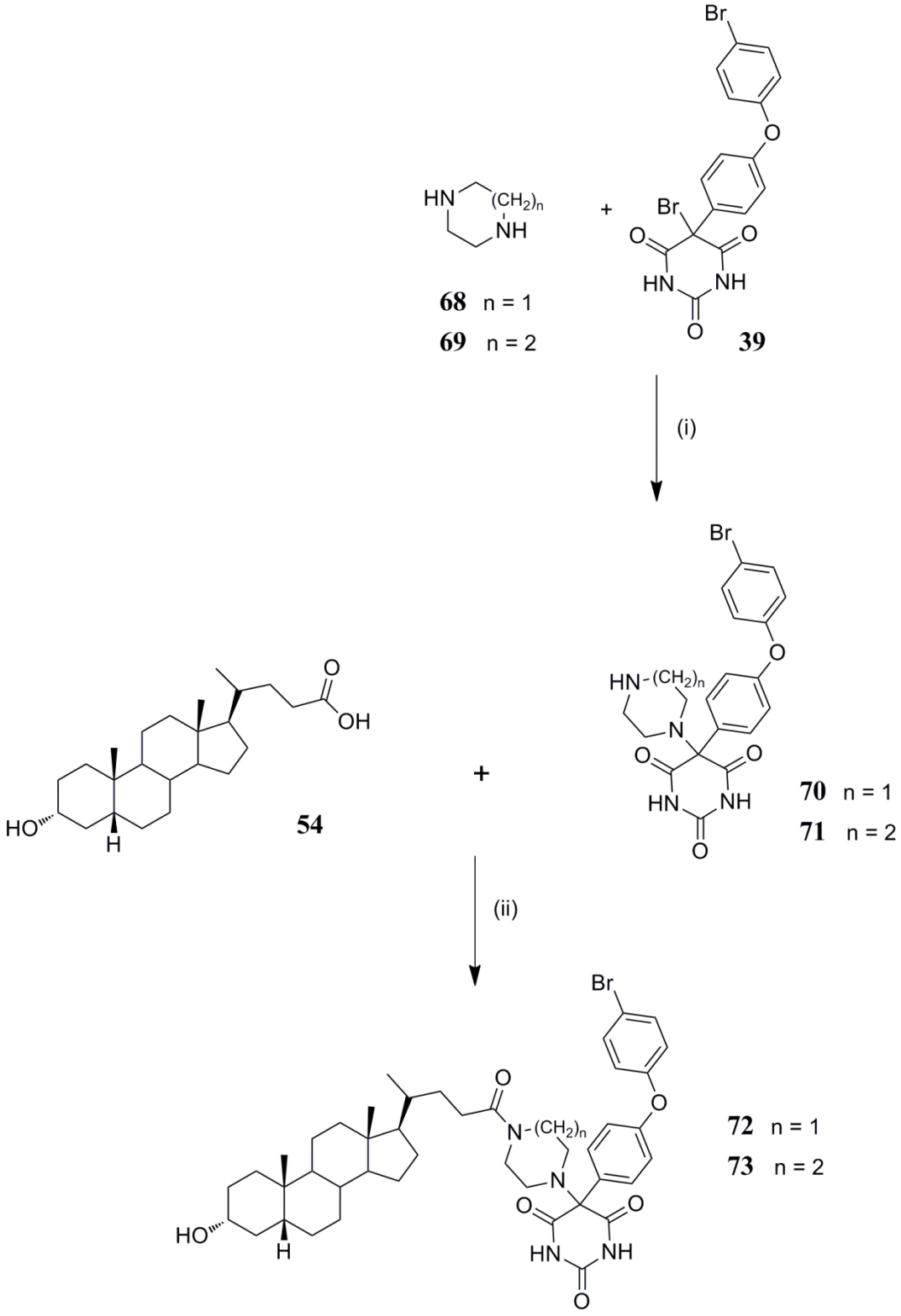

(i) MeOH, RT, 24 h (ii) COMU, DIPEA, anhydrous DMF, 0°C – RT, N_2

Scheme 6. Synthesis of compounds 72 and 73

3.5.1.2 Synthesis of a triazole-linked conjugate

Huisgen 1,3-dipolar cycloaddition of alkynes to azides to afford 1,4-disubstituted-1,2,3-triazoles as in Figure 66 is an excellent example of a click chemistry reaction.

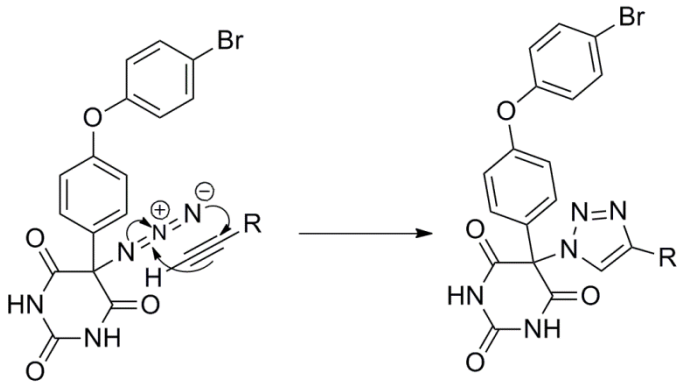

Figure 66. Proposed mechanism of triazole formation by Huisgen 1,3-dipolar cycloaddition

This reaction can be carried out under mild conditions, at room temperature, in aqueous solvent and in ambient air. It should be high yielding and often product purification does not require chromatography. Heating a substituted azide and an alkyne together will give a triazole as a mixture of two regioisomers. However a catalytic amount of Cu(I) increases the reaction rate and affords the 1,4-disubstituted triazole selectively.[248] Triazoles are useful in that they are not prone to cleavage, oxidation or reduction. The unreactivity of the azide and alkyne functionalities facilitates bioconjugation applications. In our case, copper sulfate pentahydrate with sodium ascorbate as reducing agent was used as the source of Cu(I) and water:*tert*-butanol (1:1) as the solvent. Compound **75**, a triazole derivative (Figure 67), was found to be a potent inhibitor of MMP-9 producing 90% inhibition at 10 µM in the fluorogenic assay. This indicated that the MMP-9 binding site could tolerate a triazole substitution at C-5.

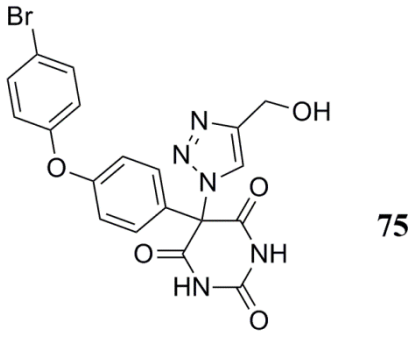

75

*Figure 67. Chemical structure of compound **75***

A triazole linked MMP inhibitor-LCA conjugate, compound **77**, was synthesized as outlined in Scheme 7. The azide derivative **74** was synthesized by treatment of **39** with azide ion in the polar, aprotic solvent 1,3-dimethyl-3,4,5,6-tetrahydro-2(1H)-pyrimidinone (DMPU). Initially a large excess of 10 equivalents of sodium azide was used but this was found to be unnecessary and a slight excess of 1.1 equivalents sufficed. LCA was functionalized to an alkyne by COMU amide coupling to propargyl amine and clicked to the barbiturate azide **74** to yield compound **77**.

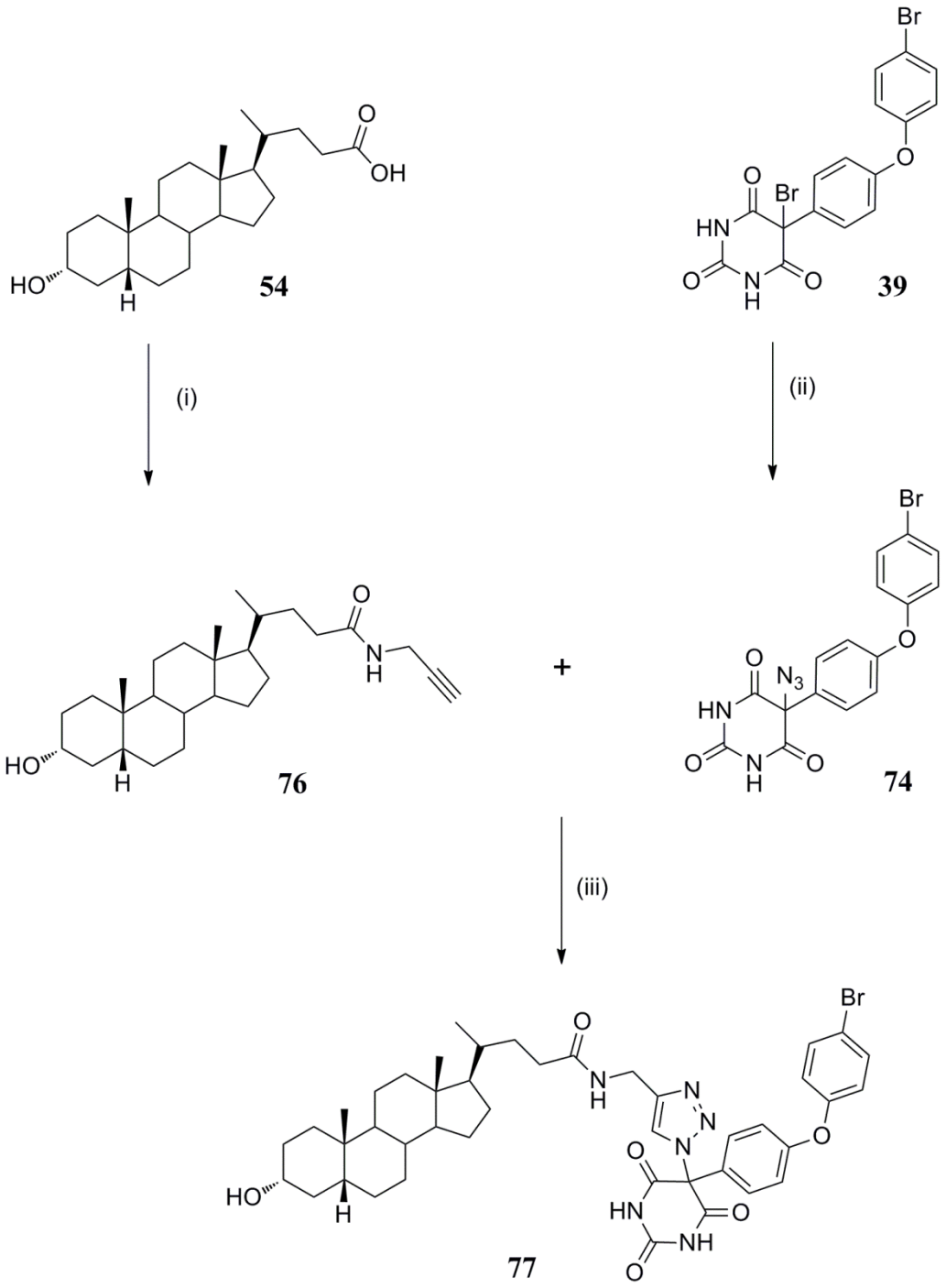

(i) Propargyl amine, DIPEA, COMU, anhydrous DMF, 0°C – RT, N_2, 12 h (ii) NaN_3, DMPU, RT, 24 h (iii) $CuSO_4.5H_2O$, sodium ascorbate, *t*-butanol, H_2O, 24 h

Scheme 7. Synthesis of compound 77

3.5.1.3 Synthesis of conjugates by direct substitution of an LCA-derived amine on compound 39

While piperazine, homopiperazine or triazole substituents will have affinity for the lip of the S2' pocket of the MMPs, accommodation of such heterocycles may be too much to ask of the TGR5 binding site. Coupling of LCA directly to compound **39** was pursued and options for functionalising the C-24 acid of LCA to a nucleophile for substitution of the bromine at C-5 of **39** were considered. The Schmidt reaction can convert a carboxylic acid to a primary amine. In this acid-catalysed reaction, the carboxylic acid is protonated and loses a molecule of H_2O to give an acylium ion. Hydrogen azide (HN_3), formed *in situ* by acidification of sodium azide, reacts with it to yield a protonated azido ketone which rearranges to the isocyanate with extrusion of N_2. This can be hydrolysed to the carbamic acid which decomposes when deprotonated to the amine with release of CO_2. However, this reaction was not suitable in this case. HN_3 also reacts with tertiary alcohols to yield imines and may also react with secondary alcohols such as the 3-OH of LCA. Under the strong acid conditions employed, the alcohol would also be prone to dehydration to the alkene and suitable protection of the alcohol would not be trivial. Amides are amenable to reduction to amines. By conversion of an acid to a simple amide, it can then be reduced to the corresponding amine. We prepared the primary amide derivative of LCA, **79**, by first converting the acid to an activated ester of N-hydroxysuccinimide by DCC coupling. The crude activated ester was reacted with ammonia solution in DMF to yield the primary amide. A simple secondary amide, **82**, was also prepared by COMU coupling of LCA to methylamine hydrochloride. Reduction of these amides with lithium aluminium hydride ($LiAlH_4$) yielded the corresponding amines which were reacted immediately with **39** to yield conjugates **81** and **84** as outlined in Scheme 8 and Scheme 9 .

In the proposed $LiAlH_4$ reduction mechanism, the carbonyl carbon is nucleophilically attacked by a hydride supplied by the $LiAlH_4$ reagent. Electrons from the C=O move to O facilitating the formation of a metal alkoxide complex with the remaining aluminium species or perhaps with the Li^+. The tetrahedral intermediate collapses displacing the metal alkoxide producing an iminium ion. The electrophilic carbon is attacked by a hydride and electrons from the C=N bond move to the N neutralizing the positive charge and yielding the amine product.

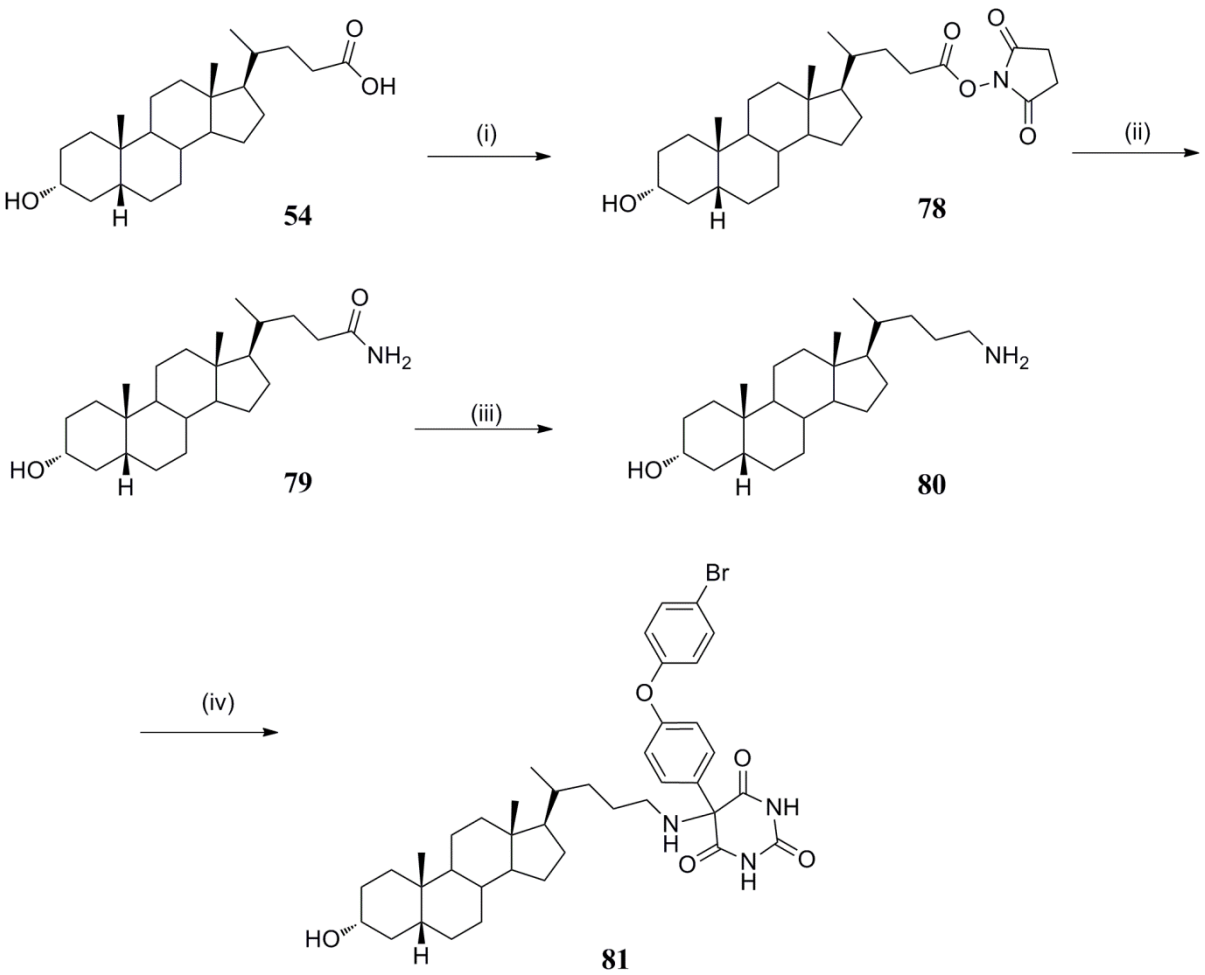

(i) DCC, N-hydroxysuccinimide, THF, ACN, RT, 24 h (ii) ammonia solution 28%, DMF, 50°C, 20 h (iii) $LiAlH_4$, anhydrous THF, N_2, 65°C, 5 h (iv) compound **39**, MeOH, RT, 24 h

Scheme 8. Synthesis of compound 81

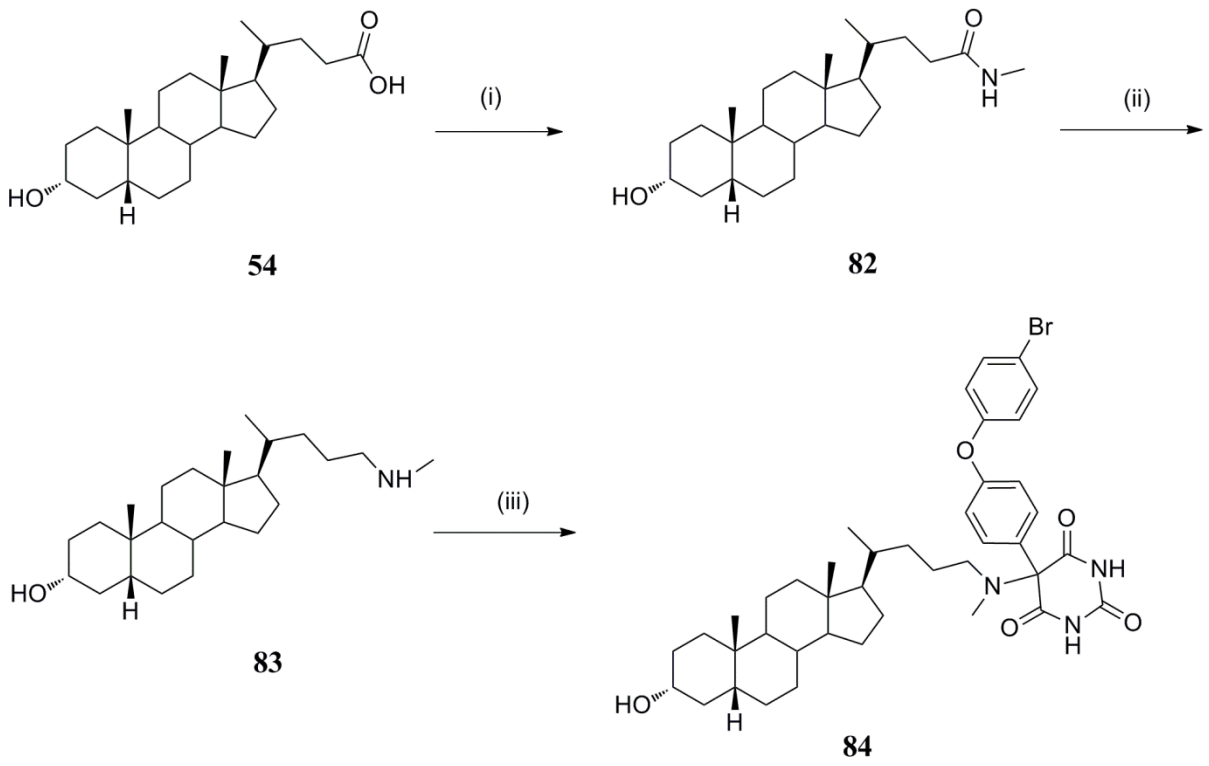

(i) CH_3NH_2.HCl, DIPEA, anhydrous DMF, 0°C – RT, N_2 (ii) $LiAlH_4$, anhydrous THF, N_2, 65°C, 5h (iii) compound **39**, MeOH, RT, 24 h

Scheme 9. Synthesis of compound 84

3.5.2 Synthesis of TGR5 agonist – MMP inhibitor conjugates with lysine as a linker – Group 2

In parallel, we sought to synthesize a hybrid where the barbiturate and LCA are connected by a linker which would retain a carboxylic acid group and perhaps have improved binding. Lysine was chosen as a suitable linker. The alpha-amine of a commercial BOC-protected epsilon N methyl ester derivative of lysine was coupled to LCA using COMU. The BOC protecting group was removed in 10% v/v TFA in DCM and from the deboced derivative **86**, an acetamide was prepared by treatment with acetic anhydride in DCM using DIPEA as base. The primary amine is released from its TFA salt by DIPEA. The nitrogen lone pair attacks the partially positive carbon of a carbonyl group of acetic anhydride forcing the electrons from the carbonyl group onto the O. The now positively charged N loses a proton to a base species in the system and the electron pair on the O reforms the carbonyl bond expelling the carboxylate leaving group (Figure 68).

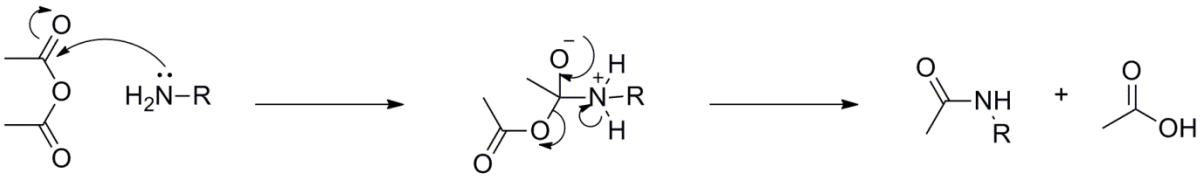

Figure 68. Proposed mechanism of acetamide formation

Base hydrolysis of **87** removed the methyl ester protecting group to yield the final product, compound **88** (Scheme 10). The acetamide, **88**, would allow us to assess whether binding could tolerate the lysine acid group and its alkyl chain that we hoped could serve as a linker chain.

Conjugation of **86** to the MMP inhibitor **39** was pursued in a similar manner. However, when the TFA salt of the deboced amine was reacted with **39** in MeOH using DIPEA as base there was no product formed. Changing the solvent or the equivalency of base did not change this. Compound **39** is a demanding reaction substrate and does not react as predicted in the presence of sterically hindered amines generally used to free the reactant amine for reaction and to mop up acid by-product produced. Instead, the reaction was carried out by first freeing the amine from the TFA salt, isolating it and reacting two equivalents with one equivalent of **39** in the absence of any other base to yield the conjugate compound **89.** Base hydrolysis of the methyl ester protecting group yielded the final product, compound **90** (Scheme 10).

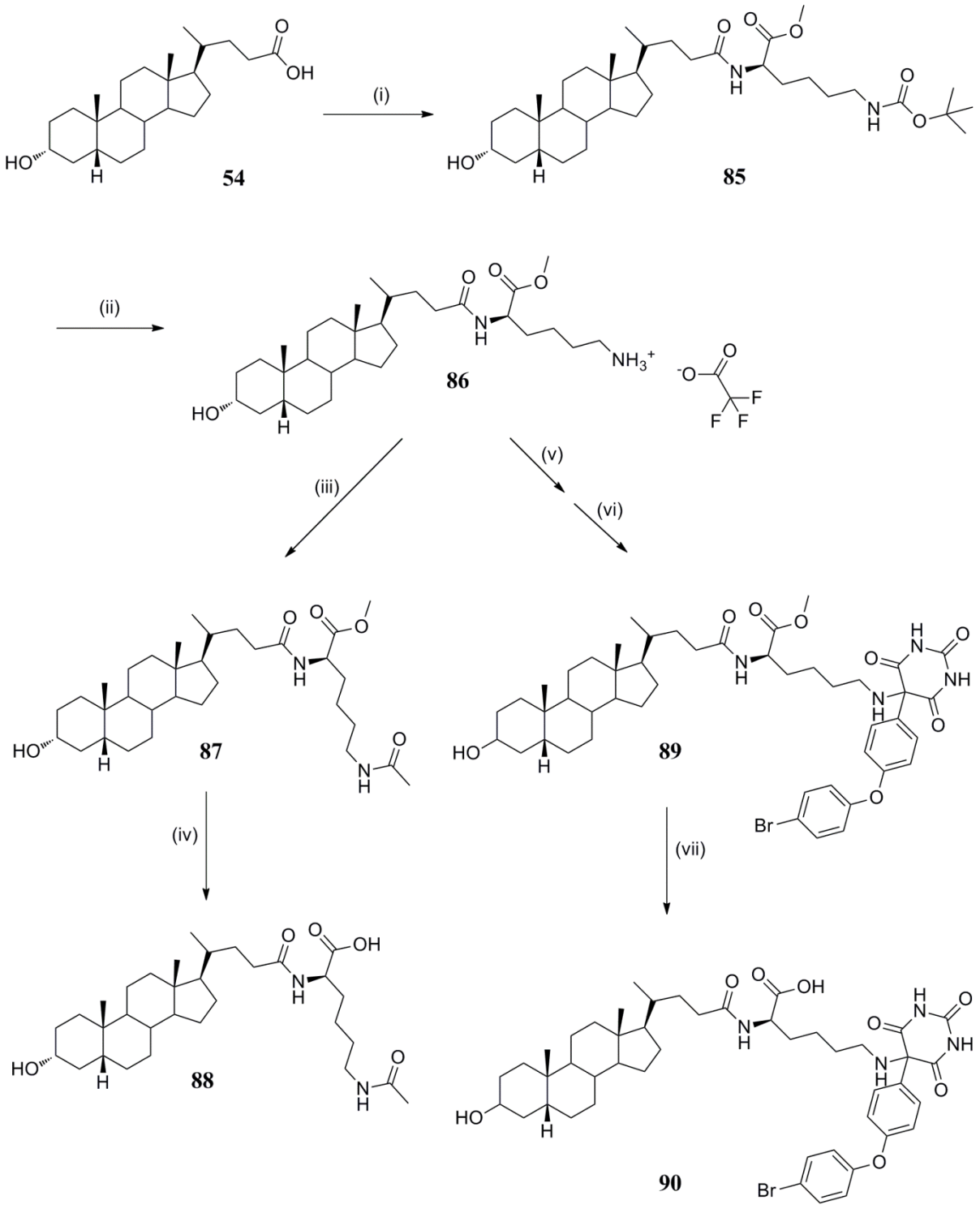

(i) H-Lys(Boc)-OMe.HCl, DIPEA, COMU, anhydrous DMF, 0°C – RT, N_2 (ii) 10% v/v TFA in DCM, RT, 1 h (iii) acetic anhydride, DIPEA, DCM, RT, 2h (iv) aqueous 2M NaOH, MeOH, RT, 22 h (v) aqueous 2 M NaOH, DCM (vi) compound **39**, MeOH, RT, 24 h (vii) aqueous 2M NaOH, MeOH, RT, 17 h

Scheme 10. Synthesis of compounds 88 and 90

3.6 Conjugation of LCA to homoserine

Other amino acids were considered for introduction of a linker while retaining a carboxylic acid. Serine or homoserine would provide a primary alcohol for further derivations. Amide coupling of homoserine to LCA by a method such as COMU coupling would require protection of the amino acid carboxylic acid. By conventional acid-catalysed esterification in methanol with one equivalent of acid to occupy the amino acid -NH_2 group and a slight excess for catalysis, there was formation of the desired ester product but the reaction would not complete and isolation of the small yield of esterified material was not trivial. Esterification was also pursued by generating HCl gas *in situ* from thionyl chloride in dry methanol but this gave a similarly low yield. Chlorotrimethylsilane based methods were not suitable in the presence of the alcohol group and most of the commonly used amine protecting groups such as BOC are acid labile and would likely not withstand the acid catalysis conditions required for esterification. Reassessment of the synthesis led us to an alternative approach where we would first activate the carboxylic acid of LCA and thereby hope to achieve selectivity of reaction for LCA with the amino acid amine in the presence of its unprotected acid group. This was achieved by generation of an anhydride. In the presence of base, the reaction between a carboxylate and a chloroformate yields a mixed carbonic anhydride which reacts quickly with an amine to form an amide. A mixed anhydride of LCA and ethyl chloroformate was prepared in diethyl ether at 0°C. When TLC indicated full conversion to the anhydride, homoserine and 1 eq. NEt_3 in MeOH were gradually added with which the anhydride reacted readily at 0°C to yield compound **91**.

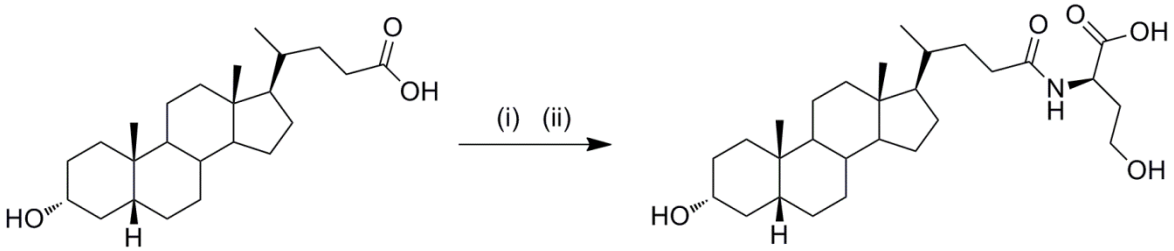

54 **91**

(i) ethyl chloroformate, NEt_3, Et_2O, 0°C, 10 min (ii) homoserine, NEt_3, MeOH, 0°C – RT, overnight

Scheme 11. Synthesis of compound 91

3.7 Synthesis of the hydroxymate derivative of LCA

Synthesis of the hydroxymate derivative **92** was achieved using a method reported by Reddy *et al*. for the conversion of carboxylic acids to hydroxamic acids[249] as in Scheme 12.

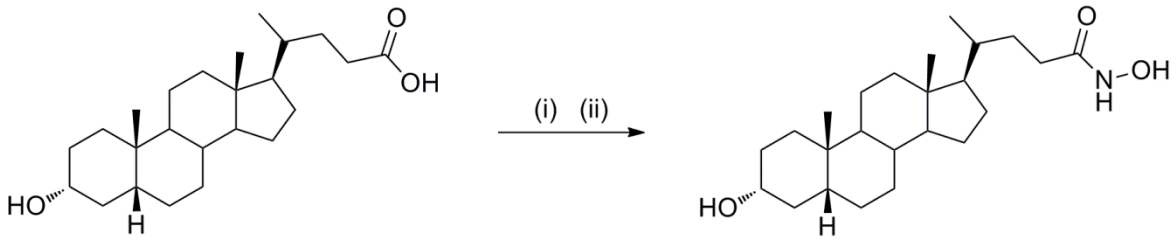

54 **92**

(i) ethyl chloroformate, NEt_3, Et_2O, 0°C, 10 min (ii) hydroxylamine solution in MeOH, 0°C – RT, 2 h

Scheme 12. Synthesis of compound 92

Briefly, the acid is reacted with ethyl chloroformate in Et_2O with NEt_3 as base. The deprotonated acid attacks the electrophilic carbon of the ethyl chloroformate carbonyl forming a mixed anhydride. As the chloroformate-derived carbonyl in the anhydride is flanked by two oxygens, delocalization diminishes its reactivity (Figure 69)

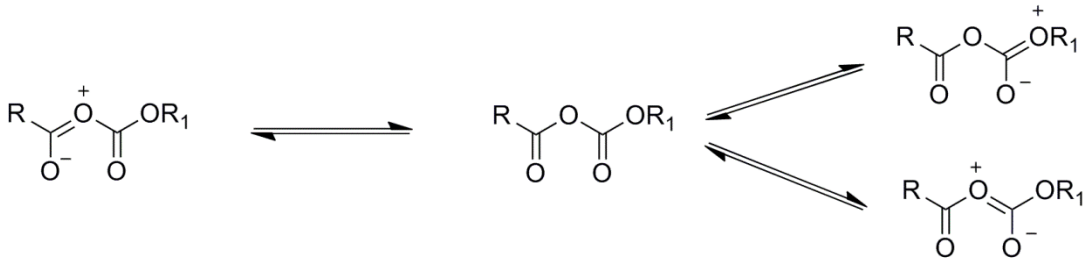

Figure 69. Resonance delocalization in a mixed anhydride derivative of a carbonic acid

When freshly prepared hydroxylamine is added, it preferentially attacks the LCA derived carbonyl group (Figure 70).

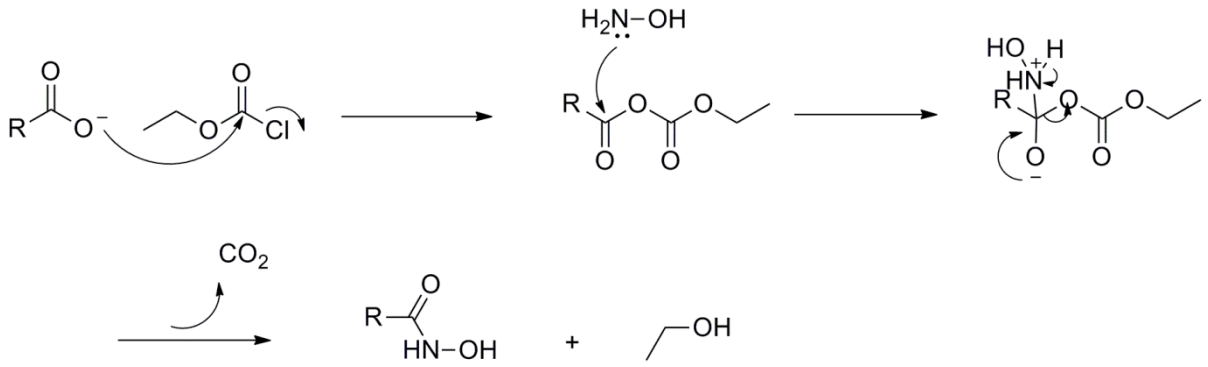

*Figure 70. Proposed mechanism of synthesis of compound **92***

3.8 Synthesis of the 3-ketone derivative of LCA

The 3-OH of LCA was derivatised to a ketone to probe the H-bond donor requirement at this position. The acid group of LCA was protected as a methyl ester (**93**) and pyridinium chlorochromate (PCC) was used to oxidise the secondary alcohol to a ketone yielding compound **94**. PCC is the orange salt of a pyridinium cation and a tetrahedral chlorochromate anion. A PCC oxidation can be carried out by stirring the alcohol with PCC in DCM at room temperature. The chromium byproduct deposits with pyridine as a sticky black tar during the reaction but passage of the reaction mixture through a celite plug simplified the work up. The alcohol oxygen attacks the chromium (VI) forming a Cr-O bond and the chloride is displaced. A base species present extracts the C-3 proton and the electrons move to form the C-O bond breaking the O-Cr bond in the process releasing the Cr(IV) by-product. The methyl ester protecting group was then removed by base hydrolyis to yield compound **95** (Scheme 13).

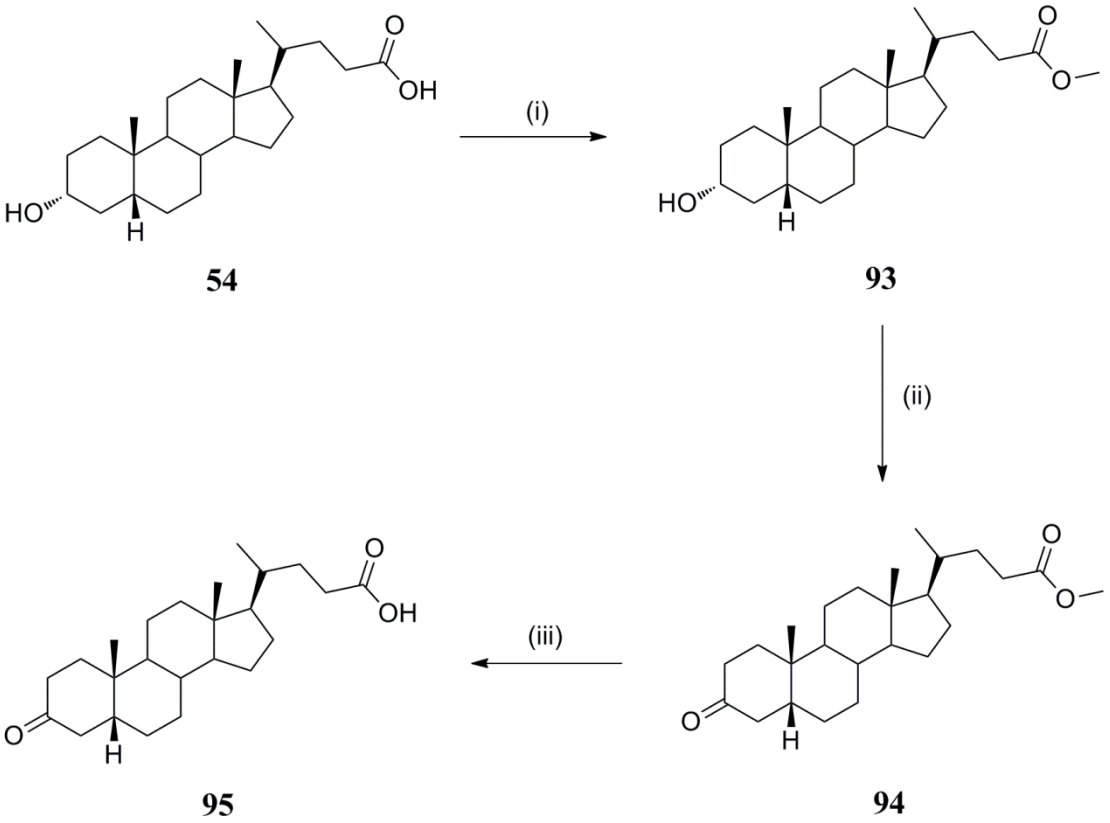

(i) conc. HCl, MeOH, 70°C, 8 h (ii) PCC, DCM, RT, 15 h (iii) aqueous 2M NaOH, MeOH, RT, 40 h

Scheme 13. Synthesis of compound 95

3.9 Synthesis of a ciprofloxacin MMP inhibitor conjugate

The fluoroquinolone antibiotic ciprofloxacin was reported as an agonist of TGR-5 by Cipriani *et al.*[69] Systemic administration had a protective effect against TNBS induced colitis in mice and reduced local generation of inflammatory mediators such as IL-1β, Il-6, IFNγ and TNF-α. These clinical and immunomodulatory effects were lost when administered to *TGR5*$^{-/-}$ mice. Ciprofloxacin-associated tendinopathy has prompted study on its effects on the gelatinases. In tendon cells, it has been found to upregulate MMP-2 at gene level and at protein level while levels of MMP-9, TIMP-1 and TIMP-2 remained unchanged.[250] Upregulation of MMP-2 may be desirable at some stages in IBD, as can TGR5 activation, and so ciprofloxacin warrants further study.

The piperazine ring of ciprofloxacin enabled direct nucleophilic substitution at C-5 of the barbiturate ring of compound **39**. It was necessary to first prepare the methyl ester of ciprofloxacin (**97**) and the acid was subsequently regenerated by base hydrolysis yielding compound **99** (Scheme 14).

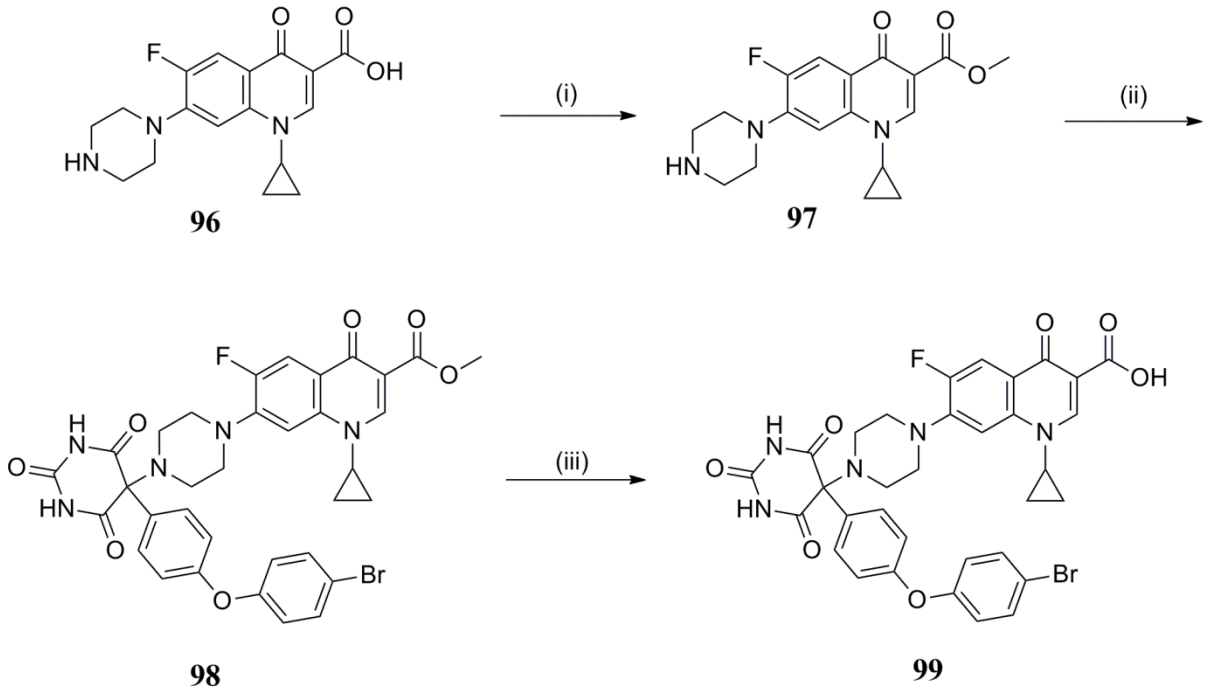

(i) conc. H_2SO_4, MeOH, 80°C, 12 h (ii) compound **39**, MeOH, 48 h (iii) aqueous 2M NaOH, MeOH, RT, 12 h

Scheme 14. Synthesis of compound 99

3.10 Synthesis of gut-confined TGR5 agonist candidates based on LCA

3.10.1 Introduction of a positive charge

In pursuit of a non-absorbable TGR5 agonist, we sought to derivatise LCA to a permanently charged DABCO derivative. This was achieved by reduction of the carboxylic acid to the alcohol, selective mesylation of this primary alcohol and subsequent displacement of the mesylate with DABCO as outlined in Scheme 15. The acid reduction was carried out using $LiAlH_4$ as the reducing agent. The proposed mechanism is similar to that proposed for amide reduction. Initially, the carboxylate anion is generated. The carbonyl carbon is nucleophilically attacked by a hydride supplied by aluminium hydride while the carbonyl oxygen is complexed by the remaining aluminium species. Elimination of an oxoaluminium hydride anion yields the aldehyde. This aldehyde intermediate is more reactive than the acid starting material and its electrophilic carbonyl C is attacked by a further hydride anion supplied by $LiAlH_4$. Subsequent hydrolysis yields the primary alcohol.

Selective mesylation of the 24-OH (primary) was achieved under conventional mesylation conditions. The alcohol derivative was dissolved in anhydrous DCM with NEt_3 as base. Methanesulfonyl chloride was added dropwise in DCM over 20 min. To avoid mesylation of the secondary 3-OH of LCA, this gradual addition was found to be necessary and the methanesulfonyl chloride was restricted to one equivalency. Initially it was deemed prudent to cool the reaction mixture over an ice-water bath but this was not pursued as there was some loss of starting material solubility at this lower temperature. At RT, the alcohol was fully in solution.

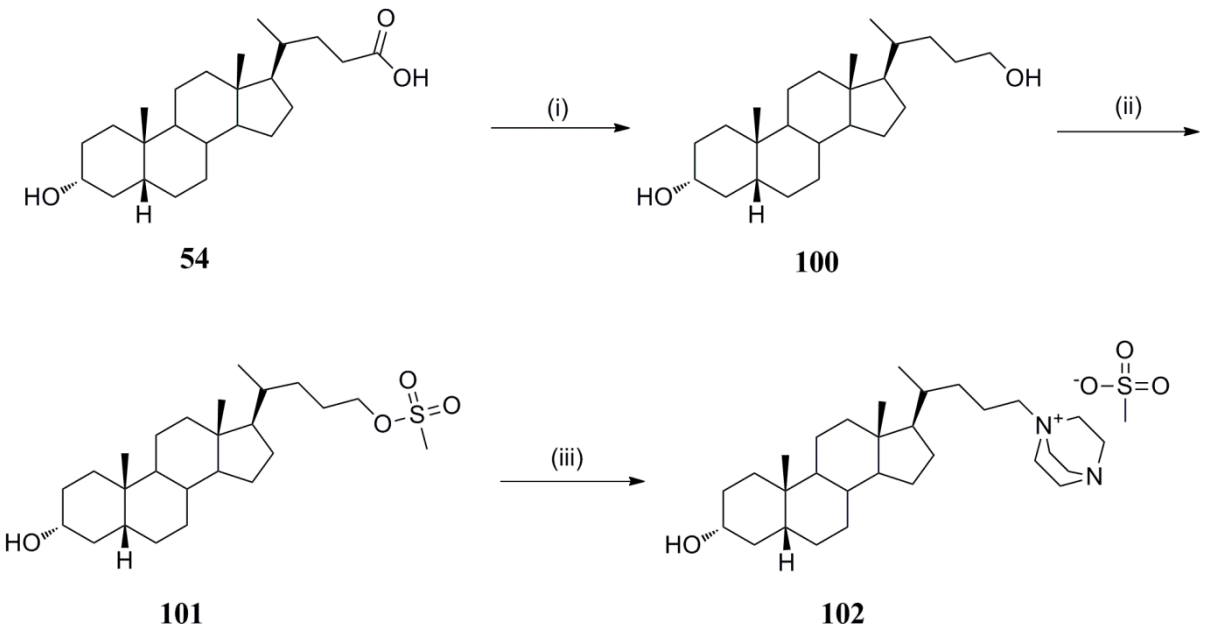

54 **100** **101** **102**

(i) $LiAlH_4$, anhydrous THF, 65°C, N_2, 6 h (ii) mesyl chloride, NEt_3, anhydrous DCM, RT, 4.5 h (iii) DABCO, ACN, RT, 48 h

Scheme 15. Synthesis of compound 102

3.10.2 Introduction of a functionality that is negatively charged at physiological pHs

While not permanent, the pK_a of a sulfonic acid means that it will be deprotonated over the range of physiological pH. For derivatisation to the sulfonate, we proposed to benzyl protect the acid and OH groups of LCA. The ester derivative could then be reduced to the alcohol and halogenated selectively while the protecting benzyl ether would remain intact. Generally, a secondary alcohol will be more reactive in a halogenation reaction than a primary alcohol and so alcohol protection was required. The halogen would then be a suitable substrate for generation of the sulfonate by reaction with Na_2SO_3 in the Strecker reaction. The benzylation reaction did not proceed as favourably as expected. Initially the reaction would not proceed in THF but DMF was found to be suitable. However, while selective halogenation without protection is unlikely, selective mesylation had been achieved and displacement of a mesylate with a halogen should be possible. The Finkelstein reaction is commonly used to exchange one halogen for another. In the classical version, an alkyl halide is treated with excess alkali metal halide in acetone and

the halogens are exchanged through an S_N2 mechanism. In a modified version of the Finkelstein reaction, a tosylate or mesylate can be treated with a metal halide to yield the alkyl halide,[251] the reaction driven by the excellent leaving group ability of the sulfonate. This modified Finkelstein reaction was used to convert the mesylate **101** to an iodate. The reaction was carried out by treatment of **101** with sodium iodide in a mixture of acetone and H_2O with microwave heating.[252] The crude iodate product, **103**, was treated with Na_2SO_3 in a mixture of acetone and water with microwave heating and the product **104** was isolated by solid phase extraction on reverse phase silica.

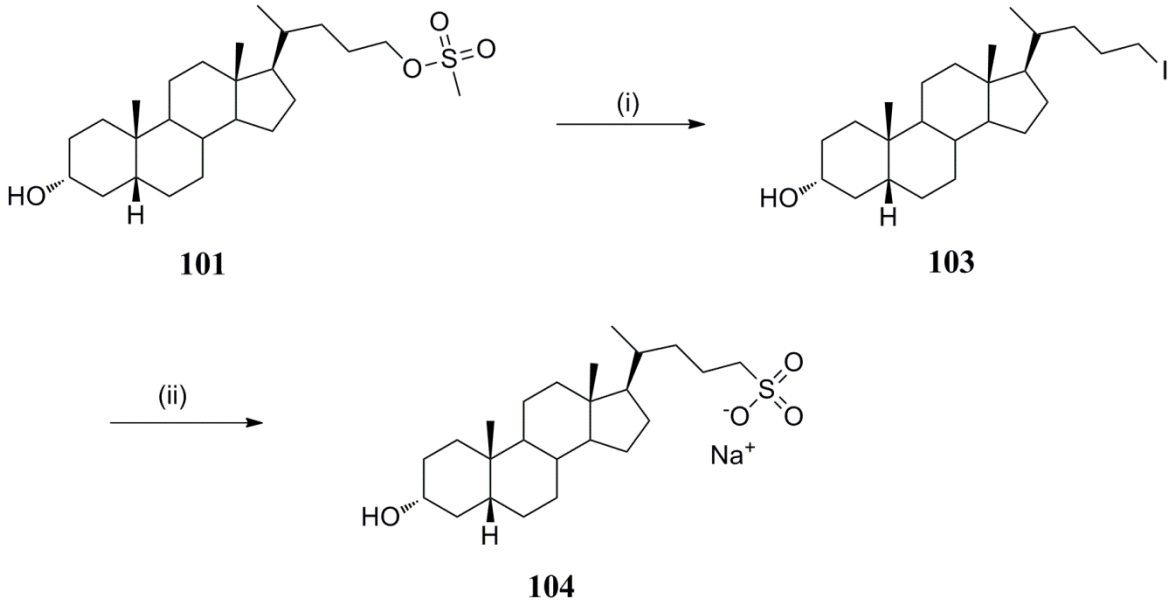

101 **103** **104**

(i) NaI, acetone, MW 85°C, 1h (ii) Na_2SO_3, acetone, H_2O, MW 120°C, 3h

Scheme 16. Synthesis of compound 104

3.10.3 Pursuit of small molecular weight gelatinase inhibitors

Previous work in the Gilmer group had identified 5-fluoro-2-(methylsulfonamido)benzoic acid (**105**, Figure 71) as a potential lead compound for gelatinase inhibitors.

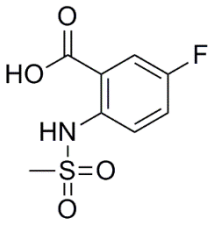

*Figure 71. Structure of 5-fluoro-2-(methylsulfonamido)benzoic acid, compound **105***

Based on this, we decided to prepare a series of anthranilate sulfonamides for evaluation as MMP inhibitors. An MMP inhibitor of small size and molecular weight could be useful in the preparation of conjugates with a TGR5 agonist. Review of the available literature showed that diverse pharmacological effects have been reported for anthranilate sulfonamides. Derivatives have been reported as methionine aminopeptidase inhibitors,[253] penicillin binding protein inhibitors,[254] aldo-keto reductase inhibitors[255] and cholecystokinin receptor antagonists.[256] As MMP inhibitors, the carboxylic acid group could coordinate to the Zn atom at the enzyme active site. The sulfonamide group could also contribute to Zn binding or may direct a substituent to the S1' pocket of the enzyme.[257]

Sulfonamides can be readily synthesized from an amine and a sulfonyl chloride. Sulfonamide formation is the basis for the Hinsberg test which is used to demonstrate whether an amine is primary, secondary or tertiary. The test involves shaking the test amine with benzenesulfonyl chloride in excess potassium hydroxide and after allowing time for reaction, acidifying the mixture. The visible results, before and after acidification, indicate the amine type. In the case of a primary amine, the N-substituted benzenesulfonamide reaction product forms a water-soluble potassium salt with the excess potassium hydroxide and so a clear solution. The hydrogen attached to the nitrogen is made sufficiently acidic by the electron withdrawing SO_2 group. On addition of acid, the now water-insoluble sulfonamide is seen to precipitate. In the case of a secondary amine, the N, N-disubstituted sulfonamide precipitates after the first step as it lacks an acidic hydrogen and acidification does not change the visible result. Deng *et al.* reported successful synthesis of sulfonamides in water based on this principle and we used this method in the synthesis of our series.

The method involves reaction of a primary amine and a sulfonyl chloride in water at pH 8. As the reaction proceeds and HCl is produced, 1M Na_2CO_3 is added to maintain the reaction mixture at pH 8. Sulfonyl chlorides are sensitive to water hydrolysis and so using water as the solvent may seem surprising. This was not found to be problematic however. It is thought that eliminating organic solvent from the reaction conditions allows the sulfonyl chloride to slowly get into the reaction system and so hydrolysis is minimised. Optimal pH is approximately 8. At lower pH, little reaction occurs and at higher pH more hydrolysis will occur. Monitoring of the reaction by TLC indicated no side reactions. When the reaction was complete, the sulfonamide product was precipitated by addition of conc. HCl. In some cases, the product did not require further purification but in others recrystallisation was necessary to remove amine starting material. The reaction of anthranilic acid and benzenesulfonyl chloride was also investigated under conventional conditions in anhydrous DCM with triethylamine as base. TLC indicated that the desired sulfonamide product was formed but there were also several side-products and so this method was not pursued further. Yields obtained were not high, particularly when recrystallisation was required, but were considered acceptable considering the ease of work-up.

The reactivity of a sulfonyl chloride can be attributed to a polar effect in which the electron withdrawing chlorine creates an electron deficient centre at the tetra co-ordinated sulfur. This allows approach of a nucleophile to the sulfur and nucleophilic substitution reactions to proceed following an S_N2 mechanism. As well as the anthranilate series, a series of derivatives was prepared from 5-fluoro-2-aminobenzoic acid and 5-chloro-2-aminobenzoic acid as outlined in Table 3.

Table 3. Benzoic acid derivatives synthesized as candidate MMP inhibitors

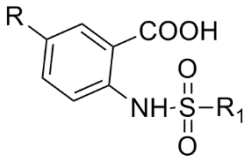

Compound	**R**	**R_1**	**Yield %**
106	H	-Ph-CH_3	23.9
107	H	-Ph	43.6
108	H	-CH_2-Ph	34.3
109	H	-CH_3	18.7
110	H	-CH_2CH_3	28.5
111	H	-$CH_2CH_2CH_3$	12.9
112	H	-Ph-Br	54.3
113	F	-Ph	51.2
114	F	-CH_2-Ph	63.4
115	F	-CH_3	38.5
116	F	-CH_2CH_3	71.2
117	F	-$CH_2CH_2CH_3$	41.7
118	F	-Ph-Br	27.3
119	Cl	-Ph-CH_3	57.3
120	Cl	-Ph	56.2
121	Cl	-CH_2-Ph	48.4
122	Cl	-CH_3	20.5
123	Cl	-CH_2CH_3	31.9
124	Cl	-Ph-Br	24.4

Disappointingly, the compounds showed negligible MMP-9 inhibitory activity. Therefore, it was decided to further derivatise the R_1 group to a diaryl or phenoxyphenyl substituent for greater binding affinity in the S1' pocket of MMP-9.

3.10.4 Synthesis of compounds 126 and 127

The diaryl derivative, **126**, was synthesized in two steps as in Scheme 17.

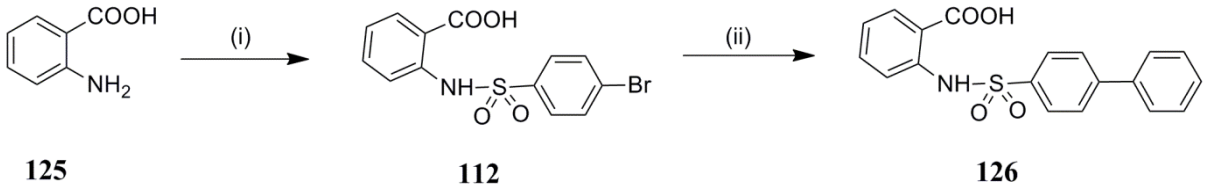

125 **112** **126**

(i) 4-bromobenzenesulfonyl chloride, NEt_3, H_2O:THF (1:1), RT (ii) phenylboronic acid, tetrakis(triphenylphosphine)palladium, K_2CO_3, anhydrous THF, N_2, RT - 75°C, 12 h

Scheme 17. Synthesis of compound 126

Anthranilic acid (**125**) was treated with 4-bromophenylsulfonyl chloride to yield the intermediate, **112**, in H_2O:THF (1:1) with NEt_3 as base. The sulfonyl chloride starting material was poorly water soluble and THF was required as a co-solvent in this case. Compound **112** was a suitable substrate for Suzuki coupling. In the Suzuki reaction the coupling partners are a boronic acid or ester with a vinyl or aryl halide or triflate catalysed by a palladium (0) complex. The mechanism of the Suzuki reaction involves oxidative addition of the aromatic halide to the palladium (0) complex which generates a palladium (II) intermediate. The intermediate undergoes a transmetallation reaction with the alkenyl boronate species. The product is then expelled from this by reductive elimination resulting in the palladium (0) catalyst being regenerated. The base used in this reaction aids the transmetallation step. Compound **112** was treated with phenylboronic acid with K_2CO_3 as base and tetrakis(triphenylphosphine)palladium as the source of palladium (0).

Compound **127** (Figure 72) was synthesized by treating anthranilic acid with phenoxyphenylsulfonyl chloride in H_2O:THF (1:1) with NEt_3 as base.

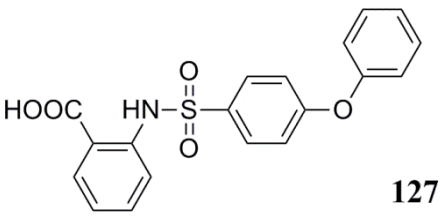

127

*Figure 72. Chemical structure of compound **127***

Disappointingly, derivation of R_1 did not greatly enhance MMP-9 inhibitory potency. Inhibition was negligible at 10 µM in both cases. At 50 µM, compound **127** produced 40% inhibition.

3.11 *In vitro* assessments

3.11.1 Assessment of TGR5 activation

Activation of TGR5 was quantitatively assessed by measuring the increase in the intracellular messenger cAMP in NCI-H716 cells following incubation with relevant bile acid agonists. NCI-H716 cells constitutively express TGR5 and the cell line was selected to avoid the sometimes technically challenging transfection of GPCRs. The aim was to achieve a read-out of potential TGR5 activation rather than quantitative estimation of e.g. EC_{50}. LCA and sodium TLCA were used as positive controls in the assay. This assay was carried out in a procedure adapted from that reported by Sato *et al*. Their work in NCI-H716 and in TGR5-transfected CHO cells indicates that the increased cAMP levels observed in NCI-H716 cells in response to bile acids is due to TGR5 activation.

The Tropix® cAMP-Screen® System (Applied Biosystems), a competitive immunoassay with chemiluminescence detection, was used to determine cAMP in cell lysates. After treatment and lysis in the cell culture plate, a portion of the lysate was transferred to a white assay plate precoated with goat anti-rabbit IgG as secondary antibody. The lysate was incubated with a cAMP-AP conjugate and a rabbit anti-cAMP antibody and the resulting immune complexes were captured in the plate. Unbound materials were then washed from the plate and CSPD® substrate with a luminescence enhancer is added. The substrate detects the AP conjugate, the AP degradation of the substrate causing light emission that can be measured in a luminometer. The light signal generated is measured in a Luminoskan™ Ascent Microplate Luminometer (Thermo Scientific™). Intracellular cAMP and cAMP-AP conjugate compete for the antibody and so with increasing intracellular cAMP, less conjugate is captured and the lower the luminometer response. Included in the assay media, 3-isobutyl-1-methylxanthine (IBMX) acts as a phosphodiesterase inhibitor. Physiologically, cAMP is a phosphodiesterase substrate and degradation limits signalling. Inclusion of IBMX allows intracellular cAMP accumulation.

NCI-H716 cell line is a human colorectal carcinoma cell line derived from the ascites fluid of a colorectal adenocarcinoma patient. Its morphology is epithelial but under standard culture conditions it remains undifferentiated growing as amorphous floating cell aggregates. The cytoplasm contains dense core granules characteristic of endocrine secretion.[258] Adherence and enhancement of endocrine differentiation can be induced *in vitro* by culture in contact with specific extracted basement membrane components or

natural extracellular matrix.[259] BD Matrigel™ Basement Membrane Matrix can be used to do this. It is a solubilized basement membrane preparation extracted from the Engelbreth-Holm-Swarm (EHS) mouse sarcoma. The matrix is rich in ECM proteins containing collagen IV for adherence of NCI-H716 and heparin sulfate proteoglycans and a host of growth factors which induce differentiation. NCI-H716 is used as a model of the enteroendocrine L-cells and has been shown to process proglucagon into GLP-1, GLP-2, glicentin and oxyntomodulin similar to human gut.[260]

3.11.2 Assessment of MMP-9 inhibitory potency

Candidate MMP-9 inhibitors were assessed for inhibitory potency using recombinant human MMP-9 in a fluorgenic assay as described in Chapter 2 of this thesis.

3.12 Results and discussion of *in vitro* assessments

In the cAMP assay, LCA (**54**) and sodium TLCA (**58**) were included as positive controls. Treatment with LCA 10 µM for 30 min significantly increased intracellular cAMP compared to the control cells treated with DMSO vehicle ($p < 0.0001$). Treatment with sodium TLCA 10 µM also increased cAMP significantly ($p = 0.0027$). In contrast to the literature, where the tauro conjugate is described as more potent than the parent acid, we saw a trend to greater stimulation by LCA but the results are not significantly different from each other. The concentration of DMSO in the treatment media of DMSO vehicle treated cells and in compound treated cells was 1% v/v.

3.12.1 *In vitro* assessment of Group 1 conjugates

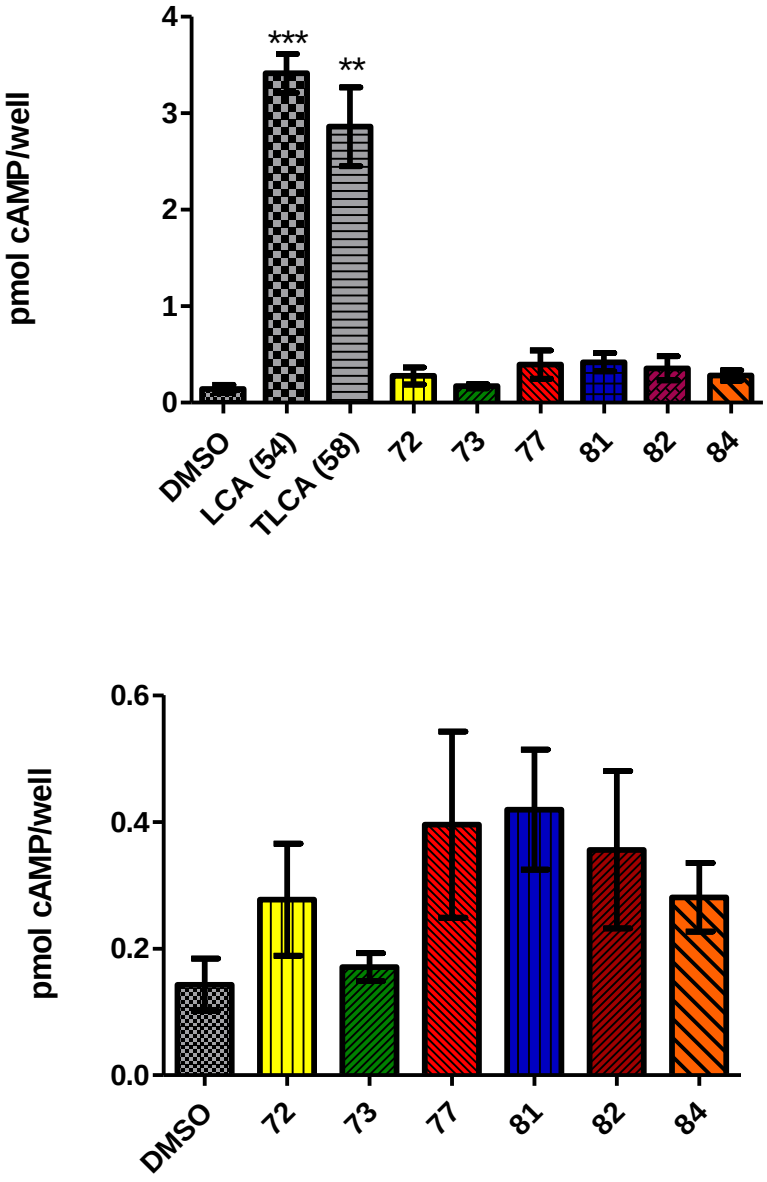

*Figure 73. Results of in vitro cAMP assay for Group 1 conjugates. NCI-H716 cells were stimulated with DMSO vehicle 1% v/v or test compound at 10 µM for 30 min and intracellular cAMP in pmol/well was determined. The values represent the mean ± SEM of the experiment in triplicate. *** $p < 0.001$; ** $p < 0.01$ versus vehicle (DMSO)-treated cells*

Treatment of NCI-H716 cells with group 1 compounds for 30 min did not significantly increase intracellular cAMP. There was a non-significant trend to cAMP production by the treatments and treatment with **81** was almost significant ($p = 0.0554$) which was between a

two and four-fold increase in cAMP accumulation compared to the control cells (Figure 73). While there may have been a non-significant trend to increased cAMP by some of the treatments, the compounds were far less active than LCA. In these Group 1 conjugates, the carboxylic acid group of LCA has been utilised for conjugation and derivatised to an amide or an amine in each case with the hope that the barbiturate ring would be able to provide affinity for the proposed polar subsite in the TGR5 binding site normally occupied by the carboxylic acid. A di-substituted barbiturate may not be sufficiently acidic to perform this function or the barbiturate ring may be too bulky particularly when substituted by a large brominated phenoxyphenyl substituent. It must be remembered that an *in vitro* assay may not model physiological pH and results may not reflect potential activity *in vivo*.

The conjugate compounds retained MMP-9 inhibitory potency and the results can be seen in Table 4.

Table 4. MMP-9 IC_{50} values for group 1 compounds

Compound No.	MMP-9 IC_{50} nM (95% CI)
72	4712.0 (3778, 5878)
73	907.2 (740.5, 1111.0)
77	8169.0 (6025, 11075)
81	276.0 (72.2, 1055.0)
84	512.0 (247.8, 1058.0)

With an MMP-9 IC_{50} of 276 nM, compound **81** was the most potent MMP-9 inhibitor of the group 1 conjugates. Interestingly, **81** and **84** (IC_{50} = 512 nM) were the most potent inhibitors. These compounds were produced by direct substitution of simple amine derivatives of LCA at C-5 of the barbiturate and are devoid of heterocycle linkers. Compounds **72**, **73** and **77** incorporate piperazine, homopiperazine or a triazole respectively. While **73** is a high nanomolar inhibitor of MMP-9 (IC_{50} = 907.2 nM), **72** and **77** are low micromolar inhibitors with IC_{50} values of 4.7 µM and 8.2 µM respectively. This order of potency was surprising as piperazine and homopiperazine have documented affinity for the S2' pocket of MMP-9.

3.12.2 *In vitro* assessment of group 1 synthetic intermediates 76 and 82

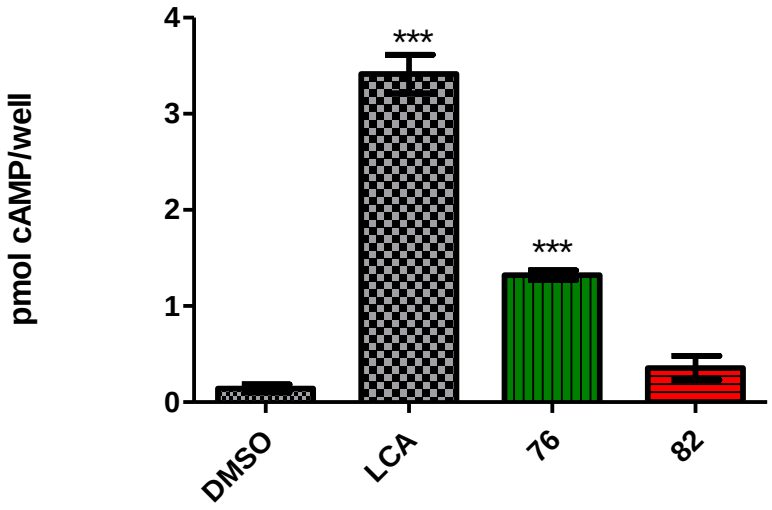

*Figure 74. Results of in vitro cAMP assay for group 1 synthetic intermediates **76** and **82**. NCI-H716 cells were stimulated with DMSO vehicle 1% v/v or test compound at 10 μM for 30 min and intracellular cAMP in pmol/well was determined. The values represent the mean ± SEM of the experiment in triplicate. *** $p < 0.001$ versus vehicle (DMSO)-treated cells*

Compounds **76** and **82**, synthetic intermediates in conjugate synthesis, were screened in the cAMP assay to probe active site tolerance. Devoid of an acid group, modification of the carboxylate of LCA to a simple secondary amide in compound **82** completely abrogated activity. Surprisingly, introduction of a terminal alkyne in compound **76** restored some activity, $p < 0.0001$ versus control cells, which was unexpected (Figure 74). A terminal alkyne can be considered a non-polar functionality and while more acidic than an alkane or an alkene, its pK_a is too high to be significantly deprotonated under these assay conditions. On review of the literature, we found that terminal alkynes have been used as enzyme active site-directed probes. Ekkebus *et al*. converted the C-terminal carboxy of ubiquitin to an alkyne by amide coupling to propargyl amine and this was shown to react with an active-site cysteine residue of deubiquitinase.[261] The vinyl thioether product was confirmed by X-ray crystallography. They demonstrated that this reaction was selective in the presence of excess thiol and that it was not restricted to the ubiquitin case. Similarly, they demonstrated the reaction of alkyne functionalised IL-1β with a cysteine of interleukin converting enzyme (caspase-1). The interaction of **76** at the TGR5 binding site should be examined further. If such a covalent interaction was shown to be occurring, **76** could prove a useful probe for the receptor.

3.12.3 *In vitro* assessment of group 2 conjugates

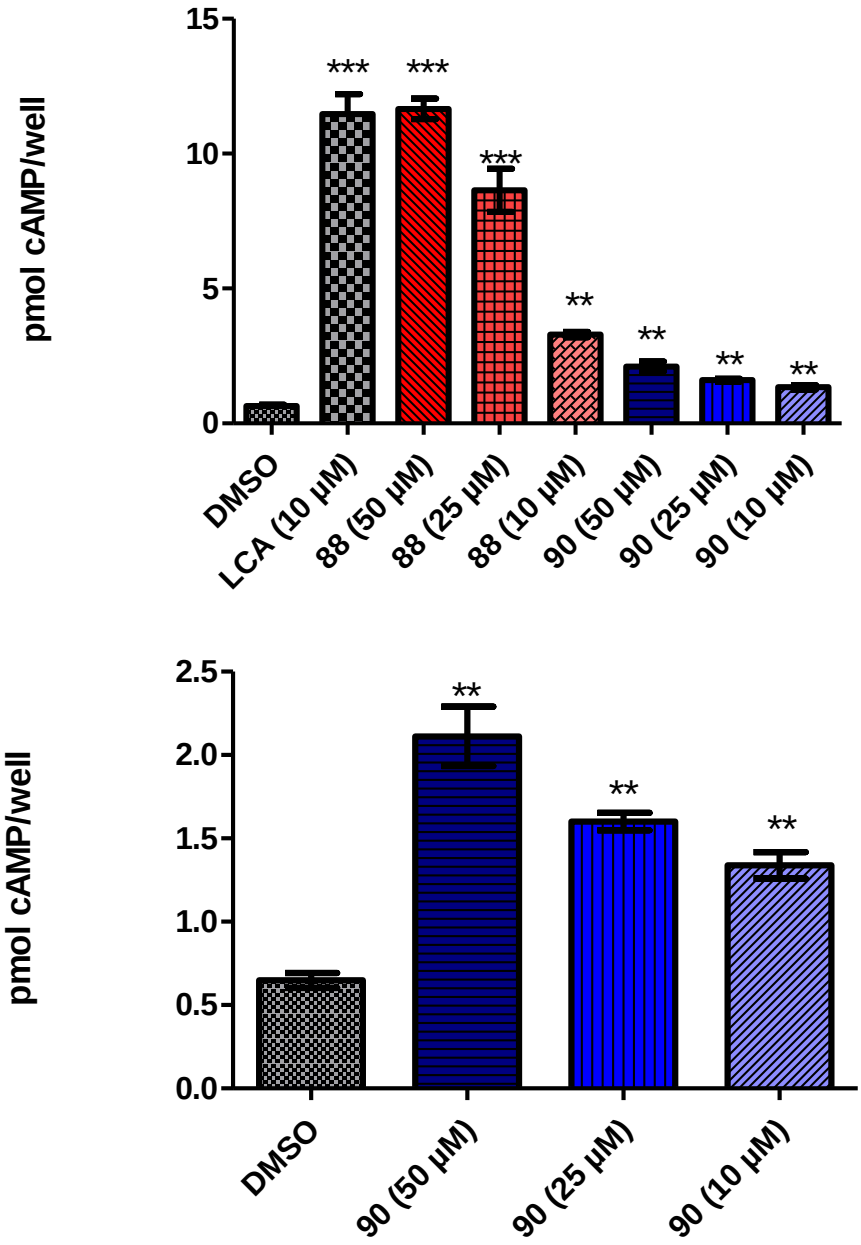

*Figure 75. Results of in vitro cAMP assay for group 2 conjugates. NCI-H716 cells were stimulated with DMSO vehicle 1% v/v or test compound for 30 min and cAMP in pmol/well was determined. The values represent the mean ± SEM of the experiment in triplicate. *** $p < 0.001$; ** $p < 0.01$ versus vehicle (DMSO)-treated cells*

Stimulation of the cells with the lysine derivatives caused cAMP accumulation greater than that of the control cells (Figure 75). The acetamide derivative, **88**, gave the strongest

stimulation, 50 µM producing an effect comparable to 10 µM LCA. Compound **90** was tested at 50 µM, 25 µM and 10 µM and while the effect was small, a dose response can be seen. At 10 µM, **90** increased intracellular cAMP 2-fold in comparison to the DMSO treated cells (p = 0.0016). MMP-9 inhibitory activity was retained in compound **90** and the IC_{50} was 439 nM (95% CI 384.8, 500.9).

Using lysine as a linker between the pharmacophores somewhat improved the response. The acetamide derivative at 50 µM produced a response comparable to LCA 10 µM which indicated that although the introduction of lysine decreased potency, pharmacologically relevant efficacy could be achieved using a higher concentration. Attaching the barbiturate or another molecule of LCA to the ε-N of the lysine derivative further decreased potency. Attaching such bulky groups did not completely abrogate activity but did dramatically reduce it. For a candidate compound such as **90**, we can see in the concentration range we have examined that the effect while small was concentration dependent. It will require further empirical studies to determine if the effect can be pharmacologically relevant.

3.12.4 *In vitro* assessment of compounds 91, 92 and 100

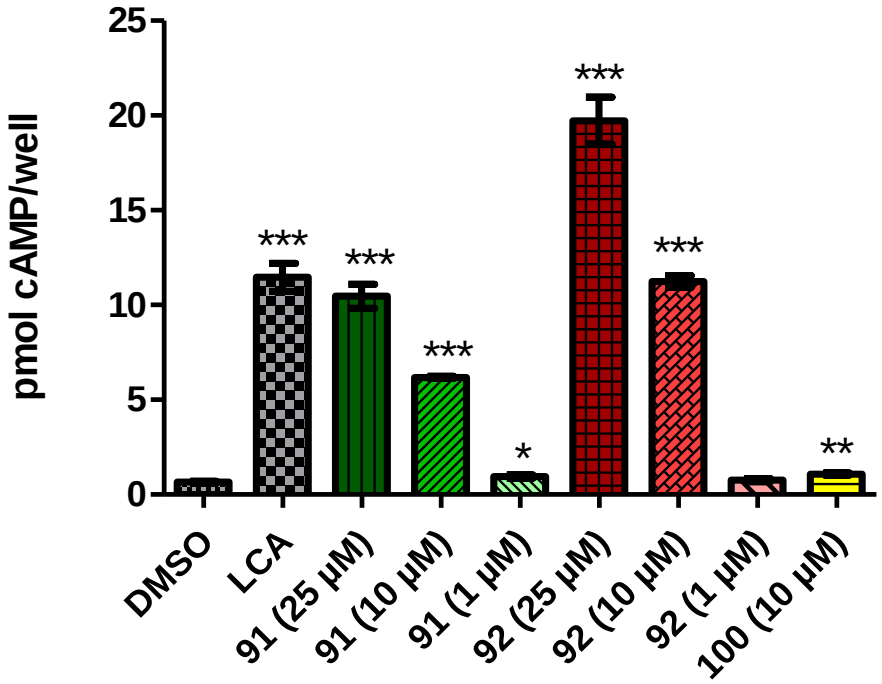

*Figure 76. Results of in vitro cAMP assay for compounds **91**, **92** and **100**. NCI-H716 cells were stimulated with DMSO vehicle 1% v/v or test compound for 30 min and cAMP in pmol/well was determined. The values represent the mean ± SEM of the experiment in triplicate. *** $p < 0.001$; ** $p < 0.01$; * $p < 0.05$ versus vehicle (DMSO)-treated cells*

Coupling to homoserine in compound **91** did reduce LCA potency but 10 µM produced an effect almost 10 times that of control cells and 25 µM gave an effect comparable to 10 µM LCA (Figure 76). The hydroxymate **92** was a good TGR5 agonist with an effect comparable to LCA at the same test concentration of 10 µM but no effect at 1 µM. Hydroxymates are excellent metal chelators and many chemical structures derivatised as hydroxymates have proved potent MMP inhibitors. Unfortunately, however, we did not find **92** to be a good inhibitor of MMP-9. The inhibition, which was inconsistent, was *circa* 25% at 50 µM but it could not be increased further with increasing concentration. Reduction of the carboxylate to an alcohol in compound **100** reduced activity greatly. While there was an increase in cAMP on treatment with **100,** the cAMP produced was less than two-fold that produced by the control cells and at 10 µM, < 5% of the effect produced by the same concentration of LCA.

3.12.5 *In vitro* assessment of compound 95

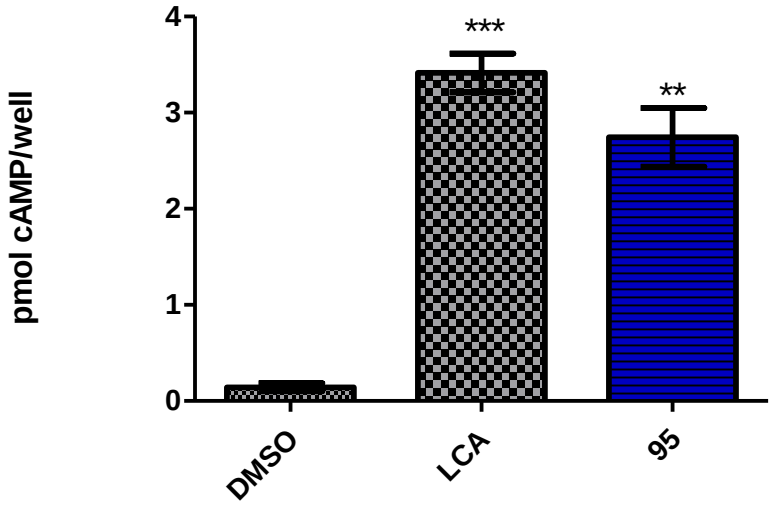

*Figure 77. Results of in vitro cAMP assay of compound **95**. NCI-H716 cells were stimulated with DMSO vehicle 1% v/v or test compound at 10 µM for 30 min and cAMP in pmol/well was determined. The values represent the mean ± SEM of the experiment in triplicate. *** $p < 0.001$; ** $p < 0.01$ versus vehicle (DMSO)-treated cells*

Oxidation of the 3-OH of LCA to a ketone in compound **95** did not significantly compromise potency relative to LCA and treatment with **95** increased cAMP significantly compared to the control cells ($p = 0.0011$) (Figure 77). A hydrogen bond donor is not a strict requirement at the 3-position of LCA.

3.12.6 In vitro assessment of ciprofloxacin and 99, a ciprofloxacin-MMP inhibitor conjugate

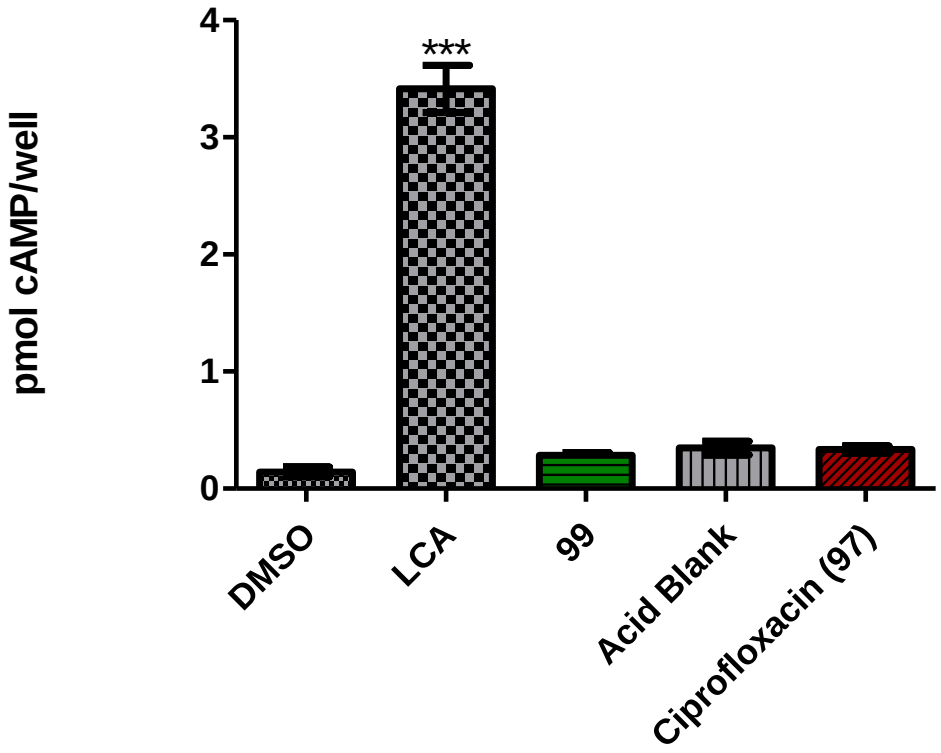

*Figure 78. Results of in vitro cAMP assay of ciprofloxacin and compound **99**. NCI-H716 cells were stimulated with vehicle or test compound at 10 µM for 30 min and cAMP in pmol/well was determined. The values represent the mean ± SEM of the experiment in triplicate. *** $p < 0.001$*

Ciprofloxacin is not sufficiently soluble in DMSO for preparation of a standard solution and so ciprofloxacin solution was prepared at 100 mM in approximately 0.1 M aqueous HCl and this solution was serially diluted to provide the test solution. An acid blank was prepared in the same manner as a control for ciprofloxacin in the assay. The ciprofloxacin conjugate **99** was prepared in DMSO and so DMSO 1% v/v treated cells are the control wells for **99**. Treatment with ciprofloxacin did not increase intracellular cAMP which was unexpected. Likewise, the conjugate **99** did not stimulate the cells (Figure 78).

In 2011, Cipriani *et al*. reported that ciprofloxacin is a TGR5 ligand and that it was nearly as potent as TLCA in a murine cell line.[69] Treatment of the NCI-H716 cells with ciprofloxacin did not induce cAMP in our model. Cipriani *et al.* found that ciprofloxacin treatment attenuated TNBS-induced colitis in mice and effects of attenuated neutrophil influx and inflammatory cytokine production unrelated to its antibiotic effects were lost

when ciprofloxacin was administered to TNBS treated *TGR5*$^{-/-}$ mice. It must be noted that the accompanying *in vitro* work was carried out in a murine GLUTag cell line and in spleen-derived monocytes from wild type and *TGR5*$^{-/-}$ mice. The lack of response to ciprofloxacin observed in human NCI-H716 cells may be due to the differences between the murine and human receptors. The amino acid sequence identity between the mouse and human receptors is 83%. Other research groups have reported widely varying potencies against the human and mouse receptor in chemical library screenings prompting some to use human TGR5 knock-in mice for *in vivo* work. Interestingly, bile acid identity and composition vary significantly between rodents and humans. Along with cholic acid, muricholic acid is synthesized in the liver of the mouse which is tri-hydroxy substituted at 3α, 6β and 7β and this is 7 dehydroxylated to the murine secondary bile acid, murideoxycholic acid. Tauro-conjugates predominate in rodents, glycol-conjugates in humans. Conjugation of the MMP inhibitor to ciprofloxacin did not dampen MMP-9 inhibitory activity and **99** is a low nM inhibitor with an IC_{50} of 17.04 nM, 95% CI (12.32, 23.55).

3.12.7 *In vitro* assessment of compounds 102 and 104

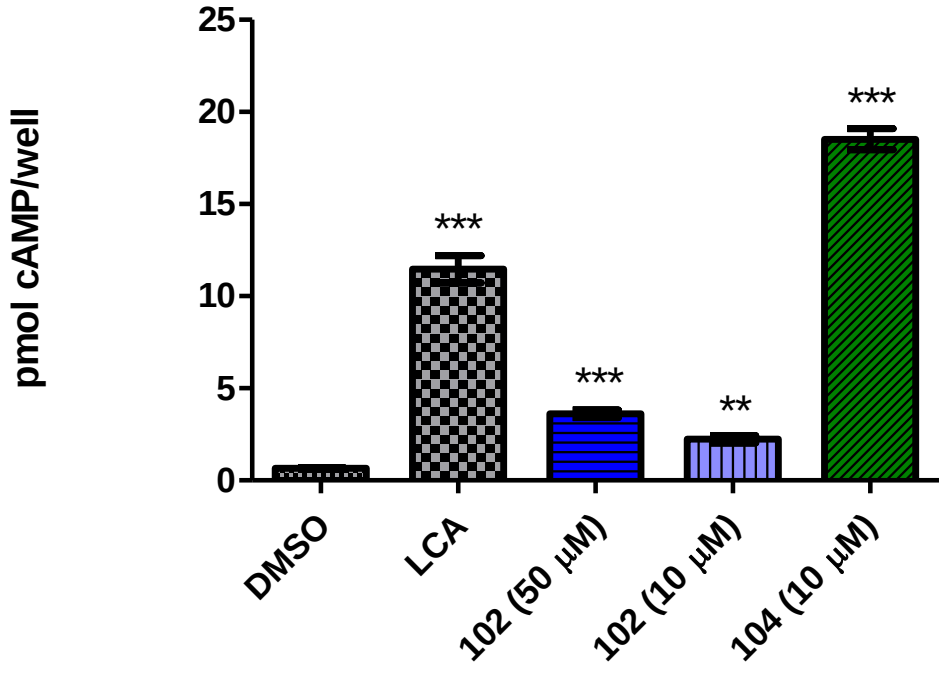

*Figure 79. Results of in vitro cAMP assay of compounds **102** and **104**. NCI-H716 cells were stimulated with DMSO vehicle 1% v/v or test compound for 30 min and cAMP in pmol/well was determined. The values represent the mean ± SEM of the experiment in triplicate. *** p < 0.001; ** p < 0.01 versus vehicle (DMSO) treated cells*

The positively charged compound **102** stimulated some cAMP accumulation and this was concentration dependent, 50 μM producing over five-fold more than control cells and 10 μM producing over three-fold more than control cells (Figure 79). The sulfonic acid derivative **104** proved to be a potent stimulator of cAMP inducing 50% more cAMP than LCA at the same test concentration of 10 μM. Compound **104** had no inhibitory effect on MMP-9.

Compound **102** holds a permanent positive charge and is a poor candidate for passive absorption but the intestine is capable of absorbing bile acids and some of their derivatives by active transport. ASBT functions as a bile acid transporter in the enterohepatic circulation. It transports the bile acids as well as the bile acid conjugates, conjugation enhancing transport. Chemistry of the C-24 position influences ASBT binding. Initially it was thought that a negative charge in this region was essential because its known endogenous bile acid and non-bile acid substrates are acids. Neutral compounds can be transported however and it is now thought that a hydrogen bond acceptor can satisfy the 'negative charge' requirement. Balakrishnan *et al*. evaluated the influence of charge and steric bulk around C-24 using conjugates of CDCA to glutamic acid and lysine derivatives. This work suggests that zwitterionic and cationic derivatives are not substrates but may still bind as ASBT inhibitors. Compound **104** is likely to be an ASBT transport substrate but the low pK_a of the sulfonic acid group means that it is ionised at physiological pH and would have limited passive absorption potential in the colon. Rectal administration of **104** or protection of orally administered **104** by a suitably designed pharmaceutical formulation for colonic delivery could bypass active absorption if necessary and achieve non-systemic activation of colonic TGR5.

3.12.8 *In vitro* assessment of a representative barbiturate, 51, and representative anthranilate sulfonamides, 107 and 127

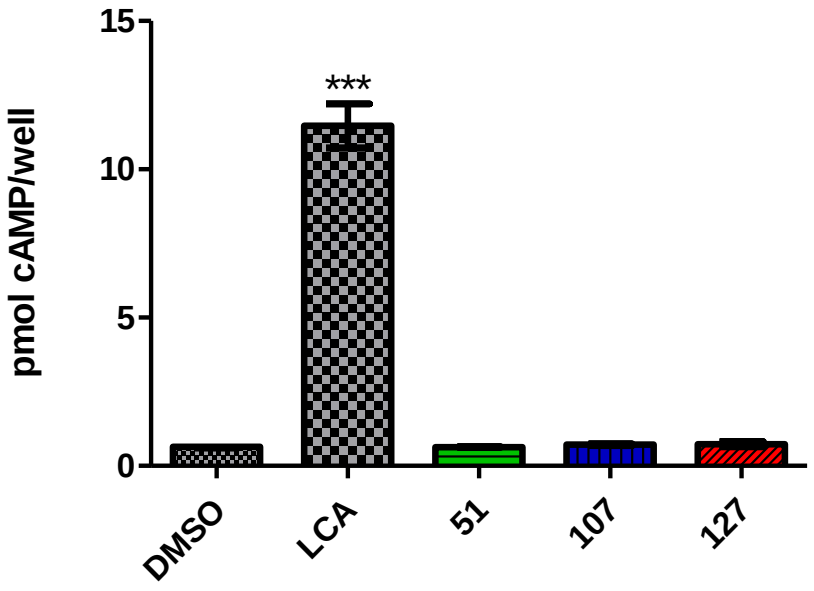

*Figure 80. Results of in vitro cAMP assay of compounds **51**, **107** and **127**. NCI-H716 cells were stimulated with DMSO vehicle 1% v/v or test compound at 10 µM for 30 min and cAMP in pmol/well was determined. The values represent the mean ± SEM of the experiment in triplicate. *** $p < 0.001$ versus vehicle (DMSO) treated cells*

Reported non-bile acid TGR5 agonists have included heterocyclic scaffolds with aromatic substitutions and sulfonamides. We screened **51** as a representative of the barbiturates and two anthranilate sulfonamides, **107** and **127**, in the cAMP assay but there was no increase in intracellular cAMP (Figure 80). We conclude that these compounds have no agonist activity at TGR5.

Chapter 4. Conclusions, limitations and future work

4.1 Conclusions, limitations and future work

On-going discovery of transporters, membrane receptors, enzymes and signalling proteins apically expressed by the intestinal epithelia has highlighted opportunities for non-systemic therapeutics. Restricted to the gut lumen, such therapeutics can achieve local or systemic effects whilst maintaining favourable safety profiles. The availability of luminally accessible drug targets also opens physicochemical space for drug development. Molecular structures with poor permeability profiles deemed not sufficiently 'drug-like' for systemic oral bioavailability could have non-systemic applications.

The pathological role of MMP-9 in IBD, its upregulation and apical secretion in the inflammatory condition and the benefits of modulation in disease models have been well established. In this work, we targeted luminal MMP-9 with compound **53** in a DSS mouse model of colitis and demonstrated that a non-systemic approach can achieve disease modifying effects. By design, **53** is a poor candidate for absorption and future work will involve full pharmacokinetic profiling in a mouse model. The measurement criteria for a non-absorbed drug are essentially the same as for a bioavailable drug and drug and metabolite levels in arterial blood, the portal vein, urine and faeces should be established.[71] In addition, any metabolites observed should be elucidated and assessed for activity at the target and considered for contribution to the pharmacological effect. The first steps in this work will involve assessment of the stability of compound **53** in mouse plasma and development of a suitable analytical method for biological matrices. Good sensitivity will be required to achieve a low nanomolar limit of detection (LOD) below the IC_{50} of **53**. We have been unable to achieve a LOD below 10 nM with the UPLC-MS/MS method developed thus far. Alternative approaches to probing the pharmacokinetics and metabolic pathways of **53** may be considered. Mass balance excretion studies using radiolabeled compound can provide much information on absorption, distribution, metabolism and excretion (ADME).[262, 263] Compound **49**, the PEG chain-linked MMP inhibitor dimer, was also a potent inhibitor of recombinant human MMP-9. Disappointingly, it had poor solubility in most solvents including DMSO. Future work may involve synthesizing dimers with PEG chain linkers of increasing length to increase polarity and solubility.

The MMP inhibitor – TGR5 agonist conjugates retained good MMP-9 inhibitory potency. Maintaining agonist activity at TGR5 proved more challenging and the receptor did not have the binding tolerance we had hoped. This work found that an acidic group in the vicinity of C-24 was favourable for activity. Conversion of the C-24 carboxylic acid to a

simple amide in compound **82** greatly reduced the effect as did reduction to an alcohol in compound **100**. Reintroduction of an acid group by coupling to lysine in the acetamide derivative, compound **88** or homoserine in compound **91** increased activity. Compound **88** at 50 µM produced an effect comparable to LCA at 10 µM. Unfortunately, conjugation to the MMP inhibitor reduced potency further indicating that bulky substituents at this position can hinder binding. Future work may include synthesis of conjugates with longer chain linkers between the pharmacophores. Conjugation to a smaller MMP inhibitory moiety is another approach worth pursuing. While our series of benzoic acid derivative candidates did not have sufficient MMP-9 inhibitory potency, an alternative MMP inhibitor may prove suitable.

Compound **90** is a potent MMP-9 inhibitor and warrants further study. Its effect on intracellular cAMP accumulation was small but it is as yet unknown if this level of TGR5 activation can produce a pharmacological effect in a gut-confined context. TGR5 does not traffic to endosomes on activation and appears to open to repeated stimulation.[264] Compound **90** is a poor candidate for passive uptake. It has a predicted Log P of 5.79, 12 H-bond acceptors, 6 H-bond donors and a molecular weight of 877.9 g/ mol[165] and so breaches Lipinski's rules.[74] With a calculated tPSA of 183.15 and 15 rotatable bonds,[165] it also contravenes Veber's rules for good absorption.[76] Future work will involve assessment of its permeability in an *in vitro* model and assessment of the stability of the amide linkage to enzymes of the GIT. If it is sufficiently stable and is poorly taken up, it may be a candidate for *in vivo* evaluation in a model of colitis. Compound **90** is a potentially non-absorbable gelatinase inhibitor and its pharmacokinetic-modifying moiety limiting absorption potential may in this case also contribute to effect.

In the course of this work, we also identified potential for synthesis of gut-confined TGR5 agonists. The permanent positive charge in compound **102** should limit uptake and treatment with **102** caused some cAMP accumulation *in vitro*. The sulfonic acid derivative, **104**, was more potent than LCA. A component of future work could be synthesis of sulfonic acid derivatives as potential gut-confined TGR5 agonists. Sulfonic acids are poor candidates for passive uptake and chemical modifications could be pursued to abolish affinity for ASBT transport if necessary.

In this work, we used intracellular accumulation of cAMP as an indirect measure of TGR5 activation. Future work could confirm that the effects we have seen are TGR5-mediated. This could be done by transfection of a TGR5 plasmid into a suitable cell line such as

CHO cells or human embryonic kidney 293 (HEK293) cells which have been widely used for this purpose.[219, 265, 266] Measured effect can be attributed to TGR5 activation if the effect is not also seen in the parent non-transfected cells. TGR5 siRNA transfection can also be used to knockdown TGR5 activity and has been used to delineate the role of TGR5 and bile acids in disease.[267, 268] TGR5 silencing treatment has also been used successfully in NCI-H716 cells.[269, 270] Incorporating TGR5 siRNA treatment with measurement of intracellular cAMP levels in future *in vitro* work would allow observed effects to be directly attributed to TGR5 activation.

Chapter 5. Experimental

5.1 Chemistry materials and methods

5.1.1 General methods

All chemicals and starting materials were commercially purchased and used as provided except where stated. All reactions were monitored by TLC and/or HPLC. Uncorrected melting points were measured on a Stuart Apparatus. Infra-red (IR) spectra were performed on a Perkin Elmer ATR FT-IR spectrometer. ^{1}H and ^{13}C nuclear magnetic resonance (NMR) spectra were recorded at 27°C on an Agilent 400 spectrometer (400 MHz, ^{1}H; 101 MHz, ^{13}C). Coupling constants are reported in Hertz. For ^{1}H-NMR assignments, chemical shifts are reported: shift value (number of protons, description of absorption, coupling constant(s) where applicable). Mass spectrometry was performed by Mr. Brian Talbot, School of Pharmacy, TCD, using a Thermo Fisher Accela LC system coupled to an LTQ – Orbitrap discovery detector. Samples were introduced by electrospray ionisation (ESI) or atomospheric pressure chemical ionisation (APCI) in the positive ion mode or in the negative ion mode. The HPLC system used consisted of a Waters 1525 Binary HPLC Pump, Waters 717 plus Autosampler, Waters 2487 Dual λ Absorbance Detector and a Waters In-Line Degasser AF. Empower® software was used for system control, data acquisition and processing.

5.1.2 TLC dip visualisation methods

Ammonium molybdate/ceric sulfate solution

A good general reagent, bile acid structures give a strong response to this dip. On strong heating, this dip gives deep blue spots on a pale background. It was prepared by dissolving **a**mmonium molybdate (5 g) and ceric sulfate (0.2 g) in 5% v/v aqueous H_2SO_4 (100 mL)

Ninhydrin

Ninhydrin was used as a dip for amines. On heating, this gives spots of purple pink to orange brown on a pale yellow background. Primary amines and BOC-protected amines give a strong response and secondary amines may sometimes give a weak response. It was prepared by dissolving ninhydrin (0.3 g) in 50 mL C_2H_5OH. Acetic acid (3 mL) was added and the solution was brought to a final volume of 100 mL with C_2H_5OH.

Potassium permanganate

Unsaturated compounds and alcohols give yellow spots on a pink purple background. Gentle heating is sometimes required. It was prepared by dissolving potassium permanganate (3 g) and potassium carbonate (20 g) in 5% aqueous NaOH (5 mL) and the solution is brought to a final volume of 300 mL with H_2O.

Vanillin

A particularly good reagent for alcohols, it gives spots of many colours on a pale grey beige background with strong heating. It was prepared by dissolving vanillin (15 g) in C_2H_5OH (250 mL) and adding conc. H_2SO_4 (2.5 mL) slowly with stirring.

5.2 Synthesis – Chapter 2

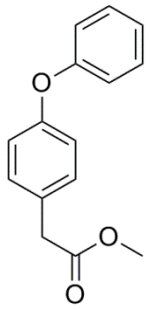

31

Methyl 2-(4-hydroxyphenyl)acetate (compound **30**) (3.3223 g, 20 mmol), phenylboronic acid (4.8772 g, 40 mmol, 2 eq.), copper (II) acetate (3.6326 g, 20 mmol, 1 eq.) and powdered 4 Å molecular sieves were dispersed in DCM (100 mL). Anhydrous pyridine (8 mL, 100 mmol, 5 eq.) was added and the mixture was stirred at RT in ambient air for 48 h. The resulting green slurry was filtered and the DCM was removed *in vacuo*. The residue was dispersed in Et_2O (150 mL) and washed with aqueous 1M HCl (2 × 100 mL), saturated $NaHCO_3$ solution (100 mL), H_2O (100 mL) and brine (50 mL). The organic layer was dried over Na_2SO_4, filtered and concentrated to a dark orange oil. The product was isolated by flash column chromatography using Hex:EtOAc (6:1) as mobile phase as a pale yellow oil (1.1074 g, 22.9%).

^{1}H NMR (400 MHz, $CDCl_3$) δ 7.37–7.41 (m, *J* = 7.53, 2H, Ar-H), 7.3 –7.32 (d, *J* = 8.53, 2H, Ar-H), 7.14–7.18 (t, *J* = 7.53, 1H, Ar-H), 7.03–7.09 (m, 4H, Ar-H), 3.76 (s, 3H, -CH_3), 3.68 (s, 2H, -CH_2); **^{13}C NMR** (101 MHz, $CDCl_3$) δ 172.2, 156.9, 156.2, 130.5, 129.6, 128.5, 123.1, 118.7, 115.2, 51.9, 40.2; **IR:** (ATR) ν cm^{-1} 1734.84, 1506.53, 1487.57, 1231.58, 1157.12; **HRMS:** Found (M+Na) = 265.0835, calculated for $C_{15}H_{14}O_3Na$ = 265.0841

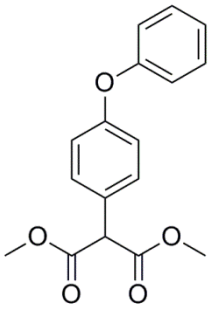

32

A 60% suspension of NaH in paraffin oil (1.4784 g, 36.96 mmol, 3 eq.) was washed with hexane and dispersed in anhydrous THF (30 mL) under N_2. Dimethyl carbonate (6.65 mL, 78.88 mmol, 6.4 eq.) was added and the mixture was heated to reflux at 90°C. Compound **31** (2.9859 g, 12.32 mmol, 1 eq.) dispersed anhydrous THF (20 mL) was added dropwise over 1 h maintaining the usual precautions for anhydrous conditions. After 5 h reflux, the dark orange reaction mixture was poured onto iced-water and the product was extracted with DCM (50 mL × 3). The combined organic layers were washed successively with water (100 mL) and brine (30 mL), dried over Na_2SO_4 and filtered. The solvent was removed *in vacuo* to yield the product which could be used in the next step without further purification as a yellow-orange solid (3.2763, 88.6%). Mp 43 - 45°C; **^{1}H NMR** (400 MHz, $CDCl_3$) δ 7.35–7.41 (m, 4H, Ar-H), 7.13–7.17 (t, *J* = 7.53, 1H, Ar-H), 7.01–7.07 (m, 4H, Ar-H), 4.68 (s, 1H, CH), 3.79 (s, 6H, 2 × CH_3); **^{13}C NMR** (101 MHz, $CDCl_3$) δ 168.5, 157.4, 156.5, 130.6, 129.7, 126.9, 123.5, 119.2, 118.4, 56.6, 52.8; **IR:** (ATR) ν cm^{-1} 3064.12, 1734.33, 1611.18, 1590.59; **HRMS:** Found (M+Na) = 323.0888, calculated for $C_{17}H_{16}O_5Na$ = 323.0895

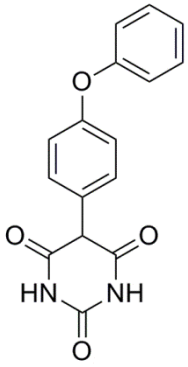

33

Sodium (0.5019 g, 21.82 mmol, 2 eq.) was dissolved in HPLC grade C_2H_5OH (20 mL) and urea (1.1139 g, 18.55 mmol, 1.7 eq.) was added and dissolved. A solution of **32** (3.2763 g, 10.91 mmol, 1 eq.) in HPLC grade C_2H_5OH was added dropwise and the reaction mixture

was heated to reflux at 100°C under N_2 for 7 h. After cooling to ambient temperature, the reaction mixture was poured onto iced-water and acidified to pH 2 with 1 M aqueous HCl. The yellow precipitate was collected by suction filtration. The solid was refluxed at 80°C in EtOAc:MeOH (3:1) for 2 h and the pure product was isolated by hot filtration as an off-white solid (1.38 g, 42.7%). Mp 250 - 253^{o}C; **^{1}H NMR** (400 MHz, DMSO-d_6) δ 11.4 (s, 2H, N-H), 7.37–7.41 (m, 2H, *J* = 7.58, Ar-H), 7.26–7.28 (m, 2H, Ar-H), 7.13–7.16 (t, 1H, *J* = 6.85, Ar-H), 7.01–7.03 (m, 2H, Ar-H), 6.95–6.97 (m, 2H, Ar-H), 4.84 (s, 1H, CH); **^{13}C NMR** (101 MHz, DMSO-d_6) δ 169.4, 156.5, 156.4, 151.1, 131.2, 130.2, 129.3, 123.9, 119.1, 118.5, 54.4; **IR:** (ATR) ν cm^{-1} 3190.17, 1742.90, 1711.07, 1519.34, 1501.54, 1371.14, 1243.72; **HRMS**: Found (M+Na) = 319.0684, calculated for $C_{16}H_{12}N_2O_4Na$ = 319.0695

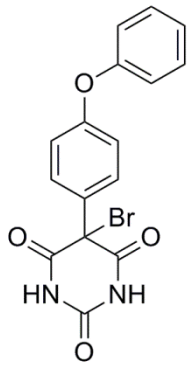

34

Compound **33** (0.5 g, 1.69 mmol, 1eq.) was dissolved in CCl_4 (20 mL). N-bromosuccinimide (0.3613 g, 2.03 mmol, 1.2 eq.) and a catalytic amount of benzoyl peroxide were added and the reaction mixture was refluxed at 78°C for 3 h. The CCl_4 solvent was removed *in vacuo* and the residue was dispersed in water. The aqueous dispersion was extracted with EtOAc (3 × 50 mL) and the combined organic layers were washed with water (5 × 30 mL) and brine (20 mL). The organic phase was dried over Na_2SO_4, filtered and concentrated to afford the product as an off-white solid (0.3969 g, 62.6%). Mp 111 - 113 ^{o}C; **^{1}H NMR** (400 MHz, DMSO-d6) δ 11.45 - 11.60 (m, 2H, N-H), 7.57 (d, J = 8.71 Hz, 1H, Ar-H), 7.32 - 7.46 (m, 3H, Ar-H), 7.12 - 7.23 (m, 1H, Ar-H), 6.93 - 7.11 (m, 4H, Ar-H); **^{13}C NMR** (101 MHz, DMSO-d6) δ 170.9, 157.3, 157.2, 156.0, 149.8, 133.0, 130.2, 128.2, 127.8, 127.8, 127.0, 123.9, 123.9, 119.1, 119.1, 119.1, 118.3, 117.7, 117.6, 75.7; **IR:** (ATR) ν cm-1 3226.73, 1735.63, 1706.71, 1585.44, 1411.20, 1335.52, 1237.09; **HRMS:** Found (M-Br) = 295.0730, calculated for $C_{16}H_{11}N_2O_4$ = 295.0724

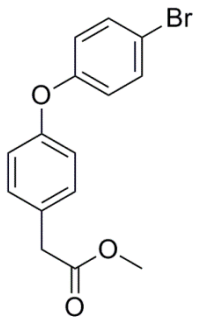

36

Methyl 2-(4-hydroxyphenyl)acetate (3g, 18.05 mmol), 4-bromophenyl boronic acid (7.25 g, 36.10 mmol, 2 eq.), copper(II) acetate (3.28 g, 18.05 mmol, 1 eq.) and powdered 4 Å molecular sieves were dispersed in DCM (100 mL). Anhydrous pyridine (7.3 mL, 90.25 mmol, 5 eq.) was added and the mixture was stirred at RT in ambient air for 48 h. The resulting green slurry was filtered and DCM was removed *in vacuo*. The residue was dispersed in Et_2O (150 mL) and washed with 1M aqueous HCl (2 × 100 mL), saturated $NaHCO_3$ solution (100 mL), H_2O (100 mL) and brine (50 mL). The organic layer was dried over Na_2SO_4, filtered and concentrated to a dark orange oil. The product was isolated by flash column chromatography using Hex:EtOAc (6:1) as mobile phase as a pale yellow oil (1.62 g, 23.68%). **^{1}H NMR** (400 MHz, $CDCl_3$) δ 7.36 - 7.45 (m, 2H, Ar-H), 7.20 - 7.27 (m, 2H, Ar-H), 6.91 - 6.97 (m, 2H, Ar-H), 6.83 - 6.91 (m, 2H, Ar-H), 3.69 (s, 3H, CH_3), 3.59 (s, 2H, CH_2); **^{13}C NMR** (101 MHz, $CDCl_3$) δ 172.0, 156.4, 155.8, 132.6, 130.7, 129.2, 120.4, 119.0, 115.6, 52.1, 40.3; **IR:** (ATR) ν cm^{-1} 1735.22, 1505.65, 1232.05, 1159.57, 820.27; **HRMS:** Found (M-H) = 318.9614, calculated for $C_{15}H_{12}BrO_3$ = 318.9975

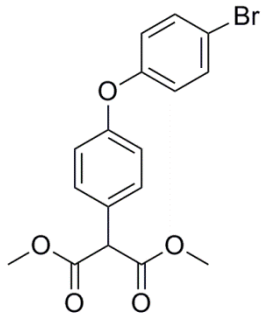

37

A 60% suspension of NaH in paraffin oil (2.2836 g, 57.09 mmol, 3 eq.) was washed with hexane and dispersed in anhydrous THF (30 mL) under N_2. Dimethyl carbonate (10.3 mL,

121.79 mmol, 6.4 eq.) was added and the mixture was heated to reflux at 90°C. Compound **36** (6.1123 g, 19.03 mmol, 1 eq.) dispersed in 20 mL anhydrous THF was added dropwise over 1 h maintaining the usual precautions for anhydrous conditions. After 5 h reflux, the dark orange reaction mixture was poured onto iced-water and the product was extracted with DCM (50 mL × 3). The combined organic layers were washed successively with H_2O (100 mL) and brine (30 mL), dried over Na_2SO_4 and filtered. The solvent was removed *in vacuo* to yield the product which could be used in the next step without further purification as a yellow-orange solid (6.1684 g, 85.5%). Mp 41 - 42°C; **^{1}H NMR** (400 MHz, $CDCl_3$) δ 7.45 (m, 2H, Ar-H), 7.38 (d, *J* = 8.71 Hz, 2H, Ar-H), 6.98 (d, *J* = 8.71 Hz, 2H, Ar-H), 6.91 (d, *J* = 8.71 Hz, 2H, Ar-H), 4.65 (s, 1H, CH), 3.78 (s, 6H, CH_3); **^{13}C NMR** (101 MHz, $CDCl_3$) δ 168.5, 157.0, 155.9, 132.7, 130.8, 127.6, 120.8, 118.7, 116.1, 56.7, 52.9; **IR:** ν cm^{-1} 2948.97, 1741.43, 1727.73, 1480.78, 1199.60, 1096.36, 823.45; **HRMS:** Found (M-H) = 377.0024, calculated for $C_{17}H_{14}BrO_5$= 377.0030

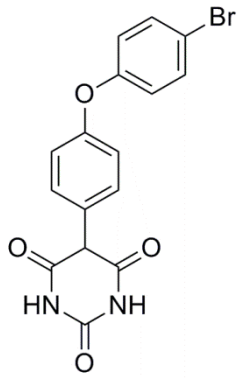

38

Sodium (0.6762 g, 29.4 mmol, 2 eq.) was dissolved in HPLC grade C_2H_5OH (20 mL) and urea (1.5009 g, 25 mmol, 1.7 eq.) was added and dissolved. A solution of **37** (3.2763 g, 10.91 mmol, 1 eq.) in HPLC grade C_2H_5OH was added dropwise and the reaction mixture was heated to reflux at 100°C under N_2 for 7 h. After cooling to ambient temperature, the reaction mixture was poured onto iced-water and acidified to pH 2 with 1 M aqueous HCl. The yellow precipitate was collected by suction filtration. The solid was refluxed at 80°C in EtOAc:MeOH (3:1) for 2 h and the pure product was isolated by hot filtration as an off-white solid (2.0596 g 37.3%). Mp 270 - 275°C decomposition; **^{1}H NMR** (400 MHz, DMSO-d_6) δ 11.34 (br. s., 1H, NH), 10.62 (br. s., 1H, NH), 7.52 (d, *J* = 8.71 Hz, 2H, Ar-H), 7.28 (br. s., 1H, Ar-H), 7.16 - 7.27 (m, 1H, Ar-H), 6.90 - 7.02 (m, 4H, Ar-H), 4.79 - 4.91 (m, 1H) **^{13}C NMR** (101 MHz, DMSO-d_6) δ 169.4, 156.5, 156.4, 151.1, 131.2, 130.2, 129.3, 123.9, 122.2, 117.8, 54.4; **IR:** (ATR) ν cm^{-1} 3249.15, 3070.17, 1755.10, 1717.00,

1598.77, 1356.03, 1235.86; **HRMS:** Found (M-H) = 372.9831, calculated for $C_{16}H_{10}BrN_2O_4$ = 372.9829

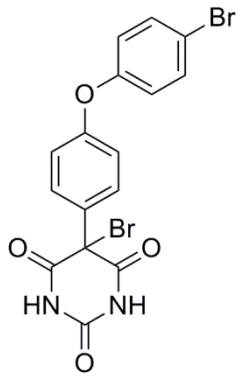

39

A suspension of **38** (4.0225 g, 10.7 mmol, 1 eq.) in H_2O 30 mL was cooled on an ice-water bath to 0°C and a mixture of Br_2 (877 µL, 17.12 mmol, 1.6 eq) and 48% HBr (2150 µL, 18.99 mmol, 1.78 eq.) was added dropwise while stirring. The mixture was stirred at 0 - 5°C for 5 h and the precipitate was collected by filtration and washed with H_2O (3 × 10 mL) to afford the product as an off-white solid (4.56 g, 93.9%). Mp 155 - 158°C decomposition; **^{1}H NMR** (400 MHz, DMSO-d_6) δ 11.54 (s, 2H, NH), 7.55 (d, *J* = 9.12 Hz, 2H, Ar-H), 7.43 (d, *J* = 8.71 Hz, 2H, Ar-H), 7.06 (d, *J* = 8.71 Hz, 2H, Ar-H), 6.98 (d, *J* = 9.12 Hz, 2H); **^{13}C NMR** (101 MHz, DMSO-d_6) δ 170.9, 156.7, 155.6, 149.9, 133.5, 132.9, 127.2, 121.1, 118.7, 115.6, 75.7; **IR:** (ATR) ν cm^{-1} 3313.67, 3250.61, 1717.98, 1694.86, 1477.83, 1328.42, 1244.48, 1203.99, 832.84; **HRMS:** Found (M-Br) =372.9832, calculated for $C_{16}H_{10}BrN_2O_4$ =372.9829

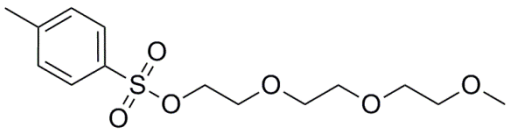

41

To a solution of triethylene glycol monomethyl ether (compound **40**) (2.5000 g, 15.2 mmol) in anhydrous DCM (20 mL), *p*-toluenesulfonyl chloride (5.80 g, 30.4 mmol, 2 eq.) and NEt_3 (4.26 mL, 30.4 mmol, 2 eq.) in DCM (2 mL) was added dropwise over an ice-water bath under anhydrous conditions. After 20 min, the ice-bath was removed and the reaction allowed to come to RT. Upon completion of the reaction in 2 h as indicated by

TLC, crushed ice was added and stirred for 10 min. The cloudy aqueous phase was extracted with DCM (3 × 50 mL). The combined organic layers were successively washed with aqueous 1M HCL (20 mL), saturated $NaHCO_3$ (20 mL), H_2O (20 mL) and brine (10 mL). The organic layer was then dried over Na_2SO_4, filtered and concentrated *in vacuo*. The product was isolated by flash column chromatography as a colourless oil (3.9182, 81.0%). **^{1}H NMR** (400 MHz, $CDCl_3$) δ 7.63 - 7.72 (m, *J* = 7.93 Hz, 2H, Ar-H), 7.19 - 7.29 (m, *J* = 7.93 Hz, 2H, Ar-H), 4.01 - 4.08 (m, 2H, CH_2), 3.54 - 3.60 (m, 2H, CH_2), 3.45 - 3.52 (m, 6H, CH_2), 3.41 (d, *J* = 5.49 Hz, 2H, CH_2), 3.25 (s, 3H, CH_3), 2.33 (s, 3H, CH_3); **^{13}C NMR** (101 MHz, $CDCl_3$) δ 144.5, 132.7, 129.5, 127.6, 71.6, 70.4, 70.2, 69.0, 68.3, 60.0, 58.6, 21.3; **IR:** (ATR) ν cm^{-1} 2877.19, 1352.62, 1174.63, 1095.42, 916.50, 662.40; **MS:** Found (M + H) = 319.3430, calculated for $C_{14}H_{23}O_6S$ = 319.1215

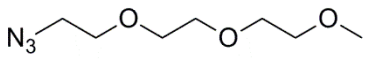

42

Compound **41** (3.1839 g, 10 mmol, 1 eq.) was dissolved in DMF (20 mL). NaN_3 (2.2754 g, 35 mmol, 3.5 eq.) was added and the reaction was stirred at 60°C for a total of 24 h over 2 days. The reaction mixture was poured onto H_2O (60 mL). The aqueous mixture was extracted with Et_2O (3 × 80 mL) and the combined organic fractions were washed with water (100 mL), dried over Na_2SO_4, filtered and concentrated to afford the product as a pale yellow oil (1.25 g, 66%). **^{1}H NMR** (400 MHz, $CDCl_3$) δ 3.55 - 3.66 (m, 8H), 3.46 - 3.51 (m, 2H), 3.27 - 3.36 (m, 5H) **^{13}C NMR** (101 MHz, $CDCl_3$) δ 71.8, 70.5, 70.5, 70.4, 69.9, 58.8, 50.5

IR: (ATR) ν cm^{-1} 2871.25, 2097.78, 1106.25. MS not found.

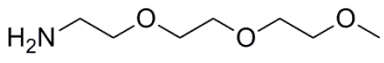

43

Compound **42** (1 g, 5.3 mmol) was dissolved in anhydrous THF (20 mL). Triphenylphosphine (1.5213 g, 5.8 mmol, 1.1 eq.) was added and the mixture was stirred under N_2 for 12 h. The reaction mixture was poured onto 30 mL of water and stirred overnight. The precipitated solids were removed by filtration and the aqueous filtrate was extracted with DCM (3 × 30 mL). The product was isolated by concentration of the aqueous phase *in vacuo* as a viscous pale yellow oil (0.7015 g, 81.1%). **^{1}H NMR** (400

MHz, $CDCl_3$) δ 3.50 - 3.60 (m, 6H), 3.37 - 3.48 (m, 4H), 3.25 – 3.30 (m, 3H), 2.76 (br. s., 2H); **^{13}C NMR** (101 MHz, $CDCl_3$) δ 73.0, 71.6, 70.3, 70.2, 70.0, 58.7, 41.4; **IR:** (ATR) ν cm^{-1} 3365.58, 2869.34, 1099.49; **MS:** Found (M + H) = 164.1766, calculated for $C_7H_{18}NO_3$ 164.1287

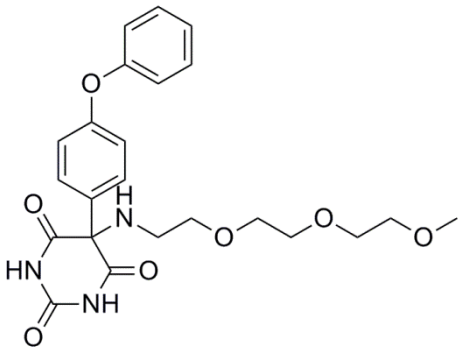

44

To a solution of **39** (0.22270 g, 0.5 mmol) in MeOH (5 mL), **43** (0.165 g, 1 mmol, 2 eq.) was added. The reaction was stirred at room temperature for 24 h. The product was isolated by flash column chromatography using EtOAc as the mobile phase as a yellow solid (0.1226 g, 54.7%). Mp 108 - 109°C; **^{1}H NMR** (400 MHz, DMSO-d_6) δ 11.60 (s, 2H, NH), 7.56 (d, *J* = 8.71 Hz, 2H, Ar-H), 7.44 (d, *J* = 8.71 Hz, 2H, Ar-H), 6.90 - 7.12 (m, 4H, Ar-H), 3.37 - 3.61 (m, 10H, CH_2), 3.22 (s, 3H, CH_3), 2.94 (br. s., 1H, NH), 2.65 (br. s., 2H, CH_2-N) **^{13}C NMR** (101 MHz, DMSO-d_6) δ 170.6, 156.6, 155.5, 149.7, 133.2, 132.9, 128.3, 121.1, 118.6, 115.5, 71.2, 70.3, 69.6, 69.6, 69.5, 69.4, 58.0, 43.9; **IR:** (ATR) ν cm^{-1} 3091.24, 2858.97, 1735.37, 1705.44, 1346.55, 1482.98, 1237.87; **HRMS:** Found (M-H) = 534.0875, calculated for $C_{23}H_{26}N_3O_7$ = 534.0881

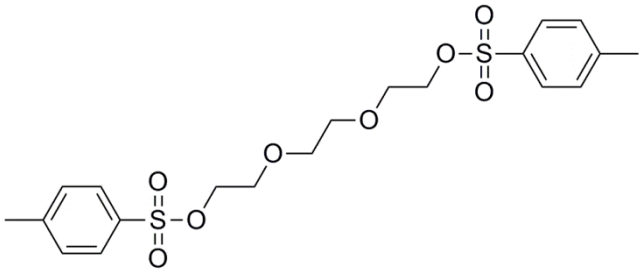

46

To a solution of triethylene glycol (2.00 g, 13.32 mmol) in anhydrous DCM (5 mL), *p*-toluenesulfonyl chloride (7.62 g, 39.96 mmol, 3 eq.) and NEt_3 (5.6 mL, 39.96 mmol, 3 eq.) in DCM (2 mL) was added dropwise over an ice-water bath under anhydrous conditions.

After 20 min, the ice-bath was removed and the reaction allowed to come to RT. Upon completion of the reaction in 1 h as indicated by TLC, crushed ice was added and stirred for 10 min. The cloudy aqueous phase was extracted with DCM (3 × 20 mL). The combined organic layers were successively washed with aqueous 1M HCL (50 mL), saturated $NaHCO_3$ (20 mL), H_2O (20 mL) and brine solution (20 mL). The organic layer was then dried over Na_2SO_4, filtered and concentrated *in vacuo*. The product was isolated by flash column chromatography as a white solid (3.528 g, 55.0%). Mp 80 - 81°C; **^{1}H NMR** (400 MHz, $CDCl_3$) δ 7.76 (d, *J* = 8.29 Hz, 4H, Ar-H), 7.32 (d, *J* = 7.88 Hz, 4H, Ar-H), 4.06 - 4.17 (m, 4H, 2 × CH_2), 3.59 - 3.67 (m, 4H, 2 × CH_2), 3.49 (s, 4H, 2 × CH_2), 2.42 (s, 6H, 2 × CH_3); **^{13}C NMR** (101 MHz, $CDCl_3$) δ 144.7, 132.7, 129.7, 127.7, 70.4, 69.1, 68.5, 21.4; **IR:** (ATR) ν cm^{-1} 1596.92, 1353.17, 1174.19, 1132.30; **MS:** Found (M + Na) = 481.2616, calculated for $C_{20}H_{26}O_8S_2Na$ = 481.0961

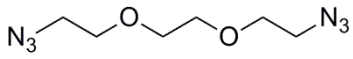

47

Compound **46** (2.50 g, 5.45 mmol) was dissolved in DMPU (20 mL). NaN_3 (0.7798 g, 11.99 mmol, 2.2 eq.) was added and the reaction mixture was stirred for 24 hours. The solution was then poured onto H_2O (50 mL) and this aqueous mixture was extracted with Et_2O (3 × 20 mL). The organic layers were combined and washed with H_2O (3 × 60 mL) and finally with saturated brine (20 mL). The organic layer was dried over Na_2SO_4, filtered and the solvent removed *in vacuo* to afford the product which did not require further purification as a yellow oil (0.9580 g, 87.8%). **^{1}H NMR** (400 MHz, CDCl3) δ 3.57 - 3.65 (m, 8H), 3.32 (t, *J* = 4.77 Hz, 4H); **^{13}C NMR** (101 MHz, $CDCl_3$) δ 70.3, 69.8, 50.3; **IR: (**ATR) ν cm^{-1} 1302.89, 1123.05; **MS**: Found (M + H) = 201.0546, calculated for $C_6H_{13}N_6O_2$ = 201.1095

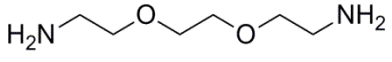

48

To a solution of **47** (0.7995 g, 3.99 mmol) in anhydrous THF (10 mL), triphenylphosphine (2.3024 g, 8.778 mmol, 2.2 equivalents) was added and the reaction mixture was stirred for 6 h under anhydrous conditions at RT. The reaction was then poured onto H_2O (20 mL) and stirred for a further 12 h. The solid precipitate was removed by filtration and the THF

removed *in vacuo*. The resulting aqueous solution was extracted with DCM (3 × 10 mL). The product was isolated from the aqueous phase by azeotropic removal of the H_2O *in vacuo* with C_2H_5OH as an orange oil (0.4376 g, 74.0%). **^{1}H NMR** (400 MHz, DMSO-d_6) δ 3.51 (s, 4H), 3.37 - 3.44 (m, 4H), 2.67 (m, 4H); **^{13}C NMR** (101 MHz, MeOD) δ 72.6, 71.2, 41.8; **IR:** (ATR) ν cm^{-1} 3513.76, 3357.88, 1250.81; **MS**: Found (M + H) = 149.1987, calculated for $C_6H_{17}N_2O_2$ = 149.1285

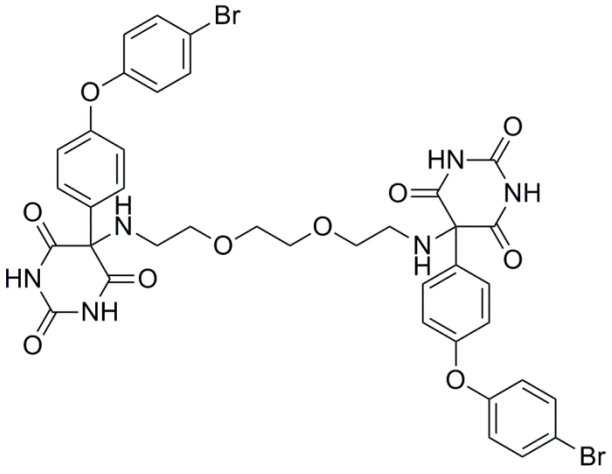

49

To a solution of **48** (0.0308 g, 0.21 mmol) in MeOH (5 mL), 39 (0.2 g, 0.46 mmol, 2.2 eq) was added and stirred at RT for 24 hours. The precipitate was collected by filtration, washed with MeOH (2 × 1 mL) and dried to yield the product which did not require further purification as an off-white solid (0.1554g, 82.7%). Mp 250 - 253°C; **^{1}H NMR** (400 MHz, DMSO-d_6) δ 9.18 (br. s., 4H, barbiturate N-Hs), 7.79 - 7.92 (m, 4H, Ar-H), 7.74 (br. s., 2H, N-H), 7.49 (d, *J* = 8.55 Hz, 4H, Ar-H), 6.90 (d, *J* = 8.55 Hz, 4H, Ar-H), 6.82 (d, *J* = 7.32 Hz, 4H, Ar-H), 3.49 - 3.63 (m, 8H, 4 × -CH_2O), 2.94 (t, *J* = 4.71 Hz, 4H, 2 × -C$\underline{H_2}$NH); **^{13}C NMR** (151 MHz, DMSO-d_6) δ 163.7, 157.7, 151.2, 150.1, 132.9, 132.4, 130.7, 119.2, 117.7, 113.6, 86.3, 69.4, 66.6, 38.6; **IR:** (ATR) ν cm^{-1} 3379.39, 1713.21, 1535.48, 1239.84, 544.3. MS not found.

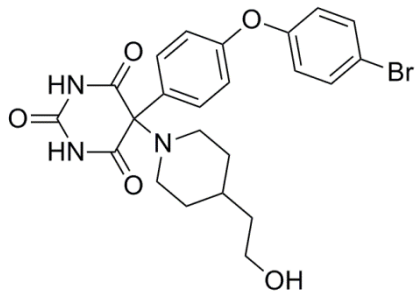

51

Compound **39** (0.7428 g. 1.6 mmol) was dispersed in MeOH (6 mL) and 4-piperidine ethanol (0.4134 g, 3.2 mmol, 2 eq.) was added. The resulting clear yellow solution was stirred at RT for 24 h. After removal of the MeOH *in vacuo*, the product was isolated by flash column chromatography with EtOAc:Hex (2:1) as the mobile phase as a white crystalline solid (0.5374 g, 66.9%). Mp 108 - 109°C; **^{1}H NMR** (400 MHz, DMSO-d_6) δ 11.59 (s, 2H, NH), 7.52 - 7.63 (m, 2H, Ar-H), 7.42 (d, *J* = 8.71 Hz, 2H, Ar-H), 6.95 - 7.11 (m, 4H, Ar-H), 3.35 - 3.48 (m, 2H, CH_2), 2.61 – 2.70 (m, 2H, CH_2), 2.36 – 2.45 (m, 2H, CH_2), 1.54 – 1.62 (m, 2H, CH_2), 1.31 – 1.41 (m, 3H, CH_2 + CH), 1.07 - 1.15 (m, 2H, CH_2); **^{13}C NMR** (101 MHz, DMSO-d_6) δ 170.1, 156.7, 155.4, 149.4, 132.9, 130.7, 129.7, 121.3, 118.3, 115.6, 74.4, 58.2, 48.0, 32.7, 32.2, 14.1; **IR:** (ATR) ν cm^{-1} 3063.98, 2927.43, 2845.15, 1701.50, 1480.69, 1235.92; **HRMS:** Found (M-H) = 500.0816, calculated for $C_{23}H_{23}BrN_3O_5$ = 500.0827

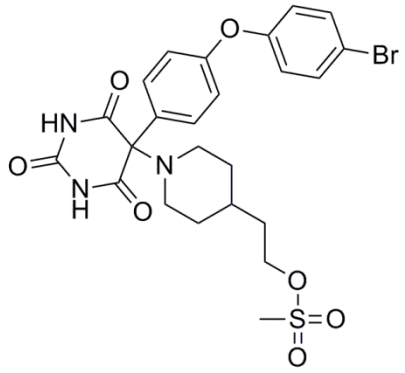

52

Compound **51** (0.4137 g, 0.82 mmol) was dissolved in anhydrous DCM (5 mL) under N_2. With usual precautions for exclusion of air, NEt_3 (114 μL, 0.82 mmol, 1 eq.) and methanesulfonyl chloride (64 μL, 0.82 mmol, 1 eq.) were added over an iced-water bath. After 30 min, the iced-water bath was removed and the reaction mixture was allowed to RT. The reaction was monitored by TLC and after 5 h a further 0.5 eq. of each of NEt_3 and methanesulfonyl chloride was added. After a total reaction time of 24 h, the reaction was poured onto iced-water (20 mL) and allowed to stir for 10 min and the cloudy aqueous layer was extracted with DCM (3 × 50 mL). The combined organic layers were washed

with aqueous 1 M HCl (20 mL), saturated $NaHCO_3$ (20 mL) and brine (20 mL), dried over Na_2SO_4 and filtered. The solvent was removed to afford the product as a white crystalline solid (0.4028 g, 84.6%). **^{1}H NMR** (400 MHz, DMSO-d_6) δ 11.87 (br. s., 2H, NH), 7.52 - 7.64 (m, 2H, Ar-H), 7.43 (d, *J* = 8.29 Hz, 2H, Ar-H), 6.95 - 7.17 (m, 4H, Ar-H), 4.22 (t, *J* = 6.43 Hz, 2H, CH_2-OS), 3.16 (s, 3H, CH_3), 2.6 - 2.8 (m, 4H, CH_2), 1.57 - 1.80 (m, 4H, CH_2), 1.50 (br. s., 1H, CH), 1.2 - 1.35 (m, 2H, CH_2); **^{13}C NMR** (101 MHz, DMSO-d_6) δ 170.3, 155.6, 154.5, 148.6, 132.6, 129.5, 121.3, 121.2, 118.2, 118.0, 115.7, 109.2, 74.0, 67.8, 48.5, 42.6, 36.1; **IR:** (ATR) ν cm^{-1} 3220.33, 2933.68, 2845.38, 1701.58, 1324.87, 1235.82, 1168.47; **HRMS:** Found (M-H) = 578.0591, calculated for $C_{24}H_{25}BrN_3O_7S$ = 578.0597

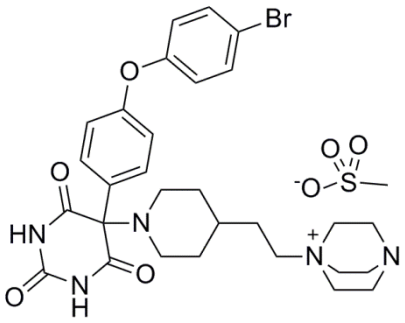

53

To a solution of **52** in ACN (2 mL), DABCO (0.0606 g, 0.54 mmol, 2 eq.) was added. The reaction mixture was stirred at RT for 7 d. The solvent was removed *in vacuo* and the residue was dissolved in 0.5 mL MeOH:H_2O (1:1). The pure product was isolated by solid phase extraction using MeOH:H_2O (1:1) as the eluting solvent as a light brown solid (0.0332 g, 20.0%). Mp 275 - 280°C decomposition; **^{1}H NMR** (400 MHz, DMSO-d_6) δ 7.56 (d, *J* = 8.71 Hz, 2H, Ar-H), 7.41 (d, *J* = 8.29 Hz, 2H, Ar-H), 6.95 - 7.07 (m, 4H, Ar-H), 3.16 - 3.27 (m, 8H, CH_2-N^+), 2.94 - 3.07 (m, 6H, DABCO CH_2), 2.62 - 2.70 (m, 2H, CH_2), 2.38 - 2.47 (m, 2H, CH_2), 1.54 – 1.66 (m, 4H, CH_2), 1.15 - 1.30 (m, 3H, CH + CH_2); **^{13}C NMR** (101 MHz, DMSO-d_6) δ 172.4, 156.1, 155.7, 152.8, 132.9, 132.4, 129.8, 121.0, 118.2, 115.4, 73.8, 61.6, 51.5, 47.8, 44.7, 33.6, 32.34, 27.4 **IR:** (ATR) ν cm^{-1} 2931.42, 1700.91, 1577.88, 1480.92, 1234.26 **HRMS:** Found (M) = 596.1875, calculated for $C_{29}H_{35}BrN_5O_4$ = 596.186

5.3 Biological methods – Chapter 2

5.3.1 Reagents and materials

Chemicals and biological materials required were commercially purchased and used as supplied except where stated. Plastic consumables were supplied by Greiner Bio-One International GmbH. Solvents were supplied by Trinity college hazardous materials facility (HMF) solvent stores.

5.3.2 Cell culture

Caco-2 (ATCC® HTB-37™) cells were purchased from American Type Culture Collection (ATCC) (Manassas, VA). Cells were cultured in Dulbecco's Modified Eagle's Medium (DMEM) supplemented to contain 1 mM sodium pyruvate, 20% v/v FBS, gentamicin 5 mg/L, streptomycin 10 mg/L, and penicillin G 6 mg/L. The cells were cultured in T-75 cm^2 vented cap cell culture flasks and incubated at 37°C in a humidified atmosphere of 95% air and 5% CO_2. Medium was changed approximately every second day until the cells reached 70 – 80% confluence at which point they were detached with trypsin and pelleted by centrifugation at 900 rpm in 10% v/v FBS containing medium. The pellet was resuspended in fresh 20% v/v FBS containing medium and split to new flasks at a subcultivation ratio of 1:3. Cryopreservation was carried out in complete growth medium supplemented with 5% v/v DMSO as cryoprotective agent and vials were stored in the liquid nitrogen vapour phase.

5.3.3 MMP-9 inhibition assay

Recombinant human MMP-9 protein, (R & D Systems, Ireland) was activated by a final concentration of 1 mM APMA at 37°C for 24 h in TCNB buffer (50 mM Tris, 10 mM $CaCl_2$, 150 mM NaCl and 0.05% w/v Brij® 35 adjusted to pH 7.5). The enzyme was then incubated at 2 nM in TCNB buffer with the test inhibitory compound in duplicate at 37°C for 45 min in a black flat-bottomed 96-well plate (volume/well = 90 µL). After incubation, 10 µL of 100 µM substrate for a final substrate concentration of 10 µM was added to each well and the increase in fluorescence was monitored at 10 time points over the first 10 min of reaction in a FLUOstar OPTIMA microplate reader (BMG LABTECH) with excitation and emission wavelengths set to 330 and 405 nm, respectively. The fluorescent substrate used was MCA-Pro-Leu-Gly-Leu-DPA-Ala-Arg-NH_2 (R&D systems, UK). The increase in fluorescence was proportional to product release by remaining MMP-9 proteolytic activity and is linear with time as monitored here. The increase in fluorescence was plotted

as a function of time in Microsoft® Excel and the slope was calculated. The reduction in comparison to the slope of the positive control prepared as for test wells but with buffer in place of inhibitor test solution yielded a measure of inhibition. Test concentrations covered 0% to 100% inhibition and non-linear regression analysis of the % inhibition as a function of the Log of concentration in GraphPad Prism® 5 established an IC_{50} and 95% CI for the test compound.

5.3.4 Stability of compound 53 in the environments of the GIT

5.3.4.1 Stability of compound 53 in Gastric fluid, Simulated, TS

Gastric fluid, Simulated, TS was prepared according to the test solution monograph in the USP 33-28NF (2010).[167]

To prepare a final volume of 10 mL, 0.02 g NaCl and 0.0320 g of pepsin were dissolved in 0.07 mL of conc. HCl and sufficient dd H_2O to make 10 mL.

Compound 53 was prepared at a concentration of 100 µM in 1.5 mL simulated gastric fluid. An aliquot of 150 µL was removed immediately as the time zero sample and the test solution was incubated in a water-bath at 37°C. Further sample aliquots were taken at time 10 min, 20 min, 30 min, 1 h, 2 h and 4 h. Once taken, samples were centrifuged at 14,000 g for 5 min and 100 µL was immediately analysed by HPLC.

5.3.4.2 Stability of compound 53 in Intestinal fluid, Simulated, TS

Intestinal fluid, Simulated, TS was prepared according to the test solution monograph in the USP 33-28NF (2010).[167]

To prepare a final volume of 10 mL, 0.068 g of KH_2PO_4 was dissolved in 2.5 mL of ddH_20 and 0.77 mL of 0.2 M NaOH and 5 mL of ddH_2O were added. Pancreatin (0.1 g) was added and gently mixed. The pH was adjusted to pH 6.8 and the solution was brought to final volume.

Compound **53** was prepared at a concentration of 100 µM in 1.5 mL simulated intestinal fluid. An aliquot of 150 µL was removed immediately as the time zero sample and the test solution was incubated in a water-bath at 37°C. Further sample aliquots were taken at time

10 min, 20 min, 30 min, 1 h, 2 h, 4 h and 6h. Once taken, samples were centrifuged at 14,000 g for 5 min and 100 µL was immediately analysed by HPLC.

5.3.5 Caco-2 cell uptake assay

5.3.5.1 Assay procedure

Caco-2 cells were cultured in T-25 flasks until confluent. For the uptake assay, the medium was removed and replaced by the test drug solution at 10 µM in supplement-free medium. The flask was incubated at 37°C for 30 min. After incubation, a 1 mL sample of the medium was collected. Medium remaining in the flask was aspirated to waste and the cells were washed three times with 1 mL of cold PBS. The cells were then scraped into 1 mL of PBS and collected. Conditioned media samples and cell samples were stored at -20°C for future analysis by HPLC.

5.3.5.2 HPLC analysis

The conditioned media samples were centrifuged at 13,000 rpm for 5 min and the supernatant transferred to a HPLC vial for direct analysis. The cell samples in PBS were gently centrifuged at 1,000 rpm for 5 min to form a cell pellet. The PBS was removed and 200 µL of acetonitrile was added to the pellet and vortexed. The samples were sonicated for 30 min to aid cell lysis. The lysate was centrifuged at 13,000 rpm for 5 min and the supernatant transferred to a HPLC vial for analysis. HPLC analysis was performed on an XBridge C18 column (Waters, USA) in isocratic mode at 25°C. The mobile phase consisted of ddH_2O + 0.1% v/v formic acid and acetonitrile (50:50 v/v) at a flow rate of 1 mL/min. UV detection was carried out at 254 nm.

5.3.6 *In vivo* assessment of compound 53 in a murine DSS colitis model

Male BALB/c mice were randomly assigned to experimental groups and allowed to settle to conditions for 10 days before induction of colitis. Animals were ear punched for identification. On day 0, the usual drinking water of the DSS group and the treatment group was replaced with DSS 5% w/v in the usual drinking water. The DSS dispersion was sonicated to a clear solution and monitored daily for any signs of turbidity and replenished or replaced as appropriate. The sham group continued to drink the usual drinking water. The treatment group were administered compound **53** at a dose of 10 mg/Kg by oral gavage once daily in the morning from day 0 to day 6 and the DSS group received the water vehicle by oral gavage. All animals were monitored daily and assigned a disease activity index (DAI) score for weight loss, stool consistency and presence of blood. These scores were combined and averaged to generate the daily score. At the endpoint of the experiment on day 6, animals were euthanized by cervical dislocation by Dr. Carlos Medina, School of Pharmacy, Trinity College, Dublin. A mid-laparotomy was performed and the distal colon was removed and divided into three. One specimen was immediately snap frozen in liquid nitrogen for protein analysis and transferred to -80°C for storage. One specimen was retained for RNA isolation by immersing in RNA*later*® (Ambion™, Ireland) solution and stored at 4 - 8°C for 24 h to allow the solution to permeate the tissue and then transferred to -20°C for longer term storage. The final specimen for histological assessment was immersed in neutral buffered 10% formalin for 48 h before transfer to 70% v/v ethanol for longer term storage.

5.3.7 Histological analysis

5.3.7.1 Preparation of buffered 10% v/v formalin solution

A phosphate solution was prepared by dissolving 0.55 g of NaH_2PO_4 and 2.27 g of Na_2HPO_4 in 90 mL of ddH_2O. To 8 g of paraformaldehyde, a solution of two pellets of NaOH in 100 mL of ddH_2O at 65°C was added and stirred to a clear solution. If the solution is not clear, more NaOH pellets are to be added until the pH is raised enough to cause the PFA to go into solution. The phosphate solution was added to the PFA solution and allowed to cool to room temperature. The pH was adjusted to pH 7.4 and the solution brought to final volume of 200 mL with ddH_2O. The buffered 10% v/v formalin solution was stored at 4°C and given an expiry of one month.

5.3.7.2 Tissue processing

Colon tissue sections for histological analysis had been fixed in neutral buffered 10% v/v formalin for 48 h before transfer to 70% v/v ethanol for long term storage. A 5 mm section of each sample was cut and placed in an individually labelled embedding cassette and processed using the TP1020 Automatic Tissue Processor (Leica®, Microsystems, Ireland). This automated instrument subjected the tissue samples to the following 10 step treatment protocol.

Tissue processing treatments

Treatment	Duration (h)
70% ethanol	1
80% ethanol	1
95% ethanol	1
100% ethanol	1
100% ethanol	1
50% ethanol / 50% xylene	1
100% xylene	1
100% xylene	1
100% paraffin	1
100% paraffin	1

Following processing each colon sample was individually embedded in paraffin using the Leica EG1150H Heated Paraffin Embedding Module (Leica®, Microsystems, Ireland). Briefly, tissue samples were removed from their cassettes and sections were inserted into plastic moulds filled with molten liquid paraffin at 61°C. The moulds were moved to a cold plate and the samples quickly orientated with the longitudinal axis perpendicular to the base of the mould. The labeled cassette was placed on top of the mould for sample identification and set with more liquid paraffin. The moulds were kept on the cold plate until fully solidified. Paraffin wax embedded samples were stored at 4°C.

To section, the embedded samples were removed from the moulds and 5 µm sections were cut using the Leica RM2235 Manual Rotary Microtome (Leica®, Microsystems, Ireland). Sectioned tissue was mounted on labeled glass slides in a water bath at 45°C, placed in a slide rack and left at 55°C overnight to dry.

5.3.7.3 Hematoxylin and eosin (H&E) staining

Slides were stained, in a slide rack, by the following sequence of treatments. Excess was removed between each treatment

- 10 immersions in xylene
- 10 immersions in fresh xylene
- 10 immersions in 100% ethanol
- 10 immersions in 90% ethanol
- 10 immersions in 70% ethanol,
- 10 immersions in tap water
- 5 min in Sellafield's hematoxylin, dipping periodically
- 40 immersions in running tap water
- 2 min in standard eosin
- 40 immersions in running tap water
- 10 immersions in 70% ethanol
- 10 immersions in 90% ethanol
- 10 immersions in 100% ethanol
- 10 immersions in xylene

Finally, the entire slide rack was immersed in fresh xylene. The slides were removed one at a time, mounted with 2-3 drops of Surgipath® Sub-X® mounting medium (Leica®, Microsystems, Ireland) and coverslipped.

5.3.7.4 H&E histological analysis

H&E slides were viewed using the Olympus BX51 research microscope (Olympus Inc., Tokyo, Japan). Colitis severity was assessed by blind scoring of colon inflammatory cell infiltration (0-3) and tissue damage (0-3) as outlined below in Table 5.

Table 5. Histological scoring system for colon samples from the DSS colitis model

Infiltration	***Score***
Occasional infiltration in lamina propria	0
Increased infiltrate in lamina propria (predominantly at base of crypts)	1
Extension of infiltrate into mucosa	2
Transmural extension of infiltrate	3

Tissue damage	***Score***
No mucosal damage	0
Partial (<50%) loss of crypts in large areas	1
Partial to total (50-100%) loss of crypts in large areas	2
Total loss of crypts in large areas and epithelial loss	3

5.3.8 Zymography

5.3.8.1 Zymography buffer and reagent solution preparation

Stacking buffer was prepared by dissolving Tris base (6.05 g) in 40 mL ddH_2O and adjusting to pH 6.8. SDS (0.4 g) was dissolved in the Tris solution and it was brought to 100 mL final volume with ddH_2O. Stacking buffer was stored at 4 - 8°C.

Zymography loading buffer 4× was prepared by dissolving SDS (0.8 g) and bromophenol blue (0.2 mg) in stacking buffer (5 mL), glycerol (4 mL) and ddH_2O (400 µL) with sonication. The solution was stored in aliquots at -20°C.

Resolving buffer was prepared by dissolving Tris base (91 g) in 300 mL ddH_2O and adjusting to pH 8.8 before bringing to 500 mL final volume with ddH_2O. Resolving buffer was stored at 4 - 8°C.

Separating gel sufficient for two gels was prepared immediately before use by mixing acrylamide 30% (2 mL), resolving buffer (1.875 mL), gelatin (750 µL (20 mg/mL, 1% w/v SDS)) and ddH_2O (2.875 mL) before adding APS (25 µL) and TEMED (5 µL) and vortexing vigorously.

Stacking gel sufficient for two gels was prepared immediately before use by mixing acrylamide 30% (650 µL), stacking buffer (1.25 mL) and ddH_2O (3 mL) before adding APS (25 µL) and TEMED (5 µL) and vortexing vigorously.

Zymography incubation buffer was prepared by dissolving NaCl (9 g), $CaCl_2$ (0.735 g) and NaN_3 (0.5 g) in 500 mL ddH_2O, adding 2M Tris HCl pH 7.6 and making to 1000 mL final volume with ddH_2O. Zymography incubation buffer was stored at 4 - 8°C.

Staining solution was prepared by dissolving Coomassie blue G-250 (250 mg) in MeOH (250 mL), CH_3COOH (100 mL) and ddH_2O (650 mL). Staining solution was stored at RT.

Destaining solution was prepared by mixing MeOH (40 mL), CH_3COOH (80 mL) and ddH_2O (880 mL). Destaining solution was stored at RT.

5.3.8.2 Tissue preparation

Tissue samples for protein analysis were prepared in 300 µL homogenization buffer (Trizma HCl 50 mM, NaCl 150 mM, Igepal CA 640 1% w/w in ddH_2O adjusted to pH 7.5 with aprotinin 60 µg/mL and leupeptin 10 µg/mL as protease inhibitors) with a Microson™ ultrasonic cell disrupter over ice and aliquoted to avoid multiple freeze-thaw cycles.

5.3.8.3 Bradford Protein assay

The dye reagent was prepared by diluting 1 part dye reagent concentrate with 4 parts double deionised water. Bovine serum albumin was used as a protein standard and serial dilutions were prepared in ddH_2O water from 400 µg/mL to 25 µg/mL as well as a blank of 0 µg/mL. Each standard and sample (10 µL) was pipetted into separate 96-well plate wells and 200 µL of diluted dye reagent was added to each well. All samples and standards were assayed in duplicate and samples were diluted as required to within the working range of the assay. The plate was incubated at room temperature for a minimum of 5 minutes with mixing on a plate rocker. No sample was incubated for more than 60 minutes. The absorbance of each well was measured at 595 nm on a FLUOstar OPTIMA microplate reader (BMG LABTECH) and Optima software. A standard curve of absorbance as a function of concentration was prepared and used to calculate the total protein concentration in the samples.

5.3.8.4 Zymography

Samples were normalized for total protein and mixed with one part loading buffer to three parts sample (18 µL normalized sample + 6 µL loading buffer). The samples were vortexed, centrifuged briefly at 13,000 rpm to spin the contents to the bottom of the tube and placed on ice until loaded onto the gel. A positive control was prepared by taking 4 µL conditioned media from PMA stimulated HT1080 cells, 14 µL ddH_2O and 6 µL loading buffer.

The zymography gel was prepared between glass plates with spacers. The separating gel was prepared, vortexed vigorously and pipetted between the glass plates. It was overlaid with ddH_2O and allowed to set (40 – 60 mins). Once set, the H_2O was poured from the separating gel and the stacking gel was pipetted on to the separating gel. A comb was inserted between the plates to create the lanes for sample loading in the stacking gel and it was allowed to set. The gels were assembled in the electrophoresis clamp, the combs removed and 20 µL of sample was loaded into each lane using a fine gel loading tip always loading the HT1080 control on the left hand side of the gel. The electrophoresis was run in electrophoresis buffer (25 mM Tris, 192 mM glycine, 0.1% w/v SDS, pH 8.3) using a Bio-Rad Power Pac HC at 150 V for approximately 2 h until approximately 15 min after the blue dye front had exited the gel. The gels were removed from the glass, the stacking portion of the gel was removed and the gels were washed by rocking in 2.5% v/v triton buffer three times for 20 min. The gels were then washed twice for 20 min in zymography buffer before incubation at 37°C in a water-bath in fresh zymography buffer until appearance of the digested bands. The gels were stained by rocking in staining solution for three hours before destaining by rocking in destaining solution. The gels were stored in destaining solution until analysis. The gelatinase bands were detected as clear bands against a blue background and quantified by densitometry using the gel documentation system ChemiDoc™ XRS system Universal hood II (Bio-Rad laboratories, Inc.) and Quantity One 4.6 software.

5.3.9 RNA isolation, reverse transcription and PCR analysis of the retained colon samples

5.3.9.1 RNA Isolation

Total RNA was isolated using the RNAqueous® Kit (Applied Biosystems) and all reagent components required were provided in the kit. Tissue samples were removed from RNA*later*® solution and excess solution was removed by blotting on a tissue culture wipe. In a nuclease-free eppendorf, the lysate was prepared for RNA isolation by manual homogenisation with a plastic tissue disruption pestle in 200 µL of lysis/binding solution. An equal volume of 64% v/v ethanol was added and gently vortexed to mix. This lysate/ethanol mixture was pipetted on to a filter cartridge assembled in a collection tube and drawn through the filter by centrifugation at 14,000 rpm for 1 min. The flow-through was discarded and the collection tube and filter cartridge were reassembled. Wash solution #1 (700 µL) was applied to the filter cartridge, drawn through the filter by centrifugation at 14,000 rpm for 30 sec and discarded. The filter was then washed in the same manner with 500 µL of Wash Solution #2/3. The flow through was then discarded and the filter washed with a second 500 µL aliquot of wash Solution #2/3. After discarding the flow-through of the last wash, the filter cartridge was subjected to another centrifugation step to remove any remaining wash solution. The RNA was then eluted from the filter cartridge by treatment with elution solution preheated to 80°C. The cartridge was assembled in a clean collection tube and 40 µL of elution buffer was pipetted onto the centre of the filter. The RNA containing elution buffer was collected by centrifugation at 14,000 rpm for 30 sec. To maximise recovery of RNA, a second elution step was carried out using 10 µL of elution buffer. Isolated RNA was stored at -80°C.

5.3.9.2 RNA Quantification

Isolated RNA was quantified using a NanoDrop ND-1000 spectrophotometer (Fisher Scientific Ireland Ltd., Dublin, Ireland) and ND-1000 software. The instrument was initialized with 1 µL of nuclease free water and blanked with elution solution. RNA concentration wass calculated from the absorbance of the sample at 260 nm by loading 1 µL of sample onto the lower optical platform.The software returned the concentration in ng/µL as well as the 260 nm/280 nm ratio which provided a measure of RNA purity.

5.3.9.3 Reverse Transcription

Total RNA was quantitatively converted to single-stranded cDNA for PCR applications using a High Capacity cDNA Reverse Transcription Kit (Applied Biosystems) according to the manufacturer's protocol. The kit components were allowed to thaw on ice. A 2× mastermix was prepared for the number of reactions to be performed as in Table 6 with an excess of 10% to allow for losses in reagent transfer. The mastermix was mixed gently and placed on ice.

Table 6 Reaction components for reverse transcription

Kit component	**Volume (µL)/Reaction**
10× RT Buffer	2.0
25× dNTP Mix (100 mM)	0.8
10× RT Random Primers	2.0
Multiscribe™ Reverse Transcriptase	1.0
Nuclease-free H_2O	4.2
Total per reaction	**10.0**

The prepared mastermix (10 µL) was pipetted into an individual nuclease free 50 µL tube for each reaction. The RNA templates were diluted with nuclease free water to 1 µg/ 100 µL and 10 µL was added to the mastermix for a final concentration of 100 ng/20 µL for reverse transcription. The tubes were inverted several times to mix and centrifuged briefly to spin down the contents and remove air bubbles. Reverse transcription was performed in a Realplex Mastercycler (Eppendorf UK Ltd.) The reaction volume was set to 20 µL and the heat cycles programmed as in Table 7.

Table 7 Thermocycler program for reverse transcription

Settings	**Step 1**	**Step 2**	**Step 3**	**Step 4**
Temperature	25°C	37°C	85°C	4°C
Time	10 min	120 min	5 min	∞

The samples were kept at 4°C in the thermal cycler until collection, briefly centrifuged and stored at -20°C.

5.3.9.4 Polymerase chain reaction

The Taqman assays and cDNA samples were thawed on ice. When fully thawed, they were vortexed gently to resuspend and centrifuged briefly. The cDNA samples (1.5 µL) were transferred to the required wells of a MicroAmp® Fast Optical 96-well reaction plate (ThermoFisher scientific) which was chilled in a 96-well freeze block while the plate was prepared. For each sample, the assay for the endogenous control 18S was performed as well as the gene expression assay(s) of interest. The gene expression assays employed are listed in Table 8. A no template control (NTC) was also included.

Table 8 Gene symbols and assay IDs of Taqman gene expression assays used. All primer/probe sets were pre-designed by Applied Biosystems

Target gene	Taqman gene expression assay ID
18S	Hs99999901_s1
TNF	Mm00443258_m1
IL-1β	Mm00446190_m1
IL-6	Mm00446190_m1

A reaction mix was prepared for 18S and the gene(s) of interest as outlined in Table 9. Sufficient mastermix was prepared for each reaction plus 10% excess to allow for loss in pipette transfer. The reaction mixes were vortexed to mix and briefly centrifuged to spin down the contents and eliminate air bubbles. The reaction mix (18.5 µL) was transferred to the required wells and the plate was sealed with a MicroAmp® Optical Adhesive Film.

Table 9 Components of reaction mix for a PCR reaction to be mixed with 1.5 µL cDNA for a total reaction volume of 20 µL

Components	Volume (µL) per reaction
Taqman® Universal PCR MasterMix II, with UNG	10.0
Taqman® gene expression assay	1.0
Nuclease-free H_2O	7.5
	18.5 (Total volume)

The plate was centrifuged briefly to spin down the contents and eliminate air bubbles. The reaction was performed in a Viia™ 7 Real-Time PCR System (ThermoFisher Scientific Ma, USA) in standard mode with a reaction volume of 20 µL using the thermal cycling parameters in Table 10.

Table 10 Thermocycler program for PCR

Reaction Phase	**UNG Incubation**	**Polymerase activation**	**PCR** (40 cycles)	
Temp (°C)	50	95	95	60
Time (mm:ss)	2:00	10:00	00:15	1:00

5.3.10 Statistical analysis

Analysis of results was carried out using GraphPad Prism® 5 for Windows (GraphPad software, USA). Results for more than three groups were analysed using one way ANOVA and Bonferroni's post-hoc test was run only if $p < 0.05$ unless otherwise stated. Histograms are presented as the mean ± SEM and statistical significance was judged as a p value < 0.05. Linear regression analysis was used for correlations with r^2 quoted and graphs were plotted in Microsoft® Excel.

5.4 Synthesis – Chapter 3

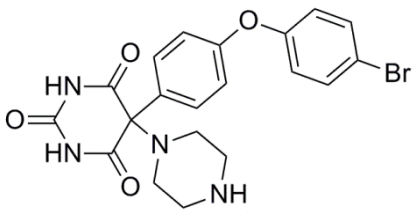

70

Compound **39** (0.3500 g, 0.77 mmol) was dissolved in MeOH (5 mL) and piperazine (0.1327 g, 2 eq.) was added. The reaction was stirred at RT. After 24 h, the precipitate formed was collected by filtration, washed with MeOH (2 × 1 mL) and allowed to dry affording the product as an off-white solid (0.1906 g, 53.9%). Mp 240 – 245°C decomposition; **^{1}H NMR** (400 MHz, DMSO-d_6) δ 9.02 (br. s., 2H, N - H), 7.85 - 7.95 (m, *J* = 8.71 Hz, 2H, Ar-H), 7.46 - 7.52 (m, *J* = 8.71 Hz, 2H, Ar-H), 6.86 - 6.92 (m, *J* = 8.71 Hz, 2H, Ar-H), 6.75 - 6.83 (m, *J* = 8.71 Hz, 2H, Ar-H), 2.72 – 2.79 (m, 4H, CH_2), 2.54 – 2.61 (m, 4H, CH_2); **^{13}C NMR** (101 MHz, DMSO-d_6) δ 170.7, 157.1, 155.9, 150.5, 133.3, 132.9, 130.3, 121.7, 118.8, 116.1, 74.7, 48.7, 46.2, 44.6; **IR:** (ATR) ν cm^{-1} 3050.71,

1699.82, 1665.72, 1541.00, 1481.31, 1395.39, 1231.14; **HRMS:** Found (M+H) = 459.0660, calculated for $C_{20}H_{20}BrN_4O_4$ = 459.0662

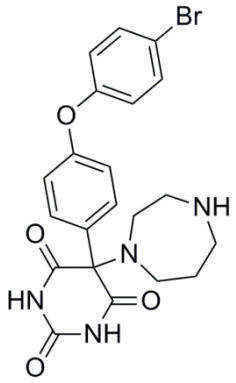

71

Compound **39** (0.3500 g, 0.77 mmol) was dissolved in MeOH (5 mL) and homopiperazine (0.1542 g, 2 eq.) was added. The reaction was stirred at RT. After 24 h, the precipitate formed was collected by filtration, washed with MeOH (2 × 1 mL) and allowed to dry affording the product as a pale yellow solid (0.1225 g, 33.6%). Mp 233 - 234°C decomposition; **^{1}H NMR** (400 MHz, DMSO-d_6) δ 7.51 - 7.69 (m, 2H, Ar-H), 7.31 - 7.51 (m, 2H, Ar-H), 6.85 - 7.14 (m, 4H, Ar-H), 2.85 – 3.06 (m, 2H, CH_2), 2.55 – 2.84 (m, 6H, CH_2), 1.50 – 1.69 (m, 2H, CH_2); **^{13}C NMR** (101 MHz, DMSO-d_6) δ 172.1,157.3,155.8, 150.6, 130.2, 129.4, 124.0, 121.3, 119.3, 118.0, 115.7, 76.3, 53.0, 50.7, 49.6, 45.7, 29.8; **IR:** (ATR) ν cm^{-1} 3060.40, 1710.28, 1660.71, 1482.64, 1396.92, 1248.83, 828.90; **MS:** Found (M – H) = 471.2906, calculated for $C_{21}H_{20}BrN_4O_4$ = 471.0668

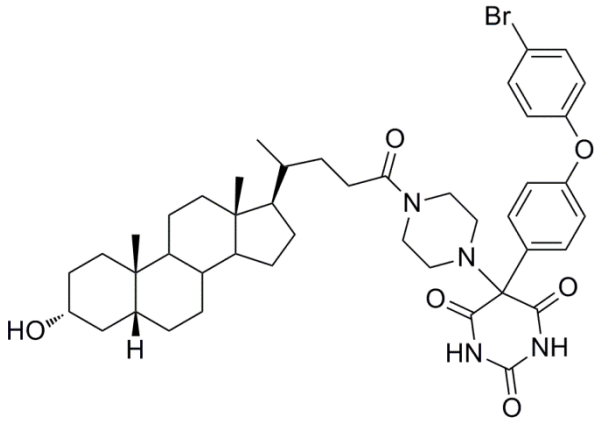

72

To a stirred solution of LCA (0.1205 g, 0.32 mmol, 1 eq.), **70** (0.1470 g, 0.32 mmol, 1 eq.) and DIPEA (111 µL, 0.0827 g, 2 eq.) in anhydrous DMF (4 mL) over an ice-water bath, COMU (0.1370 g, 0.32 mmol, 1 eq.) was added. The reaction mixture was stirred under N_2 at 0°C for 1 h before allowing to RT overnight. The yellow solution was poured onto H_2O

(50 mL) and extracted with DCM (3 × 60 mL).The combined organic layers were washed with aqueous 1 M HCl (50 mL), saturated $NaHCO_3$ solution (30 mL), H_2O (30 mL) and brine (30 mL), dried over Na_2SO_4, filtered and concentrated. The product was isolated by flash column chromatography using EtOAc:Hex (2:1) as the mobile phase as a white crystalline solid (0.1992 g, 76.1%). Mp 195 - 200°C decomposition; **^{1}H NMR** (600 MHz, DMSO-d_6) δ 11.64 (s, 2H, 2 × N-H), 7.57 (d, *J* = 9.03 Hz, 2H, Ar-H), 7.41 - 7.47 (m, *J* = 9.03 Hz, 2H, Ar-H), 7.05 - 7.10 (m, *J* = 9.04 Hz, 2H, Ar-H), 7.03 (d, *J* = 9.04 Hz, 2H, Ar-H), 4.43 (d, *J* = 4.52 Hz, 1H, 3α-OH), 3.53 - 3.59 (m, 2H, -N-CH_2), 3.34 - 3.39 (m, 1H, shouldered on H_2O peak, 3β-H), 3.03 - 3.10 (m, 2H, -N-CH_2), 2.57 – 2.62 (m, 2H, -N-CH_2), 2.51 - 2.55 (m, 2H, -N-CH_2), 0.84 - 0.89 (m, 6H, 2 × CH_3), 0.60 (s, 3H, CH_3); **^{13}C NMR** (151 MHz, DMSO-d_6) δ 170.9, 169.8, 157.0, 155.2, 149.3, 132.9, 129.8, 129.7, 121.4, 118.5, 115.8, 74.1, 69.8, 65.9, 56.0, 55.5, 47.6, 47.0, 42.3, 41.5, 40.0, 36.3, 35.4, 35.1, 35.0, 34.2, 31.0, 30.4, 29.3, 27.7, 26.9, 26.1, 23.9, 23.2, 20.4, 18.3, 11.8; **IR:** (ATR) ν cm^{-1} 2927.49, 2860.25, 1736.35, 1702.36, 1608.73, 1481.51, 1236.81, 828.19; **MS**: Found (M – H) = 815.5923, calculated for $C_{44}H_{56}BrN_4O_6$ = 815.33

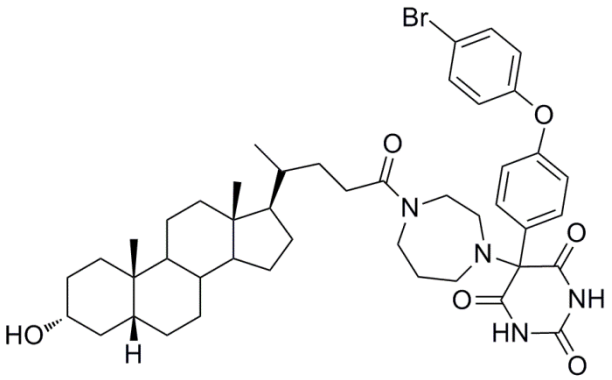

73

To a stirred solution of LCA (0.1205 g, 0.32 mmol), **71** (0.1505 g, 0.32 mmol, 1 eq.) and DIPEA (111 µL, 0.0827 g, 2 eq.) in anhydrous DMF (4 mL) over an ice-water bath, COMU (0.1370 g, 0.32 mmol, 1 eq.) was added. The reaction mixture was stirred under N_2 at 0°C for 1 h before allowing to RT overnight. The yellow-orange solution was poured onto H_2O (50 mL) and extracted with DCM (3 × 60 mL). The combined organic layers were washed with aqueous 1 M HCl (50 mL), saturated $NaHCO_3$ solution (30 mL), H_2O (30 mL) and brine (30 mL), dried over Na_2SO_4, filtered and concentrated to a white solid. The product was isolated by flash column chromatography using EtOAc:Hex (2:1) a mobile phase as a yellow solid (0.1298 g, 48.8%). Mp 185 – 189°C decomposition; **^{1}H**

NMR (600 MHz, DMSO-d_6) δ 11.54 (br. s., 2H, barbiturate N-Hs), 7.53 - 7.61 (m, 2H, Ar-H), 7.43 (d, *J* = 9.03 Hz, 2H, Ar-H), 6.99 - 7.10 (m, 4H, Ar-H), 3.54 - 3.58 (m, 1H, CH_2), 3.50 -3.52 (m, 1H, CH_2), 3.48 - 3.51 (m, 3H), 2.75 – 2.8 (m, 1H, CH_2), 2.59 - 2.69 (m, 3H, CH_2s), 0.85 - 0.90 (m, 6H, 2 × CH_3), 0.60 (d, *J* = 5.27 Hz, 3H, CH_3); **^{13}C NMR** (151 MHz, DMSO-d_6) δ 171.9, 170.7, 157.1, 155.1, 149.4, 132.9, 131.4, 129.2, 121.5, 118.4, 115.9, 76.7, 69.8, 56.0, 55.6, 53.0, 51.0, 49.3, 45.9, 42.3, 41.5, 36.3, 35.4, 35.1, 35.0, 34.2, 31.2, 31.1, 30.4, 29.4, 27.7, 26.9, 26.1, 23.8, 23.2, 20.4, 18.4, 11.9; **IR:** (ATR) ν cm^{-1} 2927.94, 2854.75, 1735.13, 1702.55, 1481.24, 1234.40, 827.43; **MS:** Found (M – H) = 829.5978, calculated for $C_{45}H_{58}BrN_4O_6$ = 829.3545

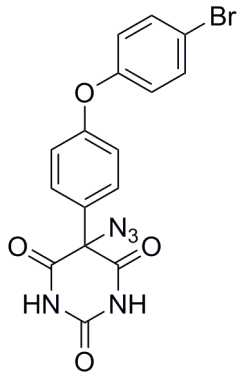

74

To a solution of **39** (0.50 g, 1.10 mmol) in DMPU (10 mL), NaN_3 (0.08 g, 1.21 mmol, 1.1 eq.) was added and the mixture was stirred at RT for 24 h. The reaction mixture was poured onto H_2O (40 mL) and extracted with EtOAc (50 mL × 3). The combined organic layers were washed successively with H_2O (100 mL × 5) and brine (50 mL), dried over Na_2SO_4, filtered and concentrated. The product was isolated by flash column chromatography with a mobile phase of hexane:ethyl acetate(2:1) as an off-white solid (0.2540 g, 55.5%). The product was stored protected from light. Mp 180ºC decomposition; **^{1}H NMR** (400 MHz, DMSO-d_6) δ 11.79 (s, 2H, 2 × N-H), 7.54 - 7.63 (m, 2H, Ar-H), 7.37 - 7.46 (m, 2H, Ar-H), 7.11 - 7.19 (m, 2H, Ar-H), 7.03 - 7.10 (m, 2H, Ar-H); **^{13}C NMR** (101 MHz, DMSO-d_6) δ 167.5, 158.3, 155.3, 149.9, 133.4, 128.9, 128.7, 122.1, 119.3, 116.6, 70.9; **IR:** (ATR) ν cm^{-1} 3099.39, 2123.11, 1723.72, 1697.35, 1247.53; **HRMS:** Found (M – H) = 413.9833, calculated for $C_{16}H_9BrN_5O_4$ = 413.9843

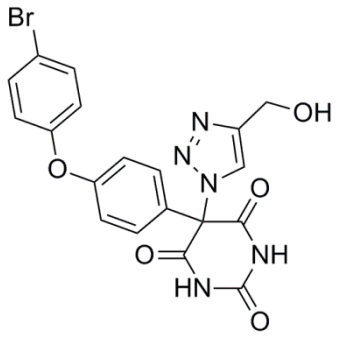

75

Copper sulfate pentahydrate (1.8 mg, 0.0072 mmol, 0.03 eq.) and sodium ascorbate (15.8 mg, 0.08 mmol, 0.33 eq.) were mixed in of *t*-butanol: H_2O (1:1) (1 mL) and added to a dispersion of **74** (0.1 g, 0.24 mmol, 1 eq.) in *t*-butanol: H_2O (1:1) (5 mL). Propargyl alcohol (28 µL, 0.48 mmol, 2 eq.) was added and the mixture was stirred at RT for 48 h. The *t*-butanol was removed *in vacuo* to an aqueous residue. H_2O (20 mL) was added and the cloudy mixture was extracted with EtOAc (3 × 30 mL). The combined organic layers were successively washed with H_2O (50 mL) and brine (20 mL), dried over Na_2SO_4, filtered and concentrated *in vacuo*. The product was isolated by flash column chromatography using a step gradient of EtOAc:Hex (2:1) to EtOAc as an off-white solid (0.0907 g, 80.27%). Mp 160 -165ºC decomposition; **^{1}H NMR** (400 MHz, DMSO-d_6) δ 12.16 (br. s., 2H, NH), 7.93 (s, 1H, triazole), 7.61 (d, *J* = 7.88 Hz, 2H, Ar-H), 7.40 (d, *J* = 7.88 Hz, 2H, Ar-H), 7.05 - 7.28 (m, 4H), 5.25 (br. s., 1H, OH), 4.53 (s, 2H, CH_2); **^{13}C NMR** (101 MHz, DMSO-d_6) δ 166.3, 158.4, 154.7, 149.1, 147.3, 133.1, 130.0, 125.4, 124.5, 121.9, 118.7, 116.3, 54.9; **IR:** (ATR) νcm^{-1} 3066.53, 1716.94, 1480.42, 1239.91; **HRMS:** Found (M – H) = 470.0112, calculated for $C_{19}H_{13}BrN_5O_5$ = 470.0106

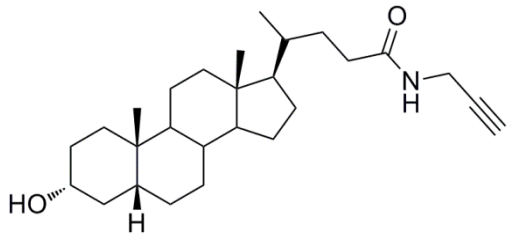

76

LCA (0.5 g, 1.33 mmol) was dissolved in anhydrous DMF (5 mL). DIPEA (464 µL, 2.66 mmol, 2 eq.) and propargyl amine (0.1217 g, 1.33 mmol, 1 eq.) were added and the mixture was cooled under N_2 over an ice-water bath before addition of COMU (1.1392 g, 2.66 mmol, 1 eq.). After 30 min the ice-water bath was removed and the reaction mixture

was allowed to RT and stirred overnight maintaining usual precautions for exclusion of air. The reaction mixture was poured onto H_2O (40 mL) and extracted with DCM (50 mL × 3). The combined organic extractions were washed sequentially with aqueous 1 M HCl (100 mL), saturated $NaHCO_3$ aqueous solution (50 mL), water (50 mL) and saturated brine solution (20 mL). The organic layer was dried over Na_2SO_4, filtered and concentrated *in vacuo* to a straw-yellow oil. The product was isolated by flash column chromatography using Hex:EtOAc (2:1) as mobile phase as a white solid. (0.2961 g, 53.83%). Mp 203 - 205 °C; **^{1}H NMR** (400 MHz, DMSO-d_6) δ 8.20 (b. s.,1H, N-H), 4.43 (d, *J* = 4.56 Hz, 1H), 3.82 (dd, *J* = 2.49, 5.39 Hz, 2H), 3.34 - 3.43 (m, 1H, 3β-H), 3.06 (t, *J* = 2.28 Hz, 1H), 0.82 - 0.91 (m, 6H, 2 × CH_3), 0.60 (s, 3H, CH_3); **^{13}C NMR** (101 MHz, $CDCl_3$) δ 173.1, 79.7, 71.8, 71.5, 56.5, 56.0, 42.7, 42.1, 40.4, 40.2, 36.4, 35.8, 35.4, 35.3, 34.6, 33.3, 31.5, 30.5, 29.2, 28.2, 27.2, 26.4, 24.2, 23.4, 20.8, 18.4, 12; **IR** (ATR) ν cm^{-1} 2934.72, 2863.08, 2848.76, 1700.50, 1479.82, 1258.65, 1231.40, 1010.87, 803.52; **MS** Found (M+H) = 414.4473, calculated for $C_{27}H_{44}NO_2$ = 414.3367

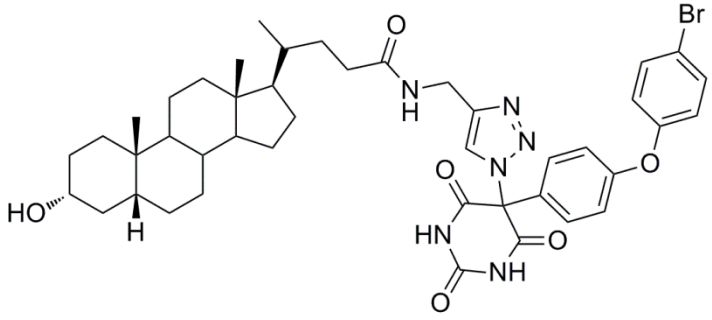

77

Copper sulfate pentahydrate (3.6 mg, 0.01 mmol, 0.03 eq.) and sodium ascorbate (31.7 mg, 0.16 mmol, 0.33 eq.) were mixed together in 1 mL of *t*-butanol: H_2O (1:1), and added to a dispersion of **74** (0.2012 g, 0.48 mmol, 1 eq.) in 5 mL *t*-butanol: H_2O (1:1). Compound **76** (0.2 g, 0.48 mmol, 1 eq.) was added and the mixture was stirred at room temperature for 24 h. The *t*-butanol was removed *in vacuo* to an aqueous residue. H_2O (50 mL) was added and the cloudy mixture was extracted three times with EtOAc (60 mL). The combined organic layers were washed with water (30 mL), brine (20 mL), dried over Na_2SO_4, filtered and concentrated. The product was isolated by flash column chromatography as a white solid (0.1026 g, 25.8%). Mp 200 - 202 °C; **^{1}H NMR** (400 MHz, DMSO-d_6) δ 12.17 (br. s., 2H, barbiturate N-Hs), 8.34 (s, 1H, C=ON-H), 7.86 (s, 1H,

triazole H), 7.67 – 7.48 (m, 2H, Ar - H), 7.43 – 7.26 (m, 2H, Ar - H), 6.95 – 7.23 (m, 4H, Ar - H), 4.40 (br. s., 1H, 3α-OH), 4.33 – 4.14 (m, 2H, C=ONHC$\underline{H_2}$), 0.92 – 0.70 (m, 6H, 2 × CH_3), 0.55 (s, 3H, CH_3); **^{13}C NMR** (151 MHz, DMSO-d_6) δ 172.5, 166.2, 158.4, 154.7, 149.0, 144.4, 133.0, 130.0, 125.3, 124.4, 121.9, 118.7, 116.3, 72.8, 69.8, 59.7, 56.0, 55.5, 42.2, 41.5, 40.0, 36.3, 35.4, 35.1, 34.9, 34.2, 33.9, 32.2, 31.4, 30.4, 27.7, 26.9, 26.1, 23.8, 23.2, 20.4, 18.2, 11.8; **IR:** (ATR**)** ν cm^{-1} 2929.21, 2863.72, 1747.97, 1719.64, 1482.07, 1352.35, 1242.39; **MS**: Found (M – H) = 829.3328, calculated for $C_{43}H_{52}BrN_6O_6$ = 827.3137

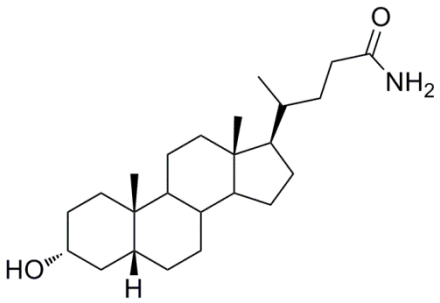

79

To a stirred solution of LCA (1 g; 2.66 mmol) in THF: ACN (17:3) (20 mL), crushed DCC (1.6465 g; 7.98 mmol; 3 eq.) and N-hydroxysuccinimide (0.9184 g; 7.98 mmol; 3 eq.) were added. The pale yellow clear solution was stirred at RT. It turned to a white precipitate within 1 h and was allowed to complete over 24 h. The white solid formed was filtered off and the filtrate was concentrated in vacuo to yield a white crude product that was used in the next step without further purification. This activated ester was dissolved with sonication in DMF (20 mL) and 28% ammonia solution (666 µL; 5.32 mmol; 2 eq.) was added. The reaction mixture was refluxed at 50°C and after 20 h TLC indicated full consumption of starting material. The reaction mixture was allowed to cool and poured onto 100 mL of saturated brine solution. The crude product was collected as a white precipitate by suction filtration and purified by flash column chromatography using ethyl acetate as the mobile phase (0.8154 g, 81.6%). **^{1}H NMR** (400 MHz, $CDCl_3$) δ 5.32 (d, 1H, C=ONH_2), 3.63 (m, 1H, 3β-H), 0.90 - 0.96 (m, 6H, 2 × CH_3), 0.65 (s, 3H, CH_3); **^{13}C NMR** (101 MHz, $CDCl_3$) δ 175.8, 71.9, 56.5, 56.0, 42.8, 42.1, 40.4, 40.2, 36.5, 35.9, 35.4, 35.3, 34.6, 32.8, 31.6, 30.6, 28.3, 27.2, 26.4, 24.2, 23.4, 20.8, 18.4, 12.1; **IR:** (ATR) ν cm^{-1} 2930.49, 2861.93, 1625.49, 727.19; **MS:** Found (M + H) = 376.3206, calculated for $C_{24}H_{42}NO_2$ = 376.321

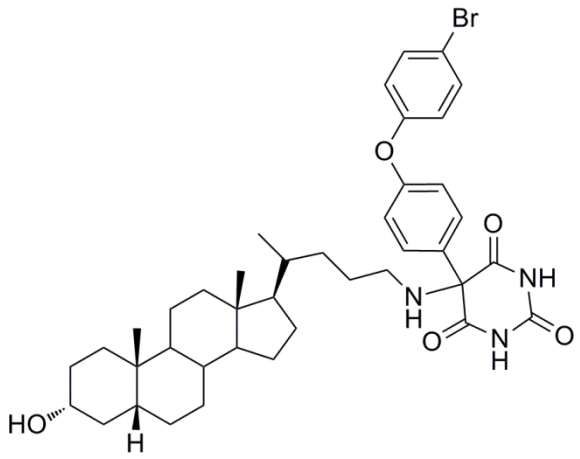

81

Required glassware was oven-dried and N_2 flushed. A commercial preparation of 1M $LiAlH_4$ in THF (9.3 mL, 9.32 mmol, 10 eq.) was added to anhydrous THF (15 mL) under N_2. To this stirred solution, **79** (0.3500 g; 0.93 mmol; 1 eq.) dispersed in anhydrous THF (15 mL) was added dropwise at RT maintaining usual precautions for exclusion of air. The reaction mixture was refluxed for 5 h at 65°C at which time TLC indicated full consumption of starting material. The reaction mixture was allowed to cool to RT. Over an ice-water bath and under N_2, methanol was added dropwise to deactivate remaining $LiAlH_4$. Aqueous sulfuric acid 10% v/v (10 mL) was added and stirred for 10 min. The solution was brought to pH 12 by addition of 2M aqueous NaOH and extracted three times with DCM (50 mL). The combined organic layers were washed with 10 mL saturated brine solution, dried over Na_2SO_4, filtered and solvent removed to a white-pink solid which was used immediately in the next step. The crude amine intermediate was dissolved in MeOH (5 mL) and **39** (0.2134 g, 0.47 mmol, 0.5 eq.) was added and stirred at RT for 24 h. The product was isolated by flash column chromatography in two steps, using EtOAc:MeOH 9:1 as the mobile phase in the first column and EtOAc:DCM 1:1 in a second column, as a white solid (0.0386, 11.18%). Mp 145 - 147°C; **^{1}H NMR** (400 MHz, DMSO-d_6) δ 11.64 (br. s., 2H, 2 × C=ON-H), 7.56 (d, *J* = 8.55 Hz, 2H, Ar-H), 7.45 (d, *J* = 8.55 Hz, 2H, Ar-H), 6.93 - 7.10 (m, 4H, Ar-H), 4.42 (d, *J* = 4.27 Hz, 1H, 3α-OH), 3.35 - 3.42 (m, 1H, 3β-H), 2.79 (br. s., 1H, N-H), 2.25 – 2.41 (m, 2H, C$\underline{H}_2$-NH), 0.83 - 0.90 (m, 6H, 2 × CH_3), 0.61 (s, 3H, CH_3); **^{13}C NMR** (101 MHz, DMSO-d_6) δ 170.9, 156.5, 155.6, 149.5, 133.2, 132.9, 128.3, 121.0, 118.6, 115.5, 70.1, 69.8, 56.1, 55.8, 45.0, 42.2, 41.5, 36.3, 35.4, 35.1, 35.0, 34.2, 32.9, 30.4, 29.3, 27.8, 26.9, 26.2, 23.8, 23.3, 20.4, 18.5, 11.9; **IR:** (ATR) ν cm^{-1} 2929.88, 2858.67, 1702.10, 1480.91, 1235.08, 823.95; **MS:** Found (M – H) = 732.5678, calculated for $C_{40}H_{51}BrN_3O_5$ = 732.5678

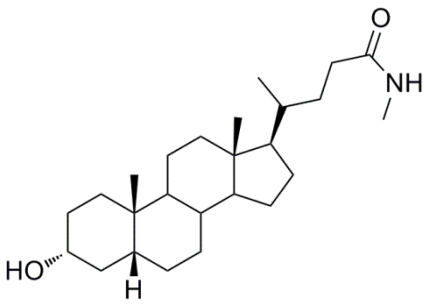

82

To a stirred solution of LCA (0.5 g, 1.33 mmol) in DMF (15 mL), DIPEA (695 µL, 3.99 mmol, 3 eq.) and methylamine hydrochloride (0.0898 g, 1.33 mmol, 1 eq.) were added under N_2 and sonicated to a cloudy mixture. The reaction was cooled over an ice-water bath and COMU (0.5696 g; 1.33 mmol; 1 eq.) was added to immediately give a clear yellow solution. After 30 min, the ice-water bath was removed and the solution was allowed to come to RT and stirred overnight under N_2. The reaction mixture was poured onto 50 mL of water and DCM (3 × 60 mL). The combined organic layers were washed with aqueous 1 M HCl (50 mL), saturated $NaHCO_3$ solution (30 mL), water (30 mL) and brine (30 mL), dried over Na_2SO_4, filtered and concentrated to a white solid. The product was isolated by flash column chromatography using EtOAc as the mobile phase as a white crystalline solid (0.4625, 89.3%). **^{1}H NMR** (400 MHz, $CDCl_3$) δ 3.63 (ddd, *J* = 5.39, 6.22, 9.95 Hz, 1H, 3β-H), 2.80 (s, 3H, C=ONH-C$\underline{H}_3$), 0.83 - 0.95 (m, 6H, 2 × CH_3), 0.64 (s, 3H, CH_3); **^{13}C NMR** (101 MHz, $CDCl_3$) δ 174.2, 71.9, 56.5, 56.0, 42.7, 42.1, 40.4, 40.2, 36.5, 35.8, 35.5, 35.3, 34.6, 33.5, 31.8, 30.5, 28.2, 27.2, 26.4, 26.3, 24.2, 23.4, 20.8, 18.4, 12.0; **IR:** (ATR) ν cm^{-1} 3367.19, 2929.95, 2863.06, 1647.38, 1445.61, 1042.48; **MS:** Found (M + H) =390.3355, calculated for $C_{25}H_{44}NO_2$ = 390.3372

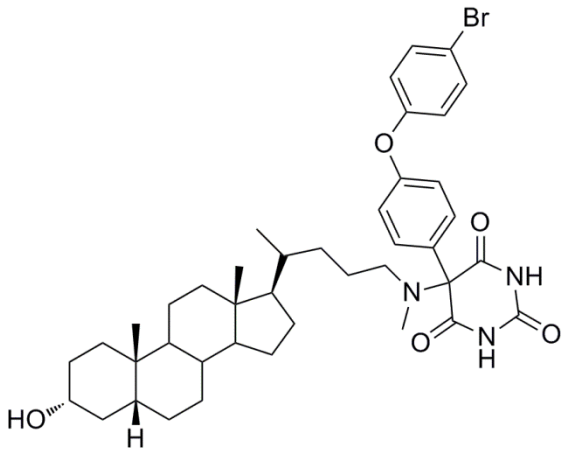

84

Required glassware was oven-dried and N_2 flushed. A commercial preparation of 1M $LiAlH_4$ in THF (4.7 mL; 4.7 mmol; 10 eq.) was added to anhydrous THF (15 mL) under N_2. To this stirred solution, **82** (0.1825 g; 0.47 mmol; 1 eq.) dispersed in anhydrous THF (15 mL) was added dropwise at RT maintaining usual precautions for exclusion of air. The reaction mixture was refluxed for 5 h at 65°C at which time TLC indicated full consumption of starting material. The reaction mixture was allowed to cool to RT. Over an ice-water bath and under N_2, methanol was added dropwise to deactivate remaining $LiAlH_4$. Aqueous sulfuric acid 10% (10 mL) was added and stirred for 10 min. The solution was brought to pH 12 by addition of aqueous 2M NaOH and extracted with DCM (3 × 50 mL). The combined organic layers were washed with 10 mL saturated brine solution, dried over Na_2SO_4, filtered and solvent removed to a white-pink solid which was used immediately in the next step. The crude amine intermediate was dissolved in methanol (5 mL) and **39** (0.1058g; 0.233 mmol; 0.5 eq.) was added and stirred at RT for 24 h. The product was isolated by flash column chromatography using EtOAc:Hex 1:1 as mobile phase (0.0422 g, 24.2%). Mp 154 - 157°C; **^{1}H NMR** (400 MHz, DMSO-d_6) δ 11.57 (br. s., 2H, N-H), 7.49 – 7.72 (m, 2H, Ar-H), 7.30 -7.48 (m, 2H, Ar-H), 6.93 - 7.10 (m, 4H, Ar-H), 4.42 (b., s, 1H, 3α-OH), 2.25 (s, 1H, N-CH_3), 0.73 - 0.93 (m, 6H, 2 × CH_3), 0.58 (s, 3H, CH_3); **^{13}C NMR** (151 MHz, DMSO-d_6) δ 170.4, 156.8, 155.4, 149.4, 132.9, 129.6, 127.5, 121.2, 118.4, 115.7, 75.4, 69.8, 56.0, 55.7, 52.9, 42.2, 41.5, 40.0, 36.8, 36.3, 35.4, 35.1, 34.9, 34.2, 32.6, 30.4, 27.7, 26.9, 26.1, 24.5, 23.8, 23.2, 20.4, 18.5, 11.9; **IR:** (ATR) ν cm^{-1} 1655.54, 1617.76, 1495.98, 1249.86, 1154.60, 1131.28 **HRMS:** Found (M-H) =746.3154, calculated for $C_{41}H_{53}BrN_3O_5$ = 746.3174

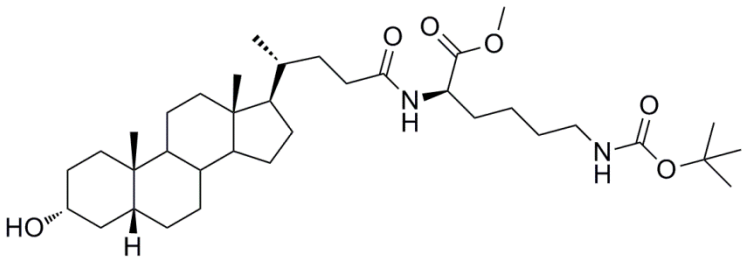

85

LCA (1 g, 2.66 mmol) was dissolved in 10 mL of anhydrous DMF (10 mL). DIPEA (0.9260 mL, 5.32 mmol, 2 eq.) and H-Lys(Boc)-OMe.HCl (0.7894 g, 2.66 mmol, 1 eq.) were added and the mixture was cooled under N_2 over an ice-water bath before addition of COMU (1.1392 g; 2.66 mmol; 1 eq.). The orange solution was stirred over the ice water bath for 30 min before allowing to room temperature maintaining usual precautions for exclusion of air. After 6 h, TLC indicated remaining starting material in the reaction mixture and a further 0.2 eq. (0.2278 g) of COMU were added and the reaction mixture was stirred at RT overnight. The reaction mixture was poured onto H_2O (40 mL) and extracted with DCM (50 mL × 3). The combined DCM extractions were washed sequentially with aqueous 1 M HCl (100 mL), saturated $NaHCO_3$ aqueous solution (50 mL), water (50 mL) and saturated brine solution (30 mL). The organic layer was dried over Na_2SO_4, filtered and concentrated *in vacuo* to a straw yellow oil. The product was isolated by flash column chromatography using EtOAc:DCM (1:1) as mobile phase as a white crystalline solid. (1.55 g, 94.13%). Mp 115 - 117°C; **^{1}H NMR** (400 MHz, DMSO-d_6) δ 8.12 (d, *J* = 7.32 Hz, 1H, NHC=O), 6.75 (br. s., 1H, NHC=O), 4.43 (d, *J* = 4.27 Hz, 1H, 3α-OH), 4.10 - 4.23 (m, 1H, C=ONHC<u>H</u>C=OOCH_3), 3.60 (s, 3H, -OCH_3), 3.33 - 3.44 (m, 1H, 3β-H), 2.79 - 2.97 (m, 2H, C<u>H</u>$_2$NH-BOC), 1.37 (s, 9H, NHC=OOC(C<u>H</u>$_3$)$_3$), 0.81 - 0.92 (m, 6H, 2 × CH_3), 0.61 (s, 3H, CH_3); **^{13}C NMR** (101 MHz, $CDCl_3$) δ 173.5, 173.1, 156.1, 79.1, 71.7, 56.4, 55.9, 52.3, 51.8, 42.7, 42.0, 40.4, 40.1, 36.4, 35.8, 35.4, 35.3, 34.5, 33.3, 32.0, 31.5, 30.4, 29.6, 28.4, 28.2, 27.1, 26.4, 24.1, 23.3, 22.4, 20.8, 20.6, 18.3, 12.0; **IR:** (ATR) ν cm^{-1} 3315.59, 2928.53, 2863.63, 1741.43, 1689.26, 1654.13, 1529.63, 1249.37, 1168.44; **MS**: Found (M+H) = 619.2587, calculated for $C_{36}H_{62}N_2O_6$ =619.4686

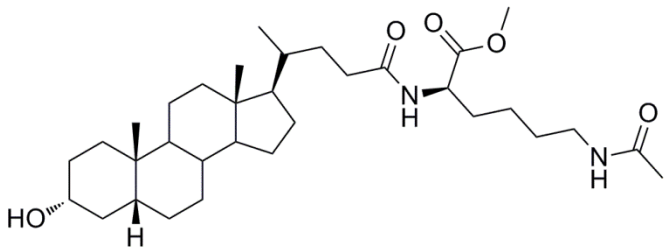

87

Compound **85** (0.2 g, 0.32 mmol) was deboced in TFA 10% v/v in DCM (10 mL). After 1 h, TLC indicated the deprotection was finished and the DCM solvent was removed *in vacuo*. DCM (5 mL) was added and removed *in vacuo* 5 times to aid in removal of TFA. The residue was dissolved in DCM (10 mL) and DIPEA (111 µL, 0.64 mmol, 2 eq.) and acetic anhydride (30.2 µL 0.32 mmol, 1 eq) were added. The reaction was stirred at RT. After 2 h, the reaction was poured onto H_2O (30 mL) and extracted with DCM (3 × 50 mL). The combined organic layers were washed with aqueous 1M HCl (50 mL), saturated $NaHCO_3$ solution (20 mL), H_2O (20 mL) and brine (10 mL), dried over Na_2SO_4, filtered and concentrated *in vacuo*. The product was isolated by flash column chromatography as a white solid (0.0994 g, 55.2%). Mp 128 -130°C; **^{1}H NMR** (400 MHz, $CDCl_3$) δ 6.41 (d, *J* = 7.88 Hz, 1H, N-H), 6.24 (t, *J* = 5.18 Hz, 1H, N-H), 4.53 (dt, *J* = 4.77, 8.19 Hz, 1H, -C=ONHC<u>H</u>C=O), 3.70 (s, 3H, -C=OOCH_3), 3.58 (ddt, *J* = 4.56, 5.39, 10.57 Hz, 1H, 3β-H), 3.15 – 3.22 (m, 2H, -C<u>H_2</u>NHC=OCH_3), 1.94 (s, 3H, CH_3, -NHC=OCH_3), 0.82 - 0.92 (m, 6H, 2 × CH_3), 0.60 (s, 3H, CH_3); **^{13}C NMR** (101 MHz, $CDCl_3$) δ 173.8, 173.0, 170.5, 71.6, 56.4, 55.9, 52.3, 51.5, 42.6, 42.0, 40.3, 40.1, 38.8, 36.3, 35.7, 35.3, 35.3, 34.5, 33.1, 31.9, 31.5, 30.4, 28.6, 28.1, 27.1, 26.3, 24.1, 23.3, 23.1, 22.3, 20.7, 18.3, 11.9; **IR:** (ATR) ν cm^{-1} 3262.38, 2933.76, 2855.41, 1751.16, 1649.50, 1560.27, 1231.94; **MS:** Found (M+H) = 561.5818, calculated for $C_{33}H_{57}N_2O5$ = 561.4262

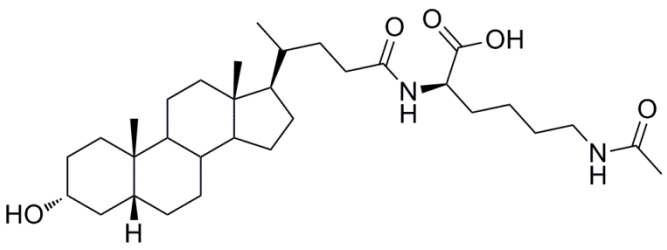

88

Compound **87** (0.1728 g, 0.31 mmol) was dissolved in MeOH (9.5 mL) and 2M aqueous NaOH (500 µL) for a final NaOH concentration of 0.1 M. After 22 h, TLC indicated full consumption of starting material. The reaction mix was acidified to pH 1 – 2 by addition of 1M aqueous HCl. H_2O (40 mL) was added and the product was seen to precipitate. The product was extracted into EtOAc (3 × 75 mL). The combined organic layers were successively washed with H_2O (2 × 100 mL) and brine (100 mL), dried over Na_2SO_4 and filtered. Removal of the solvent *in vacuo* afforded the product as a white solid (0.1558 g, 92.46%). Mp 145 - 148°C; **^{1}H NMR** (400 MHz, DMSO-d_6) δ 12.42 (br. s., 1H, -COOH), 7.98 (d, *J* = 7.88 Hz, 1H, N-H), 7.79 (t, *J* = 4.98 Hz, 1H, N-H), 4.43 (br. s., 1H, 3α-OH), 4.06 - 4.19 (m, 1H, -C=ONHC<u>H</u>C=O), 2.91 – 3.07 (m, 2H, -C<u>H$_2$</u>NHC=OCH$_3$), 1.77 (s, 3H, -NHC=OCH$_3$), 0.77 - 0.94 (m, 6H, 2 × CH$_3$), 0.60 (s, 3H, CH$_3$); **^{13}C NMR** (101 MHz, DMSO-d_6) δ 173.8, 172.7, 168.9, 69.8, 56.1, 55.6, 51.7, 42.2, 41.5, 40.0, , 38.2, 36.3, 35.4, 35.1, 34.9, 34.2, 32.0, 31.5, 30.7, 30.4, 28.7, 27.7, 26.9, 26.2, 23.8, 23.3, 22.9, 22.6, 20.4, 18.3, 11.8; **IR:** (ATR) ν cm^{-1} 3051.66, 2940.58, 2853.52, 1700.25, 1611.44, 1539.55, 1480.43, 1231.95; **MS:** Found (M+H) = 547.5377, calculated for $C_{32}H_{54}N_2O_5$ = 547.4105

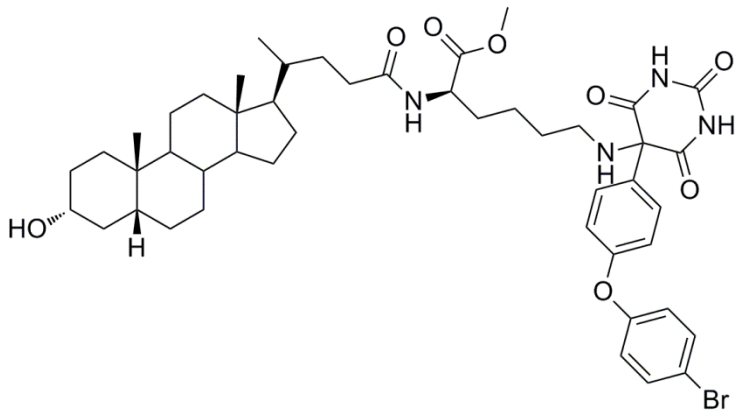

89

Compound **85** (0.2 g, 0.32 mmol) was deboced in 10% TFA v/v TFA in DCM (10 mL). After 1 h, TLC indicated the deprotection was finished and the DCM solvent was removed *in vacuo*. DCM (5 mL) was added and removed *in vacuo* 5 times to aid in removal of TFA. The amine was freed from the TFA salt with 1 M NaOH, extracted into DCM and the DCM was removed *in vacuo*. The amine residue was reacted immediately with **39** (0.1453 g, 0.16 mmol) in MeOH (5 mL). After 24 h, the MeOH was removed *in vacuo* and the product was isolated by flash column chromatography using a step gradient of DCM: EtOAC (1:1) to EtOAc as a white solid (22 mg, 8%). Mp 195 – 200°C decomposition; **^{1}H NMR** (400 MHz, DMSO-d_6) δ 11.65 (br. s., 2H, barbiturate ring N-Hs), 8.13 (d, *J* = 7.83 Hz, 1H, C=ONH), 7.56 (d, *J* = 8.80 Hz, 2H, Ar-H), 7.45 (d, *J* = 8.80 Hz, 2H, Ar-H), 7.05 (d, *J* = 9.29 Hz, 2H, Ar-H), 6.98 (d, *J* = 9.29 Hz, 2H, Ar-H), 4.45 (d, *J* = 4.40 Hz, 1H, C3-αOH), 4.11 - 4.20 (m, 1H, C=ONHC<u>H</u>C=O), 3.59 (s, 3H, -C=OOCH_3), 2.31 – 2.40 (m, 2H, -C<u>H_2</u>NH), 0.84 – 0.88 (m, 6H, 2 × CH_3), 0.59 (s, 3H, CH_3); **^{13}C NMR** (101 MHz, $CDCl_3$) δ 173.8, 173.4, 170.2, 158.1, 155.3, 148.6, 132.9, 131.0, 128.3, 121.1, 118.8, 116.7, 71.9, 71.4, 56.5, 55.8, 52.4, 51.9, 44.7, 42.7, 42.0, 40.4, 40.2, 36.3, 35.8, 35.4, 35.3, 34.5, 33.1, 32.1, 31.5, 30.4, 29.5, 28.2, 27.1, 26.4, 24.2, 23.3, 22.5, 20.8, 18.3, 12.0; **IR:** (ATR) ν cm^{-1} 2927.76, 2860.82, 1735.22, 1709.22, 1655.08, 1481.56, 1236.94; **MS:** Found (M+H) = 891.5123, calculated for $C_{47}H_{64}BrN_4O_8$ = 891.3902

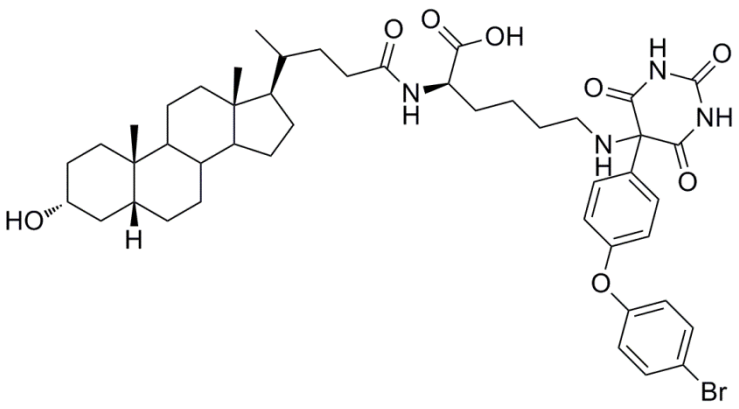

90

Compound (0.0540 g, 0.06 mmol) was dissolved in MeOH (9.5 mL) and 2M aqueous NaOH (500 µL) for a final NaOH concentration of 0.1 M. After 17 h, TLC indicated full consumption of starting material. The reaction mix was acidified to pH 1 – 2 by addition of 1M aqueous HCl. H_2O (20 mL) was added and the product was extracted into ethyl acetate (50 mL) three times. The combined organic layers were successively washed with H_2O (2 × 60 mL) and brine (20 mL), dried over Na_2SO_4 and filtered. Removal of the solvent *in vacuo* afforded the product as a white solid (0.0531g, 99.7%). Mp 225 – 230°C decomposition; **^{1}H NMR** (400 MHz, DMSO-d_6)) δ 11.61 (br. s., 2H, barbiturate ring N-H), 7.94 (d, *J* = 7.93 Hz, 1H, C=ONH), 7.52 (d, *J* = 9.16 Hz, 2H, Ar-H), 7.39 - 7.45 (m, *J* = 9.16 Hz, 2H, Ar-H), 6.98 - 7.04 (m, *J* = 9.16 Hz, 2H, Ar-H), 6.92 - 6.98 (m, 2H, Ar-H), 4.42 (br. s., 1H, 3α-OH), 4.05 - 4.11 (m, 1H, C=ONHC<u>H</u>C=O), 2.34 (t, *J* = 6.41 Hz, 2H, -C<u>H$_2$</u>NH), 0.80 - 0.85 (m, 6H, 2 × CH_3), 0.55 (s, 3H, CH_3); **^{13}C NMR** (151 MHz, DMSO-d_6) δ 173.9, 172.6, 170.8, 156.5, 155.6, 149.5, 133.2, 132.9, 128.3, 120.9, 118.6, 115.5, 70.2, 69.8, 56.1, 55.6, 51.7, 44.2, 42.2, 41.5, 40.0, 36.3, 35.4, 35.1, 34.9, 34.2, 32.1, 31.5, 30.8, 30.4, 29.3, 27.7, 26.9, 26.1, 23.8, 23.3, 23.1, 20.4, 18.3, 11.8; **IR:** (ATR) ν cm^{-1} 2926.38, 2860.94, 1711.11, 1646.76, 1482.14, 1239.62; **MS**: Found (M + H) = 877.6574, calculated for $C_{46}H_{62}BrN_4O_8$ = 877.3746

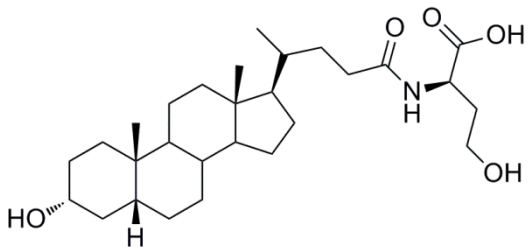

91

LCA (0.5 g, 1.33 mmol) was dispersed in Et_2O (20 mL) and cooled over an ice-bath. NEt_3 (241.2 µL, 1.73 mmol, 1.3 eq.) was added followed by ethyl chloroformate (151.3 µL, 1.59 mmol, 1.2 eq.). The reaction was stirred for 10 min. Homoserine (0.1743 g, 1.46 mmol, 1.1 eq.) was dispersed in MeOH (10 mL) and NEt_3 (389 µL, 2.79 mmol, 2.1 eq.) was added. This was sonicated for 5 min and then added dropwise to the stirring anhydride intermediate. The reaction mixture was stirred over an ice-water bath for 1 h by which time it had become a clear solution. The ice-water bath was removed and the reaction stirred at RT overnight. The solvent was removed *in vacuo* and the crude material was dispersed in aqueous 1 M HCl (30 mL) and extracted with DCM (3 × 50 mL). The combined organic layers were washed with H_2O (2 × 50 mL) and brine (20 mL), dried over Na_2SO_4, filtered and concentrated *in vacuo*. The product was isolated by flash column chromatography using a mobile phase step gradient of EtOAc:DCM 1:1 + 0.33% v/v CH_3COOH to EtOAc + 0.33% v/v CH_3COOH as a white solid. (0.1204 g, 19.0%). **^{1}H NMR** (400 MHz, MeOD) δ 4.30 (dd, *J* = 4.98, 8.29 Hz, 1H, N-H), 3.48 - 3.68 (m, 4H), 3.29 - 3.33 (m, 1H), 0.91 - 1.00 (m, 6H, 2 × CH_3), 0.69 (s, 3H, CH_3); **^{13}C NMR** (101 MHz, MeOD) δ 178.8, 176.0, 72.3, 60.2, 57.8, 57.4, 53.7, 43.8, 43.5, 41.8, 41.5, 37.2, 37.1, 36.9, 36.4, 35.6, 34.2, 33.2, 31.1, 29.2, 28.3, 27.6, 25.2, 23.9, 21.9, 18.9, 18.3, 12.4; **IR:** (ATR) ν cm^{-1} 3302.12, 2927.75, 2862.34, 1589.44, 1542.28, 1399.94 **MS:** Found (M – H) = 476.4900, calculated for $C_{28}H_{46}NO_5$ = 476.3381

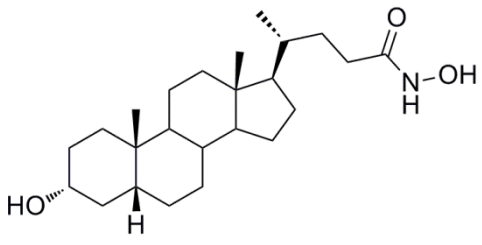

92

To a stirred solution of KOH (0.84 g, 15 mmol) in MeOH (4 mL) at 0°C, hydroxylamine hydrochloride (1 g, 15 mmol) was added and stirred at 0°C. After 15 min, the KCl precipitate was filtered off and the free hydroxylamine solution filtrate was used

immediately in the next step. LCA (2 g, 5.31 mmol) was dispersed in $E_{t2}O$ (20 mL) and cooled over an ice-bath. NEt_3 (962 µL, 6.90 mmol, 1.3 eq.) was added followed by ethyl chloroformate (607 µL, 6.37 mmol, 1.2 eq.). The reaction was stirred for 10 min. Freshly-prepared hydroxylamine solution (7 mL, 10.62 mmol, 2 eq.) was added and the reaction was stirred at RT for 2 h. Precipitated solids were filtered off and the filtrate was concentrated *in vacuo* to a crude white solid. The pure product was isolated by a double recrystallisation from C_2H_5OH as a white solid (0.2622 g, 12.6%). Mp 205°C; **^{1}H NMR** (400 MHz, DMSO-d_6) δ 10.31 (s, 1H), 8.63 (s, 1H), 4.43 (d, *J* = 4.15 Hz, 1H, 3α-OH), 3.36 - 3.49 (m, 1H, 3β-H), 0.87 (br. s., 6H, 2 × CH_3), 0.61 (s, 3H, CH_3); **^{13}C NMR** (101 MHz, DMSO-d_6) δ 169.4, 69.8, 56.1, 55.5, 42.2, 41.5, 36.3, 35.4, 35.1, 34.8, 34.2, 31.4, 30.4, 29.2, 27.7, 26.9, 26.1, 23.8, 23.3, 20.4, 18.2, 11.9; **IR:** (ATR) ν cm^{-1} 3189.39, 2923.47, 2860.89, 1702.20, 1447.38, 1039.31; **MS:** Found (M+H) = 392.3972, calculated for $C_{24}H_{42}NO_3$ = 392.3159

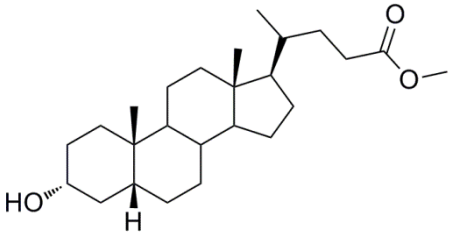

93 (LCA methyl ester)

To a stirred solution of LCA (2.000 g, 5.31 mmol) in MeOH (50 mL), conc. HCl (0.5 mL) was added and the mixture was refluxed at 70°C. After 8h, TLC indicated that the reaction was complete and the solvent was evaporated to a white solid. This residue was dissolved in DCM (50 mL) and washed successively with saturated aqueous $NaHCO_3$ solution (2 × 20 mL), water (20 mL) and brine (20 mL). The organic layer was dried over Na_2SO_4, filtered and the solvent removed *in vacuo* to yield the product as a white solid which did not require further purification (2.0388 g, 98.3%). Mp 129°C; **^{1}H NMR** (400 MHz, $CDCl_3$) δ 3.66 (s, 3H, O-CH3), 3.58 - 3.65 (m, 1H, 3β-H), 0.88 - 0.94 (m, 6H), 0.64 (s, 3H); **^{13}C NMR** (101 MHz, $CDCl_3$) δ 174.8 (C=O, 24-C), 71.8 (3-C), 56.4, 55.9, 51.5, 42.7, 42.0, 40.4, 40.1, 36.4, 35.8, 35.3, 35.3, 34.5, 31.0, 31.0, 30.5, 28.2, 27.1, 26.4, 24.2, 23.3, 20.8, 18.2, 12.0; **IR:** (ATR) ν cm^{-1} 3516.55, 2932.75, 2861.62, 1712.57; **MS:** Found (M-H) = 389.3251, calculated for $C_{25}H_{41}O_3$ =389.3056

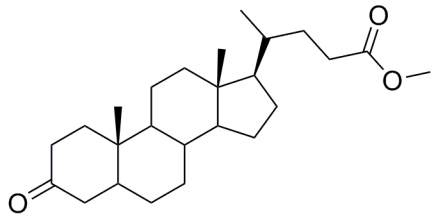

94

To a stirred solution of LCA (0.2 g, 0.51 mmol, 1 eq.) in HPLC grade DCM (15 mL), PCC (0.1324 g, 0.61 mmol, 1.2 eq.) was added and the reaction was stirred at RT for 15 h at which time TLC indicated the starting material was fully consumed. The reaction mixture was filtered through a plug of celite and the product was washed through with DCM. The filtrate was washed with water (50 mL × 3) and saturated brine solution (20 mL), dried over Na_2SO_4, filtered and concentrated *in vacuo* to a red-brown oil. The product was isolated as a white crystalline solid by flash column chromatography using Hex:EtOAc (2:1) as the mobile phase (0.1782 g, 89.91%). Mp 132 – 134°C; **^{1}H NMR** (400 MHz, $CDCl_3$) δ 3.66 (s, 3H), 1.02 (s, 3H), 0.92 (d, *J* = 6.63 Hz, 3H), 0.68 (s, 3H); **^{13}C NMR** (101 MHz, $CDCl_3$) δ 213.3, (C=O, 3-C) 174.7 (C=O, 24-C), 56.4, 55.9, 51.5, 44.3, 42.7, 42.3, 40.7, 40.0, 37.2, 37.0, 35.5, 35.3, 34.9, 31.0, 30.9, 28.1, 26.6, 25.7, 24.1, 22.6, 21.2, 18.2, 12.0; **IR:** (ATR) ν cm^{-1} 3190.14, 2924.98, 2862.61, 1735.70, 1708.65, 1447.84, 1223.26; **MS:** Found (M - H) = 389.2960, calculated for $C_{25}H_{41}O_3$ = 389.3056

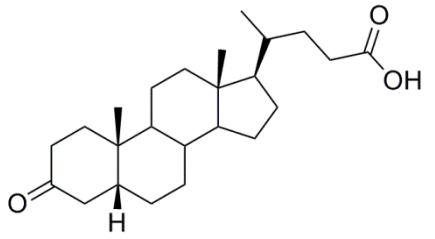

95

Compound **94** (0.15 g, 0.38 mmol) was dissolved in MeOH (18 mL) and aqueous 2 M NaOH (2 mL) was added for a final NaOH concentration of 0.2 M. The reaction was stirred at RT. After 40 h, TLC indicated full consumption of the starting material. The mixture was acidified to pH 1 -2 by the addition of aqueous 1M HCl and poured onto 100 mL of H_2O precipitating the product. The aqueous layer was extracted three times with EtOAc (3 × 150 mL). The combined organic layers were washed with H_2O (100 mL) and brine (50 mL), dried over Na_2SO_4 and filtered. The solvent was removed *in vacuo* to afford

the product as a white solid which did not require further purification (0.1408 g, 97.2%). Mp 144 - 145°C; **^{1}H NMR** (400 MHz, DMSO-d_6) δ 11.94 (s, 1H, -COOH), 0.96 (s, 3H, CH_3), 0.88 (d, *J* = 6.22 Hz, 3H, C-21 CH_3), 0.64 (s, 3H, CH_3); **^{13}C NMR** (101 MHz, DMSO-d_6) δ 211.6 (C-3 C=O), 174.8 (C-24 COOH), 55.6, 55.6, 43.6, 42.3, 41.8, 39.6, 39.5, 36.7, 36.4, 35.1, 34.8, 34.4, 30.7, 30.7, 27.7, 26.2, 25.3, 23.8, 22.2, 20.8, 18.1, 11.8; **IR:** ν cm^{-1} 3180.92, 2925.03, 2862.04, 1699.72, 1666.21, 1447.36; **MS:** Found (M-H) = 373.1667, calculated for $C_{24}H_{38}O_3$ = 373.2748

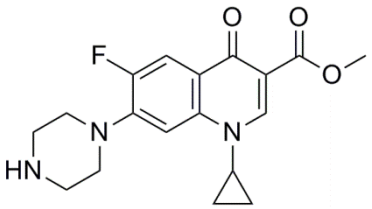

97 (ciprofloxacin methyl ester)

Ciprofloxacin (1 g, 3.02 mmol) was dispersed in MeOH (50 mL). Ten drops of conc. H_2SO_4 were added and the mixture was refluxed at 80°C for a total of 12 h over 2 d. The MeOH solvent was removed and the yellow residue was neutralised with saturated $NaHCO_3$ solution. The aqueous solution was extracted with DCM (3 × 50 mL). The combined organic layers were washed with saturated $NaHCO_3$ solution (30 mL), H_2O (30 mL) and brine (20 mL), dried over Na_2SO_4 and filtered. The solvent was removed *in vacuo* to afford the product as a white solid (0.64 g, 61.3%) which was stored protected from light. Mp 226 - 230°C decomposition; **^{1}H NMR** (400 MHz, DMSO-d_6) δ 8.52 (s, 1H, -N-CH=C), 8.00 (d, *J* = 13.27 Hz, 1H, Ar-H), 7.26 (d, *J* = 7.05 Hz, 1H, Ar-H), 3.91 (s, 3H, CH_3), 3.43 (s, 1H, N–C<u>H</u>$(CH_2)_2$), 3.23 (dd, *J* = 3.52, 6.01 Hz, 4H, N-CH_2), 3.09 (dd, *J* = 3.73, 5.80 Hz, 4H, N - CH_2), 1.90 (br. s., 1H, N-H), 1.28 – 1.36 (m, 2H, CH_2s), 1.09 - 1.18 (m, 2H, CH_2s); **^{13}C NMR** (101 MHz, DMSO-d_6) δ 173.0 (d, $^{4}J_{C,F}$ = 3.03 Hz), 166.4, 153.4 (d, $^{1}J_{C,F}$ = 250.48 Hz), 148.3, 144.9, 137.9 (d, $^{4}J_{C,F}$ = 1.01 Hz), 122.9 (d, $^{3}J_{C,F}$ = 7.07 Hz), 113.2 (d, $^{2}J_{C,F}$ = 24.24 Hz), 109.98, 104.7 (d, $^{3}J_{C,F}$ = 3.03 Hz), 52.0, 51.1, 51.1(d, $^{4}J_{C,F}$ = 4.04 Hz), 45.9, 34.5, 8.1; **IR:** (ATR) ν cm^{-1} 3051.88, 1699.57, 1480.56, 1231.21, 821.16; **HRMS:** found (M + H) = 346.1581, calculated for $C_{18}H_{21}FN_3O_3$ = 346.1561

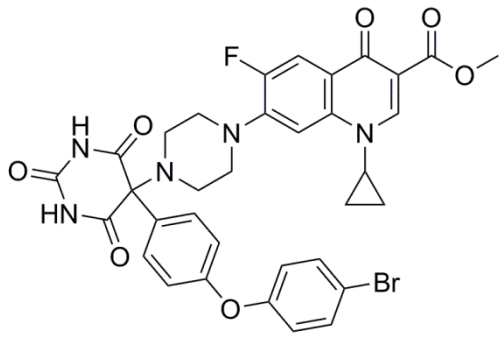

98

To a solution of **39** (0.0727 g, 0.16 mmol, 1 eq.) in MeOH (10 mL), **97** (0.1106 g, 0.32 mmol, 2 eq.) was added. The reaction was stirred at RT for 48 h. The MeOH solvent was removed *in vacuo* and the yellow residue was dispersed in EtOAc (20 mL). This organic layer was washed with aqueous 1M HCl (50 mL), saturated $NaHCO_3$ solution (50 mL) and saturated brine (20 mL). The organic phase was dried over Na_2SO_4, filtered and concentrated. The product was isolated by flash column chromatography using EtOAc:MeOH (9:1) as the mobile phase as a white solid (0.0773 g, 67.28%). Mp 245 - 249°C decomposition; **^{1}H NMR** (400 MHz, DMSO-d_6) δ 11.69 (s, 2H, N-H), 8.43 (s, 1H, -N-CH=C-), 7.73 (d, *J* = 13.27 Hz, 1H, Ar-H), 7.58 (d, *J* = 8.71 Hz, 2H, Ar-H), 7.48 (d, *J* = 8.71 Hz, 2H, Ar-H), 7.44 (d, *J* = 7.46 Hz, 1H, Ar-H), 7.00 - 7.15 (m, 4H, Ar-H), 3.73 (s, 3H, CH_3), 3.64 (br. s., 1H, CH), 3.23 (br. s., 4H, CH_2), 2.83 (br. s., 4H, CH_2), 1.26 (m, 2H, CH_2), 1.08 (br. s., 2H, CH_2); **^{13}C NMR** (101 MHz, $CDCl_3$) δ 169.9, 164.9, 157.0, 155.3, 153.9, 151.4, 149.4, 148.2, 143.9, 143.8, 138.0, 132.9, 129.9, 129.7, 122.0, 121.9, 121.4, 118.6, 115.8, 111.6, 111.3, 108.9, 106.5, 74.1, 51.2, 50.4, 47.4, 34.8, 7.5; **IR** (ATR) ν cm^{-1} 3192.68, 2957.80, 2847.74, 1734.43, 1708.65, 1612.74, 1480.42, 1235.25; **HRMS** Found (M + H) = 718.1322, calculated for $C_{34}H_{30}BrFN_5O_7$ = 718.1313

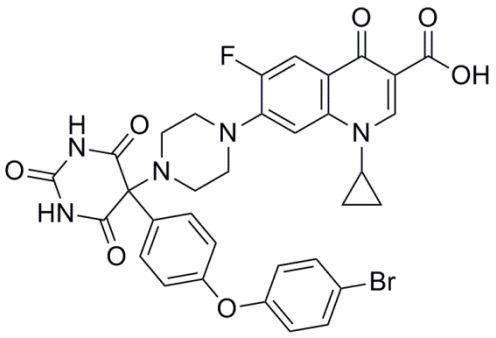

99

Compound **98** (0.05 g) was dispersed in MeOH and aqueous 2 M NaOH (5 mL) was added. The reaction was stirred at RT for 12 h. The MeOH was removed *in vacuo* to leave an aqueous residue which was neutralised and acidified by addition of aqueous 1 M HCl. The cloudy aqueous layer was extracted with EtOAc (3 × 50 mL). The combined organic layers were washed with H_2O (50 mL) and saturated brine (20 mL), dried over Na_2SO_4 and filtered. The solvent was removed *in vacuo* to afford the product as a yellow solid (0.04 g, 79%). Mp 265 - 270°C decomposition; **^{1}H NMR** (400 MHz, DMSO-d_6) δ 11.70 (s, 2H, N-H), 8.66 (s, 1H, C=CH), 7.91 (d, *J* = 13.27 Hz, 1H, Ar-H), 7.54 - 7.64 (m, 3H, Ar-H), 7.48 (d, *J* = 8.71 Hz, 2H, Ar-H), 7.01 - 7.15 (m, 4H, Ar-H), 3.82 (br. s., 1H, CH), 2.85 (br. s., 4H, CH_2), 1.32 (m, 2H, CH_2), 1.17 (m, 2H, CH_2); **^{13}C NMR** (101 MHz, DMSO-d_6) δ 176.4, 170.0, 166.1, 157.2, 155.3, 151.9, 149.4, 148.0, 145.3, 145.2, 139.2, 133.0, 133.0, 129.9, 129.8, 121.5, 121.1, 118.7, 118.6, 115.9, 106.8, 106.7, 74.2, 50.3, 47.4, 36.0, 30.8, 7.7; **IR:** (ATR) ν cm^{-1} 1763.81, 1702.22, 1625.48, 1481.77, 1230.37 **HRMS** Found (M – H) = 702.3660, calculated for $C_{33}H_{26}BrFN_5O_7$ = 702.1000

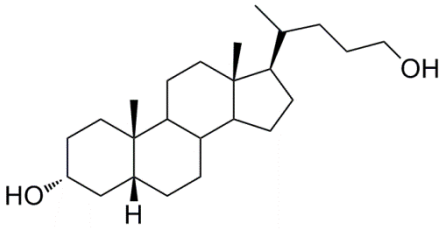

100

LCA (2 g; 5.31 mmol) dispersed in anhydrous THF (20 ml) was added dropwise to a stirred commercial 1M solution of lithium aluminium hydride in anhydrous THF (53 mL) under anhydrous conditions. When addition was complete, the mixture was refluxed at 65°C for 6 h under N_2. The reaction mixture was allowed to cool and remaining $LiAlH_4$

was deactivated by gradual addition of EtOAc. A 10% v/v aqueous solution of sulfuric acid (50 mL) was added to dissolve the formed salts and the cleared aqueous solution was extracted with Et_2O (100 mL × 3). The combined extractions were successively washed with saturated aqueous $NaHCO_3$ solution (150 mL), water (100 mL) and brine (50 mL). The organic phase was dried over Na_2SO_4, filtered and concentration to a white solid *in vacuo*. The pure product was isolated by flash column chromatography using Hex:EtOAc (1:1) as mobile phase as a white solid (1.2871 g, 51.94%). **^{1}H NMR** (400 MHz, MeOD) δ 3.45 - 3.58 (m, 3H, 3β-H and 24-CH_2), 0.90 - 0.98 (m, 6H), 0.69 (s, 3H); **^{13}C NMR** (101 MHz, MeOD) δ 72.6, 63.7, 58.1, 57.8, 44.0, 43.7, 42.1, 41.7, 37.4, 37.3, 37.1, 36.6, 35.8, 33.3, 31.3, 30.4, 29.5, 28.5, 27.8, 25.4, 24.1, 22.1, 19.3, 12.7; **IR:** (ATR) ν cm^{-1} 3053.77, 2924.38, 1479.93, 1230.55, 1011.28; **MS:** Found (M + Na) = 385.4463, calculated for $C_{24}H_{42}O_2Na$ = 385.3083

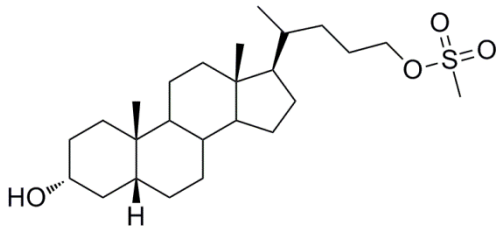

101

To a stirred solution of **100** (0.2 g, 0.55 mmol.) in anhydrous DCM (10 mL) over an ice-water bath, a solution of methanesulfonyl chloride (0.0758 g, 51.4 µL, 0.66 mmol, 1.2 eq.) and NEt_3 (0.0668 g, 92 µL, 0.66 mmol, 1.2 eq) in DCM (5 mL) was added dropwise over 30 min maintaining usual precautions for exclusion of air. When addition was complete, the ice-water bath was removed and the reaction stirred for a further 4 h at RT. When TLC indicated the reaction was not proceeding further, approximately 40 g of crushed ice was gradually added to the reaction mixture and stirred for 10 min. This mixture was extracted with DCM (60 mL × 3). The combined organic layers were washed successively with aqueous 1M HCl (100 mL), saturated aqueous $NaHCO_3$ solution (100 mL), water (100 mL) and brine (50 mL), dried over Na_2SO_4, filtered and concentrated *in vacuo*. The product was isolated from the crude residue by flash column chromatography using Hex:EtOAc (3:2) as mobile phase as a white solid (0.1629 g, 67.26%); **^{1}H NMR** (400 MHz, $CDCl_3$) δ 4.20 (tdd, *J* = 3.21, 6.58, 9.80 Hz, 2H, 24-CH_2), 3.63 (dt, *J* = 4.98, 10.37 Hz, 1H, 3β-H), 3.01 (s, 3H, -OSO_2CH_3), 0.91 - 0.96 (m, 6H), 0.65 (s, 3H); **^{13}C NMR** (101 MHz,$CDCl_3$) δ 71.8,

70.7, 56.5, 56.0, 42.7, 42.1, 40.4, 40.2, 37.4, 36.4, 35.8, 35.3, 35.3, 34.5, 31.5, 30.5, 28.3, 27.2, 26.4, 25.8, 24.2, 23.3, 20.8, 18.5, 12.0; **IR:** (ATR) ν cm^{-1} 2927.27, 2863.73, 1448.73, 1349.21, 1172.16, 914.05; **MS**:Found (M + Na) = 463.3557, calculated for $C_{25}H_{44}O_4SNa$ = 463.2858

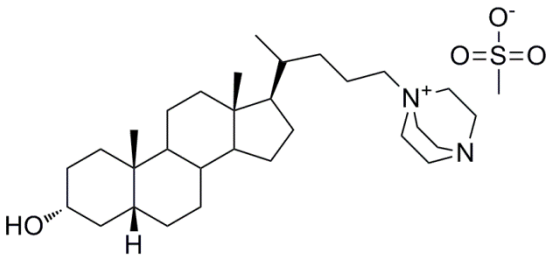

102

Compound (0.0635 g, 0.14 mmol) was dissolved in ACN (2 mL). DABCO (0.0314 g, 0.28 mmol, 2 eq.) was added and the reaction was stirred at RT for 48 h. The solid formed was isolated by filtration and washed with acetonitrile (2 × 1 mL) to afford the product as a white solid (0.0774 g, 55.0%). Mp 282 - 285°C decomposition; **^{1}H NMR** (400 MHz, MeOD) δ 3.55 (ddt, *J* = 4.58, 5.49, 10.53 Hz, 1H, 3β-H), 3.33 - 3.39 (m, 6H, 3 × N-CH_2), 3.11 - 3.26 (m, 8H, 4 × N-CH_2), 2.70 (s, 3H, -S-CH_3), 1.02 (d, *J* = 6.71 Hz, 3H, CH_3), 0.95 (s, 3H, CH_3), 0.71 (s, 3H, CH_3); **^{13}C NMR** (101 MHz, MeOD) δ 72.5, 66.3, 66.3, 66.2, 58.1, 57.5, 53.6, 53.6, 53.6, 46.2, 44.1, 43.6, 42.0, 41.7, 39.7, 37.4, 37.3, 37.0, 36.6, 35.8, 33.8, 31.3, 29.5, 28.5, 27.8, 25.4, 24.1, 22.1, 19.7, 19.1, 12.6; **IR:** (ATR) ν cm^{-1} 2928.53, 2862.69, 1590.97, 1400.14, 1377.06, 11170.33, 1039.84; **MS:** Found (M) = 457.5413, calculated for $C_{31}H_{53}N_2O$ = 457.4152

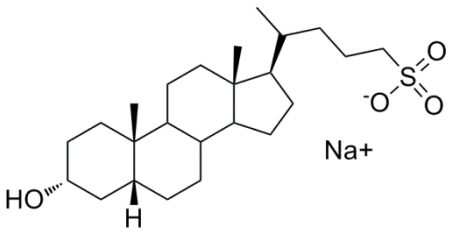

104

Compound **54** (0.0464 g, 0.11 mmol) was dissolved in acetone (1 mL) in a microwave tube and NaI (0.0173 g, 0.12 mmol, 1.1 eq.) was added. The reaction mixture was microwaved at constant temperature for 1 h at 85°C. Et_2O (10 mL) was added and precipitated solid was removed by filtration. The yellow filtrate was washed with H_2O (3 × 10 mL) and the organic layer was concentrated to yield crude iodate which was used immediately in the next step. Na_2SO_3 (0.0332 g, 0.26 mmol, 2.5 eq.) was weighed into a microwave tube and

dissolved in ddH_2O (2 mL). The crude iodate was dispersed in acetone (1.5 mL) and added to the tube. After sonication, the reaction mixture was microwaved at a constant temperature of 120°C for 3 h. The acetone was removed *in vacuo* and the product was isolated by SPE on reverse phase silica using MeOH:H_2O (1:1) as the eluting solvent as a white solid (0.02855 g, 63.9%). **^{1}H NMR** (400 MHz, MeOD) δ 3.53 (ddd, *J* = 5.49, 6.22, 10.26 Hz, 1H, 3β-H), 2.66 - 2.82 (m, 2H, CH_2SO_3), 0.97 (d, *J* = 6.63 Hz, 3H, CH_3 C-21), 0.95 (s, 3H, CH_3), 0.69 (s, 3H, CH_3); **^{13}C NMR** (101 MHz, MeOD) δ 72.6, 58.1, 57.7, 53.4, 44.0, 43.7, 42.0, 41.7, 37.4, 37.4, 37.1, 36.7, 36.4, 35.8, 31.4, 29.5, 28.5, 27.8, 25.4, 24.1, 22.9, 22.1, 19.2, 12.6; **MS**: Found (M) = 425.5649, calculated for $C_{24}H_{41}O_4S$ = 425.2731

General method A for sulfonamide synthesis by the reaction of an aminobenzoic acid derivative and a sulfonyl chloride

A dispersion of the aminobenzoic acid in water was adjusted to pH 8 by the addition of 1M Na_2CO_3. Sulfonyl chloride (1 eq.) was added and the reaction mixture was stirred at RT.The pH was maintained at approximately pH 8 as the reaction progressed by addition of aqueous 1M Na_2CO_3 as required. When the reaction was complete, the mixture was acidified to pH 1-2 with conc. HCl. The precipitate formed was collected by suction filtration and allowed to dry. Recrystallisation was carried out if required.

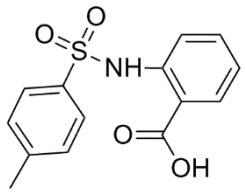

106

Compound **113** was prepared by General method A from anthranilic acid (1.00 g, 7.3 mmol) and 4-methylbenzenesulfonyl chloride (1.39 g, 7.3 mmol, 1 eq.) as an off-white solid (0.51 g, 23.9%). Mp 225 - 227°C; **^{1}H NMR** (400 MHz, DMSO-d_6) δ 11.09 (br. s., 1H), 7.85 - 7.93 (m, 1H), 7.65 - 7.75 (m, *J* = 8.29 Hz, 2H), 7.47 - 7.58 (m, 2H), 7.28 - 7.38 (m, *J* = 8.29 Hz, 2H), 7.10 (ddd, *J* = 2.07, 6.32, 8.19 Hz, 1H), 2.32 (s, 3H); **^{13}C NMR** (101 MHz, DMSO-d_6) δ 169.8, 144.1, 139.9, 135.7, 134.5, 131.5, 129.9, 126.9, 123.2, 118.2, 116.5, 21.0; **IR:** (ATR) ν cm^{-1} 3036.53, 1665.03, 1490.74, 1153.07, 1087.57; **HRMS:** Found (M + Na) = 314.0460, calculated for $C_{14}H_{13}NO_4SNa$ = 314.0463

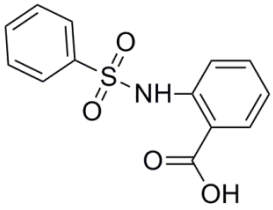

107

Compound **107** was prepared by General method A from anthranilic aicd (0.2715 g, 1.98 mmol) and benzenesulfonyl chloride (253 μL, 1.98 mmol, 1 eq.) as an off-white solid (0.2391 g, 43.6%). Mp 204 - 208°C decomposition; **^{1}H NMR** (400 MHz, DMSO-d_6) δ 13.91 (br, w., 1H, OH) 11.11 (br. s., 1H, NH), 7.89 (dd, *J* = 1.24, 7.88 Hz, 1H, Ar-H), 7.78 - 7.85 (m, 2H, Ar-H), 7.61 - 7.67 (m, 1H, Ar-H), 7.49 - 7.59 (m, 4H, Ar-H), 7.12 (dt, *J* = 3.11, 5.70 Hz, 1H, Ar-H); **^{13}C NMR** (101 MHz, DMSO-d_6) δ 169.7, 139.7, 138.5, 134.5, 133.6, 131.5, 129.5, 126.8, 123.4, 118.5, 116.7; **IR** (ATR) ν cm^{-1} 3178.69, 1671.25, 1490.20, 1254.23, 1157.56; **HRMS** Found (M + Na) = 300.0305, calculated for $C_{13}H_{11}NO_4SNa$ = 300.0306

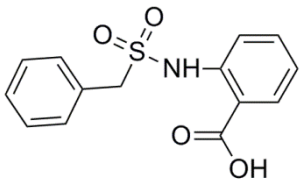

108

Compound **108** was prepared by General method A from anthranilic acid (0.1440 g, 1.05 mmol, 1 eq.) and phenylmethanesulfonyl chloride (0.2000 g, 1.05 mmol, 1 eq.) as an off-white solid (0.1049 g, 34.3%). Mp 220 - 223°C; **^{1}H NMR** (400 MHz, DMSO-d_6) δ 13.84 (br. s., 1H, OH), 10.68 (br. s., 1H, NH), 8.00 (d, *J* = 7.88 Hz, 1H, Ar-H), 7.54 - 7.64 (m, 2H, Ar-H), 7.25 - 7.37 (m, 3H, Ar-H), 7.12 - 7.24 (m, 3H, Ar-H), 4.69 (s, 2H, CH_2); **^{13}C NMR** (101 MHz, DMSO-d_6) δ 169.7, 140.8, 134.7, 131.6, 130.7, 128.9, 128.5, 128.4, 122.5, 117.2, 115.4, 57.3; **IR:** (ATR) ν cm^{-1} 2921.76, 2853.00, 1739.97, 1459.96; **HRMS:** Found (M - H) = 290.0500, calculated for $C_{14}H_{12}NO_4S$ = 290.0487

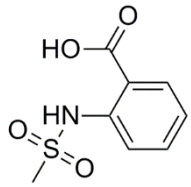

109

Compound **109** was prepared by General method A from anthranilic acid (0.2138 g, 1.56 mmol) and methanesulfonyl chloride (100 µL, 1.56 mmol, 1 eq.) as a light brown solid (0.0627 g, 18.7%). Mp 230 - 231°C; **^{1}H NMR** (400 MHz, DMSO-d_6) δ 10.68 (br., 1H, NH), 8.00 (dd, *J* = 1.66, 7.88 Hz, 1H, Ar-H), 7.62 (dd, *J* = 1.66, 7.05 Hz, 1H, Ar-H), 7.52 - 7.59 (m, 1H, Ar-H), 7.18 (m, 1H, Ar-H), 3.17 (s, 3H, CH_3); **^{13}C NMR** (101 MHz, DMSO-d_6) δ 170.0, 140.7, 134.9, 131.9, 123.0, 117.9, 116.2, 40.1; **IR:** (ATR) ν cm^{-1} 1663.33, 1491.14, 1255.40, 1140.46; **HRMS:** Found (M - H) = 214.0159, calculated for $C_8H_8NO_4S$ = 214.0174

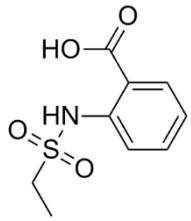

110

Compound **110** was prepared by General method A from anthranilic acid (0.3379 g, 2.4 mmol) and ethanesulfonyl chloride (227 µL, 2.4 mmol, 1 eq.) as a light brown solid (0.1566 g, 28.46%). Mp 232 - 233°C; **^{1}H NMR** (400 MHz, DMSO-d_6) δ 13.93 (br. 1H, OH), 10.72 (br. s., 1H, NH), 7.95 - 8.06 (m, 1H, Ar-H), 7.50 - 7.67 (m, 2H, Ar-H), 7.17 (ddd, *J* = 2.49, 5.80, 7.88 Hz, 1H, Ar-H), 3.29 (q, *J* = 7.46 Hz, 2H, CH_3), 1.18 (t, *J* = 7.46 Hz, 3H, CH_2); **^{13}C NMR** (101 MHz, DMSO-d_6) δ 169.9, 140.7, 134.8, 131.7, 122.7, 117.5, 115.8, 45.8, 7.9; **IR:** (ATR) ν cm^{-1} 1672.68, 1490.43, 1255.87, 1142.14 **HRMS:** Found (M - H) = 290.0332, calculated for $C_9H_{10}NO_4S$ = 228.0331

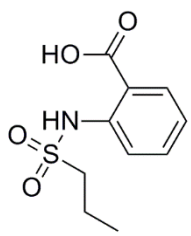

111

Compound **111** was prepared by General method A from anthranilic acid (0.4059 g, 2.96 mmol) and propanesulfonyl chloride (333 µL, 2.96 mmol, 1 eq.) as a light brown solid (0.0864 g, 12.9%). Mp 228°C; **^{1}H NMR** (400 MHz, DMSO-d_6) δ 10.73 (br. s., 1H, NH),

7.96 - 8.06 (m, 1H, Ar-H), 7.52 - 7.70 (m, 2H, Ar-H), 7.17 (ddd, *J* = 1.87, 6.22, 8.09 Hz, 1H, Ar-H), 3.21 - 3. (m, 2H, CH_2), 1.59 - 1.74 (m, 2H, CH_2), 0.93 (t, *J* = 7.46 Hz, 3H, CH_3); **^{13}C NMR** (101 MHz, DMSO-d_6) δ 169.9, 140.7, 134.8, 131.7, 122.6, 117.5, 115.7, 52.9, 16.8, 12.4 **IR** (ATR) ν cm^{-1} 3208.76, 1665.80, 1490.12, 1143.56, 1256.81; **HRMS:** Found (M - H) = 242.0501, calculated for $C_{10}H_{12}NO_4S$ = 242.0487

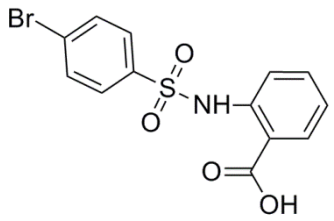

112

To a solution of anthranilic acid (0.5000 g, 3.65 mmol) in 10 mL of H_2O:THF (1:1), NEt_3 (1.5 mL, 10.95 mmol, 3 eq.) and 4-bromobenzenesulfonyl chloride (0.9326 g, 3.65 mmol, 1 eq.) were added. The reaction mixture was stirred at RT. After 16 h, 1 M HCl (50 mL) was added to the mixture and it was extracted with ethyl acetate. The combined organic layers were washed with saturated $NaHCO_3$ solution and dried over Na_2SO_4. The solvent was removed to yield a pale brown solid which did not require further purification (0.7053 g 54.3%). Mp 265 - 269°C; **^{1}H NMR** (400 MHz, DMSO-d_6) δ 11.00 - 11.30 (m, 1H, NH), 7.91 (dd, *J* = 1.87, 8.09 Hz, 1H, Ar-H), 7.67 - 7.84 (m, 4H, Ar-H), 7.44 - 7.61 (m, 2H, Ar-H), 7.11 - 7.19 (m, 1H, Ar-H); **^{13}C NMR** (101 MHz, DMSO-d_6) δ 169.6, 139.3, 137.9, 134.5, 132.6, 131.6, 128.9, 127.5, 123.7, 118.8, 117.2; **IR:** (ATR) ν cm^{-1} 3083.23, 1666.10, 1490.80, 1256.15, 1153.71; **HRMS:** Found (M - H) = 353.9413, calculated for $C_{13}H_9BrNO_4S$ = 353.9436

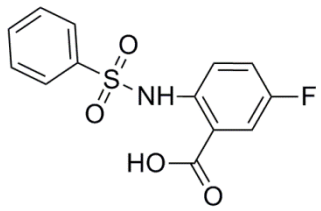

113

Compound **113** was prepared by General method A from 2-amino-5-fluorobenzoic acid (0.1800 g, 1.16 mmol) and benzenesulfonyl chloride (148 µL, 1.16 mmol, 1 eq.) as an off-white solid (0.1752 g, 51.2%). Mp 217°C; **^{1}H NMR** (400 MHz, DMSO-d_6) δ 10.83 (br. s., 1H, NH), 7.73 - 7.79 (m, 2H, Ar-H), 7.57 - 7.67 (m, 2H, Ar-H), 7.51 - 7.57 (m, 3H, Ar-H), 7.40 - 7.48 (m, 1H, Ar-H); **^{13}C NMR** (101 MHz, DMSO-d_6) δ 168.4 (d, $^4J_{H,F}$ = 2.02 Hz),

157.6 (d, $^{1}J_{H, F}$ = 243.41 Hz), 138.4, 135.8 (d, $^{4}J_{H, F}$ = 3.03 Hz), 133.6, 129.5, 126.8, 121.9 (d, $^{3}J_{H, F}$ = 8.08 Hz), 121.4 (d, $^{2}J_{H, F}$ = 23.23 Hz), 119.7 (d, $^{3}J_{H, F}$ = 7.07Hz), 117.4 (d, $^{2}J_{H, F}$ = 23.23 Hz) **IR:** (ATR) ν cm^{-1} 1686.25, 1491.81, 1167.96, 906.71; **HRMS:** Found (M -H) = 294.0238, calculated for $C_{13}H_9FNO_4S$ = 294.0236

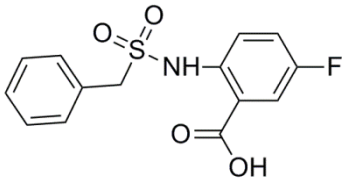

114

Compound **114** was prepared by General method A from 2-amino-5-fluorobenzoic acid (0.1551 g, 1 mmol) and 4-methylbenzenesulfonyl chloride (0.1907 g, 1 mmol, 1 eq.) as an off-white solid (0.1956 g, 63.42%). Mp 218 - 219 °C; **^{1}H NMR** (400 MHz, DMSO-d_6) δ 10.47 (br. s., 1H, NH), 7.70 (d, *J* = 7.05 Hz, 1H, Ar-H), 7.55 (m, 1H, Ar-H), 7.47 (m., 1H, Ar-H), 7.06 – 7.39 (m, 5H, Ar-H), 4.68 (br. s., 2H, CH_2); **^{13}C NMR** (101 MHz, DMSO-d_6) δ 168.5 (d, $^{4}J_{H, F}$ = 2.02 Hz), 156.9 (d, $^{1}J_{H, F}$ = 242.4 Hz), 137.1 (d, $^{4}J_{H, F}$ = 2.02 Hz), 130.8, 128.9, 128.5, 128.4, 121.6 (d, $^{2}J_{H, F}$ = 23.23 Hz), 119.9 (d, $^{3}J_{H, F}$ = 8.08 Hz), 117.6 (d, $^{3}J_{H, F}$ = 7.07 Hz), 117.2 (d, $^{2}J_{H, F}$ = 24.24 Hz), 57.42; **IR:** (ATR) ν cm^{-1} 1656.51, 1495.77, 1351.11, 1154.28; **HRMS:** Found (M-H) = 308.0396, calculated for $C_{14}H_{11}FNO_4S$ = 308.0393

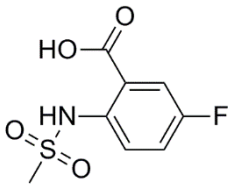

115

Compound **115** was prepared by General method A from 2-amino-5-fluorobenzoic acid (0.1551 g, 1 mmol) and methanesulfonyl chloride (65 µL, 1 mmol, 1 eq.) as a light brown solid (0.0898 g, 38.5%). Mp 208 - 209°C; **^{1}H NMR** (400 MHz, DMSO-d_6) δ 7.72 (dd, *J* = 3.11, 9.33 Hz, 1H, Ar-H), 7.59 (dd, *J* = 4.98, 9.12 Hz, 1H, Ar-H), 7.43 - 7.52 (m, 1H, Ar-H), 3.13 (s, 3H, CH_3); **^{13}C NMR** (101 MHz, DMSO-d_6) δ 168.3 (d, $^{4}J_{H, F}$ = 2.02 Hz), 157.0 (d, $^{1}J_{H, F}$ = 242.40 Hz), 136.5 (d, $^{4}J_{H, F}$ = 3.03 Hz), 121.0 (d, $^{2}J_{H, F}$ = 22.22 Hz), 120.5 (d, $^{3}J_{H, F}$ = 7.07 Hz), 119.2 (d, $^{3}J_{H, F}$ = 9.09 Hz), 117.2 (d, $^{2}J_{H, F}$ = 23.23 Hz), 20.79; **IR:** (ATR) ν

cm^{-1} 1675.65, 1494.31, 1326.87, 1156.04, 1136.89 **HRMS:** Found (M -H) = 232.0080, calculated for $C_8H_7FNO_4S$ = 232.008

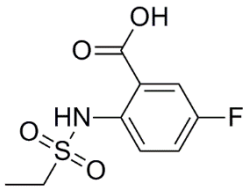

116

Compound **116** was prepared by General method A from 2-amino-5-fluorobenzoic acid (0.1551 g, 1 mmol) and ethanesulfonyl chloride (95 µL, 1 mmol, 1 eq.) as a light brown solid (0.1761 g, 71.2%). Mp 212°C; **^{1}H NMR** (400 MHz, DMSO-d_6) δ 10.46 (br. s., 1H, NH), 7.72 (dd, *J* = 3.11, 9.33 Hz, 1H, Ar-H), 7.62 (dd, *J* = 4.98, 9.12 Hz, 1H, Ar-H), 7.51 (dddd, *J* = 2.90, 3.94, 5.81, 7.26 Hz, 1H, Ar-H), 3.26 (q, *J* = 7.33 Hz, 2H, CH_2), 1.17 (t, *J* = 7.26 Hz, 3H, CH_3); **^{13}C NMR** (101 MHz, DMSO-d_6) δ 168.7 (d, $^4J_{H,F}$ = 2.02 Hz), 157.2 (d, $^1J_{H,F}$ = 242.40 Hz), 136.9 (d, $^4J_{H,F}$ = 2.02 Hz), 121.8 (d, $^2J_{H,F}$ = 23.23 Hz), 120.6 (d, $^3J_{H,F}$ = 8.08 Hz), 118.3 (d, $^3J_{H,F}$ = 7.07 Hz), 117.5 (d, $^2J_{H,F}$ = 23.23 Hz), 45.9, 7.9; **IR:** (ATR) ν cm^{-1} 1670.98, 1493.36, 1423.55, 1337.08, 1233.76, 1156.24, 1136.54; **HRMS:** Found (M - H) = 246.0243, calculated for $C_9H_9FNO_4S$ = 246.0236

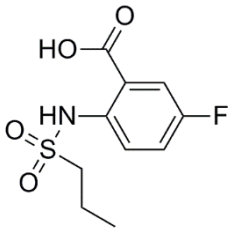

117

Compound **117** was prepared by General method A from 2-amino-5-fluorobenzoic acid (0.1551 g, 1 mmol) and propanesulfonyl chloride (113 µL, 1 mmol, 1 eq.) as a brown solid (0.1087 g 41.7%). Mp 212 - 215°C; **^{1}H NMR** (400 MHz, DMSO-d_6) δ 10.46 (br. s., 1H, NH), 7.72 (dd, *J* = 3.32, 9.12 Hz, 1H, Ar-H), 7.63 (dd, *J* = 4.98, 9.12 Hz, 1H, Ar-H), 7.52 (dddd, *J* = 3.11, 4.04, 5.80, 7.36 Hz, 1H, Ar-H) 3.14 - 3.33 (m, 2H, CH_2), 1.6 – 1.72 (m, 2H, CH_2), 0.93 (t, *J* = 7.46 Hz, 3H, CH_3); **^{13}C NMR** (101 MHz, DMSO-d_6) δ 168.7 (d, $^4J_{H,F}$ = 2.02 Hz), 157.1 (d, $^1J_{H,F}$ = 242.40 Hz), 136.8 (d, $^4J_{H,F}$ = 2.02 Hz), 121.7 (d, $^2J_{H,F}$ = 23.23 Hz), 120.5 (d, $^3J_{H,F}$ = 7.07 Hz), 118.2 (d, $^3J_{H,F}$ = 7.07 Hz), 117.4 (d, $^2J_{H,F}$ = 23.23 Hz), 53.0, 16.8, 12.4; **IR:** (ATR) ν cm^{-1} 1686.17, 1491.83, 1423.28, 1156.69, 1137.35; **HRMS:** found (M – H) 260.0402, calculated for $C_{10}H_{11}FNO_4S$ = 260.0393

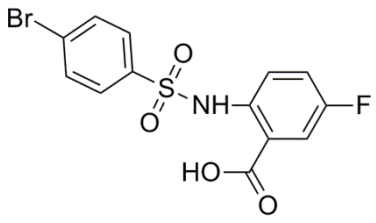

118

Compound **117** was prepared by General method A from 2-amino-5-fluorobenzoic acid (0.1551 g, 1 mmol) and 4-bromobenzenesulfonyl chloride (0.2555 g, 1 mmol, 1 eq.) as a pink-brown solid (0.0842g, 27.3%). Mp >250°C; **^{1}H NMR** (400 MHz, DMSO-d_6) δ 10.74 (br. s., 1H, NH), 7.74 - 7.80 (m, 2H, Ar-H), 7.64 - 7.70 (m, 2H, Ar-H), 7.61 (dd, *J* = 2.90, 9.12 Hz, 1H, Ar-H), 7.43 - 7.53 (m, 2H, Ar-H); **^{13}C NMR** (101 MHz, DMSO-d_6) δ 168.1 (d, $^{4}J_{H,F}$ = 1.01 Hz), 157.9 (d, $^{1}J_{H,F}$ = 244.42 Hz), 137.7, 135.8 (d, $^{4}J_{H,F}$ = 2.02 Hz), 132.6, 128.8, 127.5, 122.6 (d, $^{3}J_{H,F}$ = 8.08 Hz), 121.4 (d, $^{2}J_{H,F}$ = 23.23 Hz), 120.6 (d, $^{3}J_{H,F}$ = 7.07Hz), 117.5 (d, $^{2}J_{H,F}$ = 24.24 Hz); **IR:** (ATR) ν cm^{-1} 3169.47, 1678.28, 1493.13, 1166.37, 1140.86; **HRMS:** Found (M – H) = 371.9343, calculated for $C_{13}H_8BrFNO_4S$ = 371.9341

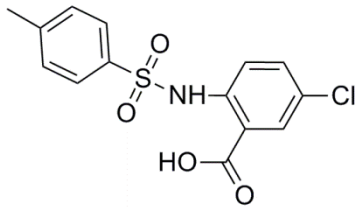

119

Compound **119** was prepared by General method A from 2-amino-5-chlorobenzoic acid (0.1716 g, 1 mmol) and *p*-toluenesulfonyl chloride (0.1907 g, 1 mmol, 1 eq.) as a white solid (0.1868 g,57.3%). Mp 162°C; **^{1}H NMR** (400 MHz, DMSO-d_6) δ 10.98 (br. s., 1H, NH), 7.83 (d, *J* = 2.49 Hz, 1H, Ar-H), 7.66 - 7.74 (m, *J* = 8.29 Hz, 2H, Ar-H), 7.58 - 7.64 (m, 1H, Ar-H), 7.49 - 7.55 (m, 1H, Ar-H), 7.32 - 7.39 (m, *J* = 7.88 Hz, 2H, Ar-H), 2.33 (s, 3H, CH_3); **^{13}C NMR** (101 MHz, DMSO-d_6) δ 168.4, 144.3, 138.6, 135.5, 134.1, 130.7, 130.0, 127.2, 126.9, 120.4, 118.6, 21.0; **IR:** (ATR) ν cm^{-1} 3222.69, 1655.10, 1483.87, 1438.32, 1244.55, 1159.98; **HRMS:** Found (M – H) = 324.0109, calculated for $C_{14}H_{11}ClNO_4S$ = 324.0097

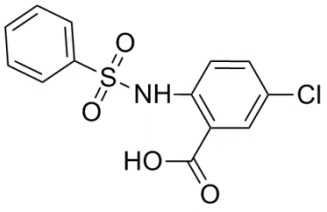

120

Compound **120** was prepared by General method A from 2-amino-5-chlorobenzoic acid (0.1716 g, 1 mmol) and benzenesulfonyl chloride (0.1551 g, 1 mmol, 1 eq.)as an off-white solid (0.1752 g, 56.2%). Mp 167-169°C; **^{1}H NMR** (400 MHz, DMSO-d_6) δ 11.01 (br. s., 1H, NH), 7.71 - 7.91 (m, 3H, Ar-H), 7.44 - 7.70 (m, 5H, Ar-H); **^{13}C NMR** (101 MHz, DMSO-d_6) δ 168.4, 138.4, 138.3, 134.1, 133.7, 130.7, 129.6, 127.4, 126.8, 120.7, 118.9; **IR:** (ATR) ν cm^{-1} 3389.67, 3257.94, 1655.28, 1482.78, 1233.31, 1141.85; **HRMS:** Found (M – H) = 309.9938, calculated for $C_{13}H_9ClNO_4S$ = 309.9941

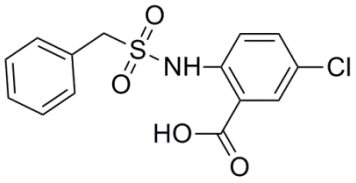

121

Compound **121** was prepared by General method A from 2-amino-5-chlorobenzoic acid (0.1716 g, 1 mmol) and benzenesulfonyl chloride (0.1907 g, 1 mmol, 1 eq.) as an off-white solid (0.1568 g 48.4%). Mp 158 - 161°C; **^{1}H NMR** (400 MHz, DMSO-d_6) δ 7.88 (br. s., 1H), 7.13-7.46 (m, 7H, Ar-H), 4.39 (s, 2H, CH_2); **^{13}C NMR** (101 MHz, DMSO-d_6) δ 168.0, 142.0, 131.1, 131.1, 130.7, 130.3, 130.0, 128.2, 127.9, 124.1, 118.4, 57.2 **IR:** (ATR) ν cm^{-1} 3575.55, 3368.90, 1479.78, 1406.73, 1365.19, 1125.97; **HRMS:** Found (M – H) = 371.9340, calculated for $C_{13}H_8BrFNO_4S$ = 371.9341

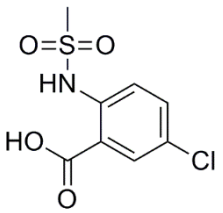

122

Compound **122** was prepared by General method A from 2-amino-5-chlorobenzoic acid (0.1716 g, 1 mmol) and methanenesulfonyl chloride (0.1907 g, 1 mmol, 1 eq.) as an off-white solid (0.5119 g 20.5%). Mp 168-169°C; **^{1}H NMR** (400 MHz, DMSO-d_6) δ 10.58

(br. s., 1H), 7.94 (d, *J* = 2.90 Hz, 1H), 7.56 - 7.64 (m, 2H), 3.21 (s, 3H); **^{13}C NMR** (101 MHz, DMSO-d_6) δ 168.5, 139.3, 133.5, 130.7, 126.6, 119.9, 118.3, 40.0; **IR:** (ATR) ν cm^{-1} 3356.97, 2825.22, 1664.10, 1236.20; **HRMS:** Found (M – H) = 247.9795, calculated for $C_8H_7ClNO_4S$ = 247.9784

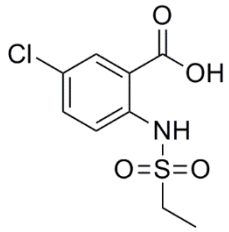

123

Compound **123** was prepared by General method A from 2-amino-5-chlorobenzoic acid (0.1716 g, 1 mmol) and ethanesulfonyl chloride (95 μL, 1 mmol, 1 eq.) as an off-white solid

(0.0841 g, 31.9%). Mp 160°C; **^{1}H NMR** (400 MHz, DMSO-d_6) δ 10.63 (br. s., 1H, NH), 7.94 (d, *J* = 2.49 Hz, 1H, Ar-H), 7.50 - 7.73 (m, 2H, Ar-H), 3.30 (q, *J* = 7.26 Hz, 2H), 1.18 (t, *J* = 7.26 Hz, 3H); **^{13}C NMR** (101 MHz, DMSO-d_6) δ 168.8, 139.5, 134.4, 130.9, 126.7, 119.8, 117.9, 46.1, 8.0; **IR:** (ATR) ν cm^{-1} 1662.54, 1482.76, 1233.48, 1141.72; **HRMS:** Found (M-H) = 261.9946, calculated for $C_9H_9ClNO_4S$

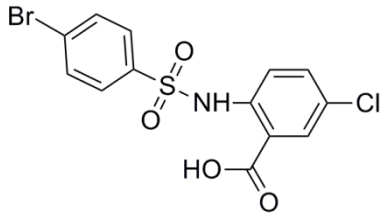

124

Compound **124** was prepared by General method A from 2-amino-5-chlorobenzoic acid (0.1716 g, 1 mmol) and 4-bromobenzenesulfonyl chloride (0.2555 g, 1 mmol, 1 eq.) as a pale brown solid (0.9545 g, 24.4%). Mp >250°C; **^{1}H NMR** (400 MHz, DMSO-d_6) δ 11.12 (br. s., 1H, NH), 7.84 (d, *J* = 2.49 Hz, 1H, Ar-H), 7.67 - 7.82 (m, 4H, Ar-H), 7.62 (dd, *J* = 2.49, 9.12 Hz, 1H, Ar-H), 7.49 (d, *J* = 8.71 Hz, 1H, Ar-H); **^{3}C NMR** (101 MHz, DMSO-d_6) δ 168.2, 138.0, 137.8, 134.0, 132.6, 130.7, 128.8, 127.7, 127.6, 121.1, 119.7; **IR:** (ATR) ν cm^{-1} 3095.05, 1655.39, 1438.17, 1245.71, 1167.5; **HRMS:** Found (M – H) = 387.9047, calculated for $C_{13}H_8BrClNO_4S$ = 387.9046

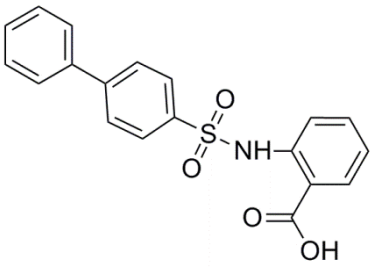

126

2-(4-bromophenylsulfonamido)benzoic acid (0.0550 g, 0.15 mmol, 1 eq.) was dissolved in 1 mL of anhydrous THF. Phenylboronic acid (0.0274 g, 0.225 mmol, 1.5 eq) tetrakis (triphenylphospine)palladium (0) (0.0087 g, 0.0075 mmol, 0.05 eq) and potassium carbonate (0.0622 g, 0.45 mmol, 3 eq.) were added at room temperature. The reaction mixture was sonicated under N_2 to degas and then refluxed under N_2 at 75°C for 12 h over 2 days. A further equivalent of phenylboronic acid was added during the course of the reaction. After 2 days, the reaction mixture was filtered through celite. THF solvent was removed under vacuum and the residue was dispersed in 1M HCL. This was extracted with ethyl acetate three times. The combined organic layers were washed with water, then brine, dried over Na_2SO_4 and concentrated. The product was isolated by flash column chromatography using a step gradient elution of Hex:EtOAc (3:2) as a pale pink solid (0.0253 g, 47.7%). Mp 239 - 242°C; **^{1}H NMR** (400 MHz, DMSO-d_6) δ 13.97 (br., 1H, OH), 11.21 (br., s., 1H, NH), 7.79 - 8.08 (m, 5H, Ar-H), 7.64 - 7.75 (m, 2H, Ar-H), 7.53 - 7.62 (m, 2H, Ar-H), 7.34 - 7.51 (m, 3H, Ar-H), 7.13 (td, *J* = 4.25, 8.09 Hz, 1H, Ar-H); **^{13}C NMR** (101 MHz, DMSO-d_6) δ 169.6, 144.7, 139.5, 137.8, 137.1, 134.4, 131.4, 128.9, 128.5, 127.4, 127.3, 126.9, 123.1, 118.1, 116.5 **IR:** (ATR) ν_{max} cm^{-1} 3025.91, 1222.36, 757.0 **HRMS:** Found (M – H) = 352.0649, calculated for $C_{19}H_{14}NO_4S$ = 352.0644

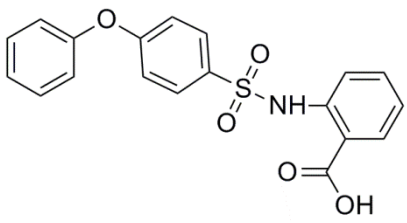

127

To a solution of anthranilic acid (0.2 g, 1.5 mmol) in H_2O:THF (1:1) (10 mL), NEt_3 (627 µL, 4.5 mmol, 3 eq.) and phenoxybenzenesulfonyl chloride (0.4031 g, 1.5 mmol, 1 eq.) were added. The reaction mixture was stirred at RT. After 16 h, aqueous 1 M HCl (30 mL) was added to the mixture and it was extracted with EtOAc (3 × 50 mL). The combined organic layers were washed with water and dried over Na_2SO_4 and filtered. The solvent was removed to yield an off-white solid which did not require further purification. (0.1270 g, 23%); **^{1}H NMR** (400 MHz, DMSO-d_6) δ 11.24 (br. s., 1H, NH), 7.87 – 7.95 (m, 1H, Ar-H), 7.77 - 7.84 (m, *J* = 9.12 Hz, 2H, Ar-H), 7.49 - 7.58 (m, 2H, Ar-H), 7.42 - 7.49 (m, 2H, Ar-H), 7.26 (t, *J* = 7.46 Hz, 1H, Ar-H), 7.08 - 7.16 (m, 3H, Ar-H), 7.02 - 7.08 (m, *J* = 9.12 Hz, 2H, Ar-H) ;**^{13}C NMR** (101 MHz, DMSO-d_6) δ 173.62, 161.2, 154.4, 145.1, 134.4, 132.4, 131.6, 130.4, 129.5, 125.1, 123.2, 120.3, 118.4, 117.5, 116.3 **IR:** (ATR) ν cm^{-1} 16661.48, 1342.25, 1157.25, 933.35; **MS**: Found (M-H) = 368.0595, calculated for $C_{19}H_{14}NO_5S$ = 368.0593

5.5 Biological methods – Chapter 3

5.5.1 Cell culture

NCI-h716 [H716] (ATCC® CCL-251™) cells were purchased form American Type Culture Collection (Manassas, VA). NCI-h716 were maintained in suspension culture in RPMI-1640 medium (ATCC® 30-2001™) supplemented with 10% v/v FBS and subsequently in RPMI-1640 (Lonza 12-167F) supplemented to contain 4.5 g/L D-glucose, 2.383 g/L HEPES, 2 mM L-Glutamine, 1 mM sodium pyruvate and 10% v/v FBS. The cells were cultured in T-75 cm^2 vented cap cell culture flasks and incubated at 37°C in a humidified atmosphere of 95% air and 5% CO_2. Cultures were maintained by the addition of fresh medium to the flask every 2 to 3 days. Subculturing was carried out by centrifugation at 130 g for 5 mins with subsequent resuspension in fresh medium at a subcultivation ratio of 1:3. Cryopreservation was carried out in complete growth medium supplemented with 5% v/v DMSO as cryoprotective agent and vials were stored in the liquid nitrogen vapour phase.

5.5.2 cAMP assay

5.5.2.1 Plating of cells

BD Matrigel™ Basement Membrane Matrix was used to coat the plates to induce adherence of the cells to the plate. The matrix was diluted from the Lot specific protein concentration of 9.5 mg/mL to a working concentration of 0.75 mg/mL using serum free Dulbecco's Modified Eagles's medium. Using cooled pipette tips and a cold block, the wells of a 96-well plate were coated with 50 µL of the diluted matrix and incubated at RT for 1 h. Unbound material was aspirated and the coating rinsed with serum free medium. Medium (100 µL) was put in each well and the plated was incubated overnight at 37°C before use. NCI-h716 cells were plated in the matrigel coated plate at a density of 6×10^4 cells per well in Dulbecco's Modified Eagles's medium modified to contain 2 mM L-glutamine, 1 mM sodium pyruvate and 10% v/v FBS and cultured for 24 h before assay.

5.5.2.2 cAMP assay procedure

After 24 h incubation, the medium was gently aspirated and the cells washed twice with PBS. The assay medium of DMEM containing 0.5 mM 3-isobutyl-1-methylxanthine (IBMX) was added to each well and the plate incubated for 30 mins at 37°C. The medium was then removed and the cells were treated with the drug candidate or vehicle in fresh

assay medium for 30 min. After treatment, the medium was removed and intracellular cAMP was determined using a Tropix® cAMP-Screen® System (Applied Biosystems) according to the kit instructions. The kit Assay/Lysis buffer (100 µL) was added to each well and the plate was incubated at 37 for 40 minutes at which time the cells were seen to be lysed by microscopic observation. Dilutions of the cAMP standard provided were prepared in Assay/Lysis buffer at 6000, 600, 60, 6, 0.6, 0.06, 0.006 and 0 pmol/60 µL. To the pre-coated assay plate, 60 µL of sample or standard and 30 µL of cAMP-AP conjugate were added to each well and mixed on a plate shaker. Each sample and standard were analysed in triplicate. Anti-cAMP antibody (60 µL) was added to each well and the plate was incubated at RT on a plate shaker for 1 h. After incubation, the solution was removed from the wells and washed well six times with the provided wash buffer. CSPD®/Sapphire-II™ RTU substrate/enhancer solution (100 µL) was added to each well and the plate was incubated at RT for 30 min. The signal from each well was measured in a Luminoskan™ Ascent Microplate Luminometer (Thermo Scientific™). A sigmoidal standard curve was prepared and fit with a weighted four-parameter logistic curve from which values for cAMP in pmol/well could be interpolated.

Chapter 6. References

1. Baumgart, D. C.; Carding, S. R. Inflammatory bowel disease: cause and immunobiology. *The Lancet* 369, 1627-1640.

2. Kaplan, G. G. The global burden of IBD: from 2015 to 2025. *Nat Rev Gastroenterol Hepatol* **2015,** 12, 720-7.

3. M'Koma, A. E. Inflammatory Bowel Disease: An Expanding Global Health Problem. *Clinical Medicine Insights. Gastroenterology* **2013,** 6, 33-47.

4. Card, T.; Hubbard, R.; Logan, R. F. A. Mortality in inflammatory bowel disease: a population-based cohort study. *Gastroenterology* 125, 1583-1590.

5. Baumgart, D. C.; Sandborn, W. J. Inflammatory bowel disease: clinical aspects and established and evolving therapies. *The Lancet* 369, 1641-1657.

6. WebMD, L. Ulcerative colitis. http://www.webmd.com/ibd-crohns-disease/ulcerative-colitis/ss/slideshow-surgery (27th March 2017).

7. The National Institute for Health and Care Excellence, N. Ulcerative colitis: management Clinical guideline CG166. https://www.nice.org.uk/guidance/CG166/chapter/1-Recommendations#inducing-remission-in-people-with-ulcerative-colitis (27th March 2017).

8. medicines.ie. Humira 40 mg solution for injection in pre-filled pen and syringe - Summary of Product Characteristics (SPC). http://www.medicines.ie/medicine/11677/SPC/Humira+40+mg+solution+for+injection+in+pre-filled+pen+and+syringe/ (27th March 2017).

9. medicines.ie. Remicade Powder for Solution for Infusion -Summary of Product Characteristics (SPC). http://www.medicines.ie/medicine/1644/SPC/Remicade+Powder+for+Solution+for+Infusion/ (27th March 2017).

10. Louis, E.; Collard, A.; Oger, A.; Degroote, E.; El Yafi, F. A. N.; Belaiche, J. Behaviour of Crohn's disease according to the Vienna classification: changing pattern over the course of the disease. *Gut* **2001,** 49, 777-782.

11. The national Institute for Health anc care Excellence, N. Crohn's disease: management Clinical guideline CG152. https://www.nice.org.uk/guidance/cg152 (27th March 2017).

12. Ng, S. C. Inflammatory Bowel Disease in Asia. *Gastroenterology & Hepatology* **2013,** 9, 28-30.

13. Ye, Y.; Pang, Z.; Chen, W.; Ju, S.; Zhou, C. The epidemiology and risk factors of inflammatory bowel disease. *International Journal of Clinical and Experimental Medicine* **2015,** 8, 22529-22542.

14. Ukwenya, A. Y.; Ahmed, A.; Odigie, V. I.; Mohammed, A. Inflammatory bowel disease in Nigerians: still a rare diagnosis? *Ann Afr Med* **2011,** 10, 175-9.

15. Probert, C. S.; Jayanthi, V.; Pinder, D.; Wicks, A. C.; Mayberry, J. F. Epidemiological study of ulcerative proctocolitis in Indian migrants and the indigenous population of Leicestershire. *Gut* **1992,** 33, 687-693.

16. Halme, L.; Paavola-Sakki, P.; Turunen, U.; Lappalainen, M.; Farkkila, M.; Kontula, K. Family and twin studies in inflammatory bowel disease. *World J Gastroenterol* **2006,** 12, 3668-72.

17. Hugot, J.-P.; Chamaillard, M.; Zouali, H.; Lesage, S.; Cezard, J.-P.; Belaiche, J.; Almer, S.; Tysk, C.; O'Morain, C. A.; Gassull, M.; Binder, V.; Finkel, Y.; Cortot, A.; Modigliani, R.; Laurent-Puig, P.; Gower-Rousseau, C.; Macry, J.; Colombel, J.-F.; Sahbatou, M.; Thomas, G. Association of NOD2 leucine-rich repeat variants with susceptibility to Crohn's disease. *Nature* **2001,** 411, 599-603.

18. Khor, B.; Gardet, A.; Xavier, R. J. Genetics and pathogenesis of inflammatory bowel disease. *Nature* **2011,** 474, 307-17.

19. Molodecky, N. A.; Kaplan, G. G. Environmental Risk Factors for Inflammatory Bowel Disease. *Gastroenterology & Hepatology* **2010,** 6, 339-346.

20. Foster, A.; Jacobson, K. Changing Incidence of Inflammatory Bowel Disease: Environmental Influences and Lessons Learnt from the South Asian Population. *Frontiers in Pediatrics* **2013,** 1, 34.

21. Kronman, M. P.; Zaoutis, T. E.; Haynes, K.; Feng, R.; Coffin, S. E. Antibiotic Exposure and IBD Development Among Children: A Population-Based Cohort Study. *Pediatrics* **2012,** 130, e794-e803.

22. Manzel, A.; Muller, D. N.; Hafler, D. A.; Erdman, S. E.; Linker, R. A.; Kleinewietfeld, M. Role of "Western Diet" in Inflammatory Autoimmune Diseases. *Current allergy and asthma reports* **2014,** 14, 404-404.

23. Klement, E.; Cohen, R. V.; Boxman, J.; Joseph, A.; Reif, S. Breastfeeding and risk of inflammatory bowel disease: a systematic review with meta-analysis. *Am J Clin Nutr* **2004,** 80, 1342-52.

24. Timm, S.; Svanes, C.; Janson, C.; Sigsgaard, T.; Johannessen, A.; Gislason, T.; Jogi, R.; Omenaas, E.; Forsberg, B.; Torén, K.; Holm, M.; Bråbäck, L.; Schlünssen, V. Place of upbringing in early childhood as related to inflammatory bowel diseases in adulthood: a population-based cohort study in Northern Europe. *European Journal of Epidemiology* **2014,** 29, 429-437.

25. Strachan, D. P. Hay fever, hygiene, and household size. *Bmj* **1989,** 299, 1259-60.

26. Ananthakrishnan, A. N. Epidemiology and risk factors for IBD. *Nat Rev Gastroenterol Hepatol* **2015,** 12, 205-217.

27. Cosnes, J. Tobacco and IBD: relevance in the understanding of disease mechanisms and clinical practice. *Best Practice & Research Clinical Gastroenterology* **2004,** 18, 481-496.

28. Thomas, G. A.; Rhodes, J.; Mani, V.; Williams, G. T.; Newcombe, R. G.; Russell, M. A.; Feyerabend, C. Transdermal nicotine as maintenance therapy for ulcerative colitis. *N Engl J Med* **1995,** 332, 988-92.

29. Neuman, M. G.; Nanau, R. M. Inflammatory bowel disease: role of diet, microbiota, life style. *Translational Research* **2012,** 160, 29-44.

30. Sellon, R. K.; Tonkonogy, S.; Schultz, M.; Dieleman, L. A.; Grenther, W.; Balish, E.; Rennick, D. M.; Sartor, R. B. Resident Enteric Bacteria Are Necessary for Development of Spontaneous Colitis and Immune System Activation in Interleukin-10-Deficient Mice. *Infection and Immunity* **1998,** 66, 5224-5231.

31. Nitzan, O.; Elias, M.; Peretz, A.; Saliba, W. Role of antibiotics for treatment of inflammatory bowel disease. *World Journal of Gastroenterology* **2016,** 22, 1078-1087.

32. Kamada, N.; Seo, S.-U.; Chen, G. Y.; Nunez, G. Role of the gut microbiota in immunity and inflammatory disease. *Nat Rev Immunol* **2013,** 13, 321-335.

33. Nell, S.; Suerbaum, S.; Josenhans, C. The impact of the microbiota on the pathogenesis of IBD: lessons from mouse infection models. *Nat Rev Micro* **2010,** 8, 564-577.

34. Frank, D. N.; St. Amand, A. L.; Feldman, R. A.; Boedeker, E. C.; Harpaz, N.; Pace, N. R. Molecular-phylogenetic characterization of microbial community imbalances in human inflammatory bowel diseases. *Proceedings of the National Academy of Sciences of the United States of America* **2007,** 104, 13780-13785.

35. Petersen, A. M.; Nielsen, E. M.; Litrup, E.; Brynskov, J.; Mirsepasi, H.; Krogfelt, K. A. A phylogenetic group of Escherichia coli associated with active left-sided Inflammatory Bowel Disease. *BMC Microbiology* **2009,** 9, 171.

36. Hapfelmeier, S.; Hardt, W.-D. A mouse model for S. typhimurium-induced enterocolitis. *Trends in Microbiology* **2005,** 13, 497-503.

37. Garrett, W. S.; Lord, G. M.; Punit, S.; Lugo-Villarino, G.; Mazmanian, S.; Ito, S.; Glickman, J. N.; Glimcher, L. H. Communicable ulcerative colitis induced by T-bet deficiency in the innate immune system. *Cell* **2007,** 131, 33-45.

38. Antoni, L.; Nuding, S.; Wehkamp, J.; Stange, E. F. Intestinal barrier in inflammatory bowel disease. *World Journal of Gastroenterology : WJG* **2014,** 20, 1165-1179.

39. Michielan, A.; D'Incà, R. Intestinal Permeability in Inflammatory Bowel Disease: Pathogenesis, Clinical Evaluation, and Therapy of Leaky Gut. *Mediators of Inflammation* **2015,** 2015, 628157.

40. Gitter, A. H.; Wullstein, F.; Fromm, M.; Schulzke, J. D. Epithelial barrier defects in ulcerative colitis: characterization and quantification by electrophysiological imaging. *Gastroenterology* **2001,** 121, 1320-8.

41. Shirazi, T.; Longman, R. J.; Corfield, A. P.; Probert, C. S. J. Mucins and inflammatory bowel disease. *Postgraduate Medical Journal* **2000,** 76, 473.

42. Smithson, J. E.; Campbell, A.; Andrews, J. M.; Milton, J. D.; Pigott, R.; Jewell, D. P. Altered expression of mucins throughout the colon in ulcerative colitis. *Gut* **1997,** 40, 234-240.

43. Geremia, A.; Biancheri, P.; Allan, P.; Corazza, G. R.; Di Sabatino, A. Innate and adaptive immunity in inflammatory bowel disease. *Autoimmun Rev* **2014,** 13, 3-10.

44. Ogura, Y.; Bonen, D. K.; Inohara, N.; Nicolae, D. L.; Chen, F. F.; Ramos, R.; Britton, H.; Moran, T.; Karaliuskas, R.; Duerr, R. H.; Achkar, J. P.; Brant, S. R.; Bayless, T. M.; Kirschner, B. S.; Hanauer, S. B.; Nunez, G.; Cho, J. H. A frameshift mutation in NOD2 associated with susceptibility to Crohn's disease. *Nature* **2001,** 411, 603-6.

45. Rosenstiel, P.; Fantini, M.; Bräutigam, K.; Kühbacher, T.; Waetzig, G. H.; Seegert, D.; Schreiber, S. TNF-α and IFN-γ regulate the expression of the NOD2 (CARD15) gene in human intestinal epithelial cells. *Gastroenterology* **2003,** 124, 1001-1009.

46. Cooney, R.; Baker, J.; Brain, O.; Danis, B.; Pichulik, T.; Allan, P.; Ferguson, D. J. P.; Campbell, B. J.; Jewell, D.; Simmons, A. NOD2 stimulation induces autophagy in dendritic cells influencing bacterial handling and antigen presentation. *Nat Med* **2010,** 16, 90-97.

47. Tan, G.; Li, R.-h.; Li, C.; Wu, F.; Zhao, X.-m.; Ma, J.-y.; Lei, S.; Zhang, W.-d.; Zhi, F.-c. Down-Regulation of Human Enteric Antimicrobial Peptides by NOD2 during Differentiation of the Paneth Cell Lineage. *Scientific Reports* **2015,** 5, 8383.

48. Cario, E.; Podolsky, D. K. Differential alteration in intestinal epithelial cell expression of toll-like receptor 3 (TLR3) and TLR4 in inflammatory bowel disease. *Infect Immun* **2000,** 68, 7010-7.

49. Iwasaki, A.; Medzhitov, R. Toll-like receptor control of the adaptive immune responses. *Nat Immunol* **2004,** 5, 987-95.

50. Rescigno, M.; Urbano, M.; Valzasina, B.; Francolini, M.; Rotta, G.; Bonasio, R.; Granucci, F.; Kraehenbuhl, J. P.; Ricciardi-Castagnoli, P. Dendritic cells express tight junction proteins and penetrate gut epithelial monolayers to sample bacteria. *Nat Immunol* **2001,** 2, 361-7.

51. Wallace, K. L.; Zheng, L.-B.; Kanazawa, Y.; Shih, D. Q. Immunopathology of inflammatory bowel disease. *World Journal of Gastroenterology : WJG* **2014,** 20, 6-21.

52. Danese, S. New therapies for inflammatory bowel disease: from the bench to the bedside. *Gut* **2012,** 61, 918-32.

53. Marafini, I.; Angelucci, E.; Pallone, F.; Monteleone, G. The IL-12/23/STAT Axis as a Therapeutic Target in Inflammatory Bowel Disease: Mechanisms and Evidence in Man. *Dig Dis* **2015,** 33 Suppl 1, 113-119.

54. Hommes, D. W.; Mikhajlova, T. L.; Stoinov, S.; Štimac, D.; Vucelic, B.; Lonovics, J.; Zákuciová, M.; D'Haens, G.; Van Assche, G.; Ba, S.; Lee, S.; Pearce, T. Fontolizumab, a humanised anti ‐ interferon γ antibody, demonstrates safety and clinical activity in patients with moderate to severe Crohn's disease. *Gut* **2006,** 55, 1131-1137.

55. Sands, B. E.; Sandborn, W. J.; Creed, T. J.; Dayan, C. M.; Dhanda, A. D.; Van Assche, G. A.; Greguš, M.; Sood, A.; Choudhuri, G.; Stempien, M. J.; Levitt, D.; Probert, C. S. Basiliximab Does Not Increase Efficacy of Corticosteroids in Patients With Steroid-Refractory Ulcerative Colitis. *Gastroenterology* 143, 356-364.e1.

56. Feagan, B. Update on Tofacitinib for Inflammatory Bowel Disease. *Gastroenterology & Hepatology* **2016,** 12, 572-574.

57. Sandborn, W. J.; Colombel, J. F.; Frankel, M.; Hommes, D.; Lowder, J. N.; Mayer, L.; Plevy, S.; Stokkers, P.; Travis, S.; Van Assche, G.; Baumgart, D. C.; Targan, S. R. Anti-CD3 antibody visilizumab is not effective in patients with intravenous corticosteroid-refractory ulcerative colitis. *Gut* **2010,** 59, 1485.

58. Feagan, B. G.; Rutgeerts, P.; Sands, B. E.; Hanauer, S.; Colombel, J. F.; Sandborn, W. J.; Van Assche, G.; Axler, J.; Kim, H. J.; Danese, S.; Fox, I.; Milch, C.; Sankoh, S.; Wyant, T.; Xu, J.; Parikh, A. Vedolizumab as induction and maintenance therapy for ulcerative colitis. *N Engl J Med* **2013,** 369, 699-710.

59. Sandborn, W. J.; Feagan, B. G.; Rutgeerts, P.; Hanauer, S.; Colombel, J. F.; Sands, B. E.; Lukas, M.; Fedorak, R. N.; Lee, S.; Bressler, B.; Fox, I.; Rosario, M.; Sankoh, S.; Xu, J.; Stephens, K.; Milch, C.; Parikh, A. Vedolizumab as induction and maintenance therapy for Crohn's disease. *N Engl J Med* **2013,** 369, 711-21.

60. Roda, G.; Jharap, B.; Neeraj, N.; Colombel, J.-F. Loss of Response to Anti-TNFs: Definition, Epidemiology, and Management. *Clinical and Translational Gastroenterology* **2016,** 7, e135.

61. Stallmach, A.; Hagel, S.; Bruns, T. Adverse effects of biologics used for treating IBD. *Best Practice & Research Clinical Gastroenterology* **2010,** 24, 167-182.

62. Olivera, P.; Danese, S.; Peyrin-Biroulet, L. Next generation of small molecules in inflammatory bowel disease. *Gut* **2016**.

63. Neurath, M. F.; Travis, S. P. Mucosal healing in inflammatory bowel diseases: a systematic review. *Gut* **2012,** 61, 1619-35.

64. Cintolo, M.; Costantino, G.; Pallio, S.; Fries, W. Mucosal healing in inflammatory bowel disease: Maintain or de-escalate therapy. *World Journal of Gastrointestinal Pathophysiology* **2016,** 7, 1-16.

65. Vandenbroucke, R. E.; Libert, C. Is there new hope for therapeutic matrix metalloproteinase inhibition? *Nat Rev Drug Discov* **2014,** 13, 904-27.

66. Guo, Y.; Lu, N.; Bai, A. Clinical use and mechanisms of infliximab treatment on inflammatory bowel disease: a recent update. *Biomed Res Int* **2013,** 2013, 581631.

67. Medina, C.; Radomski, M. W. Role of matrix metalloproteinases in intestinal inflammation. *J Pharmacol Exp Ther* **2006,** 318, 933-8.

68. O'Sullivan, S.; Gilmer, J. F.; Medina, C. Matrix metalloproteinases in inflammatory bowel disease: an update. *Mediators Inflamm* **2015,** 2015, 964131.

69. Cipriani, S.; Mencarelli, A.; Chini, M. G.; Distrutti, E.; Renga, B.; Bifulco, G.; Baldelli, F.; Donini, A.; Fiorucci, S. The bile acid receptor GPBAR-1 (TGR5) modulates integrity of intestinal barrier and immune response to experimental colitis. *PLoS One* **2011,** 6, e25637.

70. Sakanaka, T.; Inoue, T.; Yorifuji, N.; Iguchi, M.; Fujiwara, K.; Narabayashi, K.; Kakimoto, K.; Nouda, S.; Okada, T.; Kuramoto, T.; Ishida, K.; Abe, Y.; Takeuchi, T.; Umegaki, E.; Akiba, Y.; Kaunitz, J. D.; Higuchi, K. The effects of a TGR5 agonist and a dipeptidyl peptidase IV inhibitor on dextran sulfate sodium-induced colitis in mice. *J Gastroenterol Hepatol* **2015,** 30 Suppl 1, 60-5.

71. Charmot, D. Non-systemic drugs: a critical review. *Curr Pharm Des* **2012,** 18, 1434-45.

72. Donowitz, M.; Singh, S.; Salahuddin, F. F.; Hogema, B. M.; Chen, Y.; Gucek, M.; Cole, R. N.; Ham, A.; Zachos, N. C.; Kovbasnjuk, O.; Lapierre, L. A.; Broere, N.; Goldenring, J.; deJonge, H.; Li, X. Proteome of Murine Jejunal Brush Border Membrane Vesicles. *Journal of Proteome Research* **2007,** 6, 4068-4079.

73. Man, A. L.; Prieto-Garcia, M. E.; Nicoletti, C. Improving M cell mediated transport across mucosal barriers: do certain bacteria hold the keys? *Immunology* **2004,** 113, 15-22.

74. Lipinski, C. A.; Lombardo, F.; Dominy, B. W.; Feeney, P. J. Experimental and computational approaches to estimate solubility and permeability in drug discovery and development settings. *Advanced Drug Delivery Reviews* **1997,** 23, 3-25.

75. Lipinski, C. A. Lead- and drug-like compounds: the rule-of-five revolution. *Drug Discovery Today: Technologies* **2004,** 1, 337-341.

76. Veber, D. F.; Johnson, S. R.; Cheng, H. Y.; Smith, B. R.; Ward, K. W.; Kopple, K. D. Molecular properties that influence the oral bioavailability of drug candidates. *J Med Chem* **2002,** 45, 2615-23.

77. medicines.ie. Salazopyrin Tablets - Summary of Product Characteristics (SPC). http://www.medicines.ie/medicine/6862/SPC/Salazopyrin+Tablets/ (17 January 2017).

78. medicines.org.uk. Olsalazine Sodium/Dipentum 250 mg Capsules - Summary of Product Characteristics (SPC). https://www.medicines.org.uk/emc/medicine/29976 (17th January 2017).

79. Friend, D. R.; Chang, G. W. Drug glycosides: potential prodrugs for colon-specific drug delivery. *J Med Chem* **1985,** 28, 51-7.

80. Friend, D. R.; Chang, G. W. A colon-specific drug-delivery system based on drug glycosides and the glycosidases of colonic bacteria. *J Med Chem* **1984,** 27, 261-6.

81. Sawa, M.; Tsukamoto, T.; Kiyoi, T.; Kurokawa, K.; Nakajima, F.; Nakada, Y.; Yokota, K.; Inoue, Y.; Kondo, H.; Yoshino, K. New Strategy for Antedrug Application: Development of Metalloproteinase Inhibitors as Antipsoriatic Drugs. *Journal of Medicinal Chemistry* **2002,** 45, 930-936.

82. medicines.ie. Entocort CR 3 mg capsules - Summary of Product Characteristics (SPC). http://www.medicines.ie/medicine/867/SPC/Entocort+CR+3mg+Capsules/ (17th January 2017).

83. medicines.ie. Asacolon 400 mg Gastro-Resistant Tablet - Summary of Product Characteristics (SPC). http://www.medicines.ie/medicine/10838/SPC/Asacolon+400+mg+Gastro-Resistant+Tablet/ (17th January 2017).

84. Burnside, B. A.; Guo, X.; Fiske, K.; Couch, R. A.; Chang, R. K.; Treacy, D. J.; McGuiness, C. M.; Rudnic, E. M. Oral pulsed dose drug delivery system. 2011.

85. Rashmi, S.; Nitin Jain and, K. L. D. An Insight to Colon Targeted Drug Delivery System. *Drug Delivery Letters* **2013,** 3, 127-135.

86. Rajpurohit, H.; Sharma, P.; Sharma, S.; Bhandari, A. Polymers for Colon Targeted Drug Delivery. *Indian Journal of Pharmaceutical Sciences* **2010,** 72, 689-696.

87. Hans, M. L.; Lowman, A. M. Biodegradable nanoparticles for drug delivery and targeting. *Current Opinion in Solid State and Materials Science* **2002,** 6, 319-327.

88. Hua, S.; Marks, E.; Schneider, J. J.; Keely, S. Advances in oral nano-delivery systems for colon targeted drug delivery in inflammatory bowel disease: Selective targeting to diseased versus healthy tissue. *Nanomedicine: Nanotechnology, Biology and Medicine* **2015,** 11, 1117-1132.

89. Lamprecht, A.; Ubrich, N.; Yamamoto, H.; Schafer, U.; Takeuchi, H.; Maincent, P.; Kawashima, Y.; Lehr, C. M. Biodegradable nanoparticles for targeted drug delivery in treatment of inflammatory bowel disease. *J Pharmacol Exp Ther* **2001,** 299, 775-81.

90. Tremont, S. J.; Lee, L. F.; Huang, H. C.; Keller, B. T.; Banerjee, S. C.; Both, S. R.; Carpenter, A. J.; Wang, C. C.; Garland, D. J.; Huang, W.; Jones, C.; Koeller, K. J.; Kolodziej, S. A.; Li, J.; Manning, R. E.; Mahoney, M. W.; Miller, R. E.; Mischke, D. A.; Rath, N. P.; Fletcher, T.; Reinhard, E. J.; Tollefson, M. B.; Vernier, W. F.; Wagner, G. M.; Rapp, S. R.; Beaudry, J.; Glenn, K.; Regina, K.; Schuh, J. R.; Smith, M. E.; Trivedi, J. S.; Reitz, D. B. Discovery of potent, nonsystemic apical sodium-codependent bile acid transporter inhibitors (Part 1). *J Med Chem* **2005,** 48, 5837-52.

91. Huang, H. C.; Tremont, S. J.; Lee, L. F.; Keller, B. T.; Carpenter, A. J.; Wang, C. C.; Banerjee, S. C.; Both, S. R.; Fletcher, T.; Garland, D. J.; Huang, W.; Jones, C.; Koeller, K. J.; Kolodziej, S. A.; Li, J.; Manning, R. E.; Mahoney, M. W.; Miller, R. E.; Mischke, D. A.; Rath, N. P.; Reinhard, E. J.; Tollefson, M. B.; Vernier, W. F.; Wagner, G. M.; Rapp, S. R.; Beaudry, J.; Glenn, K.; Regina, K.; Schuh, J. R.; Smith, M. E.; Trivedi, J. S.; Reitz, D. B. Discovery of potent, nonsystemic apical sodium-codependent bile acid transporter inhibitors (Part 2). *J Med Chem* **2005,** 48, 5853-68.

92. Lunagariya, N. A.; Patel, N. K.; Jagtap, S. C.; Bhutani, K. K. Inhibitors of pancreatic lipase: state of the art and clinical perspectives. *EXCLI Journal* **2014,** 13, 897-921.

93. Fang, S.; Suh, J. M.; Reilly, S. M.; Yu, E.; Osborn, O.; Lackey, D.; Yoshihara, E.; Perino, A.; Jacinto, S.; Lukasheva, Y.; Atkins, A. R.; Khvat, A.; Schnabl, B.; Yu, R. T.; Brenner, D. A.; Coulter, S.; Liddle, C.; Schoonjans, K.; Olefsky, J. M.; Saltiel, A. R.; Downes, M.; Evans, R. M. Intestinal FXR agonism promotes adipose tissue browning and reduces obesity and insulin resistance. *Nature medicine* **2015,** 21, 159-165.

94. Serrano-Wu, M. H.; Coppola, G. M.; Gong, Y.; Neubert, A. D.; Chatelain, R.; Clairmont, K. B.; Commerford, R.; Cosker, T.; Daniels, T.; Hou, Y.; Jain, M.; Juedes, M.; Li, L.; Mullarkey, T.; Rocheford, E.; Sung, M. J.; Tyler, A.; Yang, Q.; Yoon, T.; Hubbard, B. K. Intestinally Targeted Diacylglycerol Acyltransferase 1 (DGAT1) Inhibitors Robustly Suppress Postprandial Triglycerides. *ACS Med Chem Lett* **2012,** 3, 411-5.

95. medicines.ie. Vancocin Matrigel 125 mg Hard Capsules - Summary of Product Characteristics (SPC). http://www.medicines.ie/medicine/15423/SPC/Vancocin+Matrigel+125mg+Hard+Capsules/ (27th March 2017).

96. Duan, H.; Ning, M.; Zou, Q.; Ye, Y.; Feng, Y.; Zhang, L.; Leng, Y.; Shen, J. Discovery of Intestinal Targeted TGR5 Agonists for the Treatment of Type 2 Diabetes. *J Med Chem* **2015,** 58, 3315-28.

97. Visse, R.; Nagase, H. Matrix metalloproteinases and tissue inhibitors of metalloproteinases: structure, function, and biochemistry. *Circ Res* **2003,** 92, 827-39.

98. Fanjul-Fernandez, M.; Folgueras, A. R.; Cabrera, S.; Lopez-Otin, C. Matrix metalloproteinases: evolution, gene regulation and functional analysis in mouse models. *Biochim Biophys Acta* **2010,** 1803, 3-19.

99. Overall, C. M.; Lopez-Otin, C. Strategies for MMP inhibition in cancer: innovations for the post-trial era. *Nat Rev Cancer* **2002,** 2, 657-672.

100. Sagi, I.; Gaffney, J. P. *Matrix metalloproteinase biology*. Wiley & Sons, Inc.: New Jersey, 2015.

101. Egeblad, M.; Werb, Z. New functions for the matrix metalloproteinases in cancer progression. *Nat Rev Cancer* **2002,** 2, 161-74.

102. Song, J.; Su, H.; Zhou, Y. Y.; Guo, L. L. Prognostic value of matrix metalloproteinase 9 expression in breast cancer patients: a meta-analysis. *Asian Pac J Cancer Prev* **2013,** 14, 1615-21.

103. Morgia, G.; Falsaperla, M.; Malaponte, G.; Madonia, M.; Indelicato, M.; Travali, S.; Mazzarino, M. C. Matrix metalloproteinases as diagnostic (MMP-13) and prognostic (MMP-2, MMP-9) markers of prostate cancer. *Urol Res* **2005,** 33, 44-50.

104. Peng, W. J.; Zhang, J. Q.; Wang, B. X.; Pan, H. F.; Lu, M. M.; Wang, J. Prognostic value of matrix metalloproteinase 9 expression in patients with non-small cell lung cancer. *Clin Chim Acta* **2012,** 413, 1121-6.

105. Tian, M.; Cui, Y. Z.; Song, G. H.; Zong, M. J.; Zhou, X. Y.; Chen, Y.; Han, J. X. Proteomic analysis identifies MMP-9, DJ-1 and A1BG as overexpressed proteins in pancreatic juice from pancreatic ductal adenocarcinoma patients. *BMC Cancer* **2008,** 8, 241.

106. Li, L. N.; Zhou, X.; Gu, Y.; Yan, J. Prognostic value of MMP-9 in ovarian cancer: a meta-analysis. *Asian Pac J Cancer Prev* **2013,** 14, 4107-13.

107. Papazafiropoulou, A.; Tentolouris, N. Matrix metalloproteinases and cardiovascular diseases. *Hippokratia* **2009,** 13, 76-82.

108. Liu, P.; Sun, M.; Sader, S. Matrix metalloproteinases in cardiovascular disease. *The Canadian Journal of Cardiology* **2006,** 22, 25B-30B.

109. Ahrens, D.; Koch, A. E.; Pope, R. M.; Stein-Picarella, M.; Niedbala, M. J. Expression of matrix metalloproteinase 9 (96-kd gelatinase B) in human rheumatoid arthritis. *Arthritis Rheum* **1996,** 39, 1576-87.

110. Maxwell, P. R.; Timms, P. M.; Chandran, S.; Gordon, D. Peripheral blood level alterations of TIMP-1, MMP-2 and MMP-9 in patients with type 1 diabetes. *Diabet Med* **2001,** 18, 777-80.

111. Yong, V. W.; Zabad, R. K.; Agrawal, S.; Goncalves Dasilva, A.; Metz, L. M. Elevation of matrix metalloproteinases (MMPs) in multiple sclerosis and impact of immunomodulators. *J Neurol Sci* **2007,** 259, 79-84.

112. Sela-Passwell, N.; Rosenblum, G.; Shoham, T.; Sagi, I. Structural and functional bases for allosteric control of MMP activities: can it pave the path for selective inhibition? *Biochim Biophys Acta* **2010,** 1803, 29-38.

113. Brew, K.; Nagase, H. The tissue inhibitors of metalloproteinases (TIMPs): An ancient family with structural and functional diversity. *Biochimica et biophysica acta* **2010,** 1803, 55-71.

114. Lovejoy, B.; Hassell, A. M.; Luther, M. A.; Weigl, D.; Jordan, S. R. Crystal structures of recombinant 19-kDa human fibroblast collagenase complexed to itself. *Biochemistry* **1994,** 33, 8207-17.

115. Jacobsen, J. A.; Major Jourden, J. L.; Miller, M. T.; Cohen, S. M. To bind zinc or not to bind zinc: an examination of innovative approaches to improved metalloproteinase inhibition. *Biochim Biophys Acta* **2010,** 1803, 72-94.

116. Rasmussen, H. S.; McCann, P. P. Matrix metalloproteinase inhibition as a novel anticancer strategy: a review with special focus on batimastat and marimastat. *Pharmacol Ther* **1997,** 75, 69-75.

117. Sparano, J. A.; Bernardo, P.; Stephenson, P.; Gradishar, W. J.; Ingle, J. N.; Zucker, S.; Davidson, N. E. Randomized Phase III Trial of Marimastat Versus Placebo in Patients With Metastatic Breast Cancer Who Have Responding or Stable Disease After First-Line Chemotherapy:

Eastern Cooperative Oncology Group Trial E2196. *Journal of Clinical Oncology* **2004,** 22, 4683-4690.

118. Coussens, L. M.; Fingleton, B.; Matrisian, L. M. Matrix metalloproteinase inhibitors and cancer: trials and tribulations. *Science* **2002,** 295, 2387-92.

119. Xu, X.; Chen, Z.; Wang, Y.; Bonewald, L.; Steffensen, B. Inhibition of MMP-2 gelatinolysis by targeting exodomain-substrate interactions. *Biochem J* **2007,** 406, 147-55.

120. Stoilova, T.; Colombo, L.; Forloni, G.; Tagliavini, F.; Salmona, M. A New Face for Old Antibiotics: Tetracyclines in Treatment of Amyloidoses. *Journal of Medicinal Chemistry* **2013,** 56, 5987-6006.

121. Compendium, e. M. Periostat 20 mg film coated tablets - Summary of Product Characteristics. https://www.medicines.org.uk/emc/medicine/16431#PRODUCTINFO (13th March 2017).

122. Brown, S.; Bernardo, M. M.; Li, Z.-H.; Kotra, L. P.; Tanaka, Y.; Fridman, R.; Mobashery, S. Potent and Selective Mechanism-Based Inhibition of Gelatinases. *Journal of the American Chemical Society* **2000,** 122, 6799-6800.

123. Jiang, X.; Dutton, C. M.; Qi, W. N.; Block, J. A.; Garamszegi, N.; Scully, S. P. siRNA mediated inhibition of MMP-1 reduces invasive potential of a human chondrosarcoma cell line. *J Cell Physiol* **2005,** 202, 723-30.

124. Kargiotis, O.; Chetty, C.; Gondi, C. S.; Tsung, A. J.; Dinh, D. H.; Gujrati, M.; Lakka, S. S.; Kyritsis, A. P.; Rao, J. S. Adenovirus-mediated transfer of siRNA against MMP-2 mRNA results in impaired invasion and tumor-induced angiogenesis, induces apoptosis in vitro and inhibits tumor growth in vivo in glioblastoma. *Oncogene* **2008,** 27, 4830-4840.

125. Kim, H. S.; Yoo, H. S. Matrix metalloproteinase-inspired suicidal treatments of diabetic ulcers with siRNA-decorated nanofibrous meshes. *Gene Ther* **2013,** 20, 378-385.

126. Martens, E.; Leyssen, A.; Van Aelst, I.; Fiten, P.; Piccard, H.; Hu, J.; Descamps, F. J.; Van den Steen, P. E.; Proost, P.; Van Damme, J.; Liuzzi, G. M.; Riccio, P.; Polverini, E.; Opdenakker, G. A monoclonal antibody inhibits gelatinase B/MMP-9 by selective binding to part of the catalytic domain and not to the fibronectin or zinc binding domains. *Biochimica et Biophysica Acta (BBA) - General Subjects* **2007,** 1770, 178-186.

127. Pruijt, J. F. M.; Fibbe, W. E.; Laterveer, L.; Pieters, R. A.; Lindley, I. J. D.; Paemen, L.; Masure, S.; Willemze, R.; Opdenakker, G. Prevention of interleukin-8-induced mobilization of hematopoietic progenitor cells in rhesus monkeys by inhibitory antibodies against the Metalloproteinase gelatinase B (MMP-9). *Proceedings of the National Academy of Sciences of the United States of America* **1999,** 96, 10863-10868.

128. Shiryaev, S. A.; Remacle, A. G.; Golubkov, V. S.; Ingvarsen, S.; Porse, A.; Behrendt, N.; Cieplak, P.; Strongin, A. Y. A monoclonal antibody interferes with TIMP-2 binding and incapacitates the MMP-2-activating function of multifunctional, pro-tumorigenic MMP-14/MT1-MMP. *Oncogenesis* **2013,** 2, e80.

129. Baugh, M. D.; Perry, M. J.; Hollander, A. P.; Davies, D. R.; Cross, S. S.; Lobo, A. J.; Taylor, C. J.; Evans, G. S. Matrix metalloproteinase levels are elevated in inflammatory bowel disease. *Gastroenterology* 117, 814-822.

130. Jakubowska, K.; Pryczynicz, A.; Iwanowicz, P.; Niewiński, A.; Maciorkowska, E.; Hapanowicz, J.; Jagodzińska, D.; Kemona, A.; Guzińska-Ustymowicz, K. Expressions of Matrix Metalloproteinases (MMP-2, MMP-7, and MMP-9) and Their Inhibitors (TIMP-1, TIMP-2) in Inflammatory Bowel Diseases. *Gastroenterology Research and Practice* **2016,** 2016, 2456179.

131. Meijer, M. J.; Mieremet-Ooms, M. A.; van der Zon, A. M.; van Duijn, W.; van Hogezand, R. A.; Sier, C. F.; Hommes, D. W.; Lamers, C. B.; Verspaget, H. W. Increased mucosal matrix

metalloproteinase-1, -2, -3 and -9 activity in patients with inflammatory bowel disease and the relation with Crohn's disease phenotype. *Dig Liver Dis* **2007,** 39, 733-9.

132. Sykes, A. P.; Bhogal, R.; Brampton, C.; Chander, C.; Whelan, C.; Parsons, M. E.; Bird, J. The effect of an inhibitor of matrix metalloproteinases on colonic inflammation in a trinitrobenzenesulphonic acid rat model of inflammatory bowel disease. *Aliment Pharmacol Ther* **1999,** 13, 1535-42.

133. Naito, Y.; Takagi, T.; Kuroda, M.; Katada, K.; Ichikawa, H.; Kokura, S.; Yoshida, N.; Okanoue, T.; Yoshikawa, T. An orally active matrix metalloproteinase inhibitor, ONO-4817, reduces dextran sulfate sodium-induced colitis in mice. *Inflammation Research* **2004,** 53, 462-468.

134. Mao, J. W.; He, X. M.; Tang, H. Y.; Wang, Y. D. Protective role of metalloproteinase inhibitor (AE-941) on ulcerative colitis in rats. *World J Gastroenterol* **2012,** 18, 7063-9.

135. Ravi, A.; Garg, P.; Sitaraman, S. V. Matrix metalloproteinases in inflammatory bowel disease: boon or a bane? *Inflamm Bowel Dis* **2007,** 13, 97-107.

136. Pirila, E.; Ramamurthy, N. S.; Sorsa, T.; Salo, T.; Hietanen, J.; Maisi, P. Gelatinase A (MMP-2), collagenase-2 (MMP-8), and laminin-5 gamma2-chain expression in murine inflammatory bowel disease (ulcerative colitis). *Dig Dis Sci* **2003,** 48, 93-8.

137. Kirkegaard, T.; Hansen, A.; Bruun, E.; Brynskov, J. Expression and localisation of matrix metalloproteinases and their natural inhibitors in fistulae of patients with Crohn's disease. *Gut* **2004,** 53, 701-9.

138. Pender, S. L.; Tickle, S. P.; Docherty, A. J.; Howie, D.; Wathen, N. C.; MacDonald, T. T. A major role for matrix metalloproteinases in T cell injury in the gut. *The Journal of Immunology* **1997,** 158, 1582.

139. Koller, F. L.; Dozier, E. A.; Nam, K. T.; Swee, M.; Birkland, T. P.; Parks, W. C.; Fingleton, B. Lack of MMP10 exacerbates experimental colitis and promotes development of inflammation-associated colonic dysplasia. *Lab Invest* **2012,** 92, 1749-59.

140. Lakatos, G.; Sipos, F.; Miheller, P.; Hritz, I.; Varga, M. Z.; Juhasz, M.; Molnar, B.; Tulassay, Z.; Herszenyi, L. The behavior of matrix metalloproteinase-9 in lymphocytic colitis, collagenous colitis and ulcerative colitis. *Pathol Oncol Res* **2012,** 18, 85-91.

141. Gao, Q.; Meijer, M. J.; Kubben, F. J.; Sier, C. F.; Kruidenier, L.; van Duijn, W.; van den Berg, M.; van Hogezand, R. A.; Lamers, C. B.; Verspaget, H. W. Expression of matrix metalloproteinases-2 and -9 in intestinal tissue of patients with inflammatory bowel diseases. *Dig Liver Dis* **2005,** 37, 584-92.

142. Sela-Passwell, N.; Kikkeri, R.; Dym, O.; Rozenberg, H.; Margalit, R.; Arad-Yellin, R.; Eisenstein, M.; Brenner, O.; Shoham, T.; Danon, T.; Shanzer, A.; Sagi, I. Antibodies targeting the catalytic zinc complex of activated matrix metalloproteinases show therapeutic potential. *Nat Med* **2012,** 18, 143-147.

143. Santana, A.; Medina, C.; Paz-Cabrera, M. C.; Díaz-Gonzalez, F.; Farré, E.; Salas, A.; Radomski, M. W.; Quintero, E. Attenuation of dextran sodium sulphate induced colitis in matrix metalloproteinase-9 deficient mice. *World Journal of Gastroenterology : WJG* **2006,** 12, 6464-6472.

144. de Bruyn, M.; Breynaert, C.; Arijs, I.; De Hertogh, G.; Geboes, K.; Thijs, G.; Matteoli, G.; Hu, J.; Van Damme, J.; Arnold, B.; Ferrante, M.; Vermeire, S.; Van Assche, G.; Opdenakker, G. Inhibition of gelatinase B/MMP-9 does not attenuate colitis in murine models of inflammatory bowel disease. *Nat Commun* **2017,** 8, 15384.

145. Garg, P.; Rojas, M.; Ravi, A.; Bockbrader, K.; Epstein, S.; Vijay-Kumar, M.; Gewirtz, A. T.; Merlin, D.; Sitaraman, S. V. Selective ablation of matrix metalloproteinase-2 exacerbates

experimental colitis: contrasting role of gelatinases in the pathogenesis of colitis. *J Immunol* **2006,** 177, 4103-12.

146. Garg, P.; Vijay-Kumar, M.; Wang, L.; Gewirtz, A. T.; Merlin, D.; Sitaraman, S. V. Matrix metalloproteinase-9-mediated tissue injury overrides the protective effect of matrix metalloproteinase-2 during colitis. *Am J Physiol Gastrointest Liver Physiol* **2009,** 296, G175-84.

147. Lehmann, F. S.; Burri, E.; Beglinger, C. The role and utility of faecal markers in inflammatory bowel disease. *Therapeutic Advances in Gastroenterology* **2015,** 8, 23-36.

148. Pedersen, G.; Saermark, T.; Kirkegaard, T.; Brynskov, J. Spontaneous and cytokine induced expression and activity of matrix metalloproteinases in human colonic epithelium. *Clinical and Experimental Immunology* **2009,** 155, 257-265.

149. Castaneda, F. E.; Walia, B.; Vijay-Kumar, M.; Patel, N. R.; Roser, S.; Kolachala, V. L.; Rojas, M.; Wang, L.; Oprea, G.; Garg, P.; Gewirtz, A. T.; Roman, J.; Merlin, D.; Sitaraman, S. V. Targeted deletion of metalloproteinase 9 attenuates experimental colitis in mice: central role of epithelial-derived MMP. *Gastroenterology* **2005,** 129, 1991-2008.

150. Al-Ghadban, S.; Kaissi, S.; Homaidan, F. R.; Naim, H. Y.; El-Sabban, M. E. Cross-talk between intestinal epithelial cells and immune cells in inflammatory bowel disease. *Scientific Reports* **2016,** 6, 29783.

151. Corry, D. B.; Kiss, A.; Song, L. Z.; Song, L.; Xu, J.; Lee, S. H.; Werb, Z.; Kheradmand, F. Overlapping and independent contributions of MMP2 and MMP9 to lung allergic inflammatory cell egression through decreased CC chemokines. *Faseb j* **2004,** 18, 995-7.

152. Wang, J.; Medina, C.; Radomski, M. W.; Gilmer, J. F. N-substituted homopiperazine barbiturates as gelatinase inhibitors. *Bioorg Med Chem* **2011,** 19, 4985-99.

153. Grams, F.; Brandstetter, H.; D'Alo, S.; Geppert, D.; Krell, H. W.; Leinert, H.; Livi, V.; Menta, E.; Oliva, A.; Zimmermann, G.; Gram, F.; Livi, V. E. Pyrimidine-2,4,6-Triones: a new effective and selective class of matrix metalloproteinase inhibitors. *Biol Chem* **2001,** 382, 1277-85.

154. Brandstetter, H.; Grams, F.; Glitz, D.; Lang, A.; Huber, R.; Bode, W.; Krell, H. W.; Engh, R. A. The 1.8-A crystal structure of a matrix metalloproteinase 8-barbiturate inhibitor complex reveals a previously unobserved mechanism for collagenase substrate recognition. *J Biol Chem* **2001,** 276, 17405-12.

155. Goodman, L.; Gilman; A.; Hardman, J.; Limbird, L. *Goodman &*

Gilman's the pharmacological basis of therapeutics. McGraw-Hill, Health

Professions Division: New York, 1996.

156. Tochowicz, A.; Maskos, K.; Huber, R.; Oltenfreiter, R.; Dive, V.; Yiotakis, A.; Zanda, M.; Pourmotabbed, T.; Bode, W.; Goettig, P. Crystal structures of MMP-9 complexes with five inhibitors: contribution of the flexible Arg424 side-chain to selectivity. *J Mol Biol* **2007,** 371, 989-1006.

157. Breyholz, H. J.; Schäfers, M.; Wagner, S.; Höltke, C.; Faust, A.; Rabeneck, H.; Levkau, B.; Schober, O.; Kopka, K. C-5-disubstituted barbiturates as potential molecular probes for noninvasive matrix metalloproteinase imaging. *J Med Chem* **2005,** 48, 3400-9.

158. Evans, D. A.; Katz, J. L.; West, T. R. Synthesis of diaryl ethers through the copper-promoted arylation of phenols with arylboronic acids. An expedient synthesis of thyroxine. *Tetrahedron Letters* **1998,** 39, 2937-2940.

159. Antonov, l. *Tautomerism*. Wiley-VCN: Weinheim, 2014.

160. Greenwald, R. B. PEG drugs: an overview. *J Control Release* **2001,** 74, 159-71.

161. Greenwald, R. B.; Conover, C. D.; Choe, Y. H. Poly(ethylene glycol) conjugated drugs and prodrugs: a comprehensive review. *Crit Rev Ther Drug Carrier Syst* **2000,** 17, 101-61.

162. Swierczewska, M.; Lee, K. C.; Lee, S. What is the future of PEGylated therapies? *Expert opinion on emerging drugs* **2015,** 20, 531-536.

163. Malla, N.; Sjoli, S.; Winberg, J. O.; Hadler-Olsen, E.; Uhlin-Hansen, L. Biological and pathobiological functions of gelatinase dimers and complexes. *Connect Tissue Res* **2008,** 49, 180-4.

164. Wang, J.; Radomski, M. W.; Medina, C.; Gilmer, J. F. MMP inhibition by barbiturate homodimers. *Bioorg Med Chem Lett* **2013,** 23, 444-7.

165. Molinspiration. http://www.molinspiration.com/ (14th march 2017).

166. Devel, L.; Rogakos, V.; David, A.; Makaritis, A.; Beau, F.; Cuniasse, P.; Yiotakis, A.; Dive, V. Development of selective inhibitors and substrate of matrix metalloproteinase-12. *J Biol Chem* **2006,** 281, 11152-60.

167. *2010 U. S. Pharmacopoeia [USP 33-28 NF]*. U.S. Pharmacopeial Convention Inc.: Rockville, Md, 2010.

168. (US), A. T. C. C. Caco-2 [Caco2](ATCC® HTB-37 ™). https://www.lgcstandards-atcc.org/Products/All/HTB-37.aspx?geo_country=ie#generalinformation (16th March 2017).

169. Hibi, T.; Ogata, H.; Sakuraba, A. Animal models of inflammatory bowel disease. *J Gastroenterol* **2002,** 37, 409-17.

170. Goyal, N.; Rana, A.; Ahlawat, A.; Bijjem, K. R.; Kumar, P. Animal models of inflammatory bowel disease: a review. *Inflammopharmacology* **2014,** 22, 219-33.

171. Dieleman, L. A.; Ridwan, B. U.; Tennyson, G. S.; Beagley, K. W.; Bucy, R. P.; Elson, C. O. Dextran sulfate sodium-induced colitis occurs in severe combined immunodeficient mice. *Gastroenterology* **1994,** 107, 1643-52.

172. Kawada, M.; Arihiro, A.; Mizoguchi, E. Insights from advances in research of chemically induced experimental models of human inflammatory bowel disease. *World J Gastroenterol* **2007,** 13, 5581-93.

173. Dieleman, L. A.; Palmen, M. J.; Akol, H.; Bloemena, E.; Pena, A. S.; Meuwissen, S. G.; Van Rees, E. P. Chronic experimental colitis induced by dextran sulphate sodium (DSS) is characterized by Th1 and Th2 cytokines. *Clin Exp Immunol* **1998,** 114, 385-91.

174. Wirtz, S.; Neufert, C.; Weigmann, B.; Neurath, M. F. Chemically induced mouse models of intestinal inflammation. *Nat Protoc* **2007,** 2, 541-6.

175. Laroui, H.; Ingersoll, S. A.; Liu, H. C.; Baker, M. T.; Ayyadurai, S.; Charania, M. A.; Laroui, F.; Yan, Y.; Sitaraman, S. V.; Merlin, D. Dextran sodium sulfate (DSS) induces colitis in mice by forming nano-lipocomplexes with medium-chain-length fatty acids in the colon. *PLoS One* **2012,** 7, e32084.

176. Zhang, L. Voluntary oral administration of drugs in mice. **2011**.

177. Jones, C. P.; Boyd, K. L.; Wallace, J. M. Evaluation of Mice Undergoing Serial Oral Gavage While Awake or Anesthetized. *J Am Assoc Lab Anim Sci* **2016,** 55, 805-810.

178. Cooper, H. S.; Murthy, S. N.; Shah, R. S.; Sedergran, D. J. Clinicopathologic study of dextran sulfate sodium experimental murine colitis. *Lab Invest* **1993,** 69, 238-49.

179. Schmittgen, T. D.; Livak, K. J. Analyzing real-time PCR data by the comparative CT method. *Nat. Protocols* **2008,** 3, 1101-1108.

180. Iyer, R. P.; Patterson, N. L.; Fields, G. B.; Lindsey, M. L. The history of matrix metalloproteinases: milestones, myths, and misperceptions. *American Journal of Physiology - Heart and Circulatory Physiology* **2012,** 303, H919-H930.

181. Vandooren, J.; Geurts, N.; Martens, E.; Van den Steen, P. E.; Opdenakker, G. Zymography methods for visualizing hydrolytic enzymes. *Nat Methods* **2013,** 10, 211-20.

182. Snoek-van Beurden, P. A.; Von den Hoff, J. W. Zymographic techniques for the analysis of matrix metalloproteinases and their inhibitors. *Biotechniques* **2005,** 38, 73-83.

183. Bradford, M. M. A rapid and sensitive method for the quantitation of microgram quantities of protein utilizing the principle of protein-dye binding. *Anal Biochem* **1976,** 72, 248-54.

184. Lohi, J.; Keski-Oja, J. Calcium ionophores decrease pericellular gelatinolytic activity via inhibition of 92-kDa gelatinase expression and decrease of 72-kDa gelatinase activation. *J Biol Chem* **1995,** 270, 17602-9.

185. Wang, J.; O'Sullivan, S.; Harmon, S.; Keaveny, R.; Radomski, M. W.; Medina, C.; Gilmer, J. F. Design of barbiturate-nitrate hybrids that inhibit MMP-9 activity and secretion. *J Med Chem* **2012,** 55, 2154-62.

186. Ramsey, K. H.; Sigar, I. M.; Schripsema, J. H.; Shaba, N.; Cohoon, K. P. Expression of Matrix Metalloproteinases Subsequent to Urogenital Chlamydia muridarum Infection of Mice. *Infection and Immunity* **2005,** 73, 6962-6973.

187. Estudante, M.; Morais, J. G.; Soveral, G.; Benet, L. Z. Intestinal drug transporters: an overview. *Adv Drug Deliv Rev* **2013,** 65, 1340-56.

188. Koepsell, H. The SLC22 family with transporters of organic cations, anions and zwitterions. *Mol Aspects Med* **2013,** 34, 413-35.

189. Koepsell, H.; Lips, K.; Volk, C. Polyspecific organic cation transporters: structure, function, physiological roles, and biopharmaceutical implications. *Pharm Res* **2007,** 24, 1227-51.

190. Zhou, S. F. Structure, function and regulation of P-glycoprotein and its clinical relevance in drug disposition. *Xenobiotica* **2008,** 38, 802-32.

191. Zihni, C.; Mills, C.; Matter, K.; Balda, M. S. Tight junctions: from simple barriers to multifunctional molecular gates. *Nat Rev Mol Cell Biol* **2016,** 17, 564-580.

192. Lingaraju, A.; Long, T. M.; Wang, Y.; Austin, J. R.; Turner, J. R. Conceptual barriers to understanding physical barriers. *Seminars in cell & developmental biology* **2015,** 42, 13-21.

193. Neurath, M. F. Cytokines in inflammatory bowel disease. *Nat Rev Immunol* **2014,** 14, 329-342.

194. Vounotrypidis, P.; Kouklakis, G.; Anagnostopoulos, K.; Zezos, P.; Polychronidis, A.; Maltezos, E.; Efremidou, E.; Pitiakoudis, M.; Lyratzopoulos, N. Interleukin-1 associations in inflammatory bowel disease and the enteropathic seronegative spondylarthritis. *Auto-Immunity Highlights* **2013,** 4, 87-94.

195. Coccia, M.; Harrison, O. J.; Schiering, C.; Asquith, M. J.; Becher, B.; Powrie, F.; Maloy, K. J. IL-1beta mediates chronic intestinal inflammation by promoting the accumulation of IL-17A secreting innate lymphoid cells and CD4(+) Th17 cells. *J Exp Med* **2012,** 209, 1595-609.

196. Reinecker, H. C.; Steffen, M.; Witthoeft, T.; Pflueger, I.; Schreiber, S.; MacDermott, R. P.; Raedler, A. Enhanced secretion of tumour necrosis factor-alpha, IL-6, and IL-1 beta by isolated lamina propria mononuclear cells from patients with ulcerative colitis and Crohn's disease. *Clinical and Experimental Immunology* **1993,** 94, 174-181.

197. Ito, H.; Takazoe, M.; Fukuda, Y.; Hibi, T.; Kusugami, K.; Andoh, A.; Matsumoto, T.; Yamamura, T.; Azuma, J.; Nishimoto, N.; Yoshizaki, K.; Shimoyama, T.; Kishimoto, T. A pilot randomized trial of a human anti-interleukin-6 receptor monoclonal antibody in active Crohn's disease. *Gastroenterology* **2004,** 126, 989-96; discussion 947.

198. Yu, Q.; Stamenkovic, I. Cell surface-localized matrix metalloproteinase-9 proteolytically activates TGF-beta and promotes tumor invasion and angiogenesis. *Genes Dev* **2000,** 14, 163-76.

199. Hamano, Y.; Zeisberg, M.; Sugimoto, H.; Lively, J. C.; Maeshima, Y.; Yang, C.; Hynes, R. O.; Werb, Z.; Sudhakar, A.; Kalluri, R. Physiological levels of tumstatin, a fragment of collagen IV alpha3 chain, are generated by MMP-9 proteolysis and suppress angiogenesis via alphaV beta3 integrin. *Cancer Cell* **2003,** 3, 589-601.

200. Lo, C. M.; Wang, H. B.; Dembo, M.; Wang, Y. L. Cell movement is guided by the rigidity of the substrate. *Biophysical Journal* **2000,** 79, 144-152.

201. Ulrich, T. A.; de Juan Pardo, E. M.; Kumar, S. The mechanical rigidity of the extracellular matrix regulates the structure, motility, and proliferation of glioma cells. *Cancer research* **2009,** 69, 4167-4174.

202. Xu, X.; Jackson, P. L.; Tanner, S.; Hardison, M. T.; Abdul Roda, M.; Blalock, J. E.; Gaggar, A. A self-propagating matrix metalloprotease-9 (MMP-9) dependent cycle of chronic neutrophilic inflammation. *PLoS One* **2011,** 6, e15781.

203. Koelink, P. J.; Overbeek, S. A.; Braber, S.; Morgan, M. E.; Henricks, P. A.; Abdul Roda, M.; Verspaget, H. W.; Wolfkamp, S. C.; te Velde, A. A.; Jones, C. W.; Jackson, P. L.; Blalock, J. E.; Sparidans, R. W.; Kruijtzer, J. A.; Garssen, J.; Folkerts, G.; Kraneveld, A. D. Collagen degradation and neutrophilic infiltration: a vicious circle in inflammatory bowel disease. *Gut* **2014,** 63, 578-87.

204. Thomas, C.; Pellicciari, R.; Pruzanski, M.; Auwerx, J.; Schoonjans, K. Targeting bile-acid signalling for metabolic diseases. *Nat Rev Drug Discov* **2008,** 7, 678-93.

205. Kawamata, Y.; Fujii, R.; Hosoya, M.; Harada, M.; Yoshida, H.; Miwa, M.; Fukusumi, S.; Habata, Y.; Itoh, T.; Shintani, Y.; Hinuma, S.; Fujisawa, Y.; Fujino, M. A G protein-coupled receptor responsive to bile acids. *J Biol Chem* **2003,** 278, 9435-40.

206. Gioiello, A.; Rosatelli, E.; Nuti, R.; Macchiarulo, A.; Pellicciari, R. Patented TGR5 modulators: a review (2006 - present). *Expert Opin Ther Pat* **2012,** 22, 1399-414.

207. Skiles, J. W.; Gonnella, N. C.; Jeng, A. Y. The design, structure, and clinical update of small molecular weight matrix metalloproteinase inhibitors. *Curr Med Chem* **2004,** 11, 2911-77.

208. Pols, T. W.; Noriega, L. G.; Nomura, M.; Auwerx, J.; Schoonjans, K. The bile acid membrane receptor TGR5 as an emerging target in metabolism and inflammation. *J Hepatol* **2011,** 54, 1263-72.

209. Masyuk, A. I.; Huang, B. Q.; Radtke, B. N.; Gajdos, G. B.; Splinter, P. L.; Masyuk, T. V.; Gradilone, S. A.; LaRusso, N. F. Ciliary subcellular localization of TGR5 determines the cholangiocyte functional response to bile acid signaling. *Am J Physiol Gastrointest Liver Physiol* **2013,** 304, G1013-24.

210. Keitel, V.; Ullmer, C.; Haussinger, D. The membrane-bound bile acid receptor TGR5 (Gpbar-1) is localized in the primary cilium of cholangiocytes. *Biol Chem* **2010,** 391, 785-9.

211. Thomas, C.; Gioiello, A.; Noriega, L.; Strehle, A.; Oury, J.; Rizzo, G.; Macchiarulo, A.; Yamamoto, H.; Mataki, C.; Pruzanski, M.; Pellicciari, R.; Auwerx, J.; Schoonjans, K. TGR5-mediated bile acid sensing controls glucose homeostasis. *Cell Metab* **2009,** 10, 167-77.

212. Watanabe, M.; Houten, S. M.; Mataki, C.; Christoffolete, M. A.; Kim, B. W.; Sato, H.; Messaddeq, N.; Harney, J. W.; Ezaki, O.; Kodama, T.; Schoonjans, K.; Bianco, A. C.; Auwerx, J. Bile acids induce energy expenditure by promoting intracellular thyroid hormone activation. *Nature* **2006,** 439, 484-9.

213. Poole, D. P.; Godfrey, C.; Cattaruzza, F.; Cottrell, G. S.; Kirkland, J. G.; Pelayo, J. C.; Bunnett, N. W.; Corvera, C. U. Expression and function of the bile acid receptor GpBAR1 (TGR5) in the murine enteric nervous system. *Neurogastroenterol Motil* **2010,** 22, 814-25, e227-8.

214. Haselow, K.; Bode, J. G.; Wammers, M.; Ehlting, C.; Keitel, V.; Kleinebrecht, L.; Schupp, A. K.; Haussinger, D.; Graf, D. Bile acids PKA-dependently induce a switch of the IL-10/IL-12 ratio and reduce proinflammatory capability of human macrophages. *J Leukoc Biol* **2013,** 94, 1253-64.

215. Yoneno, K.; Hisamatsu, T.; Shimamura, K.; Kamada, N.; Ichikawa, R.; Kitazume, M. T.; Mori, M.; Uo, M.; Namikawa, Y.; Matsuoka, K.; Sato, T.; Koganei, K.; Sugita, A.; Kanai, T.; Hibi, T. TGR5 signalling inhibits the production of pro-inflammatory cytokines by in vitro differentiated inflammatory and intestinal macrophages in Crohn's disease. *Immunology* **2013,** 139, 19-29.

216. Prawitt, J.; Caron, S.; Staels, B. Bile acid metabolism and the pathogenesis of type 2 diabetes. *Current Diabetes Reports* **2011,** 11, 160-166.

217. Pols, T. W.; Nomura, M.; Harach, T.; Lo Sasso, G.; Oosterveer, M. H.; Thomas, C.; Rizzo, G.; Gioiello, A.; Adorini, L.; Pellicciari, R.; Auwerx, J.; Schoonjans, K. TGR5 activation inhibits atherosclerosis by reducing macrophage inflammation and lipid loading. *Cell Metab* **2011,** 14, 747-57.

218. Duboc, H.; Aelion, H.; Rainteau, D.; Rajca, S.; Sokol, H.; Humbert, L.; Farabos, D.; Coffin, B.; Weber, S.; Porcher, R.; Varenne, O.; Duboc, D. Crosstalk between the hepatologist and the cardiologist: a future place for the lithocholic acid as a coronary atheroma risk factor? *Hepatology* **2012,** 56, 2426.

219. Duboc, H.; Taché, Y.; Hofmann, A. F. The bile acid TGR5 membrane receptor: From basic research to clinical application. *Digestive and Liver Disease* **2014,** 46, 302-312.

220. Alemi, F.; Kwon, E.; Poole, D. P.; Lieu, T.; Lyo, V.; Cattaruzza, F.; Cevikbas, F.; Steinhoff, M.; Nassini, R.; Materazzi, S.; Guerrero-Alba, R.; Valdez-Morales, E.; Cottrell, G. S.; Schoonjans, K.; Geppetti, P.; Vanner, S. J.; Bunnett, N. W.; Corvera, C. U. The TGR5 receptor mediates bile acid-induced itch and analgesia. *J Clin Invest* **2013,** 123, 1513-30.

221. Yuan, L.; Bambha, K. Bile acid receptors and nonalcoholic fatty liver disease. *World Journal of Hepatology* **2015,** 7, 2811-2818.

222. Li, T.; Holmstrom, S. R.; Kir, S.; Umetani, M.; Schmidt, D. R.; Kliewer, S. A.; Mangelsdorf, D. J. The G Protein-Coupled Bile Acid Receptor, TGR5, Stimulates Gallbladder Filling. *Molecular Endocrinology* **2011,** 25, 1066-1071.

223. Briere, D. A.; Ruan, X.; Cheng, C. C.; Siesky, A. M.; Fitch, T. E.; Dominguez, C.; Sanfeliciano, S. G.; Montero, C.; Suen, C. S.; Xu, Y.; Coskun, T.; Michael, M. D. Novel Small Molecule Agonist of TGR5 Possesses Anti-Diabetic Effects but Causes Gallbladder Filling in Mice. *PLoS One* **2015,** 10, e0136873.

224. Fryer, R. M.; Ng, K. J.; Nodop Mazurek, S. G.; Patnaude, L.; Skow, D. J.; Muthukumarana, A.; Gilpin, K. E.; Dinallo, R. M.; Kuzmich, D.; Lord, J.; Sanyal, S.; Yu, H.; Harcken, C.; Cerny, M. A.; Hickey, E. R.; Modis, L. K. G protein-coupled bile acid receptor 1 stimulation mediates arterial vasodilation through a K(Ca)1.1 (BK(Ca))-dependent mechanism. *J Pharmacol Exp Ther* **2014,** 348, 421-31.

225. Yasuda, H.; Hirata, S.; Inoue, K.; Mashima, H.; Ohnishi, H.; Yoshiba, M. Involvement of membrane-type bile acid receptor M-BAR/TGR5 in bile acid-induced activation of epidermal growth factor receptor and mitogen-activated protein kinases in gastric carcinoma cells. *Biochem Biophys Res Commun* **2007,** 354, 154-9.

226. Greiner, T. U.; Bäckhed, F. Microbial regulation of GLP-1 and L-cell biology. *Molecular Metabolism* **2016,** 5, 753-758.

227. Drucker, D. J.; Erlich, P.; Asa, S. L.; Brubaker, P. L. Induction of intestinal epithelial proliferation by glucagon-like peptide 2. *Proc Natl Acad Sci U S A* **1996,** 93, 7911-6.

228. Drucker, D. J.; Yusta, B.; Boushey, R. P.; DeForest, L.; Brubaker, P. L. Human [Gly2]GLP-2 reduces the severity of colonic injury in a murine model of experimental colitis. *Am J Physiol* **1999,** 276, G79-91.

229. Buchman, A. L.; Katz, S.; Shnaidman, M.; Jacobs, D. Effect of Teduglutide on Patients With Moderate-Severe Crohn’s Disease After 8 Weeks of Therapy: A Prospective, Double-Blind, Placebo-Controlled Trial. *Gastroenterology* 131, 949-950.

230. Xiao, Q.; Boushey, R. P.; Cino, M.; Drucker, D. J.; Brubaker, P. L. Circulating levels of glucagon-like peptide-2 in human subjects with inflammatory bowel disease. *Am J Physiol Regul Integr Comp Physiol* **2000,** 278, R1057-63.

231. Ichikawa, R.; Takayama, T.; Yoneno, K.; Kamada, N.; Kitazume, M. T.; Higuchi, H.; Matsuoka, K.; Watanabe, M.; Itoh, H.; Kanai, T.; Hisamatsu, T.; Hibi, T. Bile acids induce monocyte differentiation toward interleukin-12 hypo-producing dendritic cells via a TGR5-dependent pathway. *Immunology* **2012,** 136, 153-62.

232. Wu, T.; Bound, M. J.; Standfield, S. D.; Gedulin, B.; Jones, K. L.; Horowitz, M.; Rayner, C. K. Effects of rectal administration of taurocholic acid on glucagon-like peptide-1 and peptide YY secretion in healthy humans. *Diabetes Obes Metab* **2013,** 15, 474-7.

233. Harach, T.; Pols, T. W.; Nomura, M.; Maida, A.; Watanabe, M.; Auwerx, J.; Schoonjans, K. TGR5 potentiates GLP-1 secretion in response to anionic exchange resins. *Sci Rep* **2012,** 2, 430.

234. Brighton, C. A.; Rievaj, J.; Kuhre, R. E.; Glass, L. L.; Schoonjans, K.; Holst, J. J.; Gribble, F. M.; Reimann, F. Bile Acids Trigger GLP-1 Release Predominantly by Accessing Basolaterally Located G Protein-Coupled Bile Acid Receptors. *Endocrinology* **2015,** 156, 3961-70.

235. Ullmer, C.; Alvarez Sanchez, R.; Sprecher, U.; Raab, S.; Mattei, P.; Dehmlow, H.; Sewing, S.; Iglesias, A.; Beauchamp, J.; Conde-Knape, K. Systemic bile acid sensing by G protein-coupled bile acid receptor 1 (GPBAR1) promotes PYY and GLP-1 release. *British Journal of Pharmacology* **2013,** 169, 671-684.

236. Ma, S.-y.; Ning, M.-m.; Zou, Q.-a.; Feng, Y.; Ye, Y.-l.; Shen, J.-h.; Leng, Y. OL3, a novel low-absorbed TGR5 agonist with reduced side effects, lowered blood glucose via dual actions on TGR5 activation and DPP-4 inhibition. *Acta Pharmacologica Sinica* **2016,** 37, 1359-1369.

237. Sato, H.; Macchiarulo, A.; Thomas, C.; Gioiello, A.; Une, M.; Hofmann, A. F.; Saladin, R.; Schoonjans, K.; Pellicciari, R.; Auwerx, J. Novel Potent and Selective Bile Acid Derivatives as TGR5 Agonists: Biological Screening, Structure−Activity Relationships, and Molecular Modeling Studies. *Journal of Medicinal Chemistry* **2008,** 51, 1831-1841.

238. Dawson, P. A.; Karpen, S. J. Intestinal transport and metabolism of bile acids. *J Lipid Res* **2015,** 56, 1085-99.

239. Pellicciari, R.; Sato, H.; Gioiello, A.; Costantino, G.; Macchiarulo, A.; Sadeghpour, B. M.; Giorgi, G.; Schoonjans, K.; Auwerx, J. Nongenomic Actions of Bile Acids. Synthesis and Preliminary Characterization of 23- and 6,23-Alkyl-Substituted Bile Acid Derivatives as Selective Modulators for the G-Protein Coupled Receptor TGR5. *Journal of Medicinal Chemistry* **2007,** 50, 4265-4268.

240. Pellicciari, R.; Gioiello, A.; Macchiarulo, A.; Thomas, C.; Rosatelli, E.; Natalini, B.; Sardella, R.; Pruzanski, M.; Roda, A.; Pastorini, E.; Schoonjans, K.; Auwerx, J. Discovery of 6alpha-ethyl-23(S)-methylcholic acid (S-EMCA, INT-777) as a potent and selective agonist for the TGR5 receptor, a novel target for diabesity. *J Med Chem* **2009,** 52, 7958-61.

241. Sato, H.; Genet, C.; Strehle, A.; Thomas, C.; Lobstein, A.; Wagner, A.; Mioskowski, C.; Auwerx, J.; Saladin, R. Anti-hyperglycemic activity of a TGR5 agonist isolated from Olea europaea. *Biochem Biophys Res Commun* **2007,** 362, 793-8.

242. Zhao, G.; Yan, W.; Cao, D. Simultaneous determination of betulin and betulinic acid in white birch bark using RP-HPLC. *Journal of Pharmaceutical and Biomedical Analysis* **2007,** 43, 959-962.

243. Kunkel, S. D.; Elmore, C. J.; Bongers, K. S.; Ebert, S. M.; Fox, D. K.; Dyle, M. C.; Bullard, S. A.; Adams, C. M. Ursolic Acid Increases Skeletal Muscle and Brown Fat and Decreases Diet-Induced Obesity, Glucose Intolerance and Fatty Liver Disease. *PLOS ONE* **2012,** 7, e39332.

244. Genet, C.; Strehle, A.; Schmidt, C.; Boudjelal, G.; Lobstein, A.; Schoonjans, K.; Souchet, M.; Auwerx, J.; Saladin, R.; Wagner, A. Structure-activity relationship study of betulinic acid, a novel and selective TGR5 agonist, and its synthetic derivatives: potential impact in diabetes. *J Med Chem* **2010,** 53, 178-90.

245. Xu, Y. Recent Progress on Bile Acid Receptor Modulators for Treatment of Metabolic Diseases. *Journal of Medicinal Chemistry* **2016,** 59, 6553-6579.

246. Valeur, E.; Bradley, M. Amide bond formation: beyond the myth of coupling reagents. *Chemical Society Reviews* **2009,** 38, 606-631.

247. Gabriel, C. M.; Keener, M.; Gallou, F.; Lipshutz, B. H. Amide and Peptide Bond Formation in Water at Room Temperature. *Org Lett* **2015,** 17, 3968-71.

248. Pore, V. S.; Aher, N. G.; Kumar, M.; Shukla, P. K. Design and synthesis of fluconazole/bile acid conjugate using click reaction. *Tetrahedron* **2006,** 62, 11178-11186.

249. Reddy, A. S.; Kumar, M. S.; Reddy, G. R. A convenient method for the preparation of hydroxamic acids. *Tetrahedron Letters* **2000,** 41, 6285-6288.

250. Tsai, W. C.; Hsu, C. C.; Chen, C. P.; Chang, H. N.; Wong, A. M.; Lin, M. S.; Pang, J. H. Ciprofloxacin up-regulates tendon cells to express matrix metalloproteinase-2 with degradation of type I collagen. *J Orthop Res* **2011,** 29, 67-73.

251. Chen, I. T.; Baitinger, I.; Schreyer, L.; Trauner, D. Total Synthesis of Sandresolide B and Amphilectolide. *Organic Letters* **2014,** 16, 166-169.

252. Lidström, P.; Tierney, J.; Wathey, B.; Westman, J. Microwave assisted organic synthesis—a review. *Tetrahedron* **2001,** 57, 9225-9283.

253. Wang, G. T.; Mantei, R. A.; Kawai, M.; Tedrow, J. S.; Barnes, D. M.; Wang, J.; Zhang, Q.; Lou, P.; Garcia, L. A.; Bouska, J.; Yates, M.; Park, C.; Judge, R. A.; Lesniewski, R.; Sheppard, G. S.; Bell, R. L. Lead optimization of methionine aminopeptidase-2 (MetAP2) inhibitors containing sulfonamides of 5,6-disubstituted anthranilic acids. *Bioorg Med Chem Lett* **2007,** 17, 2817-22.

254. Sosič, I.; Turk, S.; Sinreih, M.; Trošt, N.; Verlaine, O.; Amoroso, A.; Zervosen, A.; Luxen, A.; Joris, B.; Gobec, S. Exploration of the chemical space of novel naphthalene-sulfonamide and anthranilic Acid-based inhibitors of penicillin-binding proteins. *Acta Chim Slov* **2012,** 59, 280-388.

255. Barski, O. A.; Tipparaju, S. M.; Bhatnagar, A. The aldo-keto reductase superfamily and its role in drug metabolism and detoxification. *Drug Metab Rev* **2008,** 40, 553-624.

256. Varga, G.; Bálint, A.; Burghardt, B.; D'Amato, M. Involvement of endogenous CCK and CCK1 receptors in colonic motor function. *Br J Pharmacol* **2004,** 141, 1275-84.

257. O'Brien, P. M.; Ortwine, D. F.; Pavlovsky, A. G.; Picard, J. A.; Sliskovic, D. R.; Roth, B. D.; Dyer, R. D.; Johnson, L. L.; Man, C. F.; Hallak, H. Structure-activity relationships and pharmacokinetic analysis for a series of potent, systemically available biphenylsulfonamide matrix metalloproteinase inhibitors. *J Med Chem* **2000,** 43, 156-66.

258. Park, J. G.; Oie, H. K.; Sugarbaker, P. H.; Henslee, J. G.; Chen, T. R.; Johnson, B. E.; Gazdar, A. Characteristics of cell lines established from human colorectal carcinoma. *Cancer Res* **1987,** 47, 6710-8.

259. de Bruine, A. P.; Dinjens, W. N.; van der Linden, E. P.; Pijls, M. M.; Moerkerk, P. T.; Bosman, F. T. Extracellular matrix components induce endocrine differentiation in vitro in NCI-H716 cells. *Am J Pathol* **1993,** 142, 773-82.

260. Kuhre, R. E.; Wewer Albrechtsen, N. J.; Deacon, C. F.; Balk-Moller, E.; Rehfeld, J. F.; Reimann, F.; Gribble, F. M.; Holst, J. J. Peptide production and secretion in GLUTag, NCI-H716, and STC-1 cells: a comparison to native L-cells. *J Mol Endocrinol* **2016,** 56, 201-11.

261. Ekkebus, R.; van Kasteren, S. I.; Kulathu, Y.; Scholten, A.; Berlin, I.; Geurink, P. P.; de Jong, A.; Goerdayal, S.; Neefjes, J.; Heck, A. J. R.; Komander, D.; Ovaa, H. On Terminal Alkynes That Can React with Active-Site Cysteine Nucleophiles in Proteases. *Journal of the American Chemical Society* **2013,** 135, 2867-2870.

262. Roffey, S. J.; Obach, R. S.; Gedge, J. I.; Smith, D. A. What is the Objective of the Mass Balance Study? A Retrospective Analysis of Data in Animal and Human Excretion Studies Employing Radiolabeled Drugs. *Drug Metabolism Reviews* **2007,** 39, 17-43.

263. Obach, R. S.; Nedderman, A. N.; Smith, D. A. Radiolabelled mass-balance excretion and metabolism studies in laboratory animals: are they still necessary? *Xenobiotica* **2012,** 42, 46-56.

264. Jensen, D. D.; Godfrey, C. B.; Niklas, C.; Canals, M.; Kocan, M.; Poole, D. P.; Murphy, J. E.; Alemi, F.; Cottrell, G. S.; Korbmacher, C.; Lambert, N. A.; Bunnett, N. W.; Corvera, C. U. The Bile Acid Receptor TGR5 Does Not Interact with β-Arrestins or Traffic to Endosomes but Transmits Sustained Signals from Plasma Membrane Rafts. *The Journal of Biological Chemistry* **2013,** 288, 22942-22960.

265. Wang, Y.-D.; Chen, W.-D.; Yu, D.; Forman, B. M.; Huang, W. The G-protein coupled bile acid receptor Gpbar1 (TGR5) negatively regulates hepatic inflammatory response through antagonizing Nuclear Factor κB. *Hepatology (Baltimore, Md.)* **2011,** 54, 1421-1432.

266. Lou, G.; Ma, X.; Fu, X.; Meng, Z.; Zhang, W.; Wang, Y.-D.; Van Ness, C.; Yu, D.; Xu, R.; Huang, W. GPBAR1/TGR5 Mediates Bile Acid-Induced Cytokine Expression in Murine Kupffer Cells. *PLOS ONE* **2014,** 9, e93567.

267. Li, D.; Cao, W. Bile acid receptor TGR5, NADPH Oxidase NOX5-S and CREB Mediate Bile Acid-Induced DNA Damage In Barrett's Esophageal Adenocarcinoma Cells. *Scientific Reports* **2016,** 6, 31538.

268. Hong, J.; Behar, J.; Wands, J.; Resnick, M.; Wang, L. J.; DeLellis, R. A.; Lambeth, D.; Souza, R. F.; Spechler, S. J.; Cao, W. Role of a novel bile acid receptor TGR5 in the development of oesophageal adenocarcinoma. *Gut* **2010,** 59, 170-80.

269. Kim, K.; Park, M.; Lee, Y. M.; Rhyu, M. R.; Kim, H. Y. Ginsenoside metabolite compound K stimulates glucagon-like peptide-1 secretion in NCI-H716 cells via bile acid receptor activation. *Arch Pharm Res* **2014,** 37, 1193-200.

270. Lo, S.-H.; Cheng, K.-C.; Li, Y.-X.; Chang, C.-H.; Cheng, J.-T.; Lee, K.-S. Development of betulinic acid as an agonist of TGR5 receptor using a new in vitro assay. *Drug Design, Development and Therapy* **2016,** 10, 2669-2676.